TURBULENT TRANSPORT PROPERTIES IN SWIRLING TWO-DIMENSIONAL BOUNDARY LAYERS

by

Marc L. Koo Sin Lin

Thesis submitted for the degree of
Doctor of Philosophy
in the Faculty of Engineering
University of London
and
for the Diploma of Membership
of Imperial College

Mechanical Engineering Department
Imperial College
London S.W.7

March 1974

ABSTRACT

This thesis records the outcome of the search for models of turbulence which are applicable to a wide range of turbulent swirling boundary layers.

The scientific and engineering relevances of swirling flows are discussed, and the governing partial differential equations for the transport of momentum, mass and enthalpy are presented. The numerical accuracy of the procedure employed to solve the finite-difference forms of the transport equations is demonstrated.

Four different models of turbulence are developed and tested. In the first, the traditional mixing-length hypothesis is adapted to swirling flows, and leads to an isotropic viscosity formulation. In the second the turbulence is characterised by its kinetic energy and a length scale, both obtained from the solution of their own differential equations. A new term involving the Richardson number is introduced in the length-scale equation to account for the effect of swirl body-forces. The third model is based on the mixing-length concept, but it accounts for the near-wall anisotropy of viscosity by postulating two mixing lengths suitably modified by Van Driest's expressions. Algebraic relations for all six Reynolds-stress components in terms of the time-average velocities and the turbulence quantities are derived in the fourth and last model for high Reynolds number flow. This model accounts analytically for the non-isotropic features of swirling boundary layers, and does not require the use of the effective viscosity concept; the Reynolds stresses are directly calculated.

The four turbulence models are tested by comparing the predictions with a large number of existing experimental data as well as data from two new experiments which were performed.

Of the models, the algebraic stress model exhibits the most promising improvement in universality of predictive power. The extension of its applicability to low Reynolds number flow to permit the prediction of the sublayer region represents an urgent future task.

ACKNOWLEDGEMENTS

Dr. F.C. Lockwood deserves my warmest thanks for his invaluable assistance and his continuous enthusiasm during the four years he supervised my work. I am also grateful to Dr. J.H. Whitelaw and Prof. D.B. Spalding for many useful suggestions, and to members of the Heat Transfer Section for their contribution to the work resulting from discussions which I had with them.

Mr. R. Church helped in the design of the experimental apparatus, which he subsequently built. Mr. R. King was always available to iron out teething problems with the apparatus and instrumentation, while Mr. S. Kasinathan helped with the assembling of the apparatus. I am deeply indebted to them for their assistance.

The excellent work of Miss M. Schertzer who typed the manuscript is very much appreciated. Finally, I would like to acknowledge my graditute to my wife, Christina, for her understanding and encouragement of my work.

The work was carried out during the tenure of a Scholarship from the University of London for the first three years. The Ministry of Defence provided financial assistance during my fourth year, and also financed the experimental programme.

M.L. Koo Sin Lin
London, March 1974.

CONTENTS

Page

CHAPTER 4

CHAPTER 1

INTRODUCTION

1.1 The Problem Considered

Swirling boundary layers are characterised by a circumferential component of velocity about a symmetry axis in addition to a main component of velocity in the dominant direction of flow. The presence of this circumferential velocity sets up centrifugal and Coriolis forces which strongly influence the structure of the flow. It is therefore not surprising that analytical work and experimental investigations have been, and still are, restricted to simplified models and approximate simulations of the geometrical and flow structure of real rotating systems.

The present work is confined to swirling flows of the boundary-layer class, where there is a single predominant direction of flow and where the diffusive fluxes are significant only normal to this direction; consequently there are no regions of recirculation. Within the context of the boundary layer restrictions the fluid flow situations considered here all fall within the general flow configuration illustrated in figure 1.1.

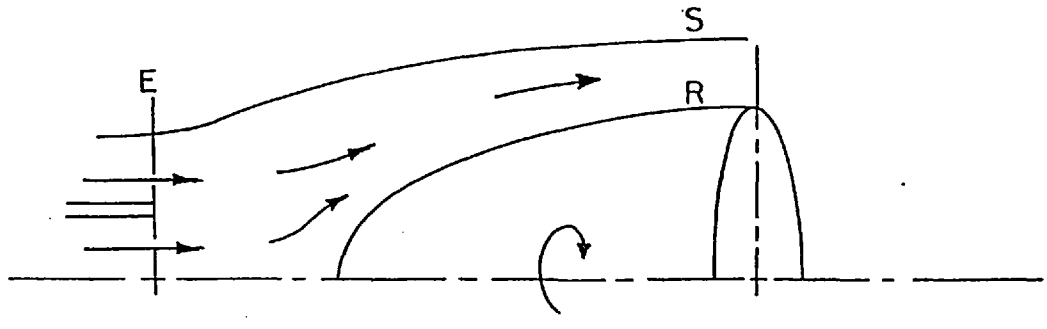

Fig. 1.1 General flow configuration

The geometry is axisymmetrical and body R rotates about the symmetry axis. The enclosure S may or may not be present, and the system is correspondingly termed 'shrouded' or 'unshrouded'. The fluid surrounding body R may be at rest, or it may move relative to R in one or more axially-directed streams issuing from the region E. The flow may be either laminar or turbulent, but most practical flows are turbulent.

Information about the dependent variables of the problem is known at the surfaces of R and S and constitutes the boundary conditions. If stagnation enthalpy is one of the dependent variables for example, then the temperature, heat flux, or heat-transfer coefficient at the surfaces is prescribed. The boundary conditions may vary with x, the coordinate measuring distance along the surface of R; but for fixed x, they are invariant with respect to the circumferential coordinate. Consequently, the dependent variables also possess axial symmetry throughout the flow field. The problem is, therefore, a two-dimensional one since it is completely specified by reference to two independent variables.

1.2 Scientific and Engineering Importance

Swirling axisymmetrical boundary layers are of considerable scientific interest; this arises from the fact that the shear stress possesses two main components. In this respect swirling boundary layers are akin to three-dimensional ones; the distinction is that, whereas the cross flow in the three dimensional layer is the result of pressure variations, the circumferential velocity component of the swirling boundary layer is not pressure driven but a result of the rotation of either a surface of revolution, or of the free-stream. Because of the two-dimensionality and the consequent ease with which

the governing partial differential equations may be computed, axisymmetrical swirling boundary layers represent a useful intermediate stage in the development of prediction procedures for three-dimensional boundary layers.

In addition to their important scientific significance swirling boundary layers are also of considerable engineering importance. Recent years have witnessed ever increasing interest in the flow and heat transfer characteristics of rotating systems. There are numerous examples of industrial applications where swirling flows are present either as a consequence of the design, or where they are purposely introduced to achieve desired results. Rotating machines and systems such as electric motors, turbines, and gas bearings, fall into the first category; engineers are primarily concerned with economical cooling arrangements which will prevent temperature limitations from being exceeded and which, ideally, will also result in size reduction. Other systems like rotating condensers and heat exchangers make use of the properties of swirling flows to obtain enhanced transfer of heat. The role played by swirling flows in some of these industrial applications is described in the following examples.

Furnace burners often employ swirl to promote rapid mixing of the fuel and air and to assist in stabilising the flame. In this case the flow is rotating relative to a stationary surface and if the swirl is not so large as to cause recirculation, the flow is of the boundary-layer type.

The heat transfer to the walls of a pipe containing a flow of hot fluid is greatly enhanced when the pipe is fitted with a twisted-tape swirl generator. Of course, the pressure drop experienced by the fluid increases as well, but twisted tapes are often employed where

compactness is essential, notably in gas-cooled nuclear reactors and sometimes in industrial boilers.

Another example of the industrial applications of swirling flows relates to high speed rotating evaporator-condensers. Through the action of centrifugal forces liquid is maintained in the form of thin films on both sides of the rotor surfaces, and large rates of heat transfer from the heated rotor are achieved. This rapid and efficient evaporation process is used for the distillation of sea water. The rotors are usually a geometrical hybrid of discs and cones, and the flow is of the two-phase, boundary-layer type.

The last example covers a sector which has received much publicity lately. The gas-turbine industry is concerned with the thermal fatigue and creep fatigue characteristics of the disc-blades system. The analysis of the thermal stresses in the metal requires knowledge of the temperatures, and hence the local heat transfer rates at the fluid/metal interfaces. The continuing demand for higher output has necessitated separate cooling of the turbine discs, as distinct from cooling of the blades, since efficient cooling allows the turbine to be operated at a higher temperature, a critical factor for improved performance. Unlike the previous three cases where the flow was of the boundary-layer type, the flow in turbines is usually of the recirculating type.

These examples illustrate the wide range of practical application of swirling flows and also demonstrate the complex nature of these flows. Consequently, empirical information is of limited value, and there is therefore a great need for reliable prediction methods in order to improve existing systems, to extend their limits of operation, and to design completely novel systems.

1.3 Previous and Current Prediction Procedures

A comprehensive survey of the various prediction procedures in existence up to about 1958 has been provided by Dorfman (1963). Another extensive review of subsequent advances in the field has been made by Krieth (1968). Both publications contribute substantially to the understanding of rotating systems and are standard references. In Appendix 1 the most relevant prediction procedures covered by these surveys are described in some detail, and the coverage is extended there to include recent contributions. This analysis of the previous theoretical work reveals that all the predictions methods solve the boundary-layer forms of the governing equations, with the exception of a few cases for which the full elliptic forms of the governing equations reduce to ordinary differential ones. Furthermore, the predictions can be classified into three distinct groups: similarity, integral-profile, and finite-difference methods.

1.3-1 Similarity Methods

For the laminar flow on axisymmetric rotating bodies, all the procedures, apart for a few integral-profile methods, are for those geometries and boundary conditions for which similarity solutions exist. Laminar flow solutions are of limited value because in most engineering applications the flow is turbulent. For turbulent non-swirling flows, it is well known that similarity solutions can only be satisfied for very special boundary conditions, see Schlichting (1968) for example; the same remark also applies to flows having a swirl component of velocity.

1.3-2 Integral-Profile Methods

All of the early methods developed for turbulent swirling flows were of the integral-profile kind, and as such they were

restricted to simple geometries, constant-property fluids, and uncomplicated boundary conditions. Using the modern digital computer, however, the computational work associated with extending the integral-profile technique to more complex flows is no longer a problem. But as the generality increases, the number of profile parameters increases correspondingly and most often the relevant ones cannot, in the absence of extensive experimental investigations, be clearly identified. Further, integral-profile methods involve a matrix inversion and the risk of singularities increases rapidly with the number of profile parameters. Although, for example, Cham and Head (1969 - 1971) have recently predicted with some success the flow near rotating discs, cylinders, and streamline-shapes using integral-profile methods, these procedures are clearly unsuited for the general problem illustrated in Fig. 1.1. Integral-profile methods are even less attractive when three-dimensional flows are considered.

1.3-3 Finite-Difference Methods

Integral-profile methods are losing their popularity in two-dimensional non-swirling flows; the same trend is also evident for swirling flows. The review in Appendix 1 reveals that finite-difference techniques are favoured by the majority of contemporary research workers. There can be little doubt that finite-difference methods, which solve the governing partial differential equations directly, are the only ones of sufficient potential to be of real interest to design engineers.

The computer-based finite-difference procedures completely master the mathematical problem of solving the time-average differential equations. However, when the flow is turbulent, these procedures require explicit information about the turbulent transport properties: the Reynolds stresses for the momentum equations, and the effective

Prandtl and Schmidt numbers for the heat and mass transfer equations. The development of relations to represent the Reynolds stresses is usually referred to as turbulence modelling. Hence, authors who employ finite-difference procedures concentrate on the search of turbulence models appropriate to their respective problems.

1.4 Previous Experimental Work

The previous experimental work relevant to the present class of boundary layer flows is reviewed in Appendix 2. The measurements surveyed relate to unshrouded rotating geometries, since the flow associated with shrouded systems is usually of the recirculating type. Only turbulent flow conditions are considered and the data reviewed are: mean flow quantities for rotating discs, cones and cylinders, and for swirling jets; turbulence quantities for rotating discs and swirling jets; heat and mass-transfer from discs and cones. The most reliable measurements, and the limitations and gaps in the available data are summarised below; the hydrodynamic, turbulence, and heat and mass-transfer measurements are considered in turn.

1.4.1 Hydrodynamic Measurements

For the case of mean velocity measurements the most useful data are probably those of Cham and Head (1969) on a free disc, and by Parr (1963) and Furuya and his co-workers (1966) on a cylinder rotating in a uniform axial stream. The circumferential drag data of Theodorsen and Regier (1944), and Owen (1969) for a free disc, are also well established.

Several authors have investigated the free swirling jet which is a boundary-layer type flow when the degree of swirl is not large. The most comprehensive measurements are those of Rose (1962), and Chigier and his co-workers (1966, 1967) of the velocity field.

1.4_2 Turbulence Measurements

Except for one incomplete set of turbulence measurements near a disc rotating in stagnant air, by Erian and Tong (1971), there exist no data of turbulence quantities for the swirling boundary layer near bodies of revolution. This dearth of data is mainly due to the experimental difficulites associated with accurate positioning of the measuring probe from, and the restricted access to rotating surfaces.

For the case of free swirling jets however, measurements of the six Reynolds stresses have been reported by Craya and Darrigol (1967), and Pratte and Keffer (1972). But very little of the data of the former authors have been published, while the data of the latter authors show considerable scatter. Pratte and Keffer (1972a) indicated that their data should not be relied on for more than trends and magnitudes.

1.4_3 Heat and Mass-Transfer Measurements

The data of Cobb and Saunders (1956), McComas and Hartnett (1970), and Dennis, Newstead and Ede (1970) for the average heat transfer from isothermal discs, and the data of Krieth, Taylor and Chong (1959), and Tien and Campbell (1963) for the average mass transfer from cones rotating in stagnant air, are the most comprehensive ones available.

The range of heat transfer data for non-isothermal surfaces is very narrow, being limited to the uniform heat flux results of Subba Rao (1967) for a disc, and the step-change mass transfer measurements of Tien (1965) for a cone. In particular, no direct measurements of local heat-transfer coefficients have been reported.

1.5 Purpose and Scope of the Present Study

In the four preceeding sections, the general swirling-flow

problem of the boundary-layer class was presented, and the scientific and engineering importance of swirling flows described. The various prediction methods employed to solve the differential equations governing these flows were discussed. The finite-difference procedures emerged as the most promising ones with sufficient potential and generality to be of real interest to design engineers. These procedures require, however, information about the turbulent transport properties, and in this area there is a major lack of knowledge. Lastly, the review of experimental work has focussed attention on the reliable measurements as well as the gaps in the existing data.

The main objective of the present work is, therefore, the development of turbulence models for swirling boundary layers. The search is for models which will give reasonably accurate predictions for several flow situations without changes in the empirical constants appearing in these models. The governing equations are solved by the finite-difference procedure of Patankar and Spalding (1970).

In addition, the present work has two secondary objectives: the provision of (a) mean velocity data for a rotating cone, and (b) local heat transfer measurements for a disc rotating in stagnant air.

1.5-1 Theoretical Work

(a) Choice of Prediction Procedure

The choice of a prediction method must be governed both by its proven capabilities and its potential for future development to tackle more complex flows. The extension of integral-profile methods to complex flow situations offers few advantages, but many disadvantages, compared with finite-difference methods. These latter methods have been shown to be flexible and general. In particular, the finite-

difference procedure of Patankar and Spalding (1970) has been applied by several workers to swirling flow problems, namely: rotating discs, Bayley and Owen (1969), free swirling jets, Siddartha (1971), Lilley (1973) and swirling flow in pipes, Roberts (1972). All these flows were efficiently and accurately handled by the procedure. The same method was chosen to solve the partial differential equations governing the class of swirling flows considered in the present study.

(b) Turbulent Transport Properties

Computers of the current generation, and probably those too of the next, are not large enough to permit the calculation of the turbulent fluctuations by solution of the time-dependent equations for any problem of engineering importance. Consequently, when the time-averaged equations are solved it is necessary to construct mathematical models which relate the turbulent transport properties to time-averaged values of the variables of the flow. These models of turbulence have been proposed in varying degrees of complexity. For example, Prandtl's (1925) mixing-length hypothesis simply relates the shear stress directly to a mean velocity gradient, while Daly and Harlow's model (1970) employs differential transport equations for all six Reynolds stress components.

Four different models of turbulence are developed and assessed in the present work:

1. A mixing-length model, which is an extension of Prandtl's hypothesis to swirling flows, leading to an isotropic effective viscosity.
2. A two-equation model, where the flow structure is characterised by two parameters determined from their own differential equations. These parameters are the turbulence energy and a length scale appropriate to the

energy containing motions.

3. A mixing-length model, modified in the near-wall region to provide anisotropic effective viscosity formulations.
4. An algebraic Reynolds stress model which provides six algebraic equations for the six Reynolds stress components, and which is employed in conjunction with the above two-equation model.

1.5-2 Experimental Work

(a) Mean Velocity Measurements on a Cone

Since the main objective of the present study is the development of turbulence models, measurements of turbulence quantities would provide the ideal data for validating the proposed models. However, these measurements, as well as presenting considerable experimental difficulties as the survey of experimental work revealed, also require expensive measuring and recording equipment. The financial resources available for the work reported in this thesis excluded such costly equipment.

The survey of experimental work also indicated a lack of data for the turbulent mean velocity field near a rotating cone. For the well documented cases of discs, and cylinders and jets, the centrifugal forces resulting from the swirl act along and normal to the predominant direction of flow respectively; but for the case of a cone, these forces have components both in the streamwise and cross-stream directions. Experimental mean velocity data for the cone therefore provide a useful test of the generality of the proposed turbulence models.

Hence an experimental investigation was initiated to obtain mean velocity data for a cone rotating in stagnant air, and also in a longitudinal air stream issuing from a concentric annulus near the

cone's apex. The dimensions and speed of the cone were large enough to ensure a substantial length of fully turbulent flow. The apparatus and experimental measurements are presented in Appendix 5. The results are compared in Section 3 of Chapter 6 with predictions obtained using a mixing-length model of turbulence.

(b) Local Heat Transfer Measurements on a Disc

In almost all situations of engineering importance, the designer wants to be able to calculate the local heat-transfer rate from a specified distribution of temperature or heat flux. However, experiments have so far been concentrated on measurements of average heat-transfer coefficients. The present experimental programme is therefore focused on obtaining information about the local heat-transfer coefficient on a disc rotating in stagnant air, for any arbitrary distribution of surface heat flux. The construction of the apparatus and the experimental techniques used are described in Appendix 7. Predictions are compared with the measurements in Chapter 8, Section 4.

1.6 Outline of Remainder of Thesis

Chapter 2 commences with the presentation of the coordinate system and the governing differential equations for the transport of momentum, enthalpy and chemical species. These equations are subsequently reduced to their parabolic forms which are appropriate to the present work.

The finite-difference method employed to solve the differential equations is briefly reviewed in Chapter 3. The accuracy of the procedure is demonstrated by comparing predictions for a laminar flow with its analytically exact solution.

The main objective of the present work, the development of suitable relations for the turbulent transport properties for flows

near rotating bodies, is covered in Chapters 4 to 7. Four models of turbulence are developed, and each is evaluated by comparing predictions with the results of experiments. At the end of each chapter, the best values of empirical parameters in the turbulence model under consideration are tabulated, and the findings are discussed.

The first model is an isotropic viscosity model, based on an extension of the mixing-length concept to swirling flows. It is employed to predict the flow near rotating free discs and cones, cylinders in axial streams, and between two parallel discs, one stationary, with radial outflow. The mixing-length is subsequently made a function of the swirling flow Richardson's number, and the predictions for the above four flows are repeated.

A two-equation energy-length model is developed in Chapter 5, where the effective viscosities are calculated from two turbulence parameters: the kinetic energy of turbulence and a length-scale, both determined from differential equations. The viscosities are assumed to be in a constant ratio. The model is evaluated by comparing predictions with experimental data for the flow near a cylinder rotating in an axial stream.

Chapter 6 deals with a mixing-length based anisotropic viscosity model. The effective viscosities are calculated from two separate Van Driest's expressions which are made functions of the corresponding Reynolds stress. These expressions are applicable to the near-wall region only; in the outer region the viscosities are assumed to be equal, and the mixing length made proportional to the boundary-layer thickness. Predictions are obtained for the free disc and cone, as well as the rotating cylinder.

A high turbulence Reynolds number model is developed in Chapter 7, where algebraic expressions are derived for all six

Reynolds stress components. Each of the two main shear-stress components, implicitly, the corresponding effective viscosity, is obtained from the mean-velocity field, the energy dissipation rate, and one or more of the remaining stresses. The model is employed to predict a free swirling jet, as well as rotating free disc and cylinder wall flows. When applied to the wall-flows, where the assumption of high Reynolds number is not valid in the near-wall region, the algebraic stress model is matched with the anisotropic mixing-length model in this region.

In Chapter 8, some calculations are presented for the heat and mass transfer from free spinning discs and cones. For these cases, where only a single quantity is required, namely the heat or mass flux, the simple isotropic mixing-length model is used to calculate the flow. The effective heat and mass exchange coefficients are made linear functions of the effective viscosity.

The principal conclusions which are the outcome of the thesis are enumerated in Chapter 9. The likely nature of the most profitable areas for further research are also discussed.

The descriptions and results of two experiments carried out as part of the present research are presented in Appendices 5 and 7. The two experiments concern the measurements of the velocity field near a cone, and the local heat transfer rate from a disc, both spinning in air. Appendices 1 and 2 are reviews of past theoretical and experimental work on swirling boundary-layer flows, while the remaining Appendices, 3, 4 and 6 are concerned with 'wall-functions', streamwise pressure gradient, and transport equations for Reynolds stresses.

CHAPTER 2

THE GOVERNING DIFFERENTIAL EQUATIONS

2.1 Introduction

The majority of swirl flows present in engineering systems are turbulent and therefore unsteady in character. These turbulent flows consist of a mean motion and a fluctuating motion, irregular velocity fluctuations being superimposed on the main stream. The resultant turbulent mixing process exerts a considerable influence on the transport of energy in the flow; and the diffusive action of the turbulence results in an apparent or eddy viscosity giving rise to large stresses, termed Reynolds stresses. Except for the occurrence of the Reynolds-stress terms, the components of the mean velocity satisfy the same equations as those which describe the corresponding velocity components in laminar flows. Schlichting (1968) reports predictions of turbulent flow in free jets and wakes, in pipes, and in boundary layers on walls, which show that the time-average character of turbulent flows can be predicted by solving the equations for steady laminar flows if the transport properties of the fluid are appropriately increased.

Section 2.2 introduces a two-dimensional curvilinear and axisymmetrical coordinate system which possesses two main features: it is general and therefore covers all axisymmetric flow configurations; it is orthogonal, hence the equations are compact. The general forms of the governing conservation equations are presented in Section 2.3, and these equations are reduced in Section 2.4 to their parabolic forms.

2.2 The Coordinate System

A general axisymmetrical coordinate system is illustrated in Fig. 2.1. The coordinates are ξ_1, ξ_2 and ξ_3 ; the first two designate two orthogonal families of surfaces of revolution while the last designates

planes through the axis of symmetry. The distance ds between two neighbouring points in the field is related to the increments in ξ_1, ξ_2 and ξ_3 by:

$$(ds)^2 = (\ell_1 d\xi_1)^2 + (\ell_2 d\xi_2)^2 + (\ell_3 d\xi_3)^2 \qquad (2.1)$$

when ℓ_1, ℓ_2 and ℓ_3 are the metric cofficients. When ξ_3 is measured in radians, ℓ_3 is identical with the radius of curvature r_3. Derivatives with respect to ξ_3 are zero because of axial symmetry.

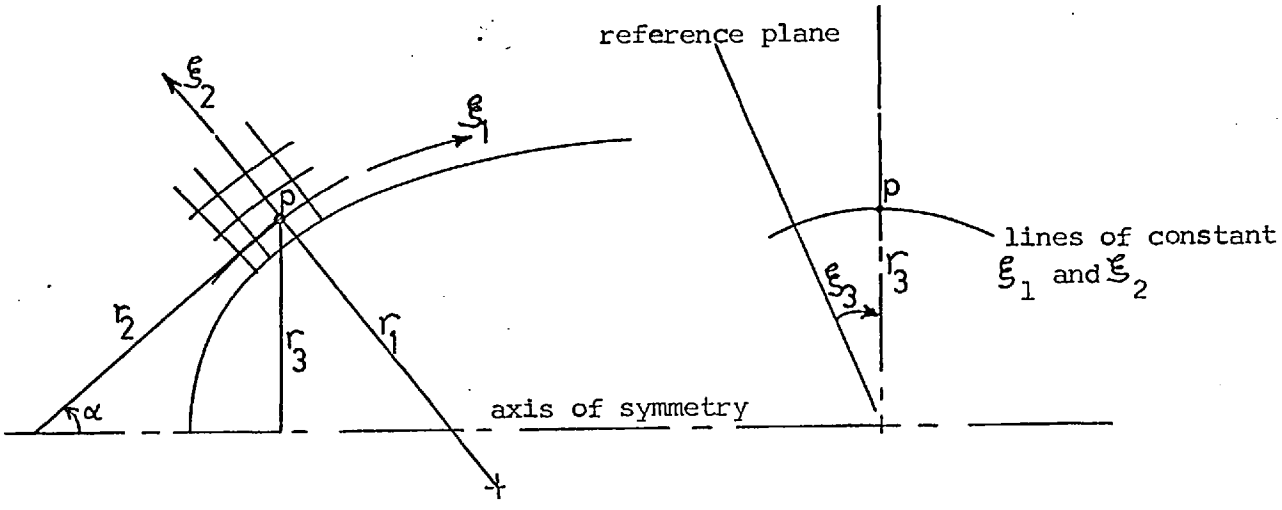

Fig. 2.1 General orthogonal coordinate system for axisymmetric flow

Geometrical Relationships

The radii of curvature can be related to α, ℓ_1 and ℓ_2 as follows:

$$\frac{1}{r_1} = -\frac{1}{\ell_1}\frac{\partial \alpha}{\partial \xi_1} = \frac{1}{\ell_1 \ell_2}\frac{\partial \ell_1}{\partial \xi_2} \quad , \qquad (2.2)$$

$$\frac{1}{r_2} = \frac{1}{\ell_2}\frac{\partial \alpha}{\partial \xi_2} = \frac{1}{\ell_1 \ell_2}\frac{\partial \ell_2}{\partial \xi_1} \qquad (2.3)$$

$$dr_3 = \ell_1 d\xi_1 \sin\alpha + \ell_2 d\xi_2 \cos\alpha \qquad (2.4)$$

2.3 General Forms of the Conservation Equations

The general elliptic forms of the conservation equation for mass, momentum, stagnation enthalpy and chemical species which describe the present axisymmetrical flows are now presented in vectorial notation, see for example Gosman and co-workers (1969). All symbols are defined in the nomenclature. The continuity equation:

$$\text{div } \mathbf{G} = 0. \qquad (2.5)$$

The momentum equation for each of the coordinate directions:

$$\mathbf{G}\cdot \text{grad } V_1 = \text{div } \mathbf{T}_1 - i_1 \cdot \text{grad} p + (V_2 G - T_2)\cdot \text{grad}\alpha + \frac{V_3 G_3 - T_{3,3}}{\ell_3}\sin\alpha \qquad (2.6)$$

$$\mathbf{G}\cdot \text{grad } V_2 = \text{div } \mathbf{T}_2 - i_2 \cdot \text{grad} p - (V_1 G - T_1)\cdot \text{grad}\alpha + \frac{V_3 G_3 - T_{3,3}}{\ell_3}\cos\alpha \qquad (2.7)$$

$$\mathbf{G}\cdot \text{grad}(\ell_3 V_3) = \text{div}(\ell_3 \mathbf{T}_3) \qquad (2.8)$$

The first Law of Thermodynamics:

$$\mathbf{G}\cdot \text{grad}\,\tilde{h} = -\text{div}\left[\mathbf{J}_h + \sum_{\text{all } j} h_j \mathbf{J}_j + \mathbf{J}_k - (V_1 \mathbf{T} + V_2 \mathbf{T} + V_3 \mathbf{T})\right] + \Phi_{rad} - \mathbf{G}\cdot g \qquad (2.9)$$

The equation for the conservation of chemical species j:

$$G \cdot \text{grad}\, m_j = -\,\text{div}\, J_j + R_j \quad ; \tag{2.10}$$

this is also the mass transfer equation when there is no reaction and only one chemical component present. All of these equations with the exception of the continuity equation have the common form:

$$G \cdot \text{grad}\, \phi = -\,\text{div}\, J_\phi + \Phi \quad , \tag{2.11}$$

where ϕ represents a dependent variable, and Φ a "source" term. The symbol $J\phi$ may stand for the diffusive fluxes of heat, mass and turbulence energy; for laminar flows they are given by the following gradient-type laws:

$$J_h = -\Gamma_h\, c_p\, \text{grad}\, T \quad , \tag{2.12}$$

$$J_j = -\Gamma_j\, \text{grad}\, m_j \quad , \tag{2.13}$$

$$\text{and} \quad J_k = -\Gamma_k\, \text{grad}\, k \quad . \tag{2.14}$$

In the case of the momentum equations, 2.6 to 2.8, the diffusive fluxes correspond to the shear stresses and are given the symbol T. For laminar flow see for example Aris (1962), the components of the shear stress vectors are:

$$T_{1,1} = \mu \left[\frac{2}{\ell_1} \frac{\partial V_1}{\partial \xi_1} + \frac{2V_2}{r_1} - \frac{2}{3}\,\text{div}\, V \right] \tag{2.15}$$

$$T_{2,2} = \mu \left[\frac{2}{\ell_2} \frac{\partial V_2}{\partial \xi_2} + \frac{2V_1}{r_2} - \frac{2}{3}\,\text{div}\, V \right] \tag{2.16}$$

$$T_{3,3} = \mu \left[\frac{2}{\ell_3} \left(V_1 \sin\alpha + V_2 \cos\alpha \right) - \frac{2}{3}\,\text{div}\, V \right] \tag{2.17}$$

$$T_{1,2} = T_{2,1} = \mu \left[\frac{\ell_1}{\ell_2} \frac{\partial}{\partial \xi_2} \left(\frac{V_1}{\ell_1} \right) + \frac{\ell_2}{\ell_1} \frac{\partial}{\partial \xi_1} \left(\frac{V_2}{\ell_2} \right) \right] \qquad (2.18)$$

$$T_{1,3} = T_{3,1} = \mu \left[\frac{\ell_3}{\ell_1} \frac{\partial}{\partial \xi_1} \left(\frac{V_3}{\ell_3} \right) \right] \qquad (2.19)$$

$$T_{2,3} = T_{3,2} = \mu \left[\frac{\ell_3}{\ell_2} \frac{\partial}{\partial \xi_2} \left(\frac{V_3}{\ell_3} \right) \right] \qquad (2.20)$$

In terms of the coordinates ξ_1, ξ_2 and ξ_3, the common form of the conservation laws, equation 2.11, expands to give:

$$\frac{G_1}{\ell_1} \frac{\partial \phi}{\partial \xi_1} + \frac{G_2}{\ell_2} \frac{\partial \phi}{\partial \xi_2} = -\frac{1}{\ell_1 \ell_2 \ell_3} \left[\frac{\partial}{\partial \xi_1} \left(\ell_2 \ell_3 J_{\phi,1} \right) + \frac{\partial}{\partial \xi_2} \left(\ell_1 \ell_3 J_{\phi,2} \right) \right] + \Phi \qquad (2.21)$$

2.4 Parabolic Forms of the Governing Equations

2.4-1 Requirement for a Boundary-Layer Flow

The general elliptic conservation equations presented in Section 2.3 may be considerably simplified for the special case of boundary-layer flow. Before making these simplifications it is important to clarify the requirements which must be fulfilled if a flow is to be of the boundary-layer kind.

Patankar and Spalding (1970) have given this particularly useful definition: "a boundary layer is a region of fluid where there is a single predominant direction of flow and where the diffusive fluxes are significant only at right angles to this direction". A consequence of this statement is that regions of recirculation must be absent.

2.4-2 The Boundary-Layer Equations

Direction-1 is chosen to be the predominant direction of flow. Diffusive fluxes are therefore negligible in that direction. The equations for the conservation of momentum in the cross-stream direction, equation 2.7, is normally ignored for non-swirling

flows unless the surface curvature is large. But for swirl velocities common in engineering practice, the last term in this equation is significant except for the special case of a rotating disc, when it is zero since cos $\alpha = 0$. The convection term is probably negligible in the absence of strong wave systems which may occur in compressible flows, and the diffusion term is certainly negligible, since V_2 is everywhere small. The following approximations are therefore valid:

$$(V_2 G - T_2) \cdot \text{grad}\,\alpha \approx \frac{V_2 G_1}{\ell_1} \frac{\partial \alpha}{\partial \xi_1} , \qquad (2.22)$$

$$G \cdot \text{grad}\, V_2 \approx 0 , \qquad (2.23)$$

$$\text{and} \quad (V_1 G - T_1) \cdot \text{grad}\,\alpha \approx \frac{V_1 G_1}{\ell_1} \frac{\partial \alpha}{\partial \xi_1} . \qquad (2.24)$$

With these considerations equations 2.5 through to 2.10 become:

$$\frac{\partial}{\partial \xi_1}(\ell_2 \ell_3 G_1) + \frac{\partial}{\partial \xi_2}(\ell_1 \ell_3 G_2) = 0 , \qquad (2.25)$$

$$\frac{G_1}{\ell_1}\frac{\partial V_1}{\partial \xi_1} + \frac{G_2}{\ell_2}\frac{\partial V_1}{\partial \xi_2} = \frac{1}{\ell_1 \ell_2 \ell_3}\frac{\partial}{\partial \xi_2}\left[\frac{\ell_1 \ell_3}{\ell_2}\Gamma_{1,2}\frac{\partial V_1}{\partial \xi_2}\right] - \frac{1}{\ell_1}\frac{\partial p}{\partial \xi_1} + \frac{V_2 G_1}{\ell_1}\frac{\partial \alpha}{\partial \xi_1} + \frac{V_3 G_3}{\ell_3}\sin\alpha , \qquad (2.26)$$

$$0 = -\frac{1}{\ell_2}\frac{\partial p}{\partial \xi_2} - \frac{V_1 G_1}{\ell_1}\frac{\partial \alpha}{\partial \xi_1} + \frac{V_3 G_3}{\ell_3}\cos\alpha , \qquad (2.27)$$

$$\frac{G_1}{\ell_1}\frac{\partial(\ell_3 V_3)}{\partial \xi_1} + \frac{G_2}{\ell_2}\frac{\partial(\ell_3 V_3)}{\partial \xi_2} = \frac{1}{\ell_1 \ell_2 \ell_3}\frac{\partial}{\partial \xi_2}\left[\frac{\ell_1 \ell_3}{\ell_2}\Gamma_{3,2}\frac{\partial(\ell_3 V_3)}{\partial \xi_2} - 2\Gamma_{3,2}\ell_1 \ell_3 V_3 \cos\alpha\right], \qquad (2.28)$$

$$\frac{G_1}{\ell_1}\frac{\partial \tilde{h}}{\partial \xi_1} + \frac{G_2}{\ell_2}\frac{\partial \tilde{h}}{\partial \xi_2} = \frac{1}{\ell_1 \ell_2 \ell_3}\frac{\partial}{\partial \xi_2}\left[\ell_1 \ell_3 \left(J_h + \sum_{all\,j} h_j \cdot J_j - V_1 T_{1,2} - V_3 T_{3,2}\right)\right] . \qquad (2.29)$$

$$\frac{G_1}{\ell_1}\frac{\partial m_j}{\partial \xi_1} + \frac{G_2}{\ell_2}\frac{\partial m_j}{\partial \xi_2} = -\frac{1}{\ell_1\ell_2\ell_3}\frac{\partial}{\partial \xi_2}\left[\ell_1\ell_3 J_j\right] + R_j \ . \qquad (2.30)$$

Equations 2.26, .28, .29, and .30 possess the common form:

$$\frac{G_1}{\ell_1}\frac{\partial \phi}{\partial \xi_1} + \frac{G_2}{\ell_2}\frac{\partial \phi}{\partial \xi_2} = -\frac{1}{\ell_1\ell_2\ell_3}\frac{\partial}{\partial \xi_2}\left[\ell_1\ell_3 J_{\phi,2}\right] + \Phi \ , \qquad (2.31)$$

where $J_{\phi,2} \equiv -\Gamma_\phi \frac{\partial \phi}{\ell_2 \partial \xi_2}$, Γ_ϕ being the exchange coefficient appropriate to the variable ϕ; Φ is a source term.

The radiation, gravitational energy, and turbulence diffusion terms have been omitted from the stagnation enthalpy equation; they are not significant in the present work. For the circumferential momentum equation the choice of $\ell_3 V_3$ as the dependent variable preserves the common form of the equations. However, it is numerically simpler and more convenient to use another form of equation 2.28, (see Patankar and Spalding (1970)); by employing V_3/ℓ_3 instead of $\ell_3 V_3$ as the dependent variable on the right hand side, the diffusion and source term are replaced by a single diffusion term:

$$\frac{G_1}{\ell_1}\frac{\partial(\ell_3 V_3)}{\partial \xi_1} + \frac{G_2}{\ell_2}\frac{\partial(\ell_3 V_3)}{\partial \xi_2} = \frac{1}{\ell_1\ell_2\ell_3}\frac{\partial}{\partial \xi_2}\left[\frac{\ell_1\ell_3^3}{\ell_2}\Gamma_{2,3}\frac{\partial(V_3/\ell_3)}{\partial \xi_2}\right] \ . \qquad (2.32)$$

The Geometrical Angle α

The present work is confined to rotating cylinders, discs and cones, and swirling jets; for these geometries and flow situations the angle α in the general orthogonal coordinates system has a constant value. Then the metric coefficients ℓ_1 and ℓ_2 are both made equal to unity while the radii r_1 and r_2 extend to infinity; the coefficient $\ell_3 = r_3 = r$. The coordinates ξ_1, ξ_2, and ξ_3 become x_1, x_2, and x_3 which are respectively the streamwise, cross-stream and

circumferential directions. Equations 2.25 to 2.30 then take on the familiar forms:

$$\frac{\partial V_1}{\partial x_1} + \frac{V_1}{r}\sin\alpha + \frac{\partial V_2}{\partial x_2} + \frac{V_2}{r}\cos\alpha = 0 \qquad (2.33)$$

$$\rho V_1 \frac{\partial V_1}{\partial x_1} + \rho V_2 \frac{\partial V_1}{\partial x_2} = \frac{1}{r}\frac{\partial}{\partial x_2}\left[r\Gamma_{1,2}\frac{\partial V_1}{\partial x_2}\right] - \frac{\partial p}{\partial x_1} + \rho\frac{V_3^2}{r}\sin\alpha \qquad (2.34)$$

$$0 = -\frac{\partial p}{\partial x_2} + \rho\frac{V_3^2}{r}\cos\alpha \qquad (2.35)$$

$$\rho V_1 \frac{\partial (rV_3)}{\partial x_1} + \rho V_2 \frac{\partial (rV_3)}{\partial x_2} = \frac{1}{r}\frac{\partial}{\partial x_2}\left[r^3\Gamma_{2,3}\frac{\partial}{\partial x_2}\left(\frac{V_3}{r}\right)\right] \qquad (2.36)$$

$$\rho V_1 \frac{\partial \tilde{h}}{\partial x_1} + \rho V_2 \frac{\partial \tilde{h}}{\partial x_2} = \frac{1}{r}\frac{\partial}{\partial x_2}\left[r\left(\Gamma_h \frac{\partial h}{\partial x_2} + V_1 T_{1,2} + V_3 T_{2,3}\right)\right] \qquad (2.37)$$

$$\rho V_1 \frac{\partial m_j}{\partial x_1} + \rho V_2 \frac{\partial m_j}{\partial x_2} = \frac{1}{r}\frac{\partial}{\partial x_2}\left[r\Gamma_j \frac{\partial m_j}{\partial x_2}\right] . \qquad (2.38)$$

In the absence of chemical reaction the generation term R_j in equation 2.30 is zero, and the contribution $\sum h_j J_j$ of the chemical components to the stagnation enthalpy equation is neglected.

2.5 Closure of the Equations

The differential equations 2.26 to 2.30 do not alone specify the problem; two kinds of additional information are required: initial and boundary conditions for all the dependent variables (V_1, V_2, rV_3, $\tilde{h}$, m_j), and auxilliary equations allowing the shear stresses and diffusion fluxes to be computed in terms of the dependent variables at each point in the field. Boundary conditions and initial values are usually readily available and present no special problem. The shear stresses and diffusion fluxes are related to the dependent variables through the

quantities $\Gamma_{1,2}$, $\Gamma_{2,3}$, Γ_h, and Γ_j which have to be specified either from known properties of the fluid or by theoretical proposals, or through empirical information. The provision of this additional information for $\Gamma_{1,2}$, $\Gamma_{2,3}$, Γ_h and Γ_j is referred to as 'the closure of the equations'.

For laminar flows $\Gamma_{1,2}$ and $\Gamma_{2,3}$ represent the molecular viscosity μ_ℓ, while Γ_h and Γ_j are equal to the μ_ℓ/σ_h and μ_ℓ/σ_j respectively; the Prandtl and Schmidt numbers, σ_h and σ_j, are well determined properties of the fluid. The molecular viscosity μ_ℓ is itself a real property of the fluid, present whether the fluid is at rest or moving.

For turbulent flows, $\Gamma_{1,2}$ and $\Gamma_{2,3}$ represent the 'effective viscosities' $\mu_{1,2}$ and $\mu_{2,3}$, in the main direction and in the circumferential direction of flow. These effective viscosities, however, only arise when the fluid is in motion, and are distinctly not physical properties of the fluid. They are nonetheless a useful concept to relate the turbulent stresses to the time-average velocity gradients in a flow field. Analogous to laminar flow (see equations 2.18 and 2.20), they have been defined as:

$$\mu_{1,2} \equiv T_{1,2} \Big/ \frac{\partial V_1}{\partial x_2} \quad , \tag{2.39}$$

$$\text{and} \quad \mu_{2,3} \equiv T_{2,3} \Big/ r\,\frac{\partial (V_3/r)}{\partial x_2} \quad ; \tag{2.40}$$

the stresses $T_{1,2}$ and $T_{2,3}$ correspond to the Reynolds-stress components $-\rho\overline{v_1 v_2}$ and $-\rho\overline{v_2 v_3}$ respectively, see for example Hinze (1959) or Schlichting (1968).

As opposed to non-swirling two-dimensional flows for which only the Reynolds stress $-\rho\overline{v_1 v_2}$ is dominant since the velocity

component V_3 is everywhere zero, axisymmetrical swirling boundary layers present special difficulties because both stress components $-\rho\overline{V_1V_2}$ and $-\rho\overline{V_2V_3}$ are important. In general, $-\rho\overline{V_1V_2} \Big/ \frac{\partial V_1}{\partial x_2}$ will not be equal to $-\rho\overline{V_2V_3} \Big/ r\frac{\partial (V_3/r)}{\partial x_2}$; that is, the effective viscosities $\mu_{1,2}$ and $\mu_{2,3}$ must be considered to possess different values at a given location in the flow. Several hypotheses relating $\mu_{1,2}$ and $\mu_{2,3}$ to other variables of the flow are described later in Chapters 4, 5, 6 and 7.

The turbulent mixing motion also increases the transfer of heat and mass in flows associated with temperature or concentration gradients; consequently further assumptions are also needed concerning the effective value of the transport coefficients Γ_h and Γ_j for heat and mass. These assumptions are discussed in Chapter 8.

However, before the turbulent transport hypotheses are considered, it is necessary to test the purely numerical accuracy of the prediction procedure. The next chapter, therefore, briefly describes the Patankar and Spalding (1970) finite-difference procedure and compares predictions of some laminar flows with established accurate analytical solutions obtained by other methods.

CHAPTER 3

THE PREDICTION PROCEDURE

3.1 Introduction

The choice of the Patankar and Spalding (1970) finite-difference procedure to solve the present class of swirling boundary layers was governed by its proven successes for two-dimensional non-swirling flows. The method is easy to use, numerically stable, and very economical of computer time. Its main features are summarised in Section 3.2.

In Section 3.3 the numerical accuracy of the solution procedure is tested by comparing predictions with exact analytical solutions for the case of a disc rotating in a uniform axial stream under laminar flow conditions. The two asymptotic cases: a disc rotating in stagnant surroundings and an axisymmetrical stagnation flow with the disc stationary, are also considered. The hydrodynamic and heat transfer predictions are shown to be in excellent agreement with the analytical results.

3.2 Outline of the Solution Procedure

The boundary-layer calculation method of Patankar and Spalding (1970) is well documented and it is only necessary to outline its main features here.

The governing partial differential equations for the transfer of momentum heat and mass in swirling boundary layers have already been presented, they are equations 2.25 to 2.30 of Section 2.4-2. It was demonstrated there that these equations all possess the common form, repeated here for convenience:

$$\frac{G_1}{\ell_1}\frac{\partial \phi}{\partial \xi_1} + \frac{G_2}{\ell_2}\frac{\partial \phi}{\partial \xi_2} = \frac{1}{\ell_1 \ell_2 \ell_3}\frac{\partial}{\partial \xi_2}\left[\frac{\ell_1 \ell_3}{\ell_2}\Gamma_\phi \frac{\partial \phi}{\partial \xi_2}\right] + \Phi \quad . \qquad (3.1)$$

This similarity of the equations allows a common numerical treatment of the variables V_1, $\tilde{h}$ and m_j, with minor modifications for V_3; only the exchange coefficient Γ_ϕ and the source term Φ are different for each dependent variable.

3.2-1 Cross-stream Variable

The central feature of the Patankar and Spalding method is the novel specification of the cross stream ξ_2 coordinate. The coordinate is a dimensionless stream function ω defined as:

$$\xi_2 = \omega \equiv \frac{\psi - \psi_I}{\psi_E - \psi_I} \quad . \tag{3.2}$$

The quantities ψ_I and ψ_E are the values of the stream function ψ at the interior and exterior edges of the boundary layer; they are functions of ξ_1 and are chosen so that the main variations in the dependent variables lie at ψ values between ψ_I and ψ_E. Thus, regardless of the width of the flow under consideration, the coordinate ω always lie between zero and unity. This practice confines the finite-difference grid to the region of flow where the changes in the values of the dependent variables are relatively large and results in great economy of computer time. Changes of the width of the finite-difference grid, hence changes in the thickness of the boundary layer, are determined from the rate of entrainment of fluid from the surroundings into the boundary layer.

3.2-2 The Common Differential Equation

The stream function ψ is defined by:

$$G_1 \equiv \frac{1}{r\ell_2} \frac{\partial \psi}{\partial \xi_2} \text{ and } G_2 \equiv -\frac{1}{r\ell_1} \frac{\partial \psi}{\partial \xi_1} \quad . \tag{3.3}$$

These relations together with equation 3.2 result in the following expressions for ℓ_2 and G_2:

$$\ell_2 = \frac{\Psi_E - \Psi_I}{rG_1} \quad , \tag{3.4}$$

and

$$G_2 = -\frac{1}{r\ell_1}\left[(1-\omega)\frac{d\Psi_I}{d\xi_1} + \omega\frac{d\Psi_E}{d\xi_1}\right] \quad . \tag{3.5}$$

The remaining metric coefficient ℓ_1, see equation 2.2, can be determined from the geometry of the general orthogonal coordinate system as:

$$\ell_1 = -\int \frac{\partial\alpha}{\partial\xi_1}\cdot\ell_2\,\partial\omega \quad . \tag{3.6}$$

This relation allows ℓ_1 to be determined as a function of the cross-stream coordinate when the streamlines are highly curved.

For the class of swirling boundary-layers considered in the present work curvature effects were not important and therefore ℓ_1 was given the value of unity. The coordinate ξ_1 becomes identical with x, the streamwise coordinate, and the difference between x as measured along the inner and outer edges of the boundary layer is ignored. Substituting the values of ℓ_2 and G_2 into the common differential equation 3.1 yields:

$$\frac{\partial\phi}{\partial x} - \frac{1}{\psi_E-\psi_I}\left[(1-\omega)\frac{\partial\psi_I}{\partial x} + \omega\frac{\partial\psi_E}{\partial x}\right]\frac{\partial\phi}{\partial\omega} = \frac{1}{(\psi_E-\psi_I)^2}\frac{\partial}{\partial\omega}\left[r^2G_1\Gamma_\phi\frac{\partial\phi}{\partial\omega}\right] + \frac{\Phi}{G_1} \quad . \tag{3.7}$$

This equation is the starting point of the finite-difference procedure. The meanings of the source term Φ can be deduced by comparing equation 2.34 to 2.38 for the transport of momentum, stagnation enthalpy and mass, with equation 3.7. The source terms are given in the following table:

When ϕ represents:	The expression for Φ is:
V_1	$-\frac{\partial P}{\partial x} + \frac{V_3 G_3}{r} \sin\alpha$
rV_3	0 , the diffusion term is however different
$\tilde{h}$	$\frac{G_1}{(\psi_E - \psi_I)^2} \frac{\partial}{\partial \omega} \left[r^2 G_1 \left\{ V_1 T_{1,2} + V_3 T_{2,3} - \frac{\Gamma_h}{2} \left(\frac{\partial V_1^2}{\partial \omega} + \frac{\partial V_3^2}{\partial \omega} \right) \right\} \right]$
m_j	0

Table 3.1 Significance of the source term Φ

3.2-3 Finite-difference Form of the Common Equation

The finite-difference equivalent of equation 3.7 is obtained by means of a micro-integral method. Each term of the equation is integrated over a small control volume around each node bounded by adjacent constant-x and constant-ω lines. On the assumption that ϕ varies linearly with ω between grid nodes and stepwise in the x-direction, each term appears as an integrated average over the small control volume. The use of the micro-integral method ensures that the integral forms of the conservation equations are satisfied over any part of the boundary layer. The result of the integration yields the following finite-difference equation:

$$\phi_i = A\phi_{i+1} + B\phi_{i-1} + C \quad , \qquad (3.8)$$

where the subscript i designates a particular grid node. A, B and C are functions of the cross-stream grid spacing, and the upstream values of ϕ and the coefficients of the differential equation 3.7. The set of equations 3.8 are solved to yield the values of the dependent variables in turn at each successive downstream grid location using a simple recurrence formula. In this way the solution progresses downstream in a marching fashion. The complete derivation of the finite-difference equations have been published by Patankar and Spalding (1970).

3.2-4 The Streamwise Pressure Gradient

The pressure gradient term which appears in the streamwise momentum equation 2.34 is determined at any cross-stream location, ω_i say, from the cross-stream momentum equation 2.35 integrated from the edge of the layer to ω_i, and differentiated with respect to x:

$$\left(\frac{\partial p}{\partial x}\right)_i = \left(\frac{\partial p}{\partial x}\right)_I + \frac{\partial}{\partial x}\int_I^{\omega_i} (\psi_E - \psi_I)\frac{\rho V_3^2}{r^2 G_1}\cos\alpha \; d\omega \quad . \qquad (3.9)$$

A similar result can be derived if $\left(\frac{\partial P}{\partial x}\right)_E$ instead of $\left(\frac{\partial P}{\partial x}\right)_I$ is known. The boundary values of the pressure gradients are determined from potential flow analyses.

3.2-5 Wall boundary layers

In the region near to a stationary or moving wall, the gradients of velocity and, if there is heat and mass transfer, of temperature and concentration are large. These steep variations are much more pronounced for turbulent flows than for laminar flows. Consequently, many grid lines must normally be deployed in such regions in order to obtain acceptable accuracy with a finite-difference procedure. Patankar and Spalding have, however, succeeded in eliminating this disadvantage by the use of a special practice.

Very close to solid boundaries convection is small since the velocities are low. When the convection terms are neglected the partial differential equations reduce to a set of ordinary ones, often referred to as Couette-flow equations. These equations are solved, employing known fluid properties for laminar flow and plausible relations for the effective transport coefficients for turbulent flow, to give algebraic relationships for the drag coefficient and the Stanton and Sherwood numbers in terms of the local properties of the flow; namely,

the Reynolds number, and the mass injection and pressure gradient parameters. These algebraic expressions, usually called wall functions, provide inner boundary conditions to which the finite-difference computations, now confined to the remainder of the boundary layer, are matched. The wall functions used in the present study are discussed in Appendix 3.

3.3 Numerical Accuracy of the Solution Procedure

Before the solution procedure is applied to turbulent flows for which assumptions are required for the transport properties, it is necessary to establish its numerical accuracy. This is accomplished by comparing the predictions with available exact analytical solutions. The test cases chosen are the hydrodynamic predictions of Hannah (1947) and the heat transfer results of several workers for a disc rotating in a uniform axial stream. All these reference solutions are for the laminar flow of fluids of uniform density and viscosity.

3.3-1 The Problem Considered

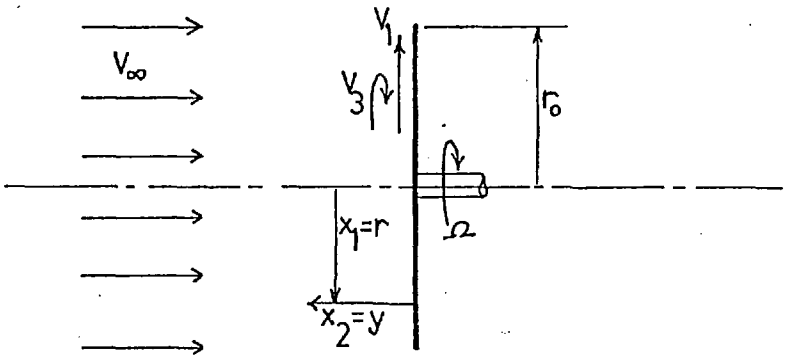

Fig. 3.1 Disc rotating in a uniform axial stream

The problem under consideration is illustrated in Fig. 3.1; the general coordinate system described in Section 2.2 reduces to cylindrical coordinates with the angle α equal to 90 degrees, x_1 equivalent to the radius r, and x_2 the normal distance y from the disc's surface. The disc rotates at a constant angular speed Ω in a free stream of uniform velocity V_∞. The boundary conditions of the problem are:

$$V_1(r,o) = o\ ,\quad V_1(r,\infty) = ar,$$
$$V_3(r,o) = \Omega r,\quad V_3(r,\infty) = o,$$
$$T(r,o) = Ar^m,\quad T(r,\infty) = o.$$

The free stream velocity boundary condition for the radial velocity V_1 is obtained from the potential flow solution, see for example Homann (1936); the constant a is equal to $2V_\infty/\pi r_o$, where r_o is the radial dimension of the disc. The surface temperature of the disc is assumed to follow a power-law distribution, for which similarity solutions exist, to facilitate comparison with the present predictions; the symbol A represents a constant.

The momentum and energy equations (2.34, 2.36 and 2.37) were solved for three flow conditions:

(1) the disc rotating in stagnant surroundings, i.e., $\Omega/a = \infty$,

(2) the disc rotating in an axial stream with $\Omega/a = 2$, and

(3) the axisymmetrical stagnation flow without rotation of the disc, i.e. $\Omega/a = 0$.

Initial Profiles

The circumferential velocity was assumed to decrease linearly with the distance y from the disc surface; the radial velocity was presumed to increase to a maximum and then decrease linearly with y:

$$V_3 = (1 - y/\delta)\ \Omega r,$$
$$V_1 = \Omega r\ y/\delta, \qquad 0 < y/\delta < 0.2$$
$$V_1 = .25\ \Omega r\ (1 - y/\delta),\ 0.2 \leqslant y/\delta \leqslant 1.0$$

The boundary layer thickness δ, Schlichting (1968), is calculated from:

$$\delta = 4.43\ (\nu/\Omega)^{\frac{1}{2}}\ .$$

The initial cross-stream profile temperature was assumed linear in y:

$$(T_{r,y} - T_\infty) = (1 - \frac{y}{\delta})\ (T_{r,o} - T_\infty)$$

Grid and Step Size

The numerical accuracy of the solution depends on the distribution of the cross-stream grid nodes, and on the size of the step chosen to advance the solution downstream. Twentyone grid nodes, concentrated near the disc surface, were found to give hydrodynamic predictions in good agreement with the exact solutions; the results are presented in Section 3.3-2 below. The step size was equal to 5% of the boundary-layer thickness. Marginally improved accuracy was obtained, at the expense of a large increase in computing time, by employing smaller steps and a larger number of grid nodes in the region of steep gradients, near the surface.

For the case of heat transfer for fluids of large Prandtl number, 100 in the case tested, the thermal boundary layer lies well within the velocity boundary layer, in a very thin region near the surface. Thirty grid nodes were then used, twenty covering the thermal layer and concentrated near the surface.

3.3-2 Hydrodynamic Predictions

The profiles of V_1 and V_3 computed by means of the finite-difference procedure are in excellent agreement (less than 0.1% maximum difference) with the analytical results of Hannah (1947) as revealed by Fig. 3.3.

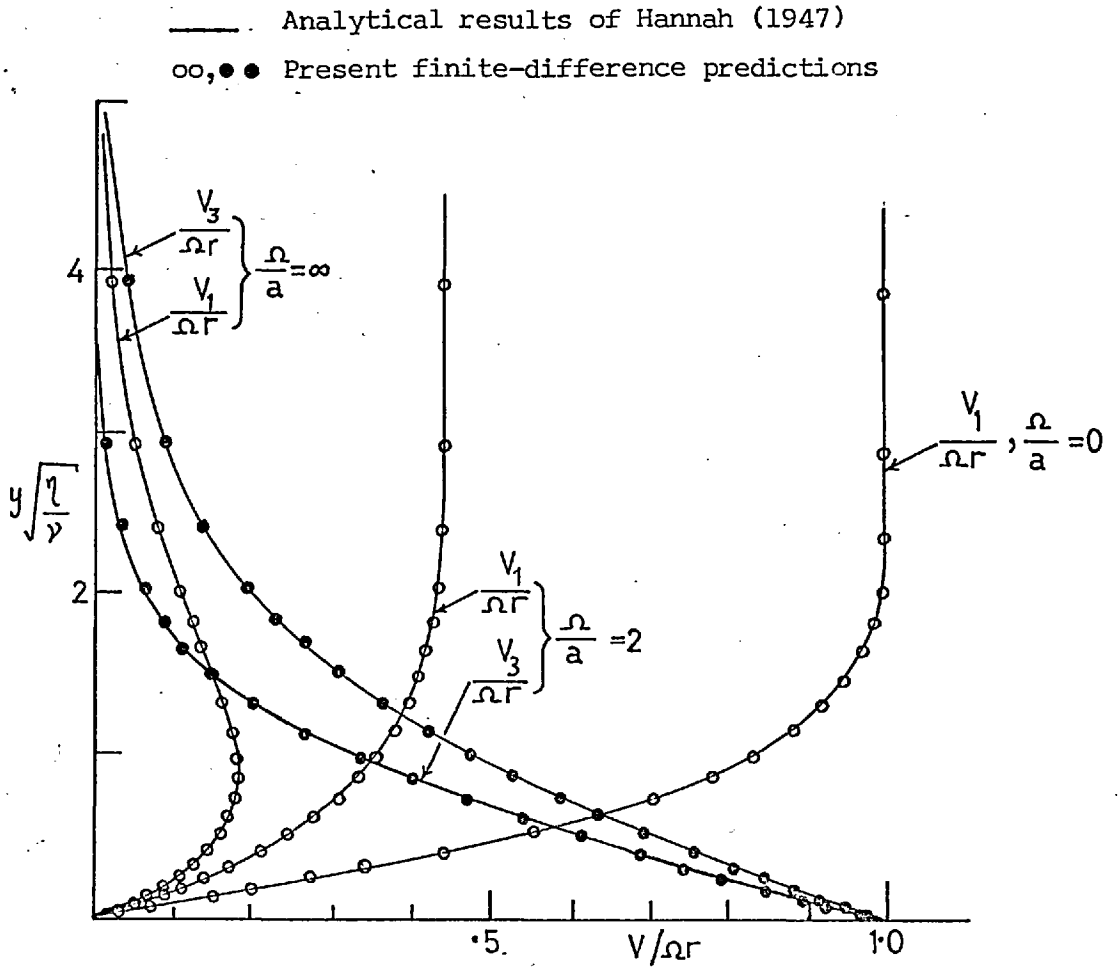

Fig. 3.3 Velocity profiles for three values of Ω/a

The drag coefficient defined as $c_f = -\left(\frac{\partial V_3}{\partial y}\right)_{y=0} \Big/ \Omega r\sqrt{\frac{\eta}{\nu}}$,

with $\eta \equiv \sqrt{a^2 + \Omega^2}$, is compared with the exact results of Hannah in Fig. 3.4.

Ω/a		c_f	
		Hannah	Present Predictions
0	Stagnation flow	1.075	1.075
2		0.800	0.801
∞	free rotating disc	0.616	0.616

Fig. 3.4 Circumferential drag coefficient

For the case of a free rotating disc Cochran (1934) also reported a value of c_f equal to 0.616. It should be remarked that, since the analytical solutions pertain to the elliptic form of the governing equations, the closeness of the present predictions to them supports the validity of the boundary-layer assumptions for the swirl flow on a rotating disc.

3.3-3 Heat Transfer Predictions

The energy equation 2.37 was solved for the three flow conditions considered in the preceeding section for an isothermal and a quadratic surface temperature distribution; that is, the index m=0 and 2. As was the case for the velocity profiles, the predicted temperature profiles were in excellent agreement with the analytical results. The local Nusselt number, defined as: $Nu = -\left(\frac{\partial T}{\partial y}\right)_{y=0} \left(\frac{\nu}{\eta}\right)^{\frac{1}{2}} \Big/ \left(T_{y=0} - T_{y=\infty}\right)$, is proportional to the Reynolds number $\Omega r^2/\nu$ to the 0.5 power. In Fig. 3.5 the predicted constant of proportionality is compared with the analytical results of several workers.

m	Pr	Ω/a			Analytical predictions of:
		0	2	∞	
0	1	.762	.557	.396	(1,2)*; (3,4) for Ω/a =∞.
		.762	.558	.397	Present predictions.
2	1	1.075	.800	.616	(1,2); (5) for Ω/a =∞ only.
		1.075	.801	.615	Present predictions.
2	100	5.19	4.18	3.79	(1)
		5.32	4.21	3.74	(2)
		5.35	4.24	3.74	Present predictions.

Fig. 3.5 Nusselt number/Reynolds number$^{0.5}$

---

* (1) Tien and Tsuji (1964), (2) Nabuchi, Tanaka and Sakakibara (1967), (3) Hartnett and Deland (1961), (4) Sparrow and Gregg (1959), (5) Hayday (1965).

For Prandtl numbers of order unity the discrepancy between the present predictions and the conventional analytical results is less than 0.25%.

3.4 Conclusions

The finite-difference procedure of Patankar and Spalding has been shown to be an accurate method for solving the partial differential equations governing swirling flows of the boundary-layer class. For the laminar flow test cases considered, with the grid distribution and step-size employed, the circumferential drag was predicted to within 0.1%, and the Nusselt number to within 0.25% of established analytical results.

In addition to its numerical accuracy, the procedure is efficient in terms of computing time. The solution of three equations (two momentum and energy), for a grid of 20 nodes, progressed through 80 steps in 1 second on a CDC6600 computer.

In the following four chapters attention is focussed on the physical problem. The Patankar and Spalding procedure is combined with various models of turbulence and applied to diverse turbulent flow problems. Predictions are compared with experimental data to assess the validity of the assumed turbulence models. Chapter 4 covers a mixing-length model leading to an isotropic effective viscosity formulation. Chapters 5, 6 and 7 deal respectively with a 'two-equation' model, a mixing-length based approach, and an algebraic stress model, all three resulting in formulations for the two effective viscosity components.

CHAPTER 4

AN ISOTROPIC VISCOSITY MIXING-LENGTH BASED MODEL OF TURBULENCE

4.1 Introduction

Prandtl's (1925) mixing-length hypothesis is one of the earliest proposed models of turbulence and it has been widely used to compute turbulent boundary layers without swirl. Considering the extreme simiplicity of the mixing-length model and its consequent meagre physical justification the results of these computations are surprisingly accurate; see for example Schlichting (1968) and Patankar and Spalding (1970). Tolerable predictions are also obtained for boundary layers for which the mixing-length concept is apparently fundamentally unsuited, boundary layers in strong adverse pressure gradients for example; see Ng, Patankar and Spalding (1968). However, the mixing-length model suffers from a number of drawbacks; it presumes that the generation and dissipation of turbulence energy are in balance and therefore excludes any influence of convection and diffusion of turbulence energy; furthermore it implies zero turbulent exchange coefficients in regions of zero velocity gradients. These limitations are obviously a direct consequence of the over-simplification of the turbulence which is assumed to be dependent on the mean velocity field, and only one other parameter, the mixing length.

Although the physical picture based upon the mixing-length concept is not correct in all details, the mixing-length model is, because of its inherent simplicity, still an attractive and useful proposition for the design engineer. For the case of swirling flows the validity of the mixing-length formulation has not been extensively explored. The present work therefore undertakes a systematic evaluation to establish the validity of the mixing-length concept when applied to the prediction of swirling boundary layers.

In Section 4.2, a viscosity formula is deduced, in terms of a mixing-length and gradients of mean velocity, from a transport equation for the kinetic energy of turbulence. The viscosity ratio $\mu_{1,2}/\mu_{2,3}$, which appears in this formula, is assumed equal to unity; that is, the viscosity is presumed to be isotropic (a scalar quantity). This is followed by the specification of the mixing-length distribution.

Comparisons are made between predictions and experimental data in Section 4.3, where the isotropic viscosity model is employed to predict the following flow configurations:

1. A disc rotating in stagnant surroundings,
2. A cone rotating in stagnant surroundings,
3. A cylinder rotating in a uniform axially-directed stream,
4. The radial outflow between a rotating and a stationary disc.

For each flow configuration and for several conditions, the optimum values of the empirical constants χ and λ in the mixing-length formulation are deduced from the comparisons of predictions with experimental data.

An overall assessment of the usefulness of the isotropic viscosity mixing-length based model of turbulence is made in Section 4.4.

4.2 A Viscosity Formulation

Until recently most authors have simply used reasonable or arbitrary extensions of the mixing-length hypothesis from two-dimensional non-swirling to swirling flows; see for example, Bayley and Owen (1969), Siddhartha (1971), Lilley (1973). The present approach to obtain a mixing-length formula is based on an analysis of the transport equation for k, the kinetic energy of turbulence. This equation, derived later in Chapter 7, comprises terms which represent four distinct physical processes: the convection, diffusion, production and dissipation of turbulence energy.

If a local balance between the production and dissipation of k is supposed (sometimes termed 'local-equilibrium'), equation 7.20 reduces to:

$$\underbrace{-\overline{v_1 v_2}\,\frac{\partial V_1}{\partial x_2} \;\; -\overline{v_2 v_3}\; r\,\frac{\partial (V_3/r)}{\partial x_2}}_{\text{Production}} \;=\; \underbrace{\epsilon}_{\text{Dissipation}} \quad . \qquad (4.1)$$

In terms of the turbulent viscosities defined previously by equations 2.39 and 2.40, equation 4.1 can be expressed as:

$$\mu_{1,2}\left(\frac{\partial V_1}{\partial x_2}\right)^2 + \mu_{2,3}\left(r\,\frac{\partial (V_3/r)}{\partial x_2}\right)^2 = \rho\epsilon \quad . \qquad (4.2)$$

Now, dimensional considerations reveal that a characteristic value of viscosity is proportional to $\rho \ell^{\frac{4}{3}} \epsilon^{\frac{1}{3}}$, where ℓ has the dimensions of a length-scale. If it is assumed that the constant of proportionality, although directionally dependent, has a unique value for each direction, then $\mu_{1,2}$ can be arbitrarily expressed as:

$$\mu_{1,2} = \rho \ell_m^{\frac{4}{3}} \epsilon^{\frac{1}{3}} \quad , \qquad (4.3)$$

where ℓ_m is a mixing-length referenced to the $\mu_{1,2}$ viscosity. Equations 4.2 and 4.3 can then be combined to produce the final form of the mixing-length formulation:

$$\mu_{1,2} = \rho \ell_m^2 \left[\left(\frac{\partial V_1}{\partial x_2}\right)^2 + \frac{1}{\sigma_{2,3}}\left(r\,\frac{\partial (V_3/r)}{\partial x_2}\right)^2\right]^{\frac{1}{2}} \quad . \qquad (4.4)$$

The viscosity ratio $\sigma_{2,3}$ has been introduced for convenience; it is defined by:

$$\sigma_{2,3} \equiv \mu_{1,2} \Big/ \mu_{2,3} \quad . \qquad (4.5)$$

This simple mixing-length formulation can be used for the prediction of swirling flows if the functional relationships for ℓ_m and $\sigma_{2,3}$ can be determined.

4.2-1 An Isotropic Viscosity Model

The basic assumption of this model in terms of the Reynolds stresses is that:

$$-\overline{v_1 v_2}/-\overline{v_2 v_3} = \frac{\partial V_1}{\partial x_2} \Big/ r \frac{\partial (V_3/r)}{\partial x_2} \quad . \tag{4.6}$$

The mixing-length expression, equation 4.4, then simply reduces to:

$$\mu_{1,2} = \mu_{2,3} = \rho \ell_m^2 \left[\left(\frac{\partial V_1}{\partial x_2} \right)^2 + \left(r \frac{\partial (V_3/r)}{\partial x_2} \right)^2 \right]^{\frac{1}{2}} , \tag{4.7}$$

where the viscosity ratio $\sigma_{2,3}$ is equal to unity. This formulation retains the basic simplicity of the mixing-length hypothesis since no new empirical constants are introduced.

4.2-2 The Mixing-length Distribution

Close to a wall, but outside the sublayer, all evidence indicates that the mixing-length ℓ_m is proportional to the normal distance y from the surface. Very near the wall ℓ_m is presumed to diminish in accordance with Van Driest's (1956) expression:

$$\ell_m = \kappa y \left[1 - \exp(-y\sqrt{\rho\tau}/A\mu_\ell) \right] \quad . \tag{4.8}$$

This formulation adequately describes the main characteristics of plane two-dimensional incompressible boundary-layers, and allows the field of calculation to be extended to the laminar sublayer. For two-dimensional non-swirling flows the constant A is about 26, and τ is the local value of the shear stress. However, it is not evident how the damping effect in the sublayer should be incorporated into a formulation for two-dimensional swirling flows or three-dimensional boundary layers, since in this case it is likely to influence the rate of change of the direction of the shear stress vector as well as the rate of change of its magnitude.

It is presumed, for the present isotropic viscosity model, that the appropriate form of the Van Driest expression for swirling

boundary layers is:

$$\ell_m = \kappa y \left[1 - \exp\left(-y\sqrt{\rho\tau_R}/A\mu_\ell\right)\right] \quad . \qquad (4.9)$$

The local value of the shear-stress vector τ_R appears in the damping term; the constant A is, based on non-swirling flow work, and some swirling-flow work, Bayley and Owen (1969), Cooper (1971), ascribed the value 26.

Further from the wall, in the wake portion of the boundary layer, ℓ_m is found to scale approximately with the thickness δ of the boundary layer, see Escudier (1965), Schlichting (1968). It is therefore assumed that:

$$\ell_m = \lambda\delta \ , \ \lambda\delta/\kappa < y \lesssim \delta \ . \qquad (4.10)$$

The mixing-length constants κ and λ are adjustable ones to be determined from experimental information.

4.3 Comparisons of Predictions with Experimental Data

4.3-1 Disc in Stagnant Surroundings

The flow induced by a disc rotating in a stagnant medium, Fig. 4.1, is the simplest flow in the class of swirling boundary-layers near walls. The flow in the central region of the disc is laminar, and undergoes transition to turbulent flow of some radial distance from the centre.

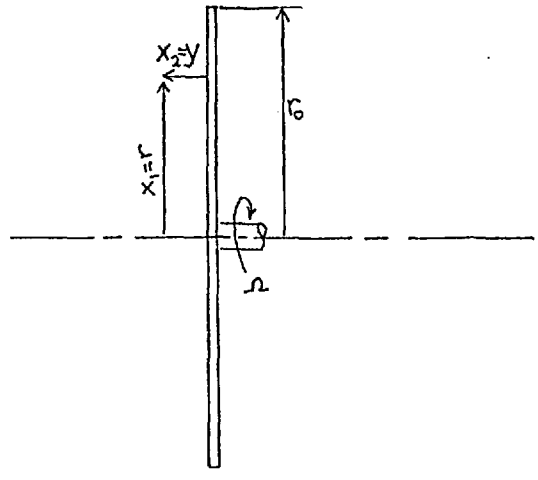

Fig. 4.1 Disc rotating in stagnant surroundings

The present computations were commenced in the region of laminar flow. The turbulent transport formulae 4.7, 4.9 and 4.10 were introduced at the radial location where the transition Reynolds number Re_{tran} is first attained; a value in the range $1.8X10^5$ and $2.8X10^5$ was assumed, depending on experimental evidence. No claim is made of physical realism for this simple transition procedure; the predictions in the vicinity of Re_{tran} clearly lack significance.

(a) Average Drag Coefficient

In Fig. 4.2 the predictions of average drag coefficient $\bar{c}_f$ are plotted against Reynolds number Re, and compared with the results of three experiments. The three panels (a), (b) and (c) display respectively the influence on the predictions of varying κ, λ, and Re_{tran}. The effect of varying λ is rather less than that for comparable variations in κ; the near-wall turbulence has a much larger influence on the wall drag than the outer layer turbulence. Varying the transition Reynolds number in the range $1.8X10^5$ to $2.8X10^5$ only influences the drag predictions in the area where the experimental data exhibit the typical scatter associated with transition from laminar to turbulent flow.

The values of κ and λ which allow the best fit with the data are 0.42 and 0.085 respectively. These values agree with those which very often provide good prediction of plane, non-swirling boundary layers. They contrast with the values 0.50 and 0.13 which have been found to give the best results for the axially symmetrical wall jet, Spalding (1967), a non-swirling flow which is geometrically comparable with the present flow. It is evident that the dominance of the swirl component of velocity and the absence of a strong axial flow directed towards the disc at its centre are sufficient to cause the present flow to be more akin to a plane one. The mean transition

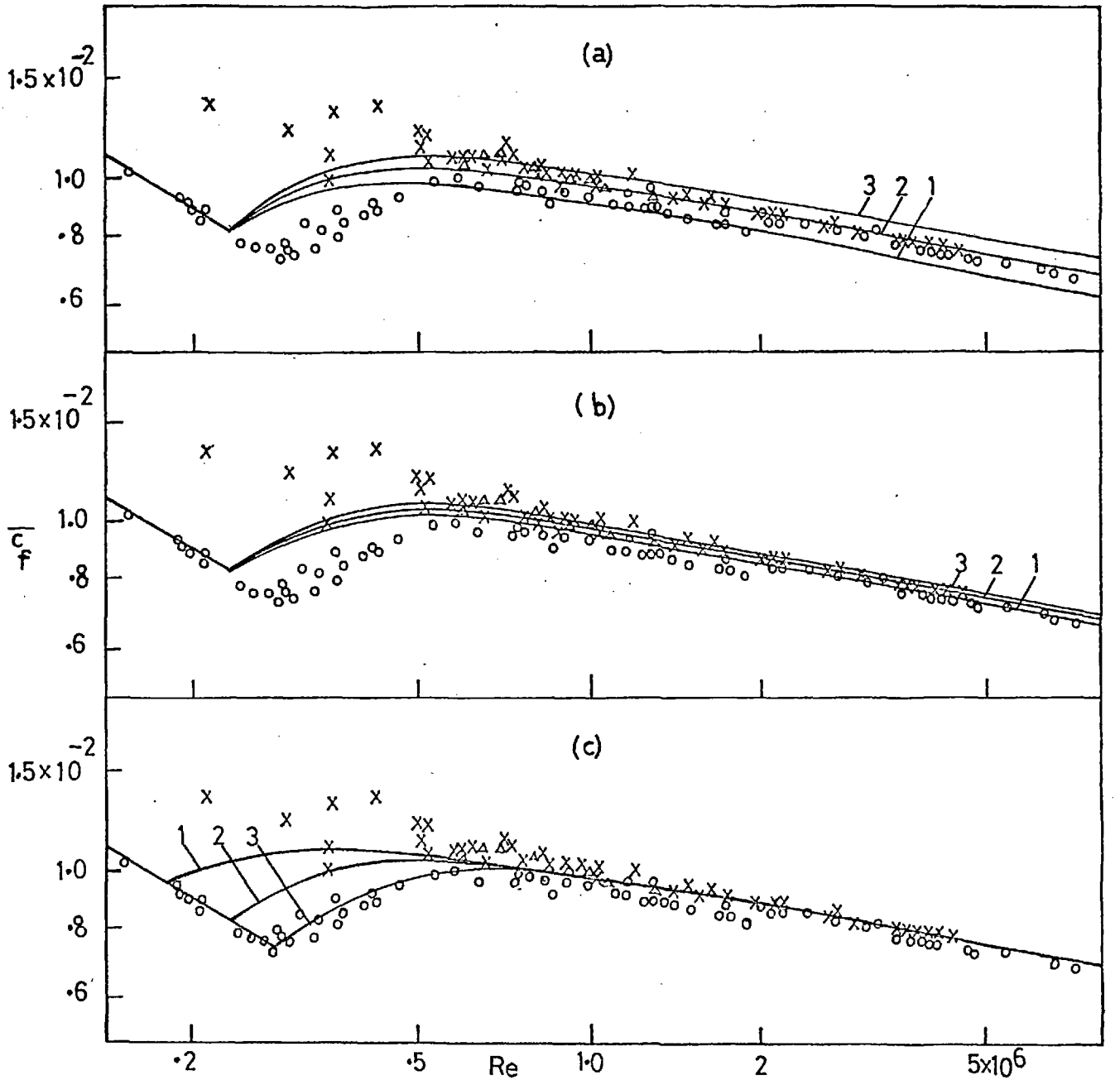

Predictions: ——— full lines					Experiments
Panel		$\varkappa$	λ	Re_{tran}	
(a)	1	.38	.08	2.3×10^5	o Theodorsen (1944)
	2	.42			
	3	.46			
(b)	1	.42	.08	2.3×10^5	Δ Kreith (1966)
	2		.09		
	3		.10		x Owen (1969)
(c)	1	.42	.08	1.8×10^5	
	2			2.3×10^5	
	3			2.8×10^5	

Fig. 4.2 Average drag on a disc rotating in stagnant air

Reynolds number $2.3X10^5$ recommended in the experimental studies, Kreith (1966), results in predictions which correspond fairly well with the mean of the experimental data.

(b) Shape Factor

Predictions of the shape factor H for the circumferential velocity profile are compared with the data of Cham and Head (1969) in Fig. 4.3. The results of varying κ, λ, and Re_{tran} are shown respectively on panels (a), (b) and (c). Since the influence of the parameter κ is felt mainly in the near-wall region, the development of the shape factor is more dependent on variations in λ than κ. The effect of varying Re_{tran} is not noticeable at the high Reynolds numbers. On panel (d) predictions obtained with $\kappa=0.42$ and $\lambda=0.085$, the values which result in the best predictions of the circumferential drag, compare favourably with the data and integral-profile predictions of Cham and Head.

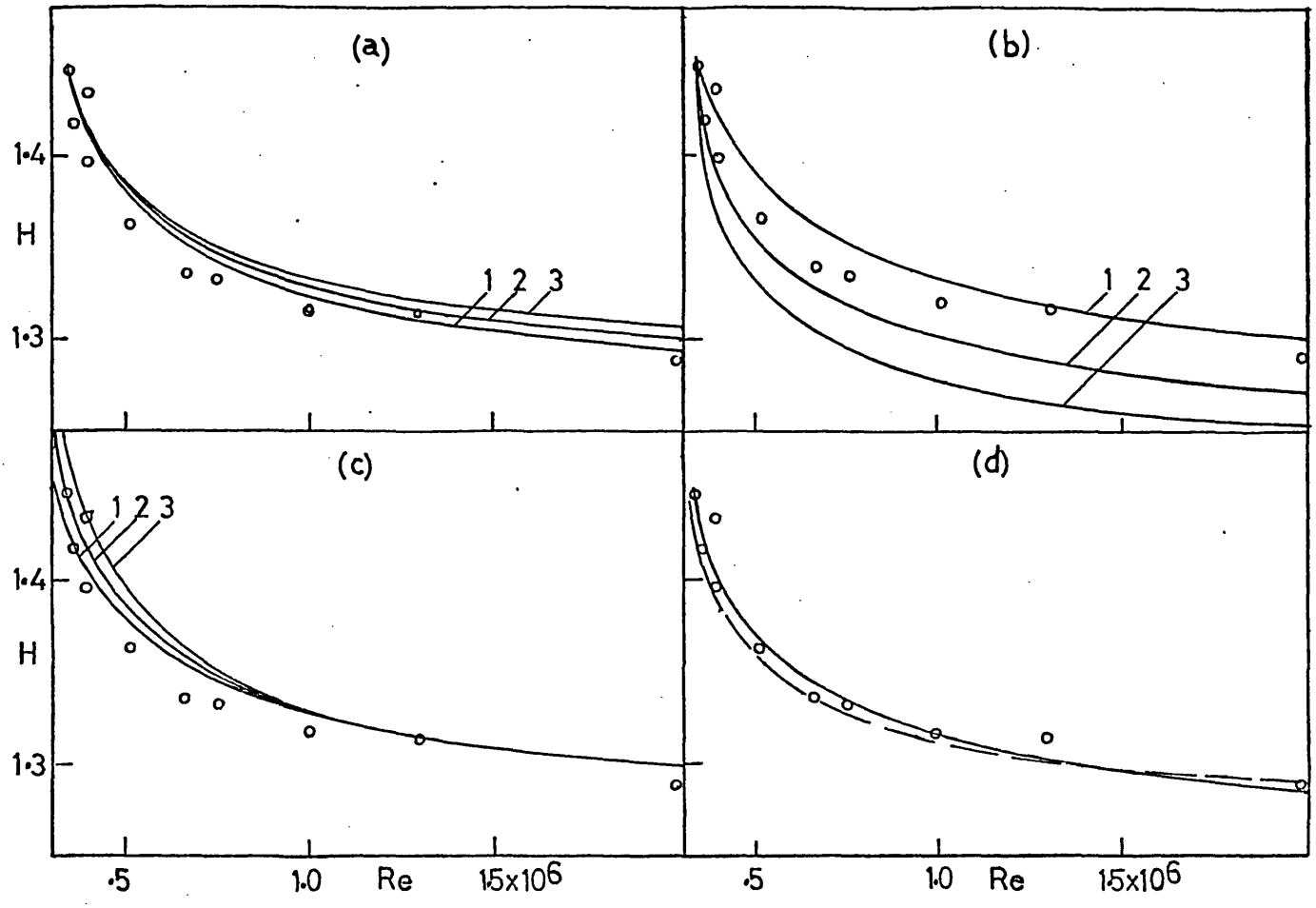

Panel		$\varkappa$	λ	Re_{tran}
(a)	1	.38		
	2	.42	.08	$2.3X10^5$
	3	.46		
(b)	1		.08	
	2	.42	.09	$2.3X10^5$
	3		.10	
(c)	1			$1.8X10^5$
	2	.42	.08	$2.3X10^5$
	3			$2.8X10^5$
(d)		.42	.085	$2.3X10^5$

o o o o Experimental data of Cham and Head (1969)

——— Present predictions

— — — Predictions of Cham and Head

Fig. 4.3 Development of shape factor for the circumferential component of velocity

(c) Volumetric Flow Rate

Fig. 4.4 displays the present predictions along with the predictions and experimental data of Cham and Head for a dimensionless radial volumetric flow rate. The overall agreement is good. The mixing-length constants were κ=0.42 and λ =0.085. The present solutions exhibit values of Q which are too high at the larger Reynolds numbers, but nevertheless the predictions show the correct trend, and the discrepancy is less than 10%.

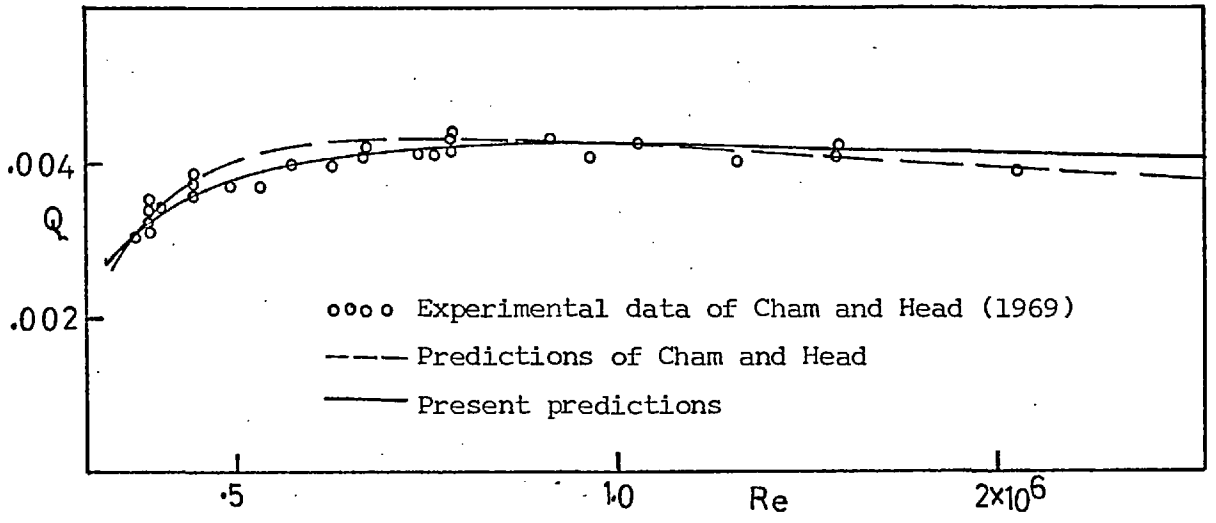

Fig. 4.4 Volumetric flow rate in the radial direction

4.3-2 Cone in Free Surroundings

The cone illustrated in Fig. 4.5 rotates in stagnant surroundings. The centrifugal forces on the fluid resolve into two components, one acting in the longitudinal direction and the other acting normal to the surface. The latter component gives rise to a cross-stream pressure gradient.

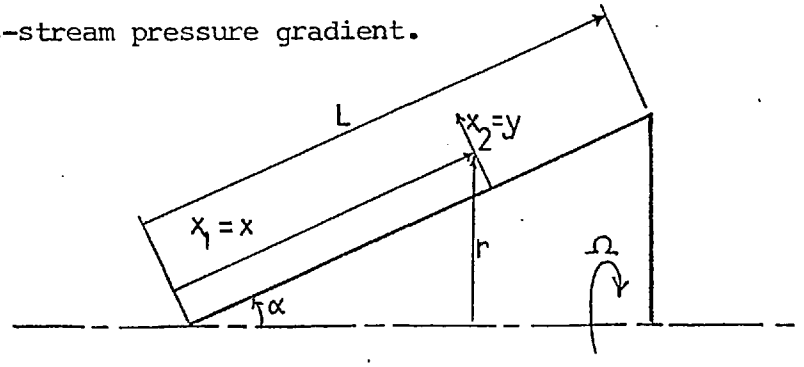

Fig. 4.5 Cone rotating in stagnant surroundings

The predictions of the average circumferential drag coefficient $\bar{c}_f$ for a cone of vertex angle 60^o are shown in Fig. 4.6; the experimental data are those of Kreith (1966). The value of 0.085 found appropriate for the disc calculations is ascribed to λ. The corresponding best value for K appears to be 0.47 instead of 0.42. The transition Reynolds number, based on the studies of Kreith, Ellis and Giesing (1962), was assumed to be $9X10^4$.

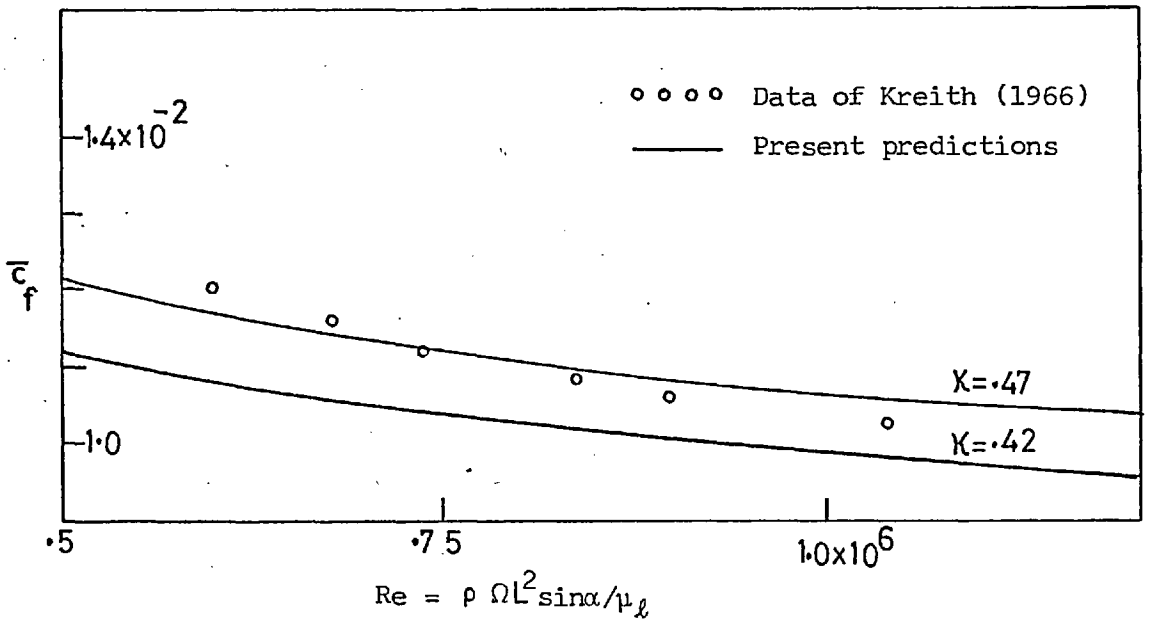

Fig. 4.6 Average circumferential drag

Within the Reynolds number range $5X10^5$ to $12X10^5$, when the influence of the laminar region near the vertex is negligible, Kreith was able to correlate his data to within 5% as: $\bar{c}_f = 0.157Re^{-0.2}$. For the present predictions the constant of proportionality relating $\bar{c}_f$ to Re can be represented by 0.156.

4.3-3 Cylinder in an Axially-Directed Stream

The turbulent boundary layer on a cylinder rotating in an axially-directed stream of uniform velocity, see Fig. 4.7, possesses some interesting characteristics. For example, the velocity vector twists through a right angle in tracing the velocity across the flow field. Furthermore, the flow is subjected to cross-stream centrifugal forces, and in this respect it is different from the disc flow which has no cross-stream pressure variation. As the speed of rotation increases, instabilities resulting from the large cross-stream centrifugal forces cause higher velocity fluctuations which in turn give rise to augmented turbulence intensities in the boundary layer.

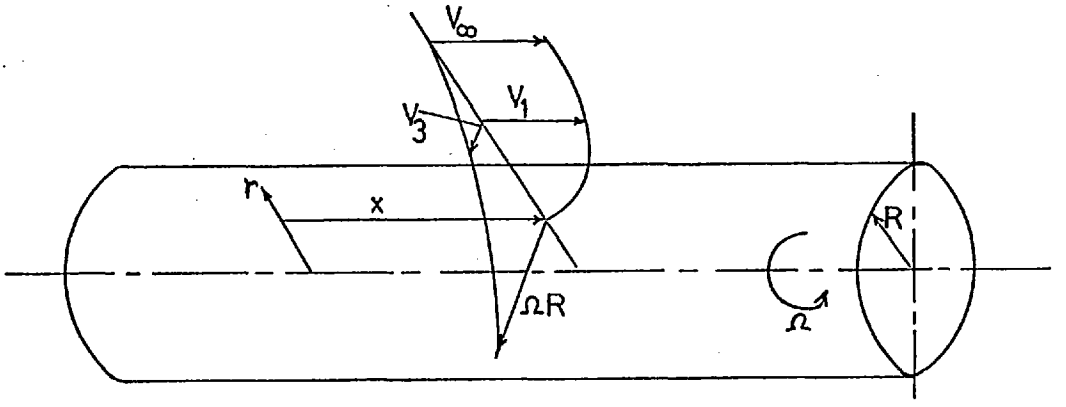

Fig. 4.7 Cylinder in Axially-directed stream

Experimental measurements of the velocity field have been reported by Parr (1963) and by Furuya and his co-workers (1966). The present predictions are for the fully turbulent downstream region of the flow; they were initiated from the furthest upstream profiles reported by the experimenters.

(a) Average Circumferential Drag Coefficient

A comparison of the average circumferential drag is made in Fig. 4.8 between one set of Parr's data and the present predictions. The values of the mixing-length constants determined from the disc studies were used. The curves marked 2 and 3 denote the effect of increasing κ and λ respectively.

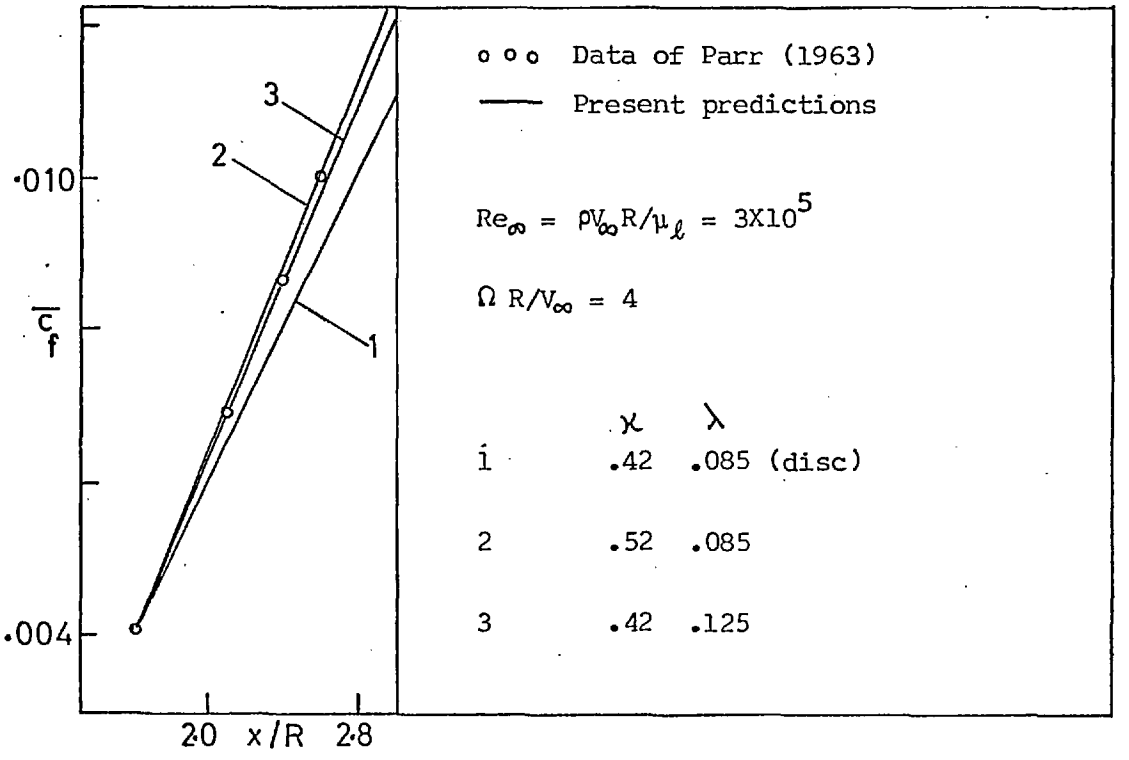

Fig. 4.8 Effect of varying mixing-length constants on the average drag for a rotating cylinder

Since the influence of κ is proportionately larger than that of λ, it was decided to adjust κ to obtain agreement with the experimental data, while keeping λ at the disc-value of 0.085. Fig. 4.9 displays predictions of the average circumferential drag coefficient for six experimental conditions. The agreement obtained between the predictions and the data is surprisingly good. However, the value

of K depends on the free stream Reynolds number as well as the ratio of rotational speed to free-stream velocity.

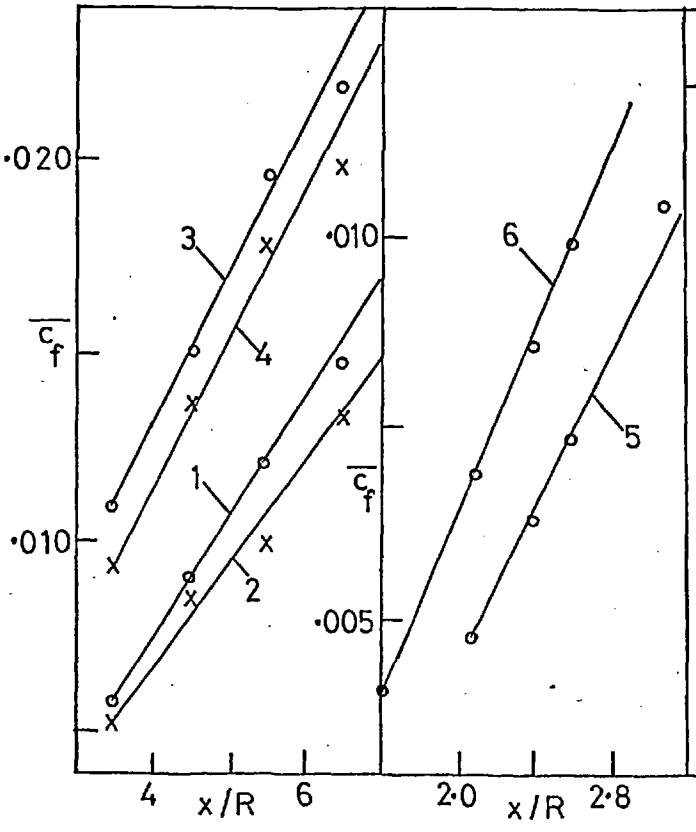

	Predictions ———			Data ooo,xxx
	Re_∞	$\Omega R/V_\infty$	χ	Ref.
1	$0.6X10^5$	1	.49	Furuya
2	$1.2X10^5$	1	.50	"
3	$0.6X10^5$	2	.50	"
4	$1.2X10^5$	2	.53	"
5	$3.0X10^5$	3	.48	Parr
6	$3.0X10^5$	4	.52	"

Fig. 4.9 Average circumferential drag for a cylinder rotating in an axially-directed stream

(b) Momentum Thicknesses

Predictions of the circumferential momentum thickness as well as the axial momentum thickness are compared in Fig. 4.10 with Parr's data for a velocity ratio of 4. The dependence of the predictions on K and λ is shown by the curves marked 2 and 3.

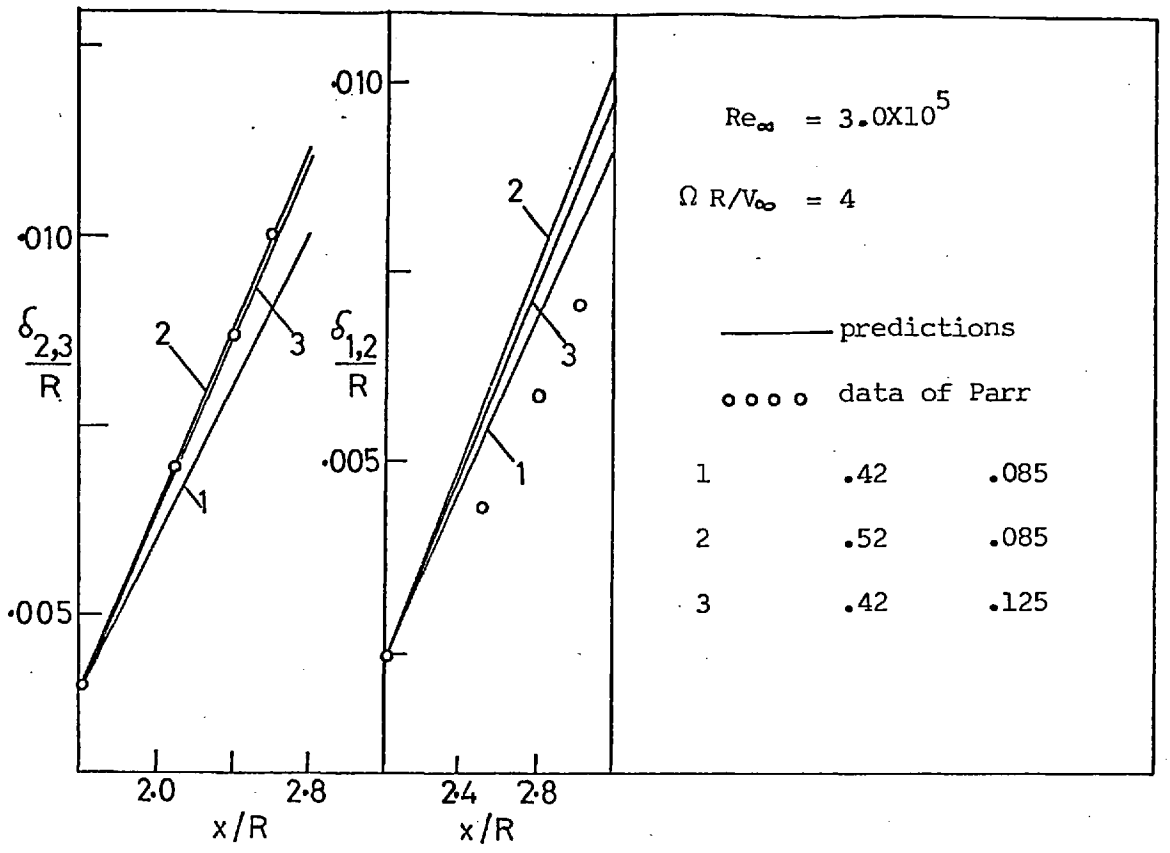

Fig. 4.10 Effect of varying the mixing-length constants on the axial and circumferential momentum thicknesses for a rotating cylinder

It is evident that accurate predictions of the overall flow field, that is, both momentum thicknesses, cannot be obtained by any combination of the constants κ and λ. The same remark also applies to the other experimental conditions of Parr and of Furuya. The explanation of the failure to predict the complete flow field lies in the original assumption of isotropic viscosity. Consequently, if the mixing-length constants are determined from the data for the circumferential velocity distribution for example, it does not follow that the same set of constants will give good predictions for the axial velocity distribution. Turbulence models which account for the non-isotropic nature of the effective viscosity are presented later in Chapters 5, 6 and 7.

4.3-4 Radial Outflow Between a Rotating and a Parallel Stationary Disc

The most comprehensive hydrodynamic study of this flow is probably that of Owen (1969) and Bayley and Owen (1969). They provide experimental results for an extensive range of conditions, and present predictions obtained using the Patankar and Spalding procedure. In order to ensure that the flow is of the boundary-layer kind, sufficient fluid must be supplied through the centre of the stationary member, as shown in Fig. 4.11, to avoid recirculation of the inter-disc fluid. The parameters governing this problem are therefore the disc Reynolds number, $Re=\Omega r_o^2/\nu$, the mass inflow coefficient, $C_w=\dot{m}/\mu r_o$, and the inter-disc gap to disc radius ratio, $G = s/r_o$.

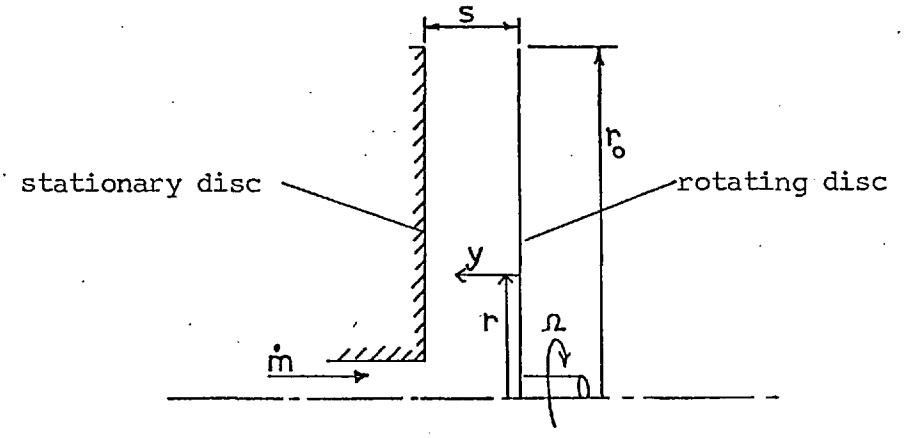

Fig. 4.11 Radial outflow between two discs

Bayley and Owen's measurements of average drag coefficient for the rotating disc, velocity profiles and radial pressure distribution for typical flow conditions are displayed in Fig. 4.12 (a), (b) and (c), along with both their own and the present predictions. As described in Section 3.1(a) of Appendix1 , Bayley and Owen presumed, in contrast to the present study, that the effective viscosities in the radial and circumferential directions are different.

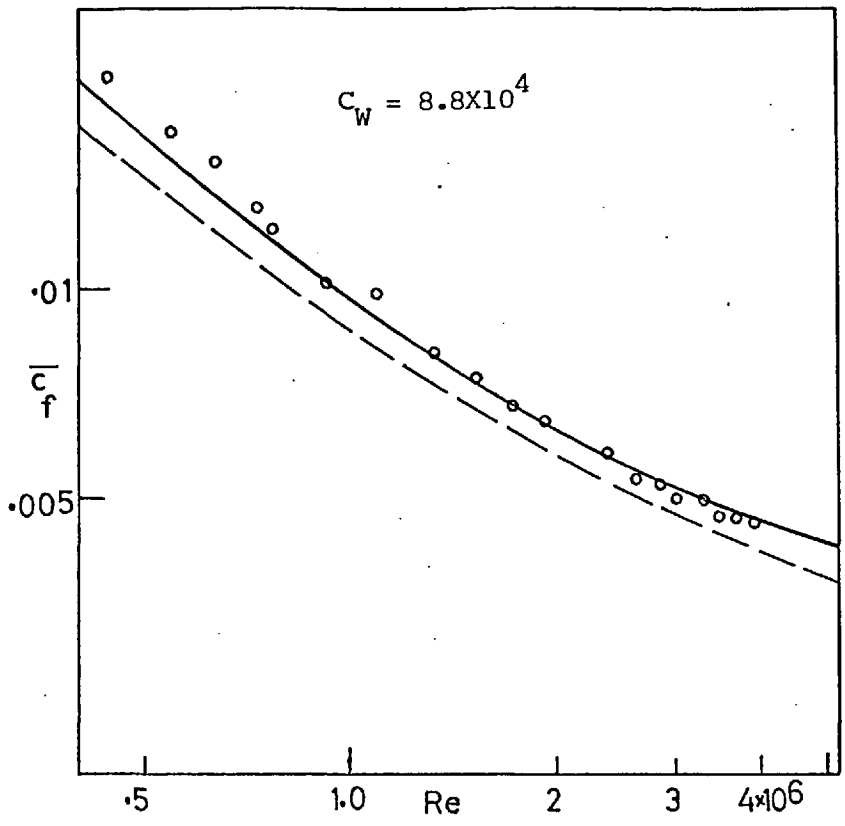

(a) Average drag on rotating disc

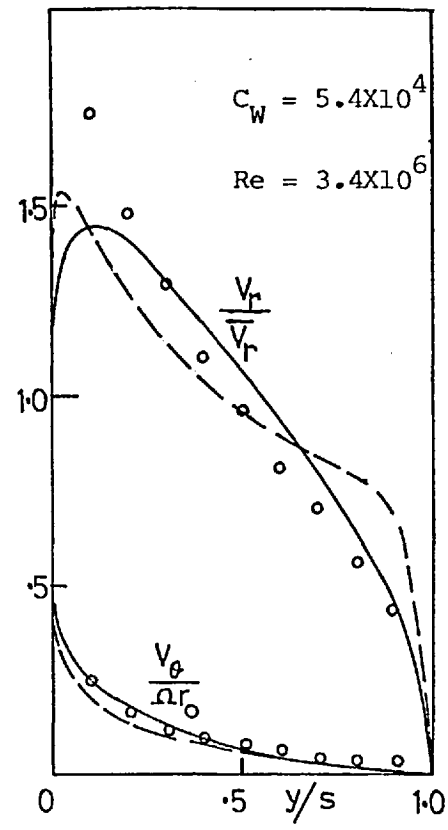

(b) Velocity profiles

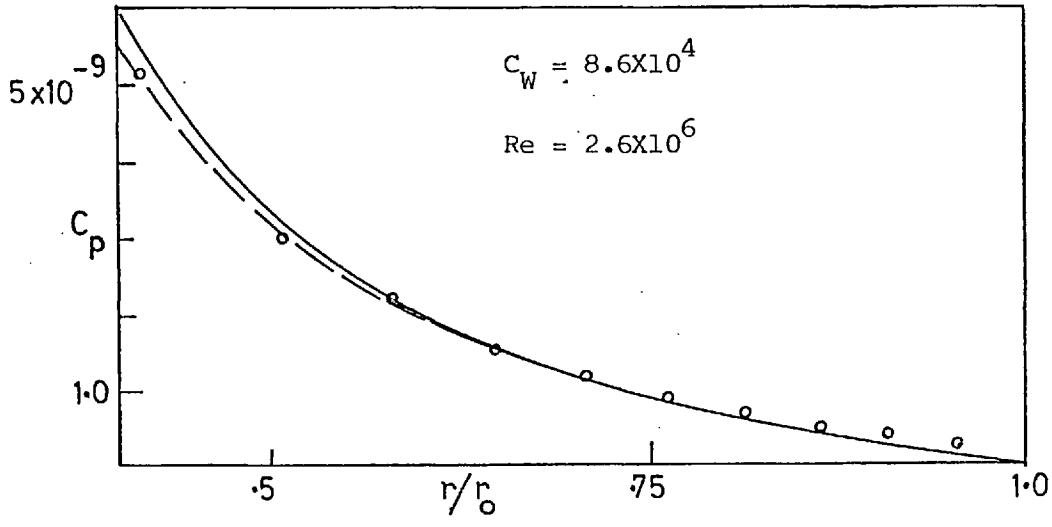

(c) Radial pressure coefficient

o o o Experimental data of Bayley and Owen (1969), G = .03

——— Present predictions

— — — Predictions of Bayley and Owen

Fig. 4.12 Radial outflow between a rotating and a parallel stationary disc

The present predictions were initiated at $r/r_o = 0.35$ where the experiments of Bayley and Owen indicated the reattachment of a separation bubble on the stator. The radial pressure gradient was calculated from the following equation:

$$\frac{dp}{dr} = -\frac{r(\tau_{rotor} + \tau_{stator})}{rs_{flow}} + \rho\frac{v_3^2}{r} + \frac{\dot{m} v_1}{(rs_{flow})^2}\frac{\delta A}{\delta r} \qquad (4.11)$$

An explanation of the symbols and origin of this equation is given in Appendix 4.

The present predictions were obtained using the same values of κ and λ as Bayley and Owen, respectively 0.40 and 0.12. These values appear to be the optimum ones for the gap ratio and mass inflow shown in Fig. 4.12. The values of κ and λ differ unfortunately from the optimum values determined for the unshrouded disc. Further exploratory comparisons with Bayley and Owen's data revealed that other values of κ and λ are required for other flow conditions.

It is evident that the present predictions for the average drag are superior to those of Bayley and Owen. There is little to choose between the two procedures in respect of the profiles and radial pressure coefficient predictions. It is indeed strange that neither procedure properly predicts the peak in the profile of radial velocity; there is no obvious explanation for this discrepancy.

4.4 Correlation of the Change in Mixing-Length Due to Swirl

When the geometrical angle α is less than 90 degrees in the present coordinate system, the circumferential component of velocity through the action of centrifugal forces may significantly alter the structure of the boundary layer. The tendency of the fluid to be flung away from the surface is balanced by the normal pressure gradient. Such a flow has an analogy with a free-convection boundary layer in which the gravitational vector crosses the heated wall boundary.

4.4-1 The 'Monin-Oboukhov' Formula

Bradshaw (1969) has presented a rather penetrating analysis of the analogy between the effect of swirl and that of buoyancy on turbulent flow. He suggests the 'Monin-Oboukhov' formula:

$$\ell_{m,c} = \ell_m \, (1-\beta.Ri) \quad , \qquad (4.12)$$

as a particularly simple approximate means of correlating the effect of the centrifugal body forces on the mixing-length. The symbol $\ell_{m,c}$ represents the correctd value of the mixing-length ℓ_m to account for centrifugal effects. β is an adjustable parameter of the turbulence model, and the Richardson number Ri, normally of meteorological interest, characterises here the ratio of the centrifugal forces, instead of the buoyancy forces, to the inertia forces. Because of the tenuous physical content of the Monin-Oboukhov formula, β cannot be expected to exhibit a refined degree of universality.

The Richardson number, as Bradshaw pointed out, can be regarded as the ratio of the square of a typical frequency scale of the circumferential velocity fluctuations to the square of a typical eddy in the boundary layer. For the former the appropriate quantity is: $\left\{\frac{2V_3}{r^2}\cos\alpha \; \frac{\partial(rV_3)}{\partial x_2}\right\}^{\frac{1}{2}}$; while for the latter, consistent with the viscosity formulation (equation 4.7), the resultant of the velocity gradients is the appropriate choice. Hence,

$$Ri = \frac{\frac{2V_3}{r^2}\cos\alpha \quad \frac{\partial(rV_3)}{\partial x_2}}{\left(\frac{\partial V_1}{\partial x_2}\right)^2 + \left(r \quad \frac{\partial(V_3/r)}{\partial x_2}\right)^2} \qquad (4.13)$$

Cham and Head (1970) have examined the suitability of the Monin-Oboukhov formula by comparing their predictions obtained using an integral-profile method with Parr's (1963) cylinder flow. Their findings indicate that, for that particular flow, β is not constant but varies in the range 0.25 to 60 across the boundary layer. In a recent paper, Hughes and Horlock (1971) obtained equations 4.12 and 4.13 by simple physical reasoning, and suggested a value of β between 7 and 8.

4.4-2 Cone and cylinder flow

The Monin-Oboukhov formula was used with the present isotropic viscosity model, equations 4.7, 4.9 and 4.10, to predict the circumferential drag for the cone experiments of Kreith (1966) and the cylinder experiments of Parr (1963). The value of ℓ_m is, of course, that appropriate to disc flow since the Richardson number is zero, the geometrical angle α being equal to 90 degrees; consequently the reference values of κ and λ are respectively 0.42 and 0.085. The value of β was adjusted until the best overall predictions were obtained. Fig. 4.13 presents the results for the cone and Fig. 4.14 provides those for the cylinder.

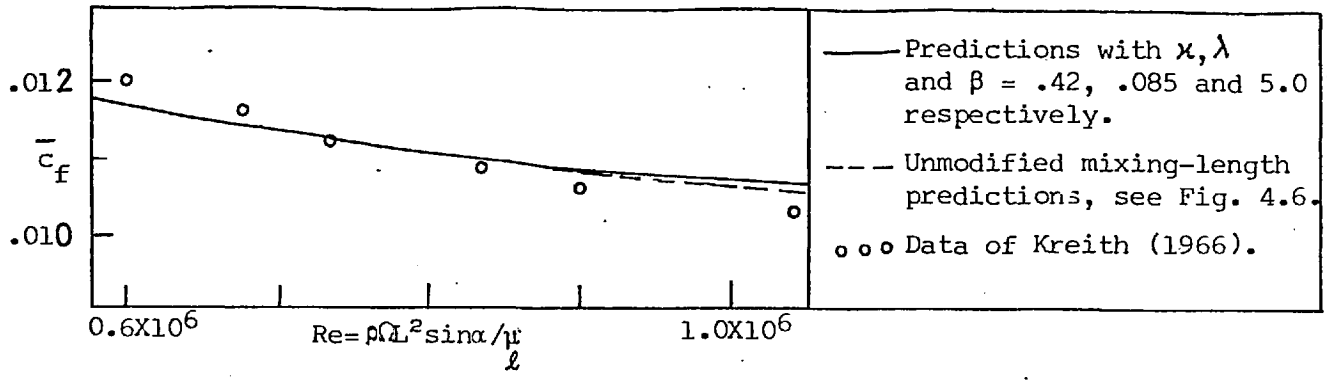

Fig. 4.13 Average circumferential drag on a 60° rotating cone

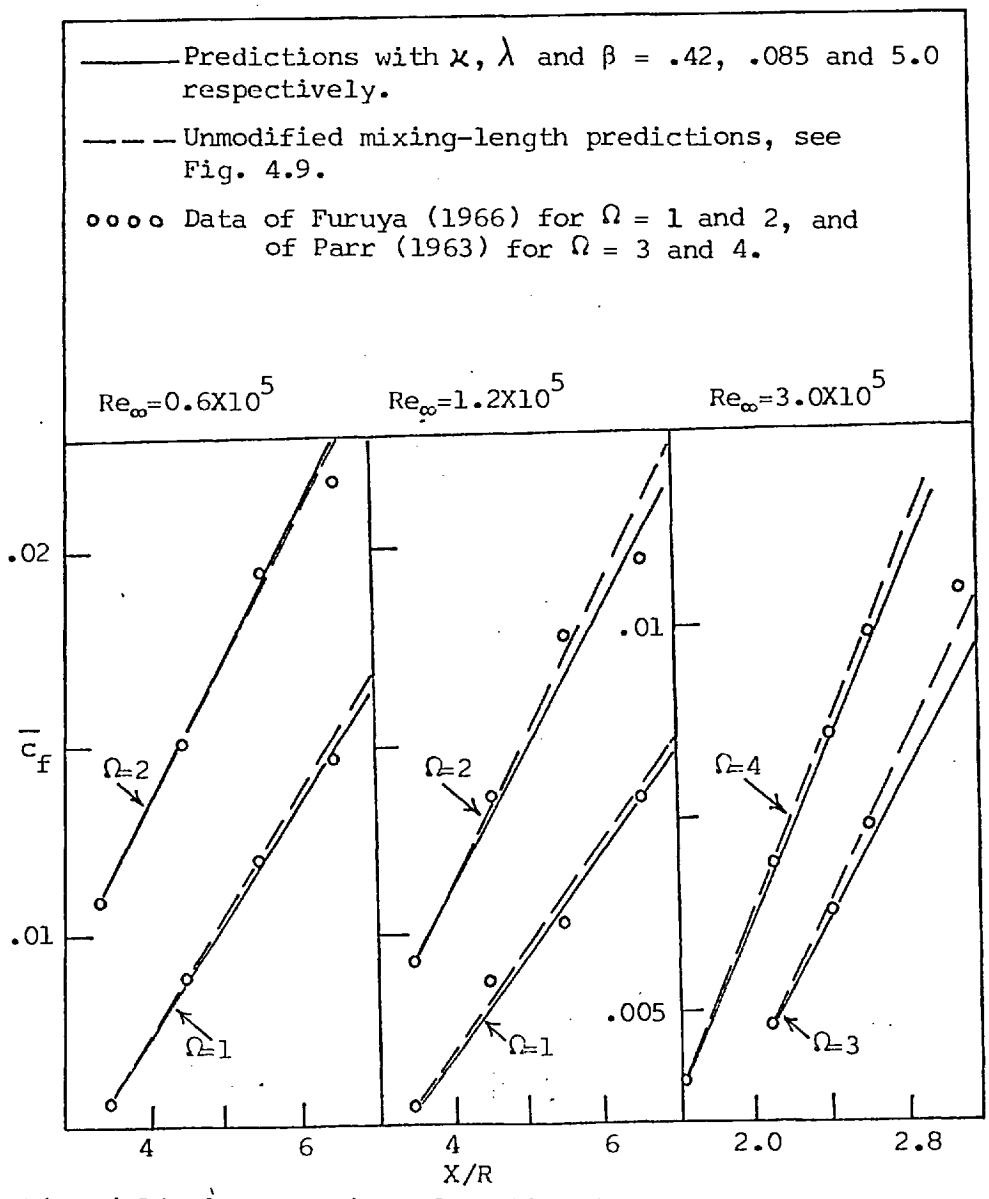

Fig. 4.14 Average circumferential drag for a cylinder rotating in an axially-directed stream

Quite good predictions are obtained when β is 5.0 for both the cone and cylinder. Also shown on the figures are the predictions for the unmodified mixing-length distribution for the previously found best values of the constants κ and λ. For these latter predictions, λ was equal to .085, but κ had to be varied in the range .48 to .53. This serves to demonstrate the useful generality of the simple recommendation of a single set of constants, $\kappa = .42$, $\lambda = .085$ and $\beta = 5.0$.

4.5 Conclusions

The folowing conclusions, on the usefulness and limitations of the isotropic viscosity mixing-length based model of turbulence, can be drawn from the comparisons which have been made of the predictions with the experimental evidence:

1. For the four flow configurations considered, free disc and cone, cylinder in axial stream, and parallel discs with outflow, the variation of average circumferential drag with rotational Reynolds number was very well predicted. However, the magnitude of the two empirical constants in the mixing-length formulation is not universal, but depends on the particular flow configuration as well as flow condition under consideration. The values of the constants, κ and λ, are summarised in Table 4.1 below; they are those which, within the limitations imposed by the accuracy of the data, predict best the experiments of the specified reference. The assumed value of Re_{tran} is also given where appropriate; it always lies within the reported experimental range of transition Reynolds number.

Experiments				Predictions λ = .085 all cases	
				κ	Re_{tran}
Disc in stagnant surroundings:					
Theordorsen and Regier	(1944)			.42	2.8×10^5
Owen	(1969)			.42	1.8×10^5
Cham and Head	(1969)			.42	2.3×10^5
Cone, 60° vertex, in stagnant surroundings:					
Kreith	(1966)			.47	0.9×10^5
Cylinder in axially-directed stream:					
		$\Omega R/V_\infty$	$V_\infty R/\nu$		
Parr	(1963)	3	3.0×10^5	.48	
		4	3.0×10^5	.52	
Furuya and co-workers	(1966)	1	0.6×10^5	.49	fully turbulent
		2	0.6×10^5	.50	
		1	1.2×10^5	.50	
		2	1.2×10^5	.53	
Radial outflow between two discs, one stationary: Owen (1969), Bayley and Owen (1969)				κ = .40 λ = .12	fully turbulent

Table 4.1 Optimum values of the mixing-length constants for several flow configurations

2. A simple modification to the mixing-length, which was correlated to a Richardson number to account for the effects of the swirl body-force, improved the universality of the mixing-length approach. A single set of constant, $\kappa = .42$, $\lambda = .085$, and $\beta = 5.0$, resulted in predictions which accorded well with the experimental data for the circumferential drag for the disc, cone, and cylinder flows.

3. The concept of an isotropic viscosity is not generally valid for swirling boundary layers (and in consequence, for non-swirling three-dimensional layers). For the case of a cylinder rotating in an axially-directed stream, where the axial and circumferential components of velocity were of the same order of magnitude, the model failed to predict the overall velocity field. If the mixing-length constants were determined from matching predictions with experimental data for the circumferential drag, then the agreement between predictions and data for the axial drag was poor, and vice versa.

4. The mixing-length concept, leading to an isotropic viscosity formula, lacks universality. This is the inevitable drawback of a model which, although conceptually simple, is lacking in physical reality. The mixing-length hypothesis implies that the local structure of the flow is determined by local conditions alone, in other words that the generation and dissipation of turbulence energy are in local equilibrum. While the equilibrium condition is satisfied near a wall, it is not satisfied, for most flows, in the outer part of the boundary layer (in practice the outer four-fifths of the layer thickness). In this region the size of a typical turbulent eddy is of the same order as the boundary-layer thickness and its lifetime corresponds to a downstream travel of several boundary-layer thicknesses. Thus, the boundary layer

has a history which is not accounted for by the mixing-length theory.

More general and physically plausible models of turbulence allow for the convection and diffusion of turbulence. In Chapter 5 which follows, the transport of turbulence is taken into account, and it is characterised by its kinetic energy and length scale; these two quantities are determined from differential transport equations.

CHAPTER 5

A TWO-EQUATION MODEL OF TURBULENCE

5.1 Introduction

The mixing-length model of turbulence described in the previous chapter can be considered a 'zero-differential-equation' model since the turbulence structure of the flow is uniquely related to the local mean flow conditions and is not characterised by any transport equation. The model works well for the boundary layers considered, but the empirical constants which it contains depend on flow configuration and flow condition. This inadequate generality of the constants was attributed to the simplified representation of turbulence by a zero-equation model.

Turbulence hypotheses which are more physically plausible than the mixing-length concept have been proposed by Kolmogorov (1942), Prandtl (1945), Chou (1945), and Rotta (1951). The local state of the fluid is assumed to depend on one or more turbulence quantities determined from the solution of transport equations. These equations are, however, complex and only ameanable to analytical solution after numerous assumptions are made, correlating these turbulence quantities (double and triple fluctuating velocity correlations) and the mean flow field. Nonetheless, these simplified equations constitute turbulence models which exhibit greater generality of application than the mixing-length model for non-swirling boundary layers, see for example Ng (1972), Hanjalic and Launder (1972), Rodi (1973). These authors, following the work of Kolmogorov (1942) and Rotta (1951), assumed that the local state of the fluid is characterised by two parameters: the kinetic energy of turbulence k, and a length scale ℓ which represents the time-averaged diameter of the energy containing

eddies; both k and ℓ are determined from the solution of their own differential equations, and the model is consequently referred to as a 'two-equation, energy-length' model. An important outcome of the work of Ng (1972) and Rodi (1973), who respectively investigated boundary layers near walls and free jets, is that a single set of empirical constants was found to be capable of accurately predicting several flow situations; this ability is not possessed by the mixing-length model.

The present work extends the two-equation energy-length model to swirling boundary layers. The equations governing the transport of k and ℓ are presented in Section 5.2, together with expressions relating the effective exchange coefficients to k and ℓ.

In Section 5.3, comparisons are made between predictions and experimental data for the flow field near a cylinder rotating in an axially-directed stream of uniform velocity. The results of Lilley's (1973) investigation of free swirling jets, using the model developed here, are also presented.

Lastly, Section 5.4 concludes with a summary of the present studies of the two-equation model of turbulence, and an evaluation of the findings.

5.2 The Turbulence Energy and Length Scale Equations

The differential equations governing the transport of turbulence quantities like k and ℓ, or other combinations such as $k\ell$ or $k^{1.5}\ell^{-1}$, are developed by a combination of physical reasoning and intuitive guess work. Discussion of these matters can be found in Rotta (1951), Rodi and Spalding (1970), and Ng and Spalding (1972). In the present work the equation for k is derived later in Chapter 7; it is equation 7.20. Following Spalding and his co-workers, and also Rotta, an equation for k times ℓ rather than an equation for ℓ is

solved. Rodi (1970) presents a partially-modelled equation for $k\ell$ in cylindrical coordinates and this constituted the starting point for the derivation of the fully-modelled form . The boundary-layer forms of the equations for k and $k\ell$, are presented in Chapter 7; in the curvilinear orthogonal system of coordinates described in Section 2.2, they are:

$$\underbrace{\rho V_1 \frac{\partial k}{\partial x_1} + \rho V_2 \frac{\partial k}{\partial x_2}}_{\text{convection}} = \underbrace{\frac{1}{r}\frac{\partial}{\partial x_2}\left[r \Gamma_k \frac{\partial k}{\partial x_2}\right]}_{\text{diffusion}} - \underbrace{\left[\overline{v_1 v_2}\frac{\partial V_1}{\partial x_2} + \overline{v_2 v_3} r \frac{\partial (V_3/r)}{\partial x_2}\right]}_{\text{production}} - \underbrace{C_D \rho \frac{k^{\frac{3}{2}}}{\ell}}_{\text{dissipation}}, \quad (5.1)$$

$$\underbrace{\rho V_1 \frac{\partial k\ell}{\partial x_1} + \rho V_2 \frac{\partial k\ell}{\partial x_2}}_{\text{convection}} = \underbrace{\frac{1}{r}\frac{\partial}{\partial x_2}\left[r \Gamma_{k\ell} \frac{\partial k\ell}{\partial x_2}\right]}_{\text{diffusion}} - \underbrace{C_B \ell \left[\overline{v_1 v_2}\frac{\partial V_1}{\partial x_2} + \overline{v_2 v_3} r \frac{\partial (V_3/r)}{\partial x_2}\right]}_{\text{production}}$$

$$\underbrace{- C_S \rho k^{\frac{3}{2}}}_{\text{dissipation}} \underbrace{- C_W \rho \left(C_D^{\frac{1}{4}} \kappa y \ell^{-1}\right)^{-C_q} k^{\frac{3}{2}}}_{\text{wall-damping effect}} \underbrace{- C_R \rho Ri\, k^{\frac{3}{2}}}_{\text{body-force effect}} . \quad (5.2)$$

The last term of equation 5.2, an outcome of the present work, is introduced to account for the influence of the centrifugual forces on the turbulence structure. Close to a wall there is no net effect from the production and dissipation of the kinetic energy of turbulence; the flow is in equilibrum. The production and dissipation terms of equation 5.1 are then equal, and the length scale ℓ is proportional to the mixing length $\ell_{m,c}$ defined by equations 4.7 and 4.12. When $\ell_{m,c}$ is substituted for ℓ in the Couette flow form of Rodi's (1970) equation for $k\ell$, compatibility and dimensional considerations indicate that an additional term, a body-force term, is required. Although this term is derived from an analysis of the flow close to a wall, it is presumed valid across the whole layer.

The equations for k and $k\ell$ are similar to the momentum

equations; they contain convection and diffusion terms, with the remaining terms regarded as source terms. They possess the same form as the general equation 2.31 and consequently are also solved using the Patankar and Spalding procedure.

5.2-1 The Effective Exchange Coefficients

Kolmogorov (1942) and Prandtl (1945) suggested on dimensional considerations that, for a non-swirling two-dimensional boundary layer, the main Reynolds shear stress $-\rho\,\overline{v_1 v_2}$ is given by:

$$-\rho\overline{V_1V_2} = \rho k^{\frac{1}{2}} \ell \frac{\partial V_1}{\partial x_2} \quad . \tag{5.3}$$

This relation is only valid for homogeneous turbulence at high Reynolds number; these conditions usually prevail, at least locally, in many flows, see for example Rodi (1973). For non-swirling boundary layers, equation 5.3 combined with the definition of effective viscosity, equation 2.39, leads to:

$$\mu_{1,2} = \rho k^{\frac{1}{2}} \ell \quad . \tag{5.4}$$

The effective viscosity is thereby related to the intensity of turbulence via k, and to the structure of turbulence via ℓ.

For swirling boundary layers, the present work assumes that the Reynolds shear stresses are given by:

$$-\rho\overline{V_1V_2} \Big/ \frac{\partial V_1}{\partial x_2} = \rho k^{\frac{1}{2}} \ell / \sigma_1 \quad , \tag{5.5}$$

and

$$-\rho\overline{V_2V_3} \Big/ r\frac{\partial (V_3/r)}{\partial x_2} = \rho k^{\frac{1}{2}} \ell / \sigma_3 \quad . \tag{5.6}$$

These two equations also represent, through the definitions 2.39 and 2.40, the effective viscosities $\mu_{1,2}$ and $\mu_{2,3}$ respectively. The viscosity ratio $\sigma_{2,3}$, defined by equation 4.5, is then equal to σ_3/σ_1. In a similar way, the exchange coefficients appearing in the turbulence equations 5.1 and 5.2 are presumed to be:

$$\Gamma_k = \rho k^{\frac{1}{2}} \ell / \sigma_k \quad , \qquad (5.7)$$

and

$$\Gamma_{k\ell} = \rho k^{\frac{1}{2}} \ell / \sigma_{k\ell} \quad ; \qquad (5.8)$$

the origin of these formulations is discussed in Sections 7.3-5 and 7.3-6. The parameters or empirical constants σ_1, σ_3, σ_k and $\sigma_{k\ell}$ are assumed constant, and their values are determined from matching predictions of mean-flow and turbulence quantities with experimental data.

5.2-2 The Empirical Constants

In total the two-equation energy-length model contains 11 empirical constants: C_B, C_D, C_R, C_S, C_W, κ, C_q, σ_1, σ_3, σ_k, and $\sigma_{k\ell}$. The constants C_B, C_D and C_S have a strong influence on the level and rate of spread of turbulence energy; the main influence of σ_k and $\sigma_{k\ell}$ is felt as a change in the shape of the profiles of the dependent variables, see Ng and Spalding (1972). The parameters σ_1 and σ_3, see equations 5.5 and 5.6, allow for the anisotropic nature of the effective viscosity, but the assumption that they are constant implies that the ratio $\mu_{1,2}/\mu_{2,3}$ is a constant over the flow field under consideration. This is no more likely to be the case than the assumption of isotropic viscosity, namely that the ratio $\mu_{1,2}/\mu_{2,3}$ is unity; short of devising elaborate empirical functions for σ_1 and σ_3, the assumption that they are constants provides a simple, but useful, approach for extending the two-equation model to account for anisotropic viscosity.

The turbulence model, represented by equations 5.1, 5.2, 5.5 to 5.8, was used to predict the flow field near a cylinder rotating in an axially-directed stream of uniform velocity. The choice of the empirical constants was guided by the values found by Ng (1972) to give good predictions for non-swirling boundary layers near walls. These values, recorded in Table 5.1 below, offer the only available

indication of the starting point for swirl-flow computations.

5.2-3 The Near-Wall Region

The above system of equations approximate to the physical situation only in the fully turbulent part of the boundary layer. The exclusion of molecular viscous terms precludes their application to the sub-layer, that is, the near wall region where the influence of the laminar viscosity predominates. To overcome this restriction the finite-difference solution is matched to values of the dependent variables, determined form 'wall-functions', at a small distance from the wall, yet in the fully-turbulent region. In practice the matching point is the first grid-node away from the surface.

The resultant velocity V_R, from the experimental findings of Backshall and Landis (1969), is presumed to obey the conventional log-law:*

$$V_R \Big/ \sqrt{\frac{\tau_R}{\rho}} = \frac{1}{0.4} \ln\left[9 \frac{y}{\mu_\ell} \sqrt{\frac{\tau_R}{\rho}} \right] \quad ; \qquad (5.9)$$

the resultant shear stress τ_R is constant in this near-wall region, and acts in the same direction as the resultant velocity. The axial and circumferential shear stress components are then obtained by straightforward resolution.

The length scale ℓ is proportional to the distance from the wall, see for example Ng and Spalding (1972), and Launder and Spalding (1972):

$$\ell = \kappa C_D^{\frac{1}{4}} y \quad . \qquad (5.10)$$

No general recommendation have yet been made about the behaviour of the turbulence energy k in the sublayer. It is presumed that, in this region, the production and dissipation of turbulence energy are in balance; the near-wall value of k is then proportional

* Pressure gradient effects are not included in equation 5.9; the influence of pressure gradient for the flow for which this equation is used, see Section 5.3, is negligible.

to the resultant wall shear stress τ_R given by equation 5.9. The relation between k and τ_R is derived in Appendix 3 and is:

$$k = C_D^{-\frac{1}{2}} \rho^{-1} \tau_R \quad . \qquad (5.11)$$

5.3 Comparisons of Predictions with Experimental Data

5.3-1 Cylinder Rotating in Axially-Directed Free Stream

The case of a cylinder rotating in an axially-directed free stream of uniform velocity, already illustrated in Fig. 4.7, is a particularly interesting one. The mixing-length studies of Chapter 4 reveal that the range of experimental data for this flow presents a trying test of the generality of the empirical constants of the assumed turbulence model, and also of the capability of the model to predict the overall flow field for a given flow situation.

Predictions of circumferential and axial momentum thicknesses for two of Parr's (1963) experimental conditions were compared with his data; these two cases were found to be a sufficient test of the generality of the model. To procure as much consistency as possible between the present work and those for non-swirling flow, the empirical constants employed are those which work well for the non-swirling flows. Consequently, all the constants in equations 5.1 and 5.2, with the exception of C_R which appears in the body-force term, are those proposed by Ng (1972). The value of C_R, as well as σ_1 and σ_3, were adjusted to values giving the overall best agreement with the data. These values and those of the remaining constants are shown in Table 5.1 below; the comparisons between predictions and experimental data are presented in Fig. 5.1.

$C_B = .985$	$C_D = .09$	$C_S = .0585$	$C_W = .078$
$\kappa = .4$	$C_q = 4.0$	$\sigma_k = 1.0$	$\sigma_{k\ell} = 1.0$

Fig. 5.1 below	$\Omega R/V_{1,\infty}$	C_R	σ_1	σ_3
1	3	0	3.0	0.2
2	3	2	3.0	0.3
3	4	0	3.0	0.3
4	4	2	4.0	0.6

Table 5.1 Constants for the energy-length turbulence model for the cylinder flow

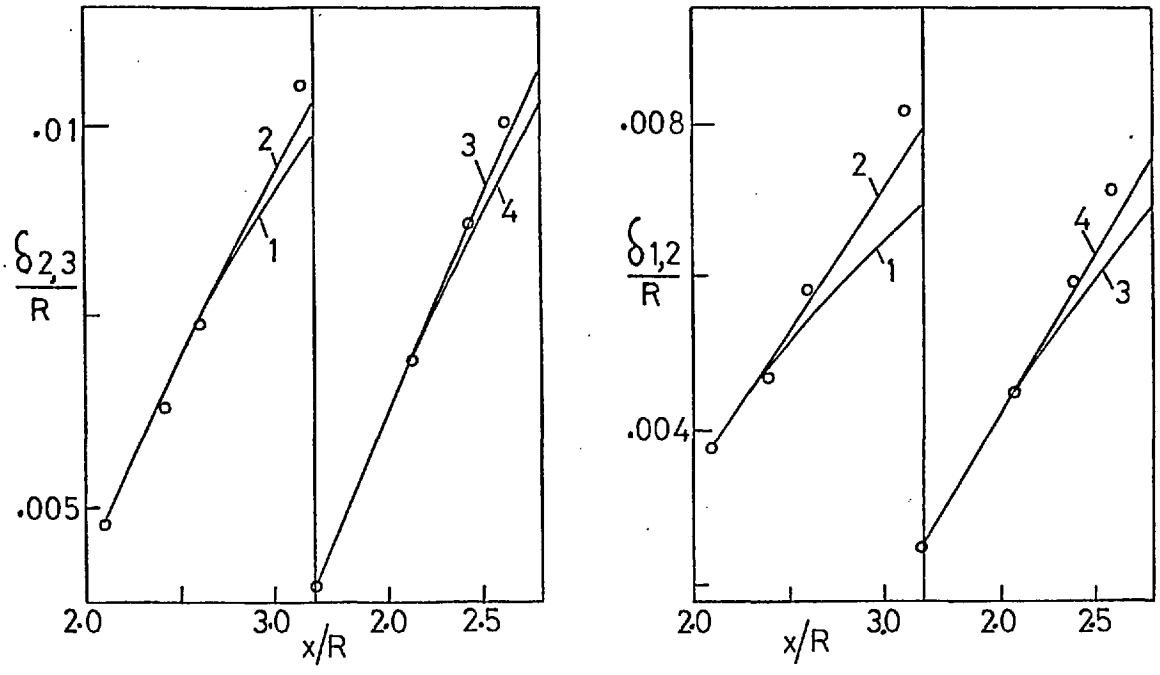

circumferential momentum thickness

axial momentum thickness

——— predictions (see also Table 5.1 above)

o o o data of Parr (1963)

Fig. 5.1 Axial and circumferential momentum thicknesses for the cylinder flow

The results are marginally better with the body-force term included and $C_R = 2.0$. The axial and circumferential momentum thicknesses are both well predicted, although different values of σ_1 and σ_3 are required for the two flow conditions considered. These values are substantially different from unity, confirming the findings of other workers, for example Lilley and Chigier (1971), that the turbulence of highly swirled flows is very anisotropic. It should also be noted that the predictions of circumferential momentum thickness on the whole do not compare very favourably with the predictions obtained using the much simpler isotropic mixing-length model of turbulence. These matters are further discussed in Section 5.4 below.

5.3-2 Free Swirling Jet

The two-equation energy-length model developed here has also recently been used by Lilley (1973) in his studies of free swirling jets issuing into stagnant surroundings. These jets, when the degree of swirl is not so large as to cause recirculation, combine the interesting characteristics of a swirling boundary layer with the mathematically simple boundary conditions associated with a free jet. There are no influences from solid surfaces, and consequently the wall-damping term in equation 5.2 for $k\ell$ vanishes.

Lilley's choice of constants was based on the work of Rodi and Spalding (1970) on non-swirling round jet flows. Having retained the same values for these constants, Lilley assumed a value of unity for σ_1 and made σ_3 a function of the local swirl number; he then determined C_R by optimising his predictions of the decay of the maxima of the axial and swirl components of velocity with the experimental data of Chigier and Chervinsky (1967). The recommended function for σ_3 is:

$$\sigma_3 = 1 + 2S_x^{\frac{1}{3}} , \qquad (5.12)$$

where the local swirl number S_x is defined as:

$$S_x = \int_0^\infty \rho V_1 V_3 r^2 \, dr \Big/ r_{0.01} \int_0^\infty (\rho V_1^2 + p - p_\infty) r \, dr ; \qquad (5.13)$$

$r_{.01}$ is the radial distance where V_1 drops to .01 of its maximum value. The constants and function employed by Lilley are summarised in Table 5.2 below; he obtained good predictions of the non-swirling jet, and two swirling jets of swirl numbers 0.2 and 0.4 measured at the orifice, with the same set of parameters.

$C_B = .98$	$C_D = .055$	$C_R = .06$	$C_S = .0397$
$\sigma_k = 1.0$	$\sigma_{k\ell} = 1.0$	$\sigma_1 = 1.0$	$\sigma_3 = 1 + 2S_x^{1/3}$

Table 5.2 Constants for the energy-length turbulence model for the swirling jet

5.4 Conclusions

1. A two-equation, energy-length model of turbulence was developed for swirling boundary layers, and a new term, a body-force term, was introduced to account for the effects of swirl on the turbulence structure. The empirical constants of the model were those found by other workers to result in good agreement between predictions and experimental data over a wide range of conditions, for non-swirling boundary layers. The introduction of the body-force term, and the assumption of non-isotropic viscosity, led to three new additional parameters, C_R, σ_1 and σ_3.

2. For the cylinder flow, the ratio of the effective viscosities was presumed constant, and good predictions were obtained for the entire

flow field under consideration. Two flow conditions were investigated, and a value of 2 was found appropriate for C_R; however, σ_1 had to be adjusted from 3 to 4, and the ratio σ_3/σ_1 from .07 to .15. The degree of variation in these parameters, for two flow conditions of the same geometrical configuration, is not acceptable for a generally applicable model of turbulence.

3. For the free jet, Lilley's predictions of axial and swirl velocity decay compared well with the experimental evidence for a non-swirling jet, and jets with swirl numbers of .2 and .4. He used a single set of parameters; C_R was equal to .06, σ_1 equal to unity, and σ_3 was made a function of the local swirl number.

4. Clearly, for the case of wall-flows, a more sophisticated approach than embodied by the turbulence model tried here is required to procure a satisfactory degree of universality. The principal task is to determine suitably general functions for σ_1 and σ_3 since the anisotropic nature of the turbulence appears to have a larger influence on the flow than the effect of the body-forces.

CHAPTER 6

AN ANISOTROPIC VISCOSITY MIXING-LENGTH BASED MODEL OF TURBULENCE

6.1 Introduction

For the cylinder flow investigated in the preceeding two chapters, the two-equation energy-length model of turbulence gave better predictions of the overall flow distribution than the simpler mixing-length, isotropic viscosity model. However, there were still variations of the order of 50% in the values of the empirical parameters in the energy-length model from one flow condition to another.

The bold assumption that the effective viscosity ratio is a constant is certainly not correct for the majority of swirling flows; its use was justified as a first step in the absence of better information on the cylinder flow. The studies of Lilley and Chigier (1971) and Syred and his co-workers (1971) have established that the ratio of the effective viscosities can vary appreciably, in the range 1 to 30 for swirling jets issuing into stagnant surroundings.

Furthermore, experimental evidence has shown that in three-dimensional non-swirling boundary layers, the assumption that the shear-stress and velocity vectors are parallel in the near-wall region is not in general valid; see for example Johnston (1970) and East (1972). It is reasonable to presume that these two vectors are also not aligned in two-dimensional swirling boundary layers. It seems likely therefore that if a generally applicable model of turbulence is required, attention must be focused on determining the anisotropic nature of the viscosity. In particular, since the transfer processes in the near-wall region have a very pronounced influence on the remainder of the flow, a proper account of the anisotropy of the viscosity in this region is indispensable. Consequently, the main purpose of this chapter is to present and assess a near-wall anisotropic vicosity model of turbulence.

A way of determining the two effective viscosities $\mu_{1,2}$ and $\mu_{2,3}$ from mixing-length expressions modified by van Driest's (1956) damping functions is presented in Section 6.2. Predictions of flow development are compared with the experimental data in Section 6.3; three cases are considered:

1. A cylinder rotating in an axial stream;
2. A disc rotating in stagnant surroundings;
3. A cone rotating in a longitudinal stream.

Section 6.4 summarises the investigations and shows that the near-wall anisotropic viscosity mixing-length based model is capable of accurately predicting the flow configurations mentioned above, with relatively minor adjustments to the empirical constants.

6.2 The Effective Viscosity Formulae

A combination of intuition and computer trials led to the following procedure in which the two effective viscosities are determined from two mixing-length expressions modified by van Driest's (1956) functions:

$$\mu_{1,2} = \mu_\ell + \rho \kappa^2 y^2 \left[1-\exp\left(-y\sqrt{\rho\tau_{1,2}}/26\mu_\ell\right)\right]^2 \left[\left(\frac{\partial V_1}{\partial x_2}\right)^2 + \frac{1}{\sigma_{2,3}}\left(r\frac{\partial (V_3/r)}{\partial x_2}\right)^2\right]^{\frac{1}{2}}, \quad (6.1)$$

$$\mu_{2,3} = \mu_\ell + \rho \kappa^2 y^2 \left[1-\exp\left(-y\sqrt{\rho\tau_{2,3}}/26\mu_\ell\right)\right]^2 \left[\left(\frac{\partial V_1}{\partial x_2}\right)^2 + \frac{1}{\sigma_{2,3}}\left(r\frac{\partial (V_3/r)}{\partial x_2}\right)^2\right]^{\frac{1}{2}}. \quad (6.2)$$

The modifications pertain to the use of the local values of the shear-stress components $\tau_{1,2}$ and $\tau_{2,3}$ in the respective damping functions. It should be noted that if the viscosity ratio $\sigma_{2,3}$, previously defined by equation 4.5 as $\mu_{1,2}/\mu_{2,3}$, is assumed equal to unity, and if the shear-stress components are replaced by the total shear stress, equation 6.1 and 6.2 are identical and revert to the isotropic viscosity model presented in Section 4.2.

Bayley and Owen (1969) and Owen (1969), in their investigation of the radial outflow between a rotor and a stator, are the only other

workers who have employed expressions like those above. However, they used the gradients of individual velocity components instead of the combined gradients of velocity components used here as the term multiplying the damping functions; their approach is described in Section 1.3-1(a) of Appendix 1.

Equations 6.1 and 6.2 are, of course, only valid in the near-wall region; further from the wall, in the wake portion of the boundary layer, the effective viscosities are presumed to be equal. This assumption is quite acceptable since it is the transfer processes in the near-wall region of the boundary layer which have most influence on the rest of the layer. In the outer region the assumed isotropic viscosity is given by equations 4.7 and 4.10; these equations can be rewritten as:

$$\mu_{1,2} = \mu_{2,3} = \mu_\ell + \rho\lambda^2\delta^2 \left[\left(\frac{\partial V_1}{\partial x_2}\right)^2 + \left(r\frac{\partial (V_3/r)}{\partial x_2}\right)^2\right]^{\frac{1}{2}}, \text{ for } \lambda\delta/\kappa < y \leqslant \delta . \qquad (6.3)$$

The combination of expressions 6.1 to 6.3 with the momentum equations forms a closed set from which the viscosity ratio $\sigma_{2,3}$ can be evaluated. In the present solution procedure, the variation of $\sigma_{2,3}$ across the boundary layer is calculated explicitly from the known information about the effective viscosities at the upstream station. This distribution is then used at the downstream station; the error thereby introduced is negligible when the forward-step size is less than 5% of the boundary-layer thickness.

6.3 Comparisons of Predictions with Experimental Data

6.3-1 Cylinder in an Axially-Directed Stream

Predictions for the growth of the axial and circumferential momentum thickness are shown compared with experimental results in Fig. 6.1; the data are those of Parr (1963) and Furuya (1966).

Axial momentum thickness

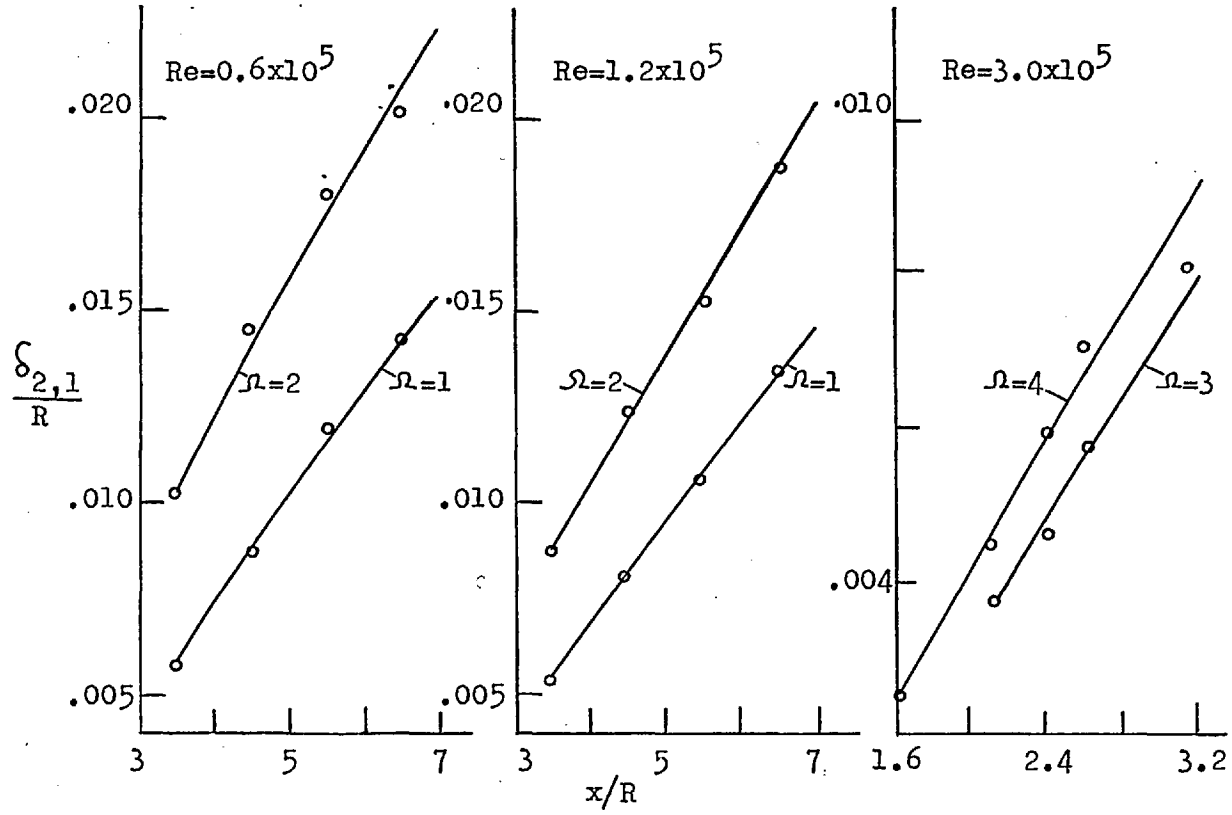

Circumferential momentum thickness

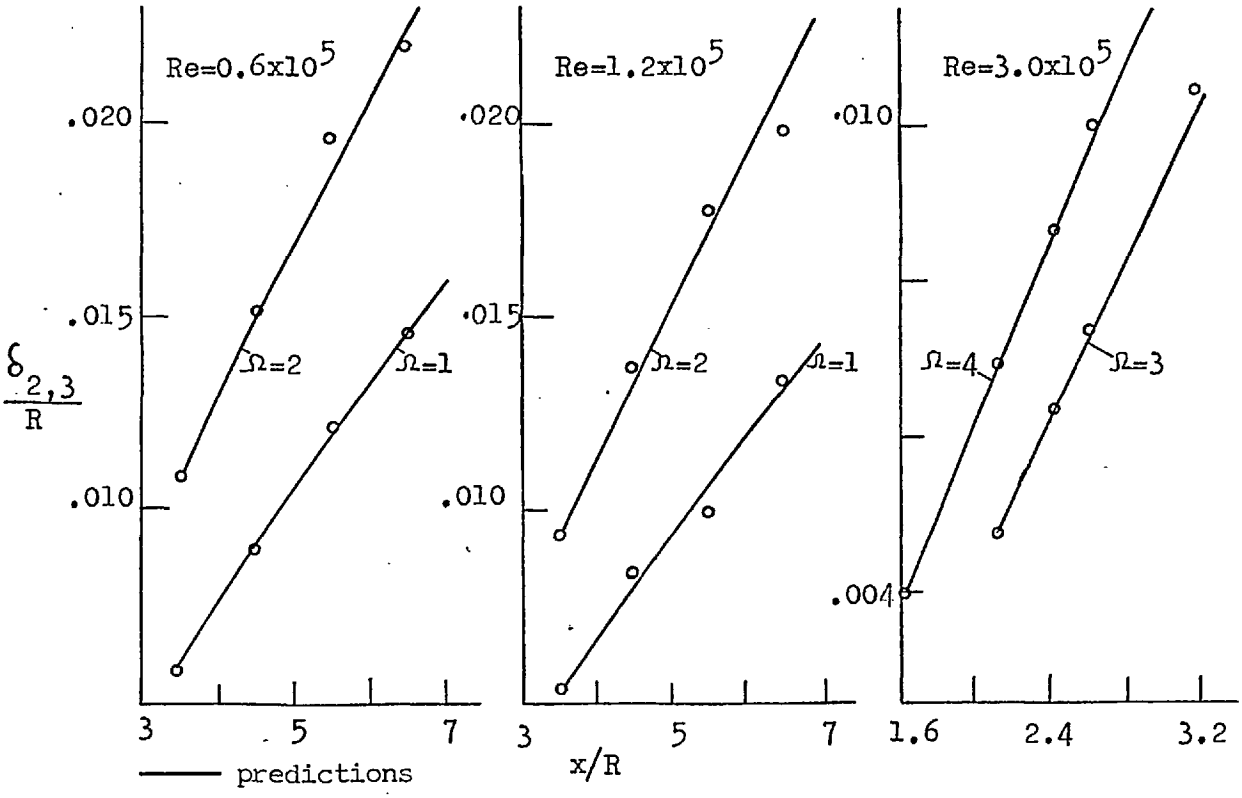

Fig. 6.1 Axial and circumferential momentum thicknesses for the cylinder flow

The values of the constants χ and λ, displayed later in Table 6.1, vary by less than 20% over the complete range of flow conditions considered. The agreement between predictions and data for both momentum thicknesses is very good. Referring back to the predictions obtained with the isotropic viscosity mixing-length, Fig. 4.10 and with the energy-length model, Fig. 5.1, the enhanced universality of the present model is evident.

Fig. 6.2 shows the predicted near-wall distribution of the viscosity ratio $\sigma_{2,3}$; its departure from unity is considerable. There exists no experimental information from which $\sigma_{2,3}$ can be deduced for the cylinder flow; however, the variation of $\sigma_{2,3}$ across the sublayer is acceptable in so far as it results in excellent agreement between the predictions and the measurements of velocity field.

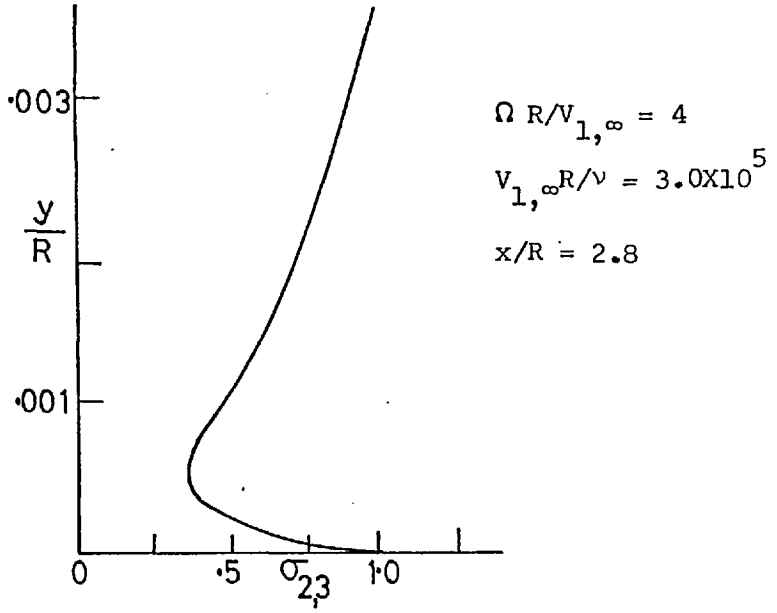

Fig. 6.2 Viscosity ratio in the sublayer for the cylinder flow

6.3-2 Disc in Stagnant Surroundings

The flow induced by a disc rotating in stagnant surroundings was predicted in Section 4.3 using the isotropic viscosity mixing-length model. The average circumferential drag variation with rotational Reynolds number, the development of shape factor, and

entrainment of fluid into the boundary layer, were all well predicted with a single set of constants: $\kappa = 0.42$ and $\lambda = 0.085$. These computations were repeated with the anisotropic viscosity mixing-length model, and the predictions are compared with the experimental measurements of Theodorsen and Regier (1944), Owen (1969), and Cham and Head (1969) in Fig. 6.3, 6.4 and 6.5 below.

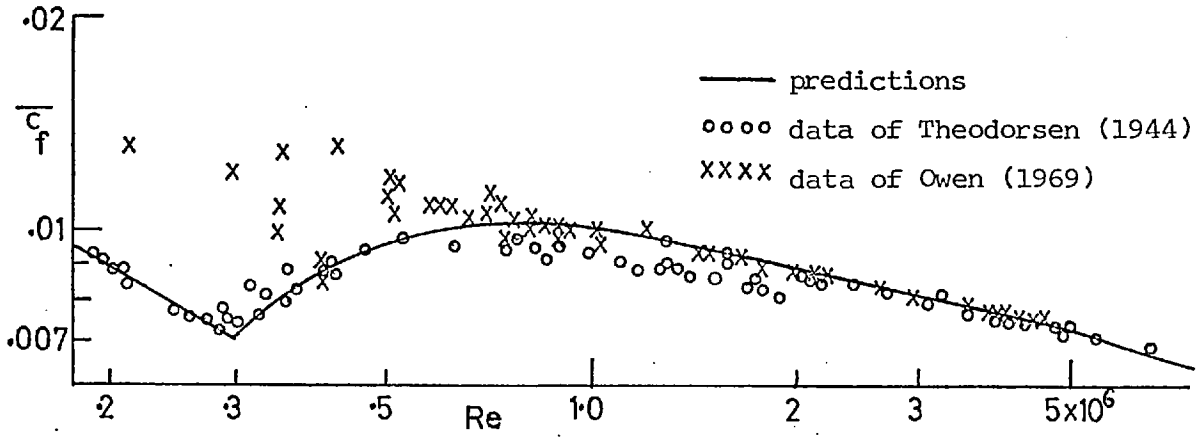

Fig. 6.3 Average circumferential drag for disc

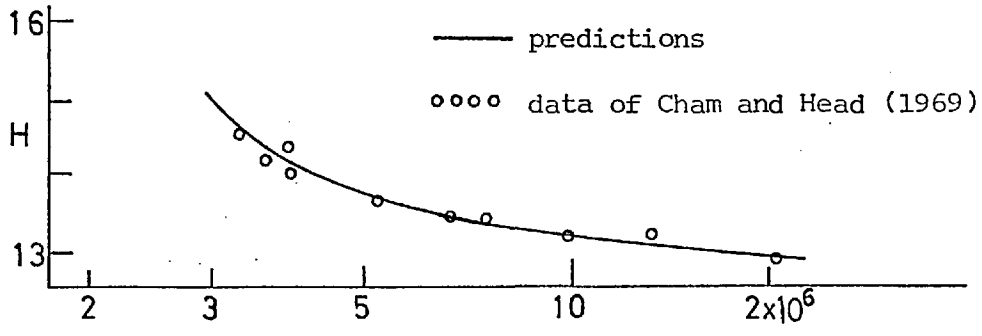

Fig. 6.4 Development of shape factor for disc

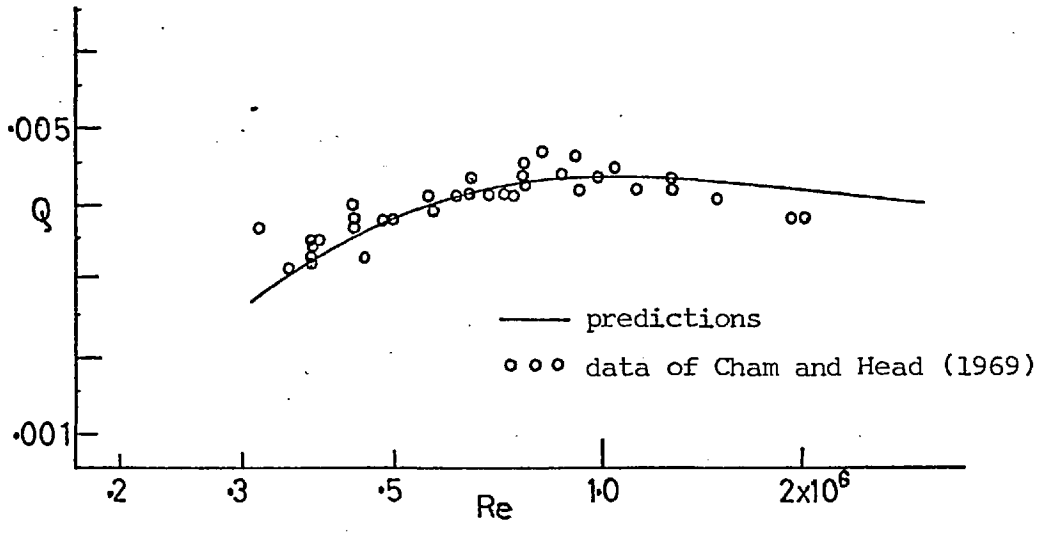

Fig. 6.5 Radial volumetric flow rate for disc

The optimum values found for κ and λ to give best agreement between predictions and experimental data were 0.34 and 0.085. The former value is surprisely low compared with the values of κ found appropriate for the cylinder flow and also with those suitable for non-swirling boundary layers, usually between 0.40 and 0.45. It may be that a relatively small adjustment to the van Driest damping constant would result in a more usual value of κ being appropriate. It was preferred, however, in the present predictions to adjust only κ and λ with the damping constant fixed at its accepted 'flat-plate' value of 26.

The computed variation of $\sigma_{2,3}$ in the near-wall region is shown in Fig. 6.6 and it is seen to depart substantially from unity. Yet good predictions of the disc flow are possible with mixing-length formulations which presume an isotropic viscosity all the way to the wall; see Chapter 4 and also Cooper (1971). The reason must be that since the circumferential component of velocity is much larger than the radial one, the flow is akin to a two-dimensional plane flow in that it is dominated by one shear stress, the circumferential one in this case.

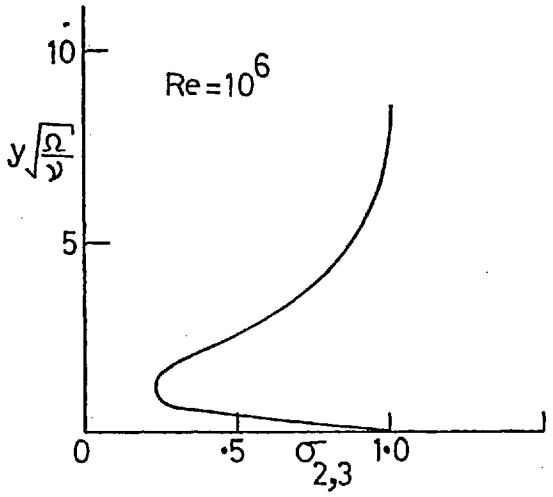

Fig. 6.6 Viscosity ratio in the sublayer for the disc flow

6.3-3 Cone in Longitudinal Stream

It was stated in Chapter 1 that the survey of previous experimental work revealed a lack of data for the turbulent mean velocity field near a rotating cone. It was therefore decided that an experimental investigation of the mean velocity field would be a useful contribution to the data on swirling boundary layers near walls, especially for assessing the generality of turbulence models.

Mean velocity measurements were therefore made for the configuration shown in Fig. 6.7. The cone rotated in stagnant surroundings and had provision for injection from an annular slot near its apex; the experimental apparatus and procedure are described in Appendix 5. Data were collected for a variety of rotational speeds, slot heights, and mass injection rates. Representative predictions, based on the anisotropic viscosity mixing-length model, of the growth of the axial and circumferential boundary layers, and the decay of axial velocity profiles are shown in Fig. 6.8 and Fig. 6.9 for three sample experimental conditions.

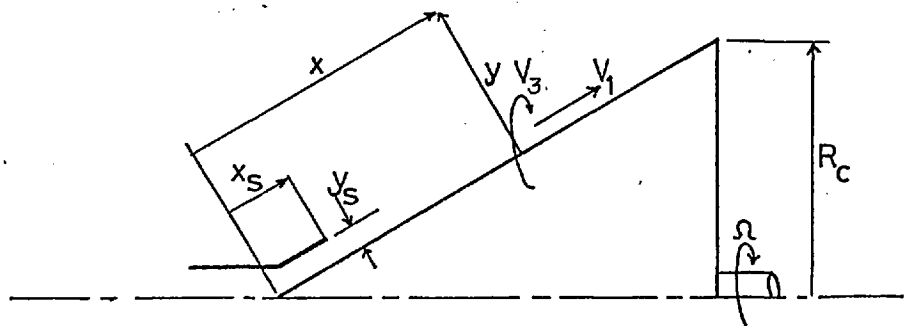

Fig. 6.7 Cone rotating in longitudinal stream

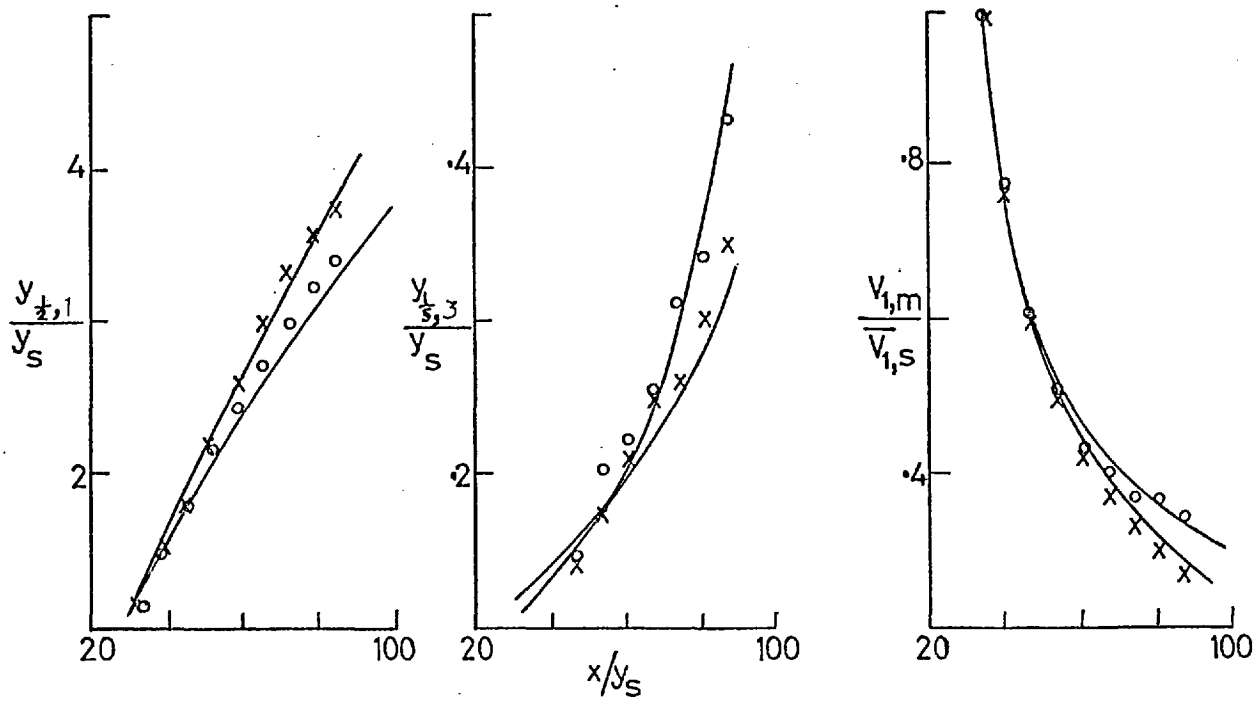

y_s = .00381 m, x_s = .094 m, $\overline{V}_{1,s}$ = 13.5 m/s.

XXXX Data for Ω = 562.5 rpm, ——— predictions with χ = .42, λ = .10.

oooo Data for Ω = 1111 rpm, ——— predictions with χ = .42, λ = .09.

Fig. 6.8 Comparisons of predictions with experimental data for a rotating cone with slot injection.

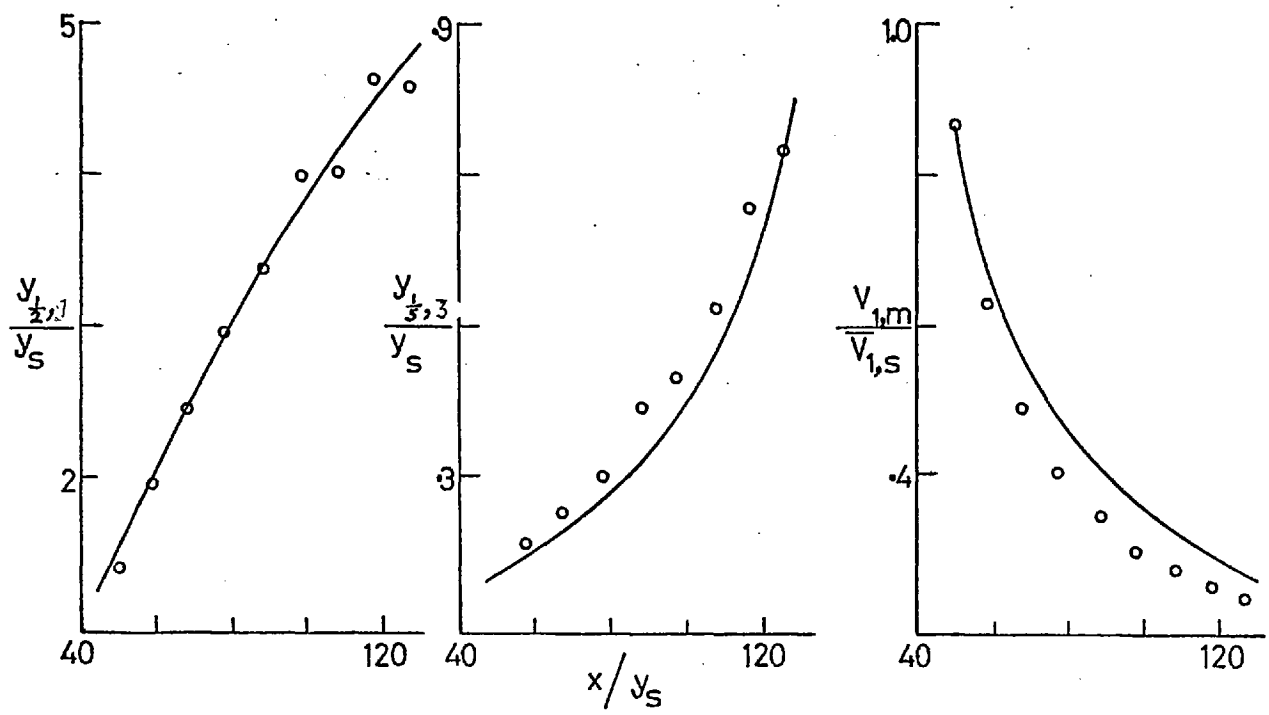

y_s = .00259 m, x_s = .0955 m, $\bar{V}_{1,s}$ = 17.0 m/s.

oooo Data for Ω = 1111 rpm.

——— Predictions with $\varkappa$ = .46, λ = .09.

Fig. 6.9 Comparisons of predictions with experimental data for a rotating cone with slot injection.

Fairly good predictions are obtained; the appropriate values of the constants are given in Table 6.1. The maximum variation in both $\varkappa$ and λ is about 10%. The influence of an increase in $\varkappa$ and λ on the axial and circumferential boundary layer growths, and on the axial velocity decay, is illustrated in Fig. 6.10 below for one of the experimental conditions. It is seen that the influence of λ is largest on the axial growth, while the influence of $\varkappa$ is most felt by the growth of the circumferential velocity profile. The decay of maximum axial velocity is hardly affected.

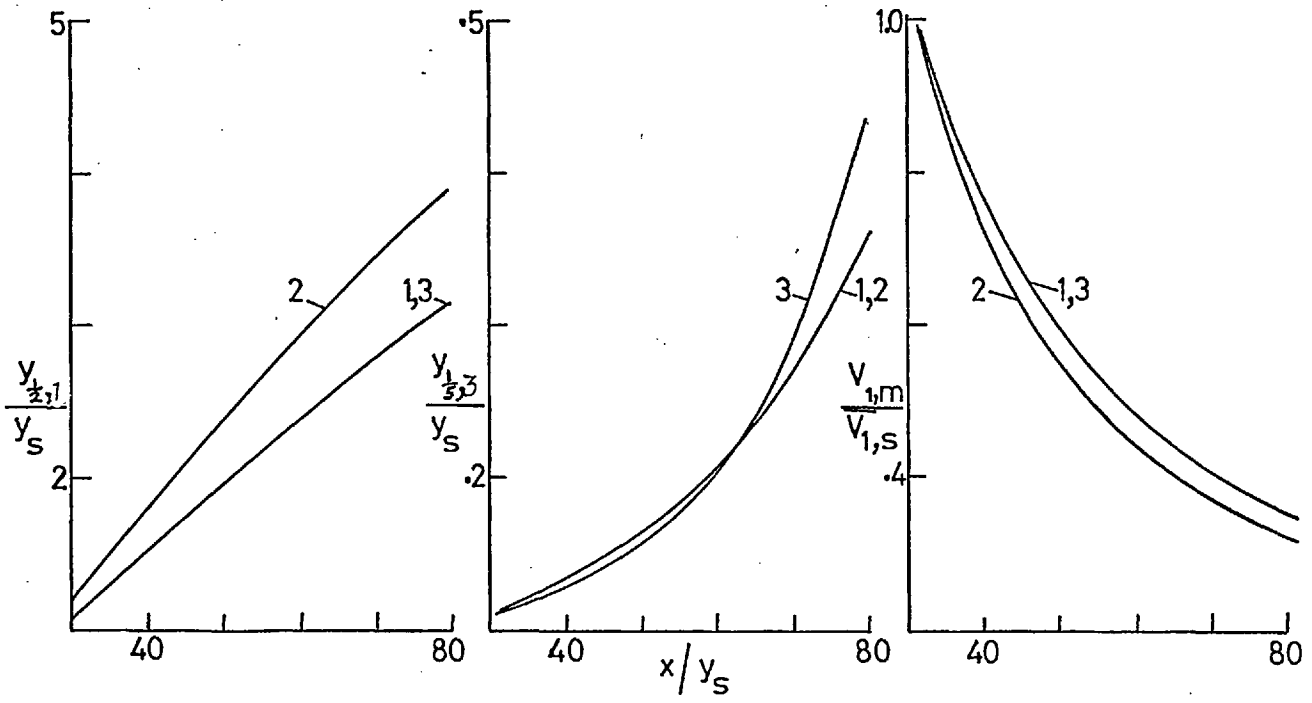

y_s = .00381m, x_s = .094m, $\overline{V}_{1,s}$ = 13.6m/s, Ω = 1111 rpm.

	1	2	3
χ	.42	.42	.50
λ	.09	.11	.09

Fig. 6.10 Influence of mixing-length constants on the mean velocity field for the cone flow

Two typical predictions of the variation of the viscosity ratio across the sublayer are shown in Fig. 6.11. A significant departure from unity is again displayed in the near-wall region, and $\sigma_{2,3}$ is revealed to be strongly dependent on the degree of swirl.

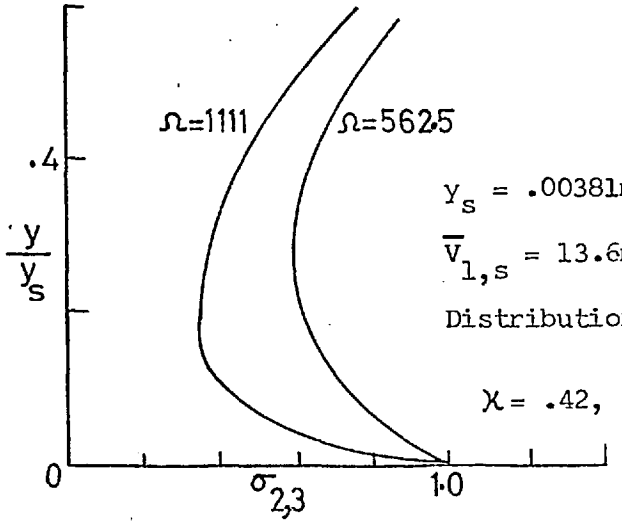

y_s = .00381m, x_s = .094m,
$\overline{V}_{1,s}$ = 13.6m/s.
Distribution of $\sigma_{2,3}$ at x/y_s = 60.
χ = .42, λ = .09.

Fig. 6.11 Viscosity ratio in the sublayer for the cone flow

6.4 Conclusions

1. In summary, although the present anisotropic viscosity mixing-length based model of turbulence required some adjustments of $\varkappa$ and λ to cope with the range of experimental conditions considered, the model nonetheless exhibited a fairly satisfactory level of universality. It is substantially more general than the isotropic mixing-length model and energy-length model considered previously. The values of $\varkappa$ and λ for the three flow configurations investigated are tabulated below.

Flow configurations				$\varkappa$	λ	Experimental reference
Cylinder	$\Omega R^2/\nu$	$\Omega R/V_{1,\infty}$				
	0.6×10^5	1		.45	.10	Furuya and co-workers (1966)
	0.6×10^5	2		.47	.10	
	1.2×10^5	1		.47	.10	
	1.2×10^5	2		.50	.10	
	3.0×10^5	3		.435	.115	Parr (1963)
	3.0×10^5	4		.425	.085	
Disc				.34	.085	Theodorsen and Regier (1944); Owen (1969); Cham and Head (1969)
Cone	y_s/R_c	$\Omega R_c^2 \sin\alpha/\nu$	$\overline{V}_{1,s}/\Omega R_c$			
	.0166	1.30×10^6	1.0	.42	.10	Appendix 5
	.0166	2.56×10^6	.51	.42	.09	
	.0113	2.56×10^6	.64	.46	.09	

Table 6.1 Optimum values of the mixing-length constants for the anisotropic viscosity model for several flow configurations

2. In the sublayer, for all the cases investigated, the viscosity ratio $\sigma_{2,3}$ differed substantially from unity. The velocity vector in this region 'twists', relative to the shear-stress vector and they do not act in the same direction as implied by isotropic viscosity assumptions.

3. Admitedly, the model presented here is not based on extensive physical reasoning, but is a result of intuition and trials. However, two aspects of the results are worthy of note. First, the model is simple and sufficiently general to be of immediate practical use to design engineers who are interested in the calculation of swirling boundary layers near rotating bodies. Second, the results positively indicate that attention must be focused on the near-wall region where $\sigma_{2,3}$ is not close to unity. If the goal of universal application and truly unified treatment is to be attained, the behaviour of the two effective viscosities, implicitly the two main Reynolds shear stresses $-\rho\,\overline{v_1 v_2}$ and $-\rho\,\overline{v_2 v_3}$, in the near-wall region must be comprehensively investigated.

CHAPTER 7

AN ALGEBRAIC REYNOLDS STRESS MODEL OF TURBULENCE

7.1 Introduction

The turbulence models considered in the previous three chapters employed the concept of turbulent viscosity to relate the Reynolds stresses to the time-average properties of the flow, namely:

$$-\rho\overline{v_i v_j} \equiv \mu_t \left(\frac{\partial V_i}{\partial x_j}\right) \quad , \qquad (7.1)$$

where the subscript i denotes either the streamwise or circumferential direction, and j denotes the cross-stream direction. The turbulent viscosity μ_t was calculated from extensions of the mixing-length hypothesis, and from a two-equation energy-length model. For all the flows considered, the viscosity was found to be anisotropic, and that the anisotropy is particularly important in the near-wall region. This vectorial nature of the turbulent viscosity has also been experimentally demonstrated; for example, the measurements of Reynolds stresses and velocity distribution by Syred, Beer and Chigier (1971) of a swirling recirculating flow, have indicated that the implied value of the turbulent viscosity varies with direction by several orders of magnitude.

In the present chapter, the anisotropic nature of the viscosity is determined from an analysis of the differential (transport) equations for the Reynolds stresses themselves. The present approach lies between the two-equation energy-length model with an algebraic relation for the viscosity ratio, and the seven-equation kind of model where all six Reynolds stresses and a length-scale are calculated from differential equations. In short, transport equations are solved for the energy and length-scale, but the Reynolds stresses are expressed

in terms of implicit algebraic relations derived under certain assumptions from their own transport equations. This approach combines the economical advantage of solving only two differential equations for turbulence quantities with the improved generality obtained from employing the algebraic relations for the Reynolds stresses; it will subsequently be referred to herein as the algebraic stress model of turbulence.

The algebraic stress relations are derived from an analysis of the transport equations for the Reynolds stresses themselves. This treatment owes its origin to the discussions of Prandtl and Weighardt (1945), Chou (1945), and Rotta (1951). Hanjalic and Launder (1972) and du P. Donaldson (1972) have recently proposed and tested turbulence models of this variety for two-dimensional, non-swirling boundary layers. The first two authors solve differential equations for the turbulence kinetic energy, turbulence dissipation rate, and the Reynolds stress $-\rho\overline{v_1 v_2}$; the third author and his colleagues solve differential equations for the turbulence energy and $-\rho\overline{v_1 v_2}$, but they employ an algebraic formulation for the energy dissipation rate. The extension of this type of procedure to swirling boundary layers represents the primary purpose of this chapter.

The equations for the Reynolds stresses, also called double velocity correlations, are presented in Section 7.2. The Cartesian forms of the equations are first introduced and discussed, followed by a derivation of the equations in curvilinear orthogonal coordinates. The boundary layer forms of these last equations are then determined, and they are subsequently reduced to algebraic equations in Section 7.3 through the modelling of the convection, diffusion, pressure-strain and dissipation terms. The turbulence energy equation is also derived and the length-scale equation presented in Section 7.3.

In Section 7.4, comparisons are made between experimental measurements and predictions obtained from the algebraic stress model. Both free flows and wall flows are considered; namely: a swirling jet issuing into stagnant surroundings, a cylinder rotating in an axial stream, and a disc rotating in free surroundings. The outcome of these studies is discussed in Section 7.5.

7.2 Transport Equations for the Double Velocity Correlations

7.2-1 Equations in Cartesian Coordinates

It is both necessary and instructive to consider here the Cartesian-coordinate form of the exact equation for the double velocity correlations; see for example Hinze (1959):

$$\underbrace{V_k \frac{\partial \overline{v_i v_j}}{\partial x_k}}_{\text{convection}} = \underbrace{-\frac{\partial}{\partial x_k}\left[\overline{v_i v_j v_k} + \left(\delta_{jk}\overline{v_i} + \delta_{ik}\overline{v_j}\right)\frac{\overline{p'}}{\rho} - \nu \frac{\partial \overline{v_i v_j}}{\partial x_k}\right]}_{\text{diffusion}} - \underbrace{\left[\overline{v_i v_k}\frac{\partial V_j}{\partial x_k} + \overline{v_j v_k}\frac{\partial V_i}{\partial x_k}\right]}_{\text{production}} + \underbrace{\left[\frac{\overline{p'}}{\rho}\left(\frac{\partial v_i}{\partial x_j} + \frac{\partial v_j}{\partial x_i}\right)\right]}_{\text{pressure-strain}} - \underbrace{2\nu\left[\frac{\partial v_i}{\partial x_k}\frac{\partial v_j}{\partial x_k}\right]}_{\text{dissipation}} \cdots \tag{7.2}$$

The transport of the double velocity correlations is governed by convection and turbulent viscous diffusion due to inhomogeneties in the flow field, by energy transfer from the main motion through the turbulence shear stresses, by energy redistribution due to the correlations between the pressure fluctuations and the derivatives of the velocity fluctuations, and finally by viscous dissipation. The terms representing each of these physical processes have been classified into distinct groups in equation 7.2.

The origin of these groups of terms can be traced if one considers the parents: the Navier-Stokes equations; for incompressible flow these latter equations, Aris (1962), are:

$$\underbrace{(V\cdot\nabla)V}_{1} = \underbrace{-\frac{1}{\rho}\nabla p}_{2} + \underbrace{\nu\nabla^2 V}_{3} \quad , \tag{7.3}$$

where 1, 2 and 3 represent the convection, pressure, and viscous diffusion effects. When equation 7.2 is compared with 7.3 some

important facts emerge regarding the Navier-Stokes parentage of the terms appearing in the double-velocity correlations equation. Term 1 of the Navier-Stokes equation gives rise to terms which express convection, diffusion and production of the double-velocity correlations; term 2 leads to pressure diffusion and pressure-strain terms; while term 3 leads to diffusion and viscous dissipation terms.

Equation 7.2 has introduced two new and unknown variables, the pressure fluctuation p', and the triple-velocity correlation $\overline{v_i v_j v_k}$. A differential equation for the triple correlation will give rise to a fourth order correlation and so on. Equation 7.2 is therefore not soluble in its present form. Most authors have chosen to model the diffusion, pressure-strain, and dissipation in terms of known quantities, namely the time-average velocity-components, the double correlations themselves, the turbulence energy and the energy dissipation rate. The modelled form of equation 7.2 can be symbolically expressed as:

$$V_k \frac{\partial \overline{v_i v_j}}{\partial x_k} + \left[\overline{v_i v_k} \frac{\partial V_j}{\partial x_k} + \overline{v_j v_k} \frac{\partial V_i}{\partial x_k} \right] = \text{Modelled [Diffusion, Pressure-strain, Dissipation]}. \qquad (7.4)$$

7.2-2 Equations in Curvilinear Orthogonal Coordinates

For the coordinate system illustrated in Fig. 2.1 of Chapter 2, the equations for the double-velocity correlations are required in curvilinear orthogonal forms. Rodi (1970) has performed a term by term transformation of the correlations from Cartesian to cylindrical coordinates; however, for the more general curvilinear orthogonal system such transformations are not straightforward and are usually very lengthy. A simpler route is to start directly from the Navier-Stokes equations as outlined by Hinze (1959), and used by Wislicenus and Yeh (1952) in order to derive the equations in cylindrical coordinates.

The derivation of the double-velocity correlations from the Navier-Stokes equations in curvilinear orthogonal coordinates is presented in Appendix 6. The constituent terms of the diffusion, pressure-strain, and dissipation are not formally determined; these three transport processes are instead modelled in Section 7.3 below in terms of known quantities. Consequently, only term 1 of the Navier-Stokes equation is analysed to yield the convection and production terms:

$$\frac{V_k}{\ell_k}\frac{\partial \overline{v_i v_j}}{\partial x_k} + \frac{V_k}{\ell_k}\left[\overline{v_i v_j}\left(\frac{\partial \ell_i}{\ell_i \partial x_k} + \frac{\partial \ell_j}{\ell_j \partial x_k}\right) - 2\left(\overline{v_i v_k}\frac{\partial \ell_k}{\ell_j \partial x_j} + \overline{v_j v_k}\frac{\partial \ell_k}{\ell_i \partial x_i}\right)\right] + \overline{v_i v_k}\frac{\partial (\ell_j V_j)}{\ell_j \ell_k \partial x_k} + \overline{v_j v_k}\frac{\partial (\ell_i V_i)}{\ell_k \ell_i \partial x_k}$$

= Modelled [Diffusion + Pressure-strain + Dissipation]; (7.5)

the ℓ's are the metric coefficients, and equation 7.5 must be summed for k = 1, 2 and 3 for each of the six values of $\overline{v_i v_j}$. It should be noted this equation reduces to its Cartesian coordinates form, equation 7.4, when the metric coefficients are all equal to unity.

7.2-3 Boundary-Layer Forms of the Equations

For the class of boundary layers considered here, that is, flow near discs, cones and cylinders, and free jets, the metric coefficients ℓ_1 and ℓ_2 of equation 7.5 are equal to unity. The coefficient ℓ_3 is equivalent to the distance r from the axis of symmetry, x_3 being the circumferential coordinate. After invoking the boundary layer assumptions, with x_1 and x_2 corresponding to the mainstream and cross-stream coordinates, (see Sections 3 and 4 of Appendix 6), there result the following equations for the double correlations:

$$V_1\frac{\partial\overline{v_1^2}}{\partial x_1}+V_2\frac{\partial\overline{v_1^2}}{\partial x_2}=4\frac{V_3}{r}\overline{v_1v_3}\frac{\partial r}{\partial x_1}-2\overline{v_1v_2}\frac{\partial V_1}{\partial x_2}+(Df+Ps+D)_{1,1} \quad (7.6)$$

$$V_1\frac{\partial\overline{v_2^2}}{\partial x_1}+V_2\frac{\partial\overline{v_2^2}}{\partial x_2}=4\frac{V_3}{r}\overline{v_2v_3}\frac{\partial r}{\partial x_2}+(Df+Ps+D)_{2,2} \quad (7.7)$$

$$V_1\frac{\partial\overline{v_3^2}}{\partial x_1}+V_2\frac{\partial\overline{v_3^2}}{\partial x_2}=-4\frac{V_3}{r}\overline{v_1v_3}\frac{\partial r}{\partial x_1}-4\frac{V_3}{r}\overline{v_2v_3}\frac{\partial r}{\partial x_2}-2\overline{v_2v_3}r\frac{\partial(V_3/r)}{\partial x_2}+(Df+Ps+D)_{3,3} \quad (7.8)$$

$$V_1\frac{\partial\overline{v_1v_2}}{\partial x_1}+V_2\frac{\partial\overline{v_1v_2}}{\partial x_2}=-\overline{v_2^2}\frac{\partial V_1}{\partial x_2}+2\frac{V_3}{r}\overline{v_2v_3}\frac{\partial r}{\partial x_1}+2\frac{V_3}{r}\overline{v_1v_3}\frac{\partial r}{\partial x_2}+(Df+Ps+D)_{1,2} \quad (7.9)$$

$$V_1\frac{\partial\overline{v_1v_3}}{\partial x_1}+V_2\frac{\partial\overline{v_1v_3}}{\partial x_2}=-\overline{v_1v_2}r\frac{\partial(V_3/r)}{\partial x_2}-\overline{v_2v_3}\frac{\partial V_1}{\partial x_2}-2\overline{v_1v_2}\frac{V_3}{r}\frac{\partial r}{\partial x_2}-2\frac{V_3}{r}(\overline{v_1^2}-\overline{v_3^2})\frac{\partial r}{\partial x_1}+(Df+Ps+D)_{1,3} \quad (7.10)$$

$$\underbrace{V_1\frac{\partial\overline{v_2v_3}}{\partial x_1}+V_2\frac{\partial\overline{v_2v_3}}{\partial x_2}}_{\text{I}}=\underbrace{-\overline{v_2^2}r\frac{\partial(V_3/r)}{\partial x_2}-2(\overline{v_2^2}-\overline{v_3^2})\frac{V_3}{r}\frac{\partial r}{\partial x_2}-2\overline{v_1v_2}\frac{V_3}{r}\frac{\partial r}{\partial x_1}}_{\text{II}}+\underbrace{(Df+Ps+D)_{2,3}}_{\text{III}} \quad (7.11)$$

where the symbols stand for:

Df diffusion;

Ps pressure-strain;

D dissipation;

I convection terms arising from term 1 of equation 7.2;

II production terms arising from term 1 of equation 7.2;

III diffusion (velocity, pressure, viscous), pressure-strain, and dissipation effects arising from terms 1, 2 and 3 of equation 7.2.

The following sections of the text describe the restrictions accepted and the assumptions made in order to model the dissipation, pressure-strain, and diffusion transport processes, and consequently simplify the stress equations to a practically useful form.

7.3 The Algebraic Stress Equations

7.3-1 Dissipation

It is the small scale eddies which are primarily responsible for the turbulence dissipation. In the regions of the flow where the local turbulence Reynolds number is high, these eddies are isotropic even though there may be anisotropy in the larger scales of motion.

Consequently, the dissipation is expressed as (see Hinze (1959) or Hanjalic and Launder (1972)):

$$D_{ij} = -\frac{2}{3}\delta_{ij}\varepsilon \quad , \qquad (7.12)$$

where δ_{ij} in the Kronecker delta, and ε is the total dissipation rate of turbulence kinetic energy.

7.3-2 Pressure-strain

The pressure rate-of-strain correlations $P_{s_{i,j}}$ arise from two physical sources: the mutual interaction of the fluctuating velocities, and the interaction of the mean rate of strain with the turbulence, Hinze (1959). The effect of the pressure-strain terms is to transfer energy from the higher-intensity to the lower-intensity normal stress components.

Most authors have adopted Rotta's (1951) proposal to model the first-mentioned part of the correlation, and the same practice is followed here. Rotta has also proposed an approximation for the second-mentioned part, as have Hanjalic and Launder (1972), and Naot, Shavit and Wolfshtein (1970). None of these has however been much tested, so the formulation of the latter authors is employed here because of its simplicity. The full form of the pressure-strain model is therefore:

$$P_{s_{i,j}} = -\underbrace{C_1 \frac{\varepsilon}{k}\left(\overline{v_i v_j} - \frac{2}{3}k\delta_{ij}\right)}_{\text{Rotta (1951)}} - \underbrace{C_2\left(P_{i,j} - \frac{2}{3}P_k\delta_{ij}\right)}_{\text{Naot (1970)}} \quad , \qquad (7.13)$$

where $P_{i,j}$ represents the production terms of equations 7.6 to 7.11, and P_k stands for the production of turbulence energy.

It should be remarked that the main source of doubt in current turbulence-modelling practice is associated with lack of knowledge about adequate, let alone accurate representation of the pressure-strain correlation, especially for the second part, even for non-swirling flow.

7.3-3 Convection and Diffusion

The differential nature of equations 7.6 to 7.11 can be very conveniently eliminated by extending the modelling one stage further through the adoption of a further, and not unreasonable, suggestion of Rodi (1973) that the local convection less the diffusion of a double velocity correlation $\overline{v_i v_j}$ is proportional to the convection less the diffusion of turbulence kinetic energy k in the ratio $\overline{v_i v_j}/k$. This approximation permits equations 7.6 to 7.11 to be represented by:

$$\left(P_k - \varepsilon\right) \overline{v_i v_j}/k = \left(P + P_s + D\right)_{i,j} \quad , \qquad (7.14)$$

where it has been recognised that the convection minus the diffusion of k is equal to the production minus the dissipation of k.

7.3-4 The Algebraic Stress Equations

When the modelled expressions 7.12 and 7.13 are inserted in equation 7.14, there results an algebraic equation for the double velocity correlations:

$$\overline{v_i v_j} = \left[\frac{k}{P_k + \varepsilon\left(C_1 - 1\right)}\right]\left[\frac{2}{3}\left\{C_2 P_k + \varepsilon\left(C_1 - 1\right)\right\}\delta_{ij} + \left(1 - C_2\right)P_{i,j}\right] \quad . \qquad (7.15)$$

It is convenient to write this equation in the concise form:

$$\overline{v_i v_j} = \frac{1}{\gamma_1}\left[\gamma_2 \delta_{ij} + P_{i,j}\right] \quad ; \qquad (7.16)$$

the expressions corresponding to γ_1 and γ_2 are evident.

The stress production terms $P_{i,j}$ are the corresponding ones of equations 7.6 to 7.11 and they are expressed wholly in terms of the stresses themselves and known mean-flow quantities. Consequently, closure of the set of stress equations necessitates only the additional knowledge of the production P_k and the dissipation rate ε

of the turbulence energy. This information is obtained by solving the transport equation for k, defined as half the sum of the normal stresses, and the equation for ϵ.

The dissipation ϵ, from dimensional arguments, can be expressed in terms of a length-scale ℓ which is proportional to the energy containing eddies; namely:

$$\varepsilon = C_D k^{\frac{3}{2}} \ell^{-1} \quad , \tag{7.17}$$

where C_D is a further constant to be determined. Now, since an equation for k is solved, it is clearly not necessary to solve an equation for ϵ itself; any variable of the form $k^a \epsilon^b$ or $k^a \ell^b$ will be suitable. Thus, for non-swirling boundary layers, Hanjalic and Launder (1972) chose to solve an equation for ϵ itself, while Rodi and Spalding (1970) and Ng and Spalding (1972) have preferred an equation for the energy-length-scale product $k\ell$. The latter approach is adopted in the present work.

7.3-5 The Turbulence Energy Equation

The transport equation for the kinetic energy of turbulence has already been employed together with an equation for $k\ell$ in Chapter 5. This equation for k is obtained from the summation of equation 7.6 to 7.8 for the three normal stresses, and division by two:

$$\underbrace{V_1 \frac{\partial k}{\partial x_1} + V_2 \frac{\partial k}{\partial x_2}}_{\text{convection}} = \underbrace{-\left(\overline{v_1 v_2} \frac{\partial V_1}{\partial x_2} + \overline{v_2 v_3}\, r \frac{\partial (V_3/r)}{\partial x_2} \right)}_{\text{production}} + \underbrace{\mathcal{D}F_k}_{\text{diffusion}} + \underbrace{\mathcal{D}_k}_{\text{dissipation}} \quad . \tag{7.18}$$

It should be noted that the troublesome pressure-strain terms vanish from the equation for the turbulence kinetic energy.

Following the practice suggested by Spalding and his co-workers (see for example Launder and Spalding (1972)) for non-swirling

two-dimensional boundary layers, it is presumed that the diffusion of k obeys a gradient-type law:

$$Df_k = \frac{1}{r}\frac{\partial}{\partial x_2}\left(r\frac{k^{\frac{1}{2}}\ell}{\sigma_k}\frac{\partial k}{\partial x_2}\right), \qquad (7.19)$$

where σ_k is a parameter which is close to unity.

The dissipation of k, which is half the sum of the dissipation of the normal stresses, is from equation 7.12 simply equal to $-\varepsilon$. With the diffusion and dissipation terms so modelled, the final form of the equation for k is:

$$\underbrace{V_1\frac{\partial k}{\partial x_1}+V_2\frac{\partial k}{\partial x_2}}_{\text{convection}} = \underbrace{-\left(\overline{v_1v_2}\frac{\partial V_1}{\partial x_2}+\overline{v_2v_3}\,r\frac{\partial(V_3/r)}{\partial x_2}\right)}_{\text{production}} + \underbrace{\frac{1}{r}\frac{\partial}{\partial x_2}\left(r\frac{k^{\frac{1}{2}}\ell}{\sigma_k}\frac{\partial k}{\partial x_2}\right)}_{\text{diffusion}} \underbrace{-\varepsilon}_{\text{dissipation}}. \qquad (7.20)$$

7.3-6 The Energy-Length-Scale Equation

As mentioned earlier, an equation for the energy-length-scale product $k\ell$ is solved in place of an equation for the dissipation. This equation was originally proposed by Rotta (1951) and subsequently used by Rodi and Spalding (1970) and Ng and Spalding (1972) in calculating two-dimensional non-swirling boundary layers. The form of Rotta's equation in curvilinear orthogonal coordinates is:

$$\underbrace{V_1\frac{\partial k\ell}{\partial x_1}+V_2\frac{\partial k\ell}{\partial x_2}}_{\text{convection}} = \underbrace{\frac{1}{r}\frac{\partial}{\partial x_2}\left[r\frac{k^{\frac{1}{2}}\ell}{\sigma_{k\ell}}\frac{\partial k\ell}{\partial x_2}\right]}_{\text{diffusion}} \underbrace{-C_3\ell\left[\overline{v_1v_2}\frac{\partial V_1}{\partial x_2}+\overline{v_2v_3}\,r\frac{\partial(V_3/r)}{\partial x_2}\right]}_{\text{production}} \underbrace{-C_s k^{\frac{3}{2}}}_{\text{dissipation}} \underbrace{-C_w\left[\kappa C_D^{\frac{1}{4}}y\ell^{-1}\right]^{-C_{\ell}}k^{\frac{3}{2}}}_{\text{wall-damping}}. \qquad (7.21)$$

Following the practice for the k equation, the diffusion transport is again represented by a gradient-type law with the exchange coefficient equal to $k^{\frac{1}{2}}\ell/\sigma_{k\ell}$. The wall-damping term was proposed by Ng and Spalding (1972) and found by these authors to result in much improved predictions for boundary layers close to stationary walls. This term is, of course, absent for the case of free flows.

7.3-7 The Empirical Constants

The complete turbulence model comprising the six algebraic stress relations represented by equation 7.15, along with equations 7.20 and 7.21 for k and $k\ell$, contains 10 empirical constants:

$$C_1,\ C_2,\ C_B,\ C_S,\ C_D,\ C_W, C_q,\ \kappa\ ,\ \sigma_k,\ \sigma_{k\ell}.$$

The model is used to predict the free swirling jet and rotating cylinder test flows, and the values assigned to the constants are given in Table 7.1 below, along with those established by other workers for non-swirling flows. It is seen that, apart for C_2, the present choice of values for the constants has been guided by those values found by others to give good predictions for related, but non-swirling flows. It should also be noted that some of the constants are common to the present model and to the energy-length model developed in Chapter 5. Unfortunately, even without swirl, changes in the constants between the wall flows and the round-jet flow are required as Table 7.1 reveals. At best, one might hope that the introduction of swirl would not give rise to any further lack of universality; whatever the case, the non-swirling flow constants are the only available indication of the starting point for swirl-flow computations.

The constant C_2, which appears in the model for the second part of the pressure-strain terms was, on the basis of tentative evidence, assigned the value 0.8 by the proposers of the model, Naot, Shavit and Wolfshtein (1970). Because of the uncertainty of the model, this parameter is allowed in the present work to assume either of two values $C_{2,n}$ and $C_{2,t}$, depending on whether it occurs in an equation for a normal or a tangential double correlation. Both values have been determined by comparing predictions with experimental data. They turn out to be rather closer to the value 0.4 which Rodi (1973) has recently found applicable to non-swirling jets,

than to 0.8. The assigning of two values to C_2 is an unappealing feature of the present turbulence model, but is represents a useful stop-gap measure in the absence of better knowledge for the simulation of the pressure-strain terms.

	C_1	C_2	C_B	C_S	C_D	σ_k	$\sigma_{k\ell}$	C_W	C_q	κ
Wall flows without swirl[a]										
Ng and Spalding (1972)			.84	.055	.10	2.	1.2	.056	4	.4
Ng (1972)			.98	.058	.09	1.	1.	.078	4	.4
Hanjalic and Launder (1972)	2.8									
Flow near a rotating cylinder										
Present study	2.8	.4[b], .2[c]	.98	.058	.09	1.	1.	.078	4	.4
Free shear flows without swirl										
Rotta (1951)	2.8									
Naot and co-workers (1970)		.8								
Hanjalic and Launder (1972)	2.8									
Round free jet without swirl										
Rodi and Spalding (1970)			.98	.0397	.055	1.	0.3			
Rodi (1973)	2.5	.4	.98	.0397	.055	1.	1.			
Free swirling jet										
Lilley (1973)			.98	.0397	.055	1.	1.			
Present study	2.8	.4[b], .5[c]	.98	.0397	.055	1.	1.			

[a]These studies have all been based on plane geometries; possible radius effects in the present rotating cylinder study will, however, be negligible since the boundary layer thickness is much less than the radius of the cylinder.

[b,c]Values of C_2, referred to in the text as $C_{2,n}$ and $C_{2,t}$, applicable to normal and tangential double correlations respectively.

Table 7.1 Values of turbulence-model constants of present study compared with those of other workers

7.3-8 The Near-Wall Region

It has been stated that the algebraic stress model of turbulence described herein is restricted to regions where the local turbulence Reynolds number is high. This condition is not satisfied in the near-wall region. To overcome this restriction the near-wall values of the two main Reynolds stresses $-\rho\overline{V_1V_2}$ and $-\rho\overline{V_2V_3}$ are determined from the modified mixing-length based expressions 6.1 and 6.2 using the constitutive equations 2.39 and 2.40.

7.3-9 Examination of the Viscosity Ratio

The viscosity ratio $\sigma_{2,3}$, previously defined by equation 4.5, was shown to be an important parameter in the turbulence models developed in Chapters 5 and 6; it accounted for the anisotropic nature of the viscosity. This ratio was either assumed to be a constant, or was obtained as an empirical function of the swirl level. It is therefore interesting to deduce an analytical expression for $\sigma_{2,3}$ from equation 7.15 in terms of local time-mean velocities and stress components.

Now, from the definitions of the effective viscosities $\mu_{1,2}$ and $\mu_{2,3}$, equations 2.39 and 2.40, the ratio $\mu_{1,2}/\mu_{2,3}$ can be written as:

$$\sigma_{2,3} = \frac{-\rho\overline{V_1V_2} \Big/ \dfrac{\partial V_1}{\partial x_2}}{-\rho\overline{V_2V_3} \Big/ r\dfrac{\partial (V_3/r)}{\partial x_2}} \quad . \tag{7.22}$$

From equation 7.15 for the double-velocity correlations $-\overline{v_1v_2}$ and $-\overline{v_2v_3}$ it follows that:

$$\sigma_{2,3} = \frac{P_{1,2} \Big/ \dfrac{\partial V_1}{\partial x_2}}{P_{2,3} \Big/ r\dfrac{\partial (V_3/r)}{\partial x_2}} \quad . \tag{7.23}$$

Substituting for the production terms $P_{1,2}$ and $P_{2,3}$ from equations 7.9 and 7.11 results in:

$$\sigma_{2,3} = \frac{1 - \frac{2}{\overline{v_2^2}} \frac{V_3/r}{\partial V_1/\partial x_2} \left[\overline{v_2 v_3} \frac{\partial r}{\partial x_1} + \overline{v_1 v_3} \frac{\partial r}{\partial x_2} \right]}{1 + \frac{2}{\overline{v_2^2}} \frac{V_3/r}{r \frac{\partial (V_3/r)}{\partial x_2}} \left[\overline{v_1 v_2} \frac{\partial r}{\partial x_1} + (\overline{v_2^2} - \overline{v_3^2}) \frac{\partial r}{\partial x_2} \right]} \quad . \qquad (7.24)$$

The behaviour of $\sigma_{2,3}$ for two special cases is worthy of note: flows for which the mainstream direction is parallel to the axis of symmetry, such as a swirling jet or a rotating cylinder in an axial stream; and flows for which the mainstream direction is normal to the axis of symmetry, for example a rotating disc.

For the former, $r = x_2$ and $\partial r/\partial x_1 = 0$. Further, the correlation $-\rho \overline{v_1 v_3}$ is the shear stress $\tau_{1,3}$. For laminar boundary layers of the kind considered here, this stress is small. It seems reasonable to expect that it is also small when such layers are turbulent, in which case equation 7.24 reduces to:

$$\sigma_{2,3} = \left(1 - \beta \, Ri\right)^{-1} \quad . \qquad (7.25)$$

The parameter β is defined by $(\overline{v_3^2} / \overline{v_2^2} - 1)$, and Ri is a Richardson number defined as $2 \frac{V_3}{r} \Big/ r \frac{\partial (V_3/r)}{\partial x_2}$. Equation 7.25 can be recognised as a relative of the Monin-Oboukhov formula which modifies the turbulence length-scale when a body force acting normal to the streamline direction exists ; see for example Bradshaw (1969), Hughes and Horlock (1971), and also Section 4.4. The equation reveals that, when a body force is due to swirl, the modification is more properly applied to the viscosity ratio $\sigma_{2,3}$.

For the latter of the above-mentioned cases, x_1 is the radial coordinate r, and $\partial r/\partial x_2 = 0$. For fully turbulent flow, above a Reynolds number of 10^6, and are of the order 0.1 and 2 respectively in the outer four-fifths of the boundary layer, see Dorfman (1963). Generally, the correlations $\overline{v_1 v_2}$ and $\overline{v_2 v_3}$ are of the same order or less than $\overline{v_2^2}$, see for example Erian and Tong (1971); it can therefore

be surmised that $\sigma_{2,3}$ is probably near to unity.

7.4 Comparison of Predictions with Experimental Results

7.4-1 The Free Swirling Jet

Strictly, the algebraic Reynolds-stress model of turbulence developed in Section 7.3-1 to 7.3-7 is applicable to two-dimensional high-Reynolds-number swirling boundary layers. The only flow which does not violate any of these restrictions is a free, fully turbulent, axisymmetrical swirling jet for which the degree of swirl is not sufficient to cause recirculation; unfortunately here, as in many other areas of fluid mechanics today, the potential of computer-based prediction methods has outstripped the supply of established experimental data. Comparisons are made with the experimental results of Pratte and Keffer (1972) and of Chigier and Chervinsky (1967). The former authors have measured all six double-correlations in a swirling jet using hot-wire techniques, a task which is by no means easy; and these authors have remarked (1972 a) that one should not attempt to rely on their data for more than trends and magnitudes.

In Fig. 7.1 the predicted Reynolds stresses are compared with those measured by Pratte and Keffer at stations 6 and 12 diameters downstream from injection respectively. Comparisons for the stress $\overline{v_1 v_3}$ are not shown because there is now some doubt surrounding those values measured by Pratte and Keffer (1972 a). With the notable exception of the stress $\overline{v_2 v_3}$ at 6 diameters downstream, the agreement is on the whole quite good, better than might have been expected considering the uncertainties in the turbulence modelling and the data.

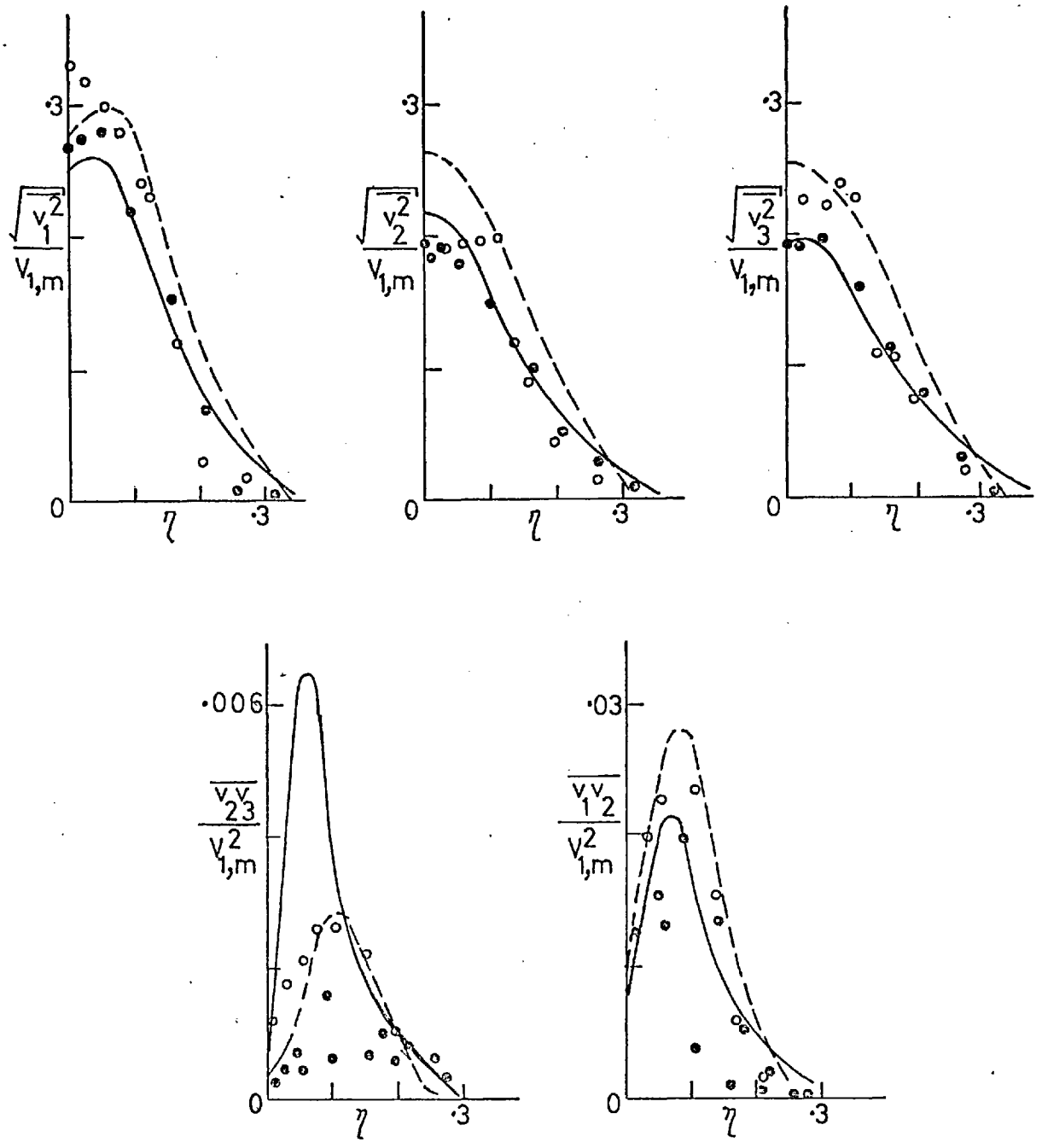

x/d	predictions	data of Pratte and Keffer (1972)
6	————	o o o o
12	– – – – – –	o o o o

Fig. 7.1 Free swirling jet. Predictions of Reynolds stresses for a swirl number of 0.3.

Shown in Fig. 7.2 are the predicted profiles of the viscosity ratio $\sigma_{2,3}$. It is noted that a rather large maximum value of about 3 occurs at the axis for x/d=6, and that this maximum falls off rapidly with downstream distance due to the rapid decay of the swirl component of velocity. The radially-averaged values of $\sigma_{2,3}$ are roughly the same as those found by Lilley (1973) by computer optimization to give satisfactory predictions of mean quantities. It should be remarked that the degree of anisotropy of turbulence displayed by the predicted normal stresses is less than that which the values of the viscosity ratio $\sigma_{2,3}$ would suggest. The latter quantity appears, therefore, to exaggerate the actual level of anisotropy, emphasising the fact that the 'effective viscosity' concept is a rather bad one for turbulent swirling flows.

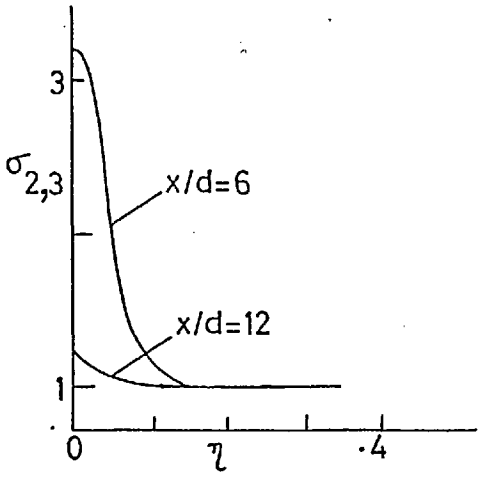

Fig. 7.2 Predicted profiles of the viscosity ratio $\sigma_{2,3}$ for a swirl number of 0.3

In Fig. 7.3 some predictions of mean velocity distribution and mean-velocity decay are compared with the measurements of Pratte and Keffer, and also with those of Chigier and Chervinsky. Since the Reynolds stresses are reasonably well predicted, not unexpectedly the predictions of mean quantities are also quite good. The decay of both the axial and the swirl velocities are well predicted and this is particularly

heartening since the less sophisticated effective-viscosity based turbulence models do not possess this universality, Lilley (1973). The prediction of the circumferential velocity V_3 for the Pratte and Keffer experiment stands out as being in poor agreement with the data. The V_3 profile of Chigier and Chervinsky is however well predicted.

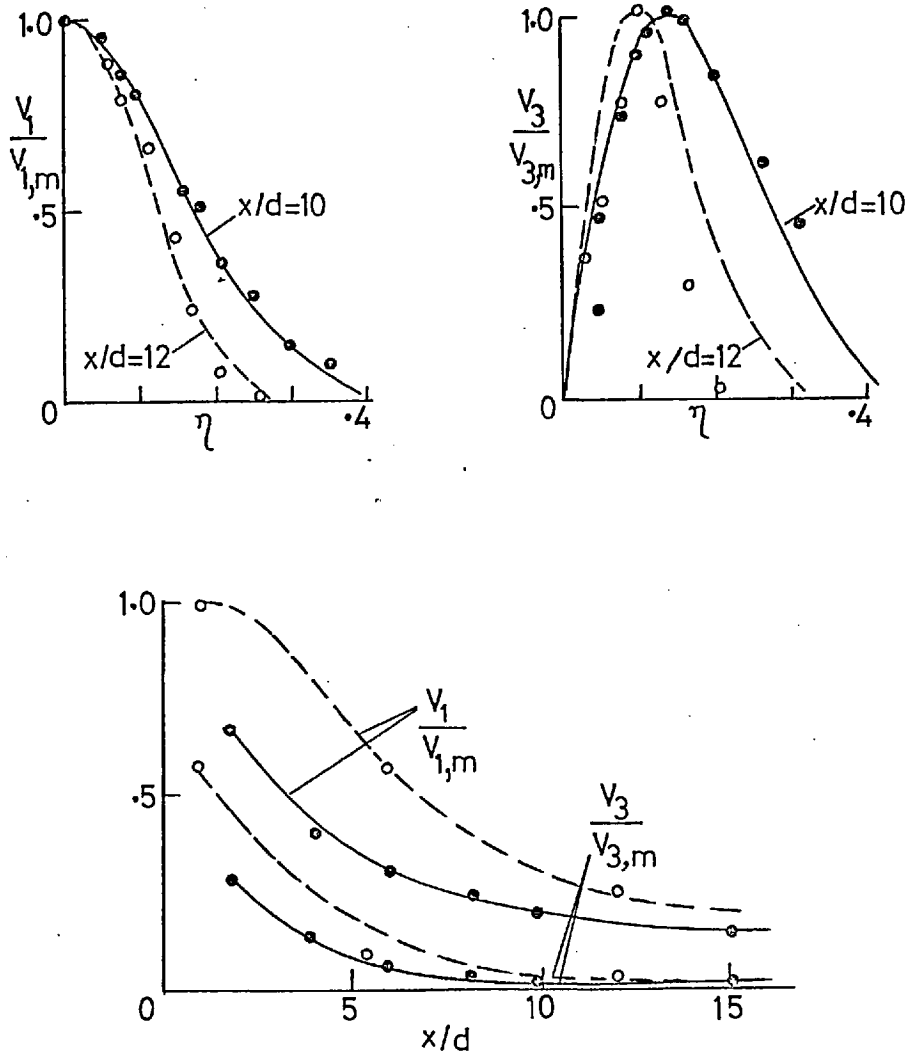

S	predictions	data
.30	— — — —	o o o o Pratte and Keffer (1972)
.416	————	• • • • Chigier and Chervinsky (1967)

Fig. 7.3 Free swirling jet. Predictions of velocity profile and velocity decay for two values of the swirl number S.

7.4-2 Swirling Flows Near Walls

(a) Rotating Disc . Erian and Tong (1971) have measured the mean-velocity components and the stresses $\overline{v_1 v_3}$, $\overline{v_1^2}$ and $\overline{v_3^2}$ near a free rotating disc. Using this data in the stress relations 7.15 alone, the remaining stresses: $\overline{v_1 v_2}$, $\overline{v_2 v_3}$ and $\overline{v_2^2}$ can be determined, along with the ratio of $(1-C_{2,n})$ upon $(1-C_{2,t})$, without the need to specify the value of any of the adjustable constants. The outcome of this exercise is presented in Fig. 7.4 for a rotational Reynolds number of 9.93×10^5. It is seen that $(1-C_{2,n})/(1-C_{2,t})$ does depart from the constant value of unity in the outer part of the flow, but perhaps this departure is not unacceptable. The viscosity ratio $\sigma_{2,3}$ has also been calculated and it is, as expected from the arguments of Section 7.3-9, near unity; but in contrast to the free-jet situation, the normal stresses now indicate significant anisotropy of turbulence.

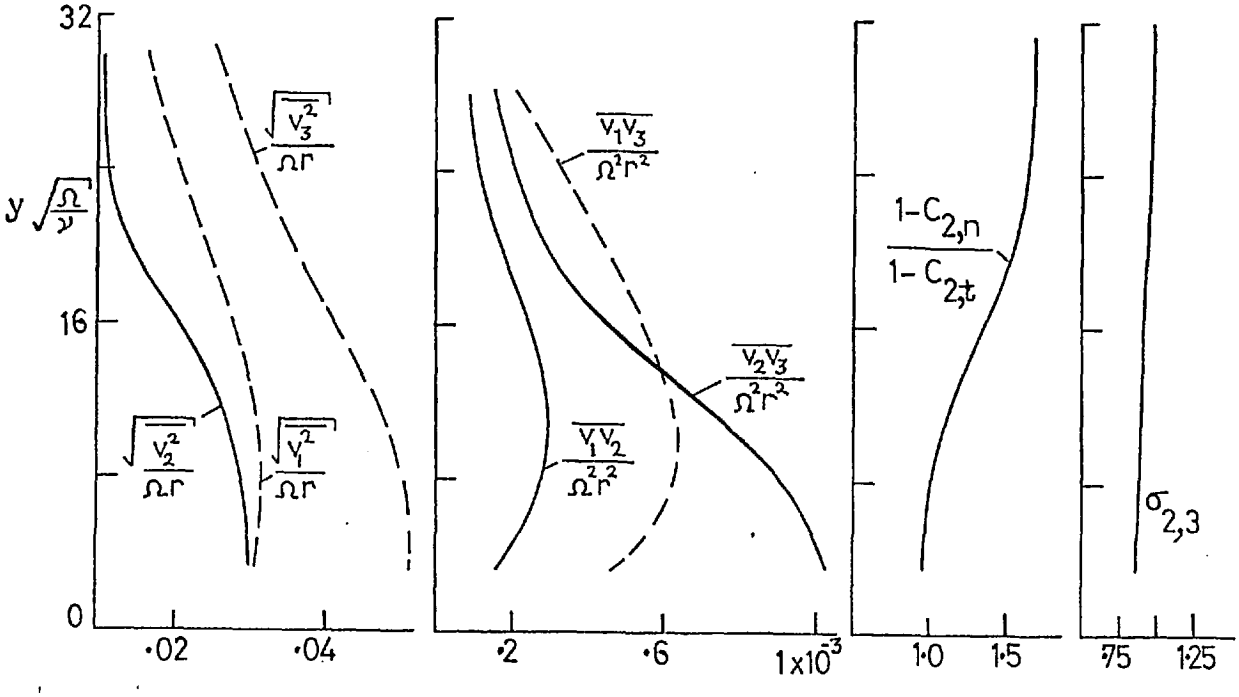

——— Experimental measurements of Erian and Tong (1971)

———— Calculated from equation 7.15.

Fig. 7.4 Calculated results applying algebraic stress relations for a free rotating disc.

(b) Rotating Cylinder. Mean flow data for a cylinder rotating in a co-axial stream have been provided by Parr (1963) and by Furuya and his co-workers (1966). Predictions of the growths of the axial and circumferential momentum thicknesses, obtained using the Reynolds-stress turbulence model matched near the wall to the relations 6.1 and 6.2 as explained in Section 7.3-8, are shown compared with the data in Fig. 7.5. The values of the constants of the stress model are those recorded in Table 7.1 for the full range of data. In the near-wall expressions 6.1 and 6.2 two values of the constant κ, 0.43 and 0.48, were respectively required to predict the data of Parr and Furuya. The enchanced universality of the present turbulence model is revealed by the predictions previously obtained in Section 4.3-3, and reproduced in Fig. 7.5, with the isotropic viscosity mixing-length model.

Although neither Parr nor Furuya made measurements of any turbulence quantities, the predictions of these quantities are nonetheless of interest. Fig. 7.6 shows the predicted profiles for one of Parr's conditions of the turbulence kinetic energy, length scale, Reynolds stresses, ratio of dissipation to production of energy, and the viscosity ratio. Two aspects of these predictions are worthy of note. Firstly, the ratio of dissipation to production $(\epsilon/p)_k$ is nowhere far from unity, as would be expected for a near-equilibrium flow, so that the rather approximate way in which the convection and diffusion contributions to the stress equations have been modelled should not be of great consequence. Secondly, the stress ratio $\sigma_{2,3}$ is near unity where the local Reynolds number of turbulence is high, as surmized in Section 7.3-9; the considerable departure from unity within the sublayer was discussed in Section 6.3-1. Since both $(\epsilon/p)_k$ and $\sigma_{2,3}$ are close to unity in the outer part of the boundary layer, application of the mixing-length formulation in place of the stress model in this region would not result in a loss of universality; the

computations performed in Section 6.3-1 and displayed in Fig. 6.1 substantiate this.

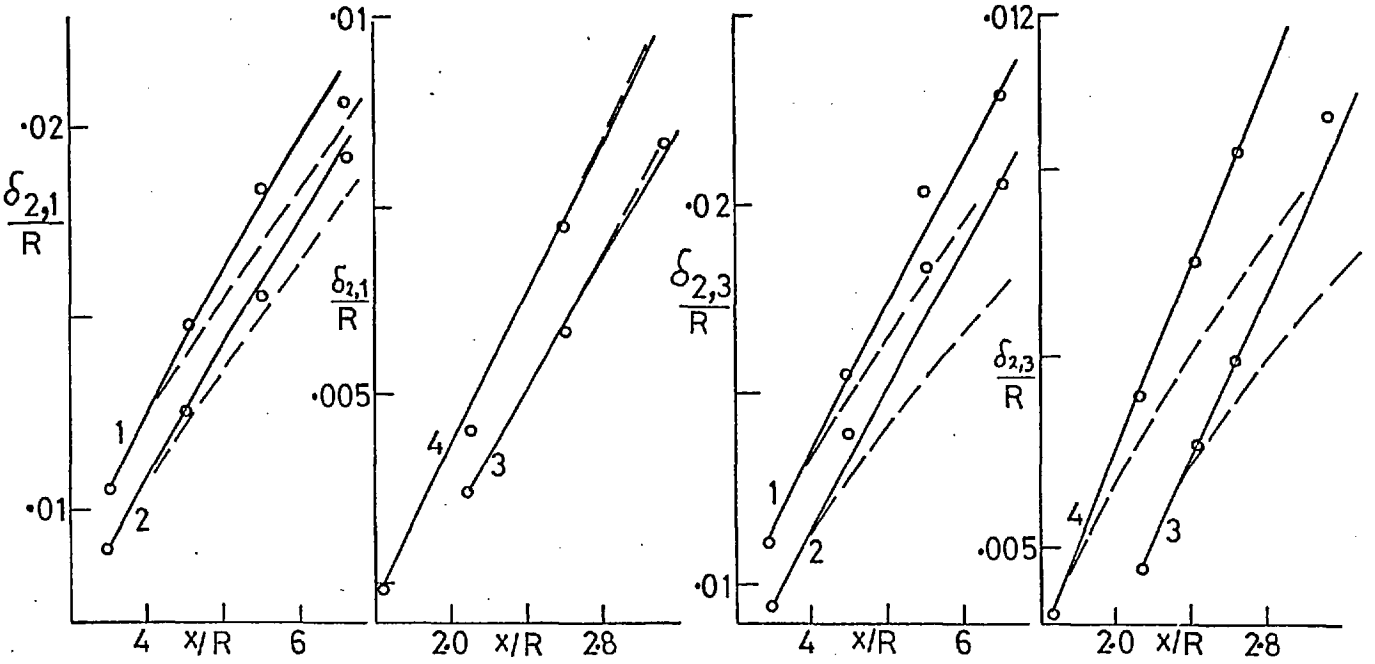

——predictions obtained with stress model and near-wall relations based on anisotropic mixing-length model

----predictions obtained with isotropic mixing-length model.

ooo Experimental data

	$\Omega R/V_{1,\infty}$	$V_{1,\infty}R/\nu$	Reference
1	2	0.6×10^5	Furuya (1966)
2	2	1.2×10^5	" "
3	3	3.0×10^5	Parr (1963)
4	4	3.0×10^5	" "

Fig. 7.5 Predictions of axial and circumferential momentum thicknesses for a cylinder rotating in an axially-directed stream.

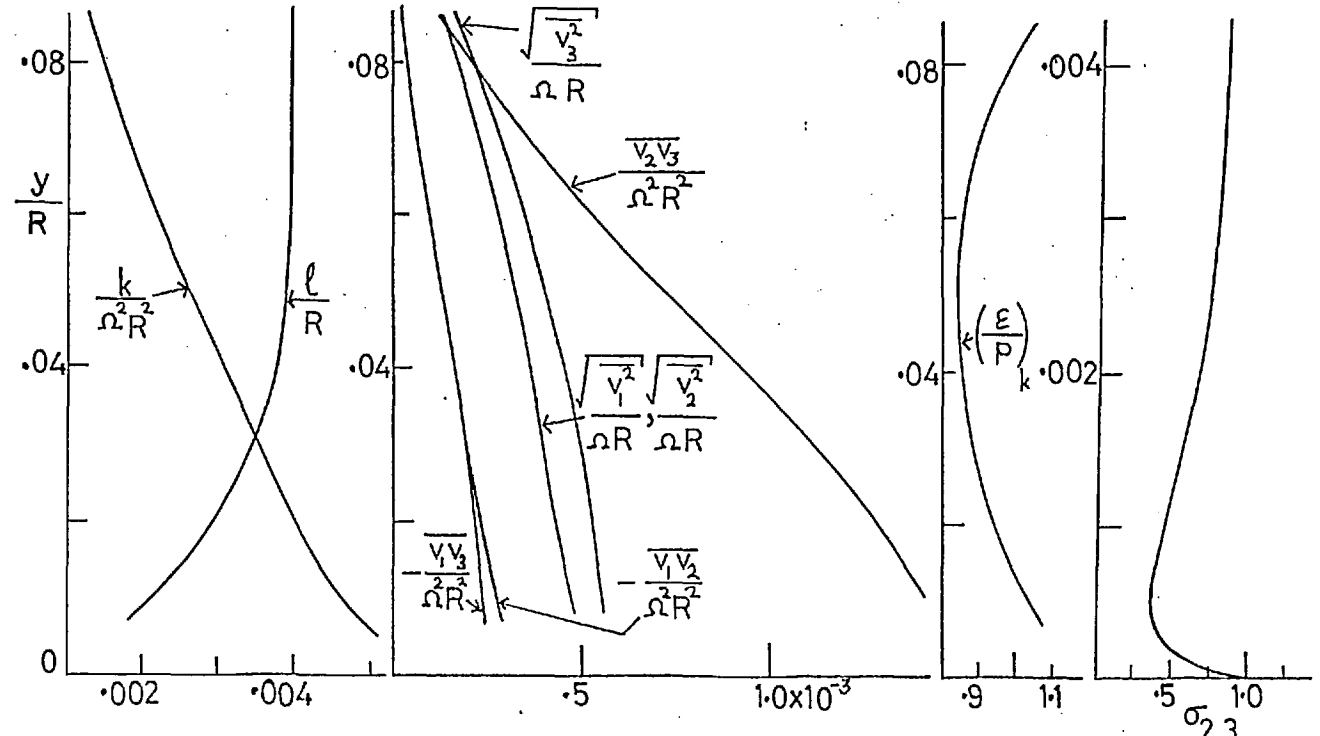

Fig. 7.6 Predictions of turbulence quantities for a cylinder rotating in an axially-directed stream: $\Omega R/V_{1,\infty}=4$, $V_{1,\infty}R/\nu=3\times10^5$, $x/R=2\cdot8$.

7.5 Summary and Conclusions

1. An algebraic Reynolds stress model of turbulence has been developed which is applicable to swirling boundary layer flows where the local Reynolds number of turbulence is high. All six Reynolds stress components were expressed in terms of the time-average velocity components, the turbulence energy and its rate of dissipation, and the stresses themselves.

2. An analytical expression for an important parameter, the viscosity ratio $\sigma_{2,3}$, has been determined from the equations for the two main Reynolds shear-stress components $-\rho\overline{v_1 v_2}$ and $-\rho\overline{v_2 v_3}$. Examination of this expression suggested that $\sigma_{2,3}$ is near unity in the fully turbulent outer part of swirling boundary layers near walls.

3. For wall-flows, the condition of high turbulence Reynolds number is not satisfied in the near-wall region; for these cases, the stress model was matched in this region to the modified mixing-length expressions described in Section 6.2. The model was subsequently employed to predict both free flows and wall flows.

4. For the free swirling jet, the predicted Reynolds stresses and mean-velocity components were in satisfactory agreement with the data within the probable accuracy of the measurements. The viscosity ratio was found to depart significantly from unity near the axis and less than about 10 diameters from injection.

5. For the case of a cylinder rotating in an axial stream, the complete velocity distribution was accurately predicted. The viscosity ratio $\sigma_{2,3}$ was found to be near unity away from the surface; this was also the result of calculations for a free rotating disc.

6. The algebraic stress model derived herein suffers from two drawbacks. First, the constant C_2 is not universal, a feature which is attributed mainly to the inadequacy of the pressure-strain simulation. Secondly, the model is not applicable to the near-wall region; it was matched with mixing-length based expressions in this region.

7. However, the stress model obviates the need to use the effective viscosity concept, the Reynolds stresses being determined directly. Furthermore, for cases where experimental data are not available, for example the rotating cylinder, the predictions of the Reynolds stresses are a useful guide to further analytical and experimental investigations.

CHAPTER 8

HEAT AND MASS TRANSFER

8.1 Introduction

The preceeding four chapters have been concerned with the development of models of turbulence, and these were employed to predict the hydrodynamic behaviour of several cases of swirling boundary layers. The present chapter deals with the prediction of heat and mass transfer from discs and cones rotating in unconfined surroundings.

The equations governing the transport of heat and mass are introduced in Section 8.2, followed in Section 8.3 by the formulae for the effective exchange coefficients. Predictions of heat and mass transfer are compared in Section 8.4 with the experimental results for the following cases:

1. An isothermal disc rotating in stagnant air.
2. A non-isothermal disc rotating in stagnant air.
3. An isothermal cone rotating in stagnant air.
4. An isothermal cone rotating in an axially-directed air stream of uniform velocity.

The comparisons are subsequently summarised and conclusions drawn in Section 8.5.

8.2 Conservation Equations

The equations which govern the transport of heat and mass in laminar swirling boundary layers were introduced in Chapter 2. They are, in curvilinear orthogonal coordinates:

$$\rho V_1 \frac{\partial \tilde{h}}{\partial x_1} + \rho V_2 \frac{\partial \tilde{h}}{\partial x_2} = \frac{1}{r} \frac{\partial}{\partial x_2} \left[r \left(\Gamma_h \frac{\partial h}{\partial x_2} + V_1 \tau_{1,2} + V_3 \tau_{2,3} \right) \right] \qquad (8.1)$$

$$\rho V_1 \frac{\partial m_j}{\partial x_1} + \rho V_2 \frac{\partial m_j}{\partial x_2} = \frac{1}{r} \frac{\partial}{\partial x_2} \left[r \Gamma_j \frac{\partial m_j}{\partial x_2} \right] \qquad (8.2)$$

For turbulent flow, in analogy with laminar flow, it is presumed that the diffusive transport of heat and of mass obey Fourier's and Fick's laws, but with the laminar exchange coefficient replaced by an effective exchange coefficient which is usually much larger than the laminar counterpart.

8.3 Effective Exchange Coefficients

The available experimental data for two-dimensional non-swirling flows, see for example Kestin and Richardson (1963), and the analytical work of Patankar and Spalding (1970), suggest that the effective exchange coefficient is proportional to the effective viscosity via the relation:

$$\Gamma_{eff} = \mu_{eff} / \sigma_{eff} \qquad (8.3)$$

This variable σ_{eff} is obviously analogous to the Prandtl or Schmidt number for laminar flow, namely $\frac{k_a}{c_p} = \frac{\mu_\ell}{Pr}$ or $\rho \mathcal{D}_j = \frac{\mu_\ell}{Sc}$. Consequently, for turbulent flow $\sigma_{h,eff}$ and $\sigma_{j,eff}$ are respectively the effective Prandtl and Schmidt numbers.

Kestin and Richardson (1963) found that $\sigma_{h,eff}$ remains roughly constant at a value of 0.8 across the fully turbulent part of the flow in pipes. In free turbulent flows the values of $\sigma_{h,eff}$ and $\sigma_{j,eff}$ appear to be lower; a value around 0.7 has been reported by Forstall and Shapiro (1950) for axisymmetrical jets. Patankar and Spalding (1970) used a value of 0.9 to predict several wall boundary layers.

In the region close to a wall, Patankar and Spalding (1970) have established that the effective exchange coefficient can be represented as the sum of its laminar and turbulent components:

$$\Gamma_{eff} = \Gamma_\ell + \Gamma_t \qquad (8.4)$$

This expression can be written in terms of the laminar and turbulent viscosity, and laminar Prandtl or Schmidt number as:

$$\Gamma_{eff} = \mu_{eff}/\sigma_{eff} = \mu_\ell/\sigma_\ell + \mu_t/\sigma_t \quad . \qquad (8.5)$$

In the fully-turbulent region the value of σ_t is, of course, the same as σ_{eff} because μ_ℓ is much less than μ_t. In the laminar sublayer, however, the laminar contribution is predominant since the turbulent viscosity tends to zero.

For swirling boundary layers the calculation of the effective exchange coefficient through equation 8.5 presents a special problem because of the anisotropic nature of the turbulent viscosity. An alternative formulation which would remove this problem would be to specify the turbulent exchange coefficient Γ_t in terms of the turbulence energy k and length scale ℓ calculated from the turbulence model described in Chapter 5. Thus,

$$\Gamma_{eff} = \mu_\ell/\sigma_\ell + \rho k^{\frac{1}{2}} \ell/\sigma_t \quad . \qquad (8.6)$$

However, in Chapter 5, it was revealed that the behaviour of k in the near-wall region is not well established even for non-swirling two-dimensional boundary layers; equation 8.6 is therefore not useful under present circumstances.

Since the more complex algebraic-stress model of turbulence of Chapter 7 is at an early stage of development, and is in its present form not directly applicable to the low turbulence near-wall region, it was decided to employ the isotropic mixing-length model of Chapter 4 to determine the turbulent viscosity. It should be noted that the hydrodynamic predictions obtained there for the disc and cone flows were in excellent agreement with the experimental data.

Since the present chapter is restricted to predictions of heat and mass transfer from discs and cones spinning in free surroundings, the assumption of isotropic viscosity, see also the report of Cooper (1971), is acceptable.

The relevant mixing-length based equations for the turbulent viscosity, equations 4.7, 4.9, 4.10 and 4.12, are repeated here for convenience:

$$\mu_t = \rho \ell_{m,c}^2 \left[\left(\frac{\partial V_1}{\partial x_2} \right)^2 + \left(r \frac{\partial (V_3/r)}{\partial x_2} \right)^2 \right]^{\frac{1}{2}} , \qquad (8.7)$$

$$\ell_m = \kappa y \left[1 - \exp\left(-y \sqrt{\rho \tau_R} / 26 \mu_\ell \right) \right] \quad \text{for } y \leqslant \lambda\delta/\kappa, \qquad (8.8)$$

$$\ell_m = \lambda\delta \quad \text{for} \quad \lambda\delta/\kappa < y \leqslant \delta , \qquad (8.9)$$

$$\ell_{m,c} = \ell_m \left(1 - \beta Ri \right) . \qquad (8.10)$$

Together with equation 8.5, and equations 2.34 to 2.38 for the transport of momentum, and heat or mass, they form a closed set containing four empirical parameters: κ, λ, β and σ_t. Predictions are compared with the experimental heat and mass transfer data in the following section; the values of κ, λ, and β found appropriate for the disc and cone studies of Chapter 4 are again used, and the optimum values of σ_t are determined by matching the predictions with the data.

8.4 Comparisons of Predictions with Experimental Data

8.4-1 Isothermal Disc in Stagnant Air

(a) Heat Transfer

Fig. 8.1 (a), (b) and (c) show the predictions of average Nusselt number for an isothermal disc compared respectively with the experimental data of Cobb and Saunders (1956), McComas and Hartnett (1970), and Dennis, Newstead and Ede (1970). The value of 0.85 was assigned to the turbulent Prandtl number for each of the three experiments. Good agreement with the data was obtained by adjusting the value of the transition Reynolds number Re_{tran} within the range quoted by the authors.

The most interesting information is contained in Fig. 8.2; here, the influence of varying Re_{tran} for a fixed value of $\sigma_{h,t}$ is exhibited along with the collected experimental data. The predicted curves converge at large Reynolds numbers to yield a single result for fully turbulent flow which is not influenced by the transition assumption. Unfortunately, the data barely extend to the fully turbulent region and, in consequence, the suggested value of $\sigma_{h,t}$ of 0.85 must be considered as tentative.

The data over-estimate the confirmed heat-transfer predictions in the purely laminar-flow region. This is probably due to heat losses which are inevitable in heat transfer experiments. Notwithstanding the remarks of the preceeding paragraph, it may be seen that a slightly higher value of $\sigma_{h,t}$ than 0.85 is appropriate.

Predictions displaying the influence of the turbulent Prandtl number $\sigma_{h,t}$ are compared in Fig. 8.3 with the collected experimental data for a single assumed value of Re_{tran} for $\sigma_{h,t}$ equal to 0.6, 0.85 and 1.0.

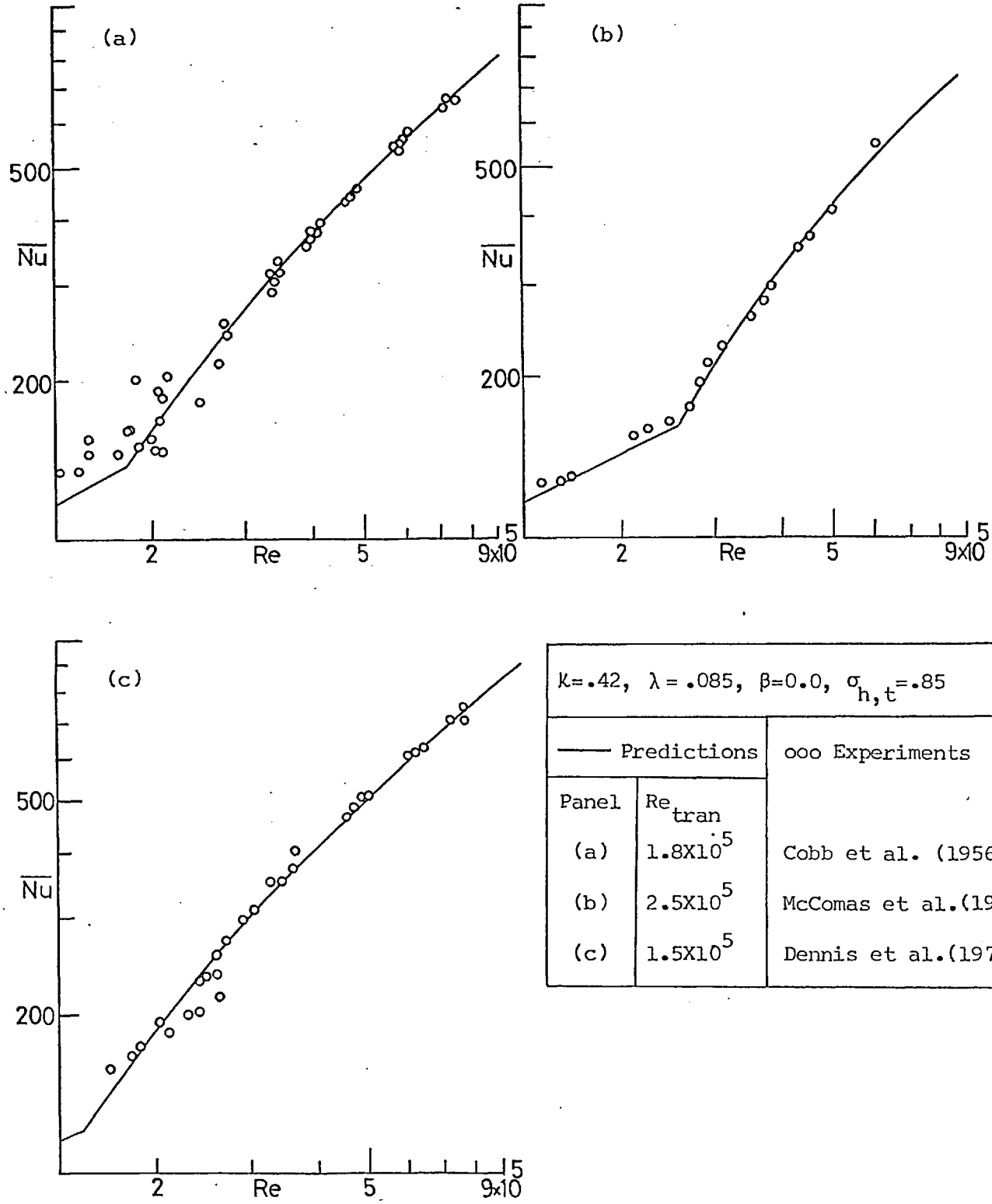

Fig. 8.1 Average heat transfer from a free rotating disc

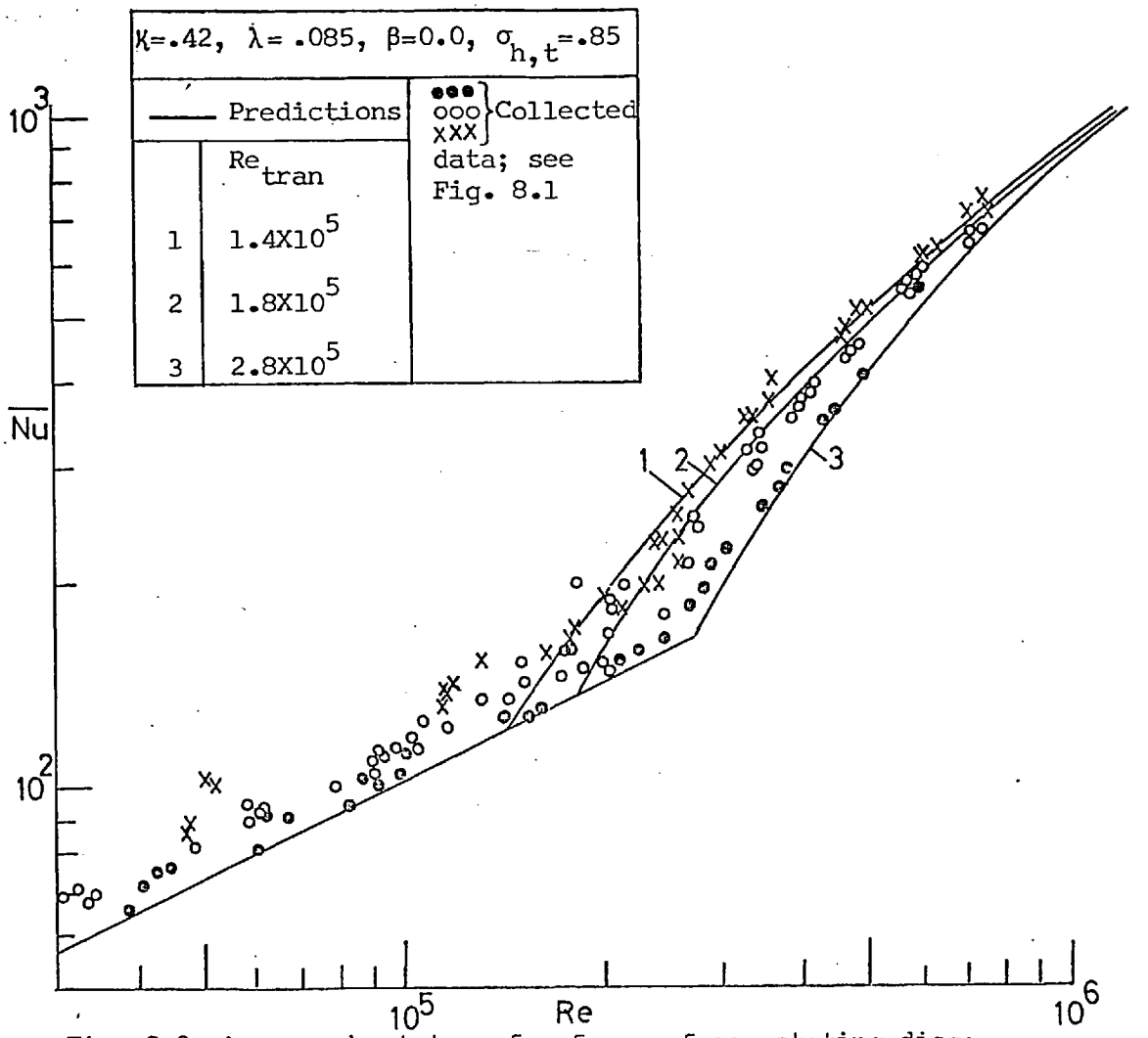

Fig. 8.2 Average heat transfer from a free rotating disc; influence of transition Reynolds number.

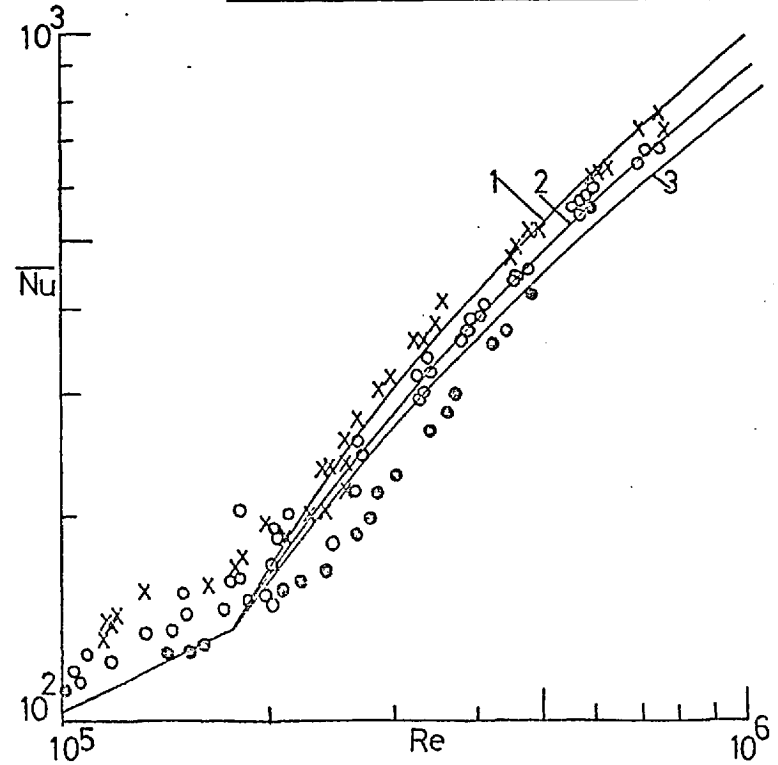

κ =.42, =.085, β=0.0

Re_{tran}=1.8X10^5

Predictions; ooo XXX Collected data; see Fig. 8.1

	$\sigma_{h,t}$
1	.60
2	.85
3	1.00

Fig. 8.3 Average heat transfer from a free rotating disc; influence of turbulent Prandtl number.

(b) Mass Transfer

Predictions of the average Sherwood number are compared with the experimental mass-transfer data of Tien and Campbell (1963), and Krieth, Taylor and Chong (1959) in Fig. 8.4 . The optimum values of κ and λ, with $\beta=0.0$, determined from the hydrodynamic investigation have again been utilised to obtain the predicted curves. In Fig. 8.4 (a) predictions are shown for a turbulent Schmidt number of 0.45 for three values of the transition Reynolds number: 1.8, 2.3 and $2.8X10^5$. It is again evident that data at higher Reynolds number is required if $\sigma_{j,t}$ is to be determined independently of the transition assumption.

This point is given further illustration in Fig. 8.4 (b). The same data are again predicted with $\sigma_{j,t}=0.35$ and $Re_{tran}=2.6X10^5$, and with $\sigma_{j,t}=0.85$ and $Re_{tran}=2.0X10^5$. The agreement for both sets of turbulent Schmidt number and transition Reynolds number is as good as that exhibited by the best predictions of Fig. 8.4 (a) obtained for a $\sigma_{j,t}$ of 0.45 and Re_{tran} of $2.3X10^5$.

In the laminar-flow region, it is of interest to note that, in contrast to the heat transfer comparisons of Fig. 8.3, the agreement with the data is good. Mass transfer experiments conveniently avoid the errors due to extraneous heat losses which are unavoidable in heat transfer experiments.

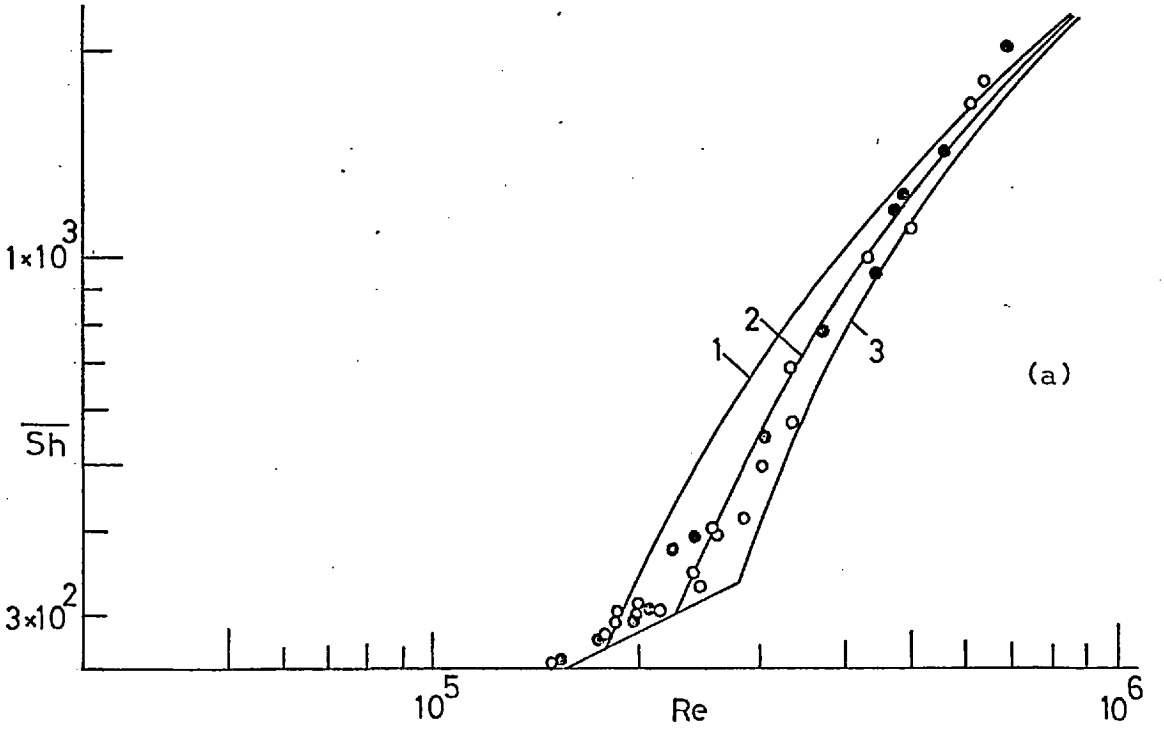

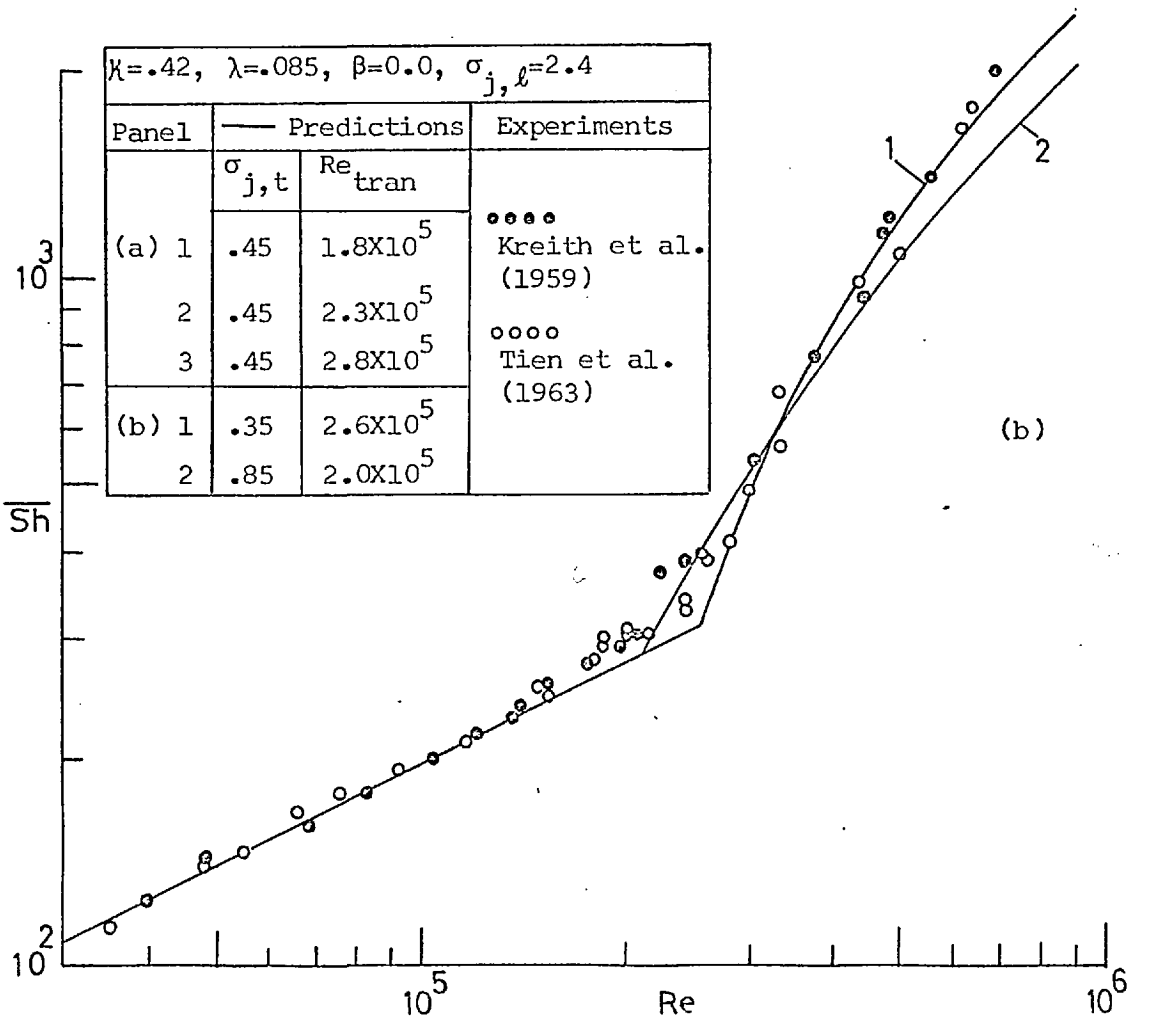

χ=.42, λ=.085, β=0.0, $\sigma_{j,\ell}$=2.4			
Panel	Predictions		Experiments
	$\sigma_{j,t}$	Re_{tran}	
(a) 1	.45	$1.8X10^5$	●●●● Kreith et al. (1959)
2	.45	$2.3X10^5$	
3	.45	$2.8X10^5$	○○○○ Tien et al. (1963)
(b) 1	.35	$2.6X10^5$	
2	.85	$2.0X10^5$	

Fig. 8.4 Average mass transfer from a disc rotating in still air

8.4-2 Non-isothermal Disc in Stagnant Air

Part of the experimental programme into the research for turbulent transport properties undertaken in the present thesis was the investigation of local heat transfer rate from a non-isothermal disc rotating in free air. The experimental apparatus and procedure are described in Appendix 7, and the measured and reduced data for four experimental conditions are recorded there.

Predictions are compared with the data in Fig. 8.5 (a) to (d). The measured temperature of the disc's surface was specified for $r/r_o \leqslant 0.45$, and the measured heat flux for $0.45 < r/r_o \leqslant 1.0$; the reasons for this choice of boundary conditions are explained in Appendix 7. The heat flux distributions, constant for each of five concentric annular segments of the disc's surface, are also shown in Fig. 8.5. They demonstrate the wide range of heat flux which can be achieved by the apparatus.

For all four cases the predictions were started in the laminar region, and immediate transition was assumed at a Reynolds number of 2×10^5; the value of the turbulent Prandtl number was 0.85. The values of the mixing-length constants κ, λ and β were the same ones used in Section 8.4-1 for the isothermal disc. The influence of a lower transition Reynolds number, 10^5, and of a lower turbulent Prandtl number, 0.6, are illustrated in Fig. 8.5 (b). It is seen that the influence of the transition Reynolds number disappears after a Reynolds number of 2.5×10^5, while the lower $\sigma_{h,t}$ results in an increase of about 15% in the heat transfer predictions.

The predictions do not compare very favourably with the measured data; the rather large errors in the experimental measurements, discussed in Appendix 7, preclude any meaningful assessment of the predictions.

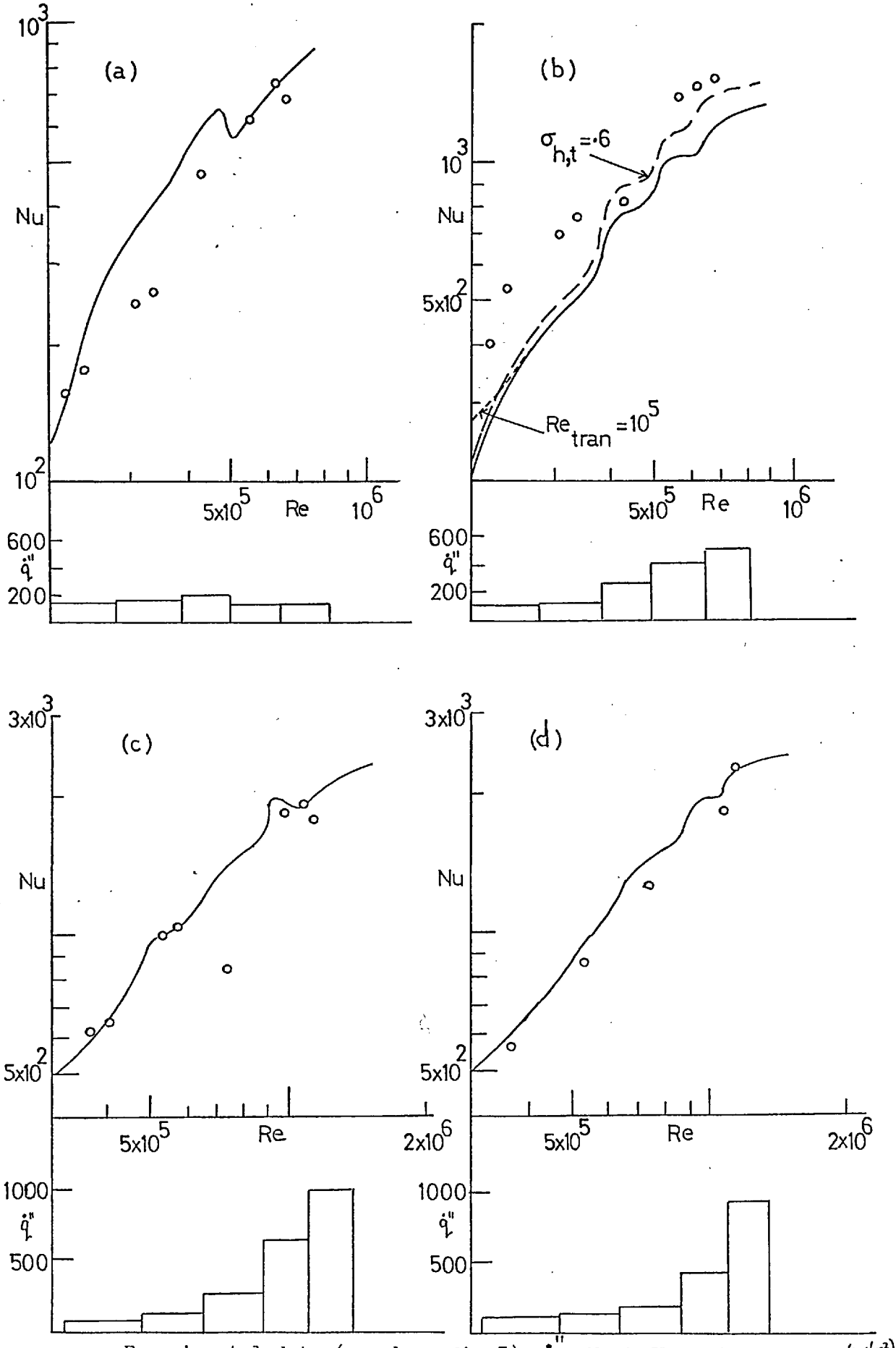

ooo Experimental data (see Appendix 7); $\dot{q}''$, Heat flux distribution (w/m^2).

——Predictions with χ=.42, λ=.085, β=0.0, $\sigma_{h,t}$=.85, $Re_{tran}=2X10^5$, except where shown otherwise.

Fig. 8.5 Local Nusselt number for a free rotating disc with non-uniform surface heat flux.

Notwithstanding the uncertainty of the data, the predictions serve to demonstrate the potential and flexibility of the prediction procedure and turbulent transport hypotheses.

8.4-3 Isothermal Cone in Stagnant Air

(a) Heat Transfer

The predicted average Nusselt number for a 60 degree vertex angle isothermal cone is compared with the data of Kreith (1966) in Fig. 8.6 (a) for three values of the transition Reynolds number. The empirical parameters $\mathcal{K}$, λ and β were the same ones used in the preceeding section in the study of heat transfer from discs. The agreement between predictions and data is good for $Re_{tran}=.9X10^5$ up to the value of $2X10^5$ for the cone Reynolds number, above which the predictions underestimate the data by about 10%.

Better results are obtained, as Fig. 8.6 (b) reveals, when the Richardson term correction is introduced with $\beta=5.0$. This is the value found appropriate for the hydrodynamic cone flow study in Section 4.4-2. The transition Reynolds number was 10^5.

It should also be noted that the laminar heat transfer data are again underestimated.

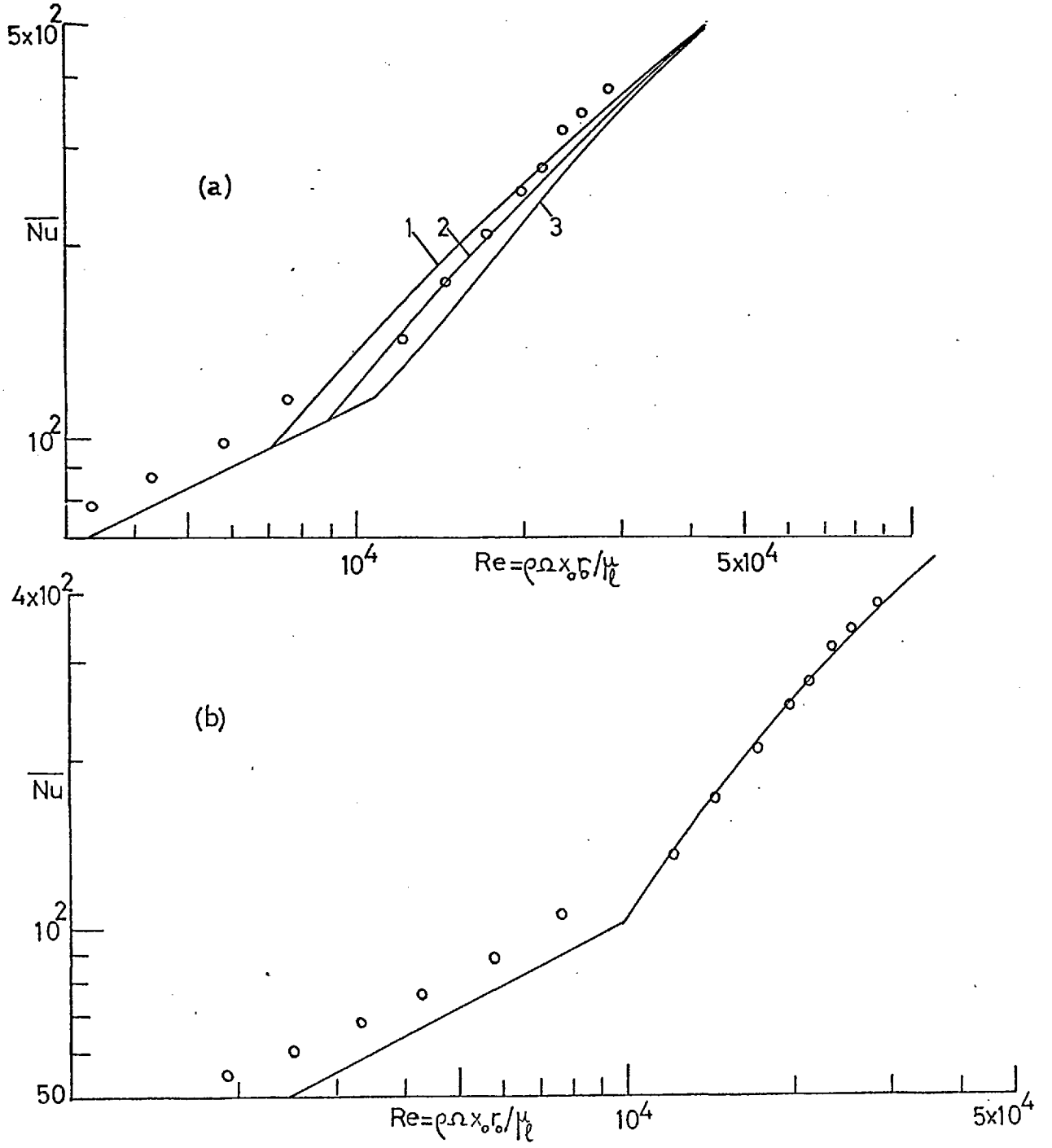

κ=.42, λ =.085, $\sigma_{h,\ell}$=.72, $\sigma_{h,t}$=.85			
—— Predictions			ooo Experiments
Panel	β	Re_{tran}	
(a) 1	0	$0.7X10^5$	Kreith (1966)
2	0	$0.9X10^5$	
3	0	$1.1X10^5$	
(b)	5	$1.0X10^5$	

Fig. 8.6 Average heat transfer from a free rotating cone

(b) Mass Transfer

Average mass-transfer predictions of Tien and Campbell's (1963) data for a 60 degree vertex angle cone are displayed in Fig. 8.7 with $Re_{tran}=1.1X10^5$. The data deviate above the calculated values for $Re > 4X10^5$. The relatively different behaviour of the heat and mass transfer data is probably associated with the different molecular Prandtl/Schmidt numbers for the processes: .72 and 2.4 respectively.

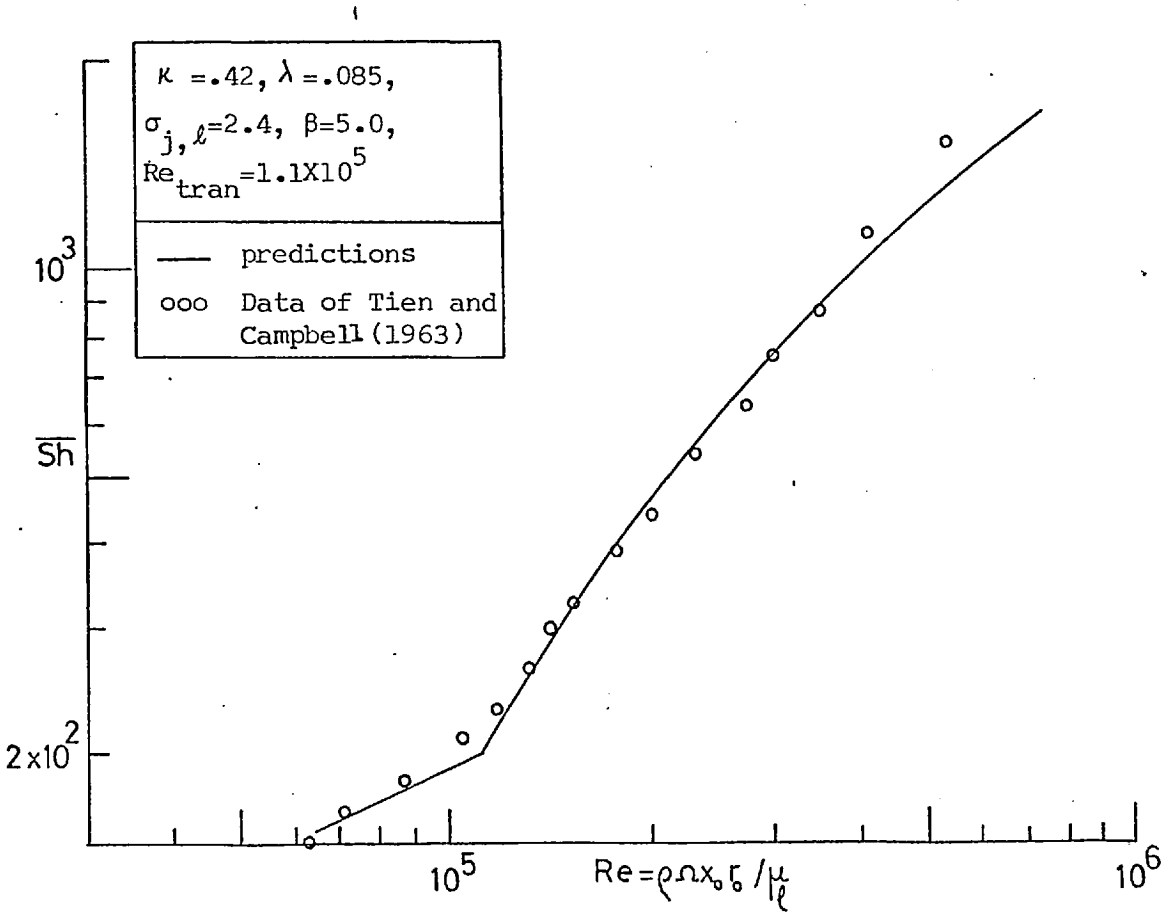

Fig. 8.7 Average mass transfer from a 60^o free rotating cone

8.4-4 Cone in Uniform Axial Stream

Predicted local Nusselt and Sherwood numbers for a 30 degree vertex angle isothermal cone spinning in a uniform-velocity air stream are compared with the data of Ruggeri and Lewis (1957), and of Salzberg and Kezios (1965) in Fig. 8.8 (a) and (b) respectively. The predictions were, as for all the previous cases, commenced in the laminar region and immediate transition to fully turbulent flow was assumed to occur at a specified Reynolds number. Both the longitudinal velocity at the edge of the boundary layer and the transition Reynolds number were deduced from the experimental data.

It is probable that the flow near the cone is akin to that near a cylinder rotating in an axial stream, and consequently the effective viscosity is highly non-isotropic. Since no hydrodynamic data exist for a 30 degree cone spinning in an axially-directed stream, the simple isotropic viscosity model was again employed, and the values of κ, λ and β were rather arbitrarily chosen. The turbulent Prandtl and Schmidt numbers were 0.9 and 0.6 respectively.

The agreement between the predictions and the experimental data is good. However, since the hydrodynamic constant κ, λ and β were assigned arbitrary values, they are not physically meaningful; the primary role of Fig. 8.8 is to provide additional evidence of the generality of the calculation procedure.

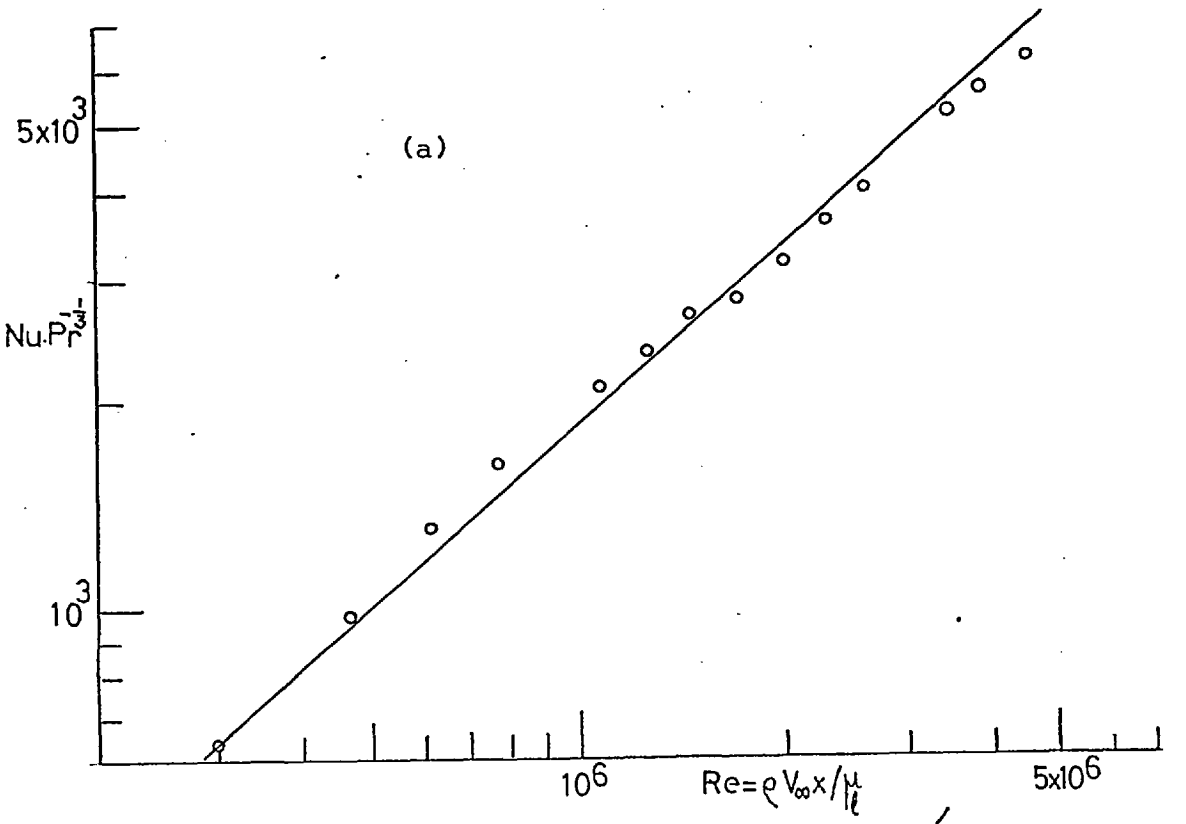

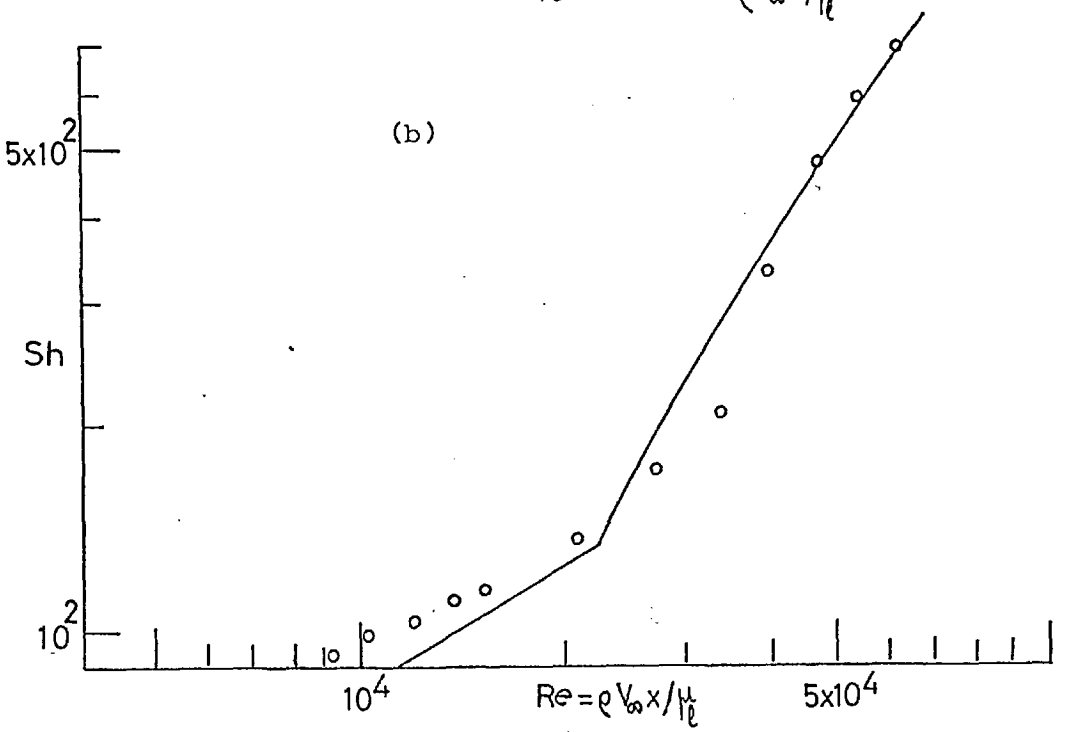

	Predictions						ooo Experiments
	$\Omega r_o/V_\infty$	$\varkappa$	λ	σ_ℓ	σ_t	Re_{tran}	
a	0.35	.4	.085	.72	.9	$8X10^4$	Ruggeri et al. (1957)
b	2.29	.4	.10	2.4	.6	10^4	Salzberg et al. (1965)

Fig. 8.8 Local heat and mass transfer from a 30° vertex angle cone in an axial stream of uniform velocity

8.5 Conclusions

1. The values of the turbulence model constants K, λ and β, the values of the turbulent Prandtl and Schmidt numbers $\sigma_{h,t}$ and $\sigma_{j,t}$, and the transition Reynolds numbers found to give the best overall agreement between predictions and experimental data are summarised in Table 8.1. The values for the non-isothermal disc are not included because of the doubt surrounding the experimental data.

2. The present enquiry has shown that use of the isotropic viscosity mixing-length hypothesis leads to generally satisfactory results provided the mixing length is made a linear function of the equivalent 'swirling flow' Richardson number.

3. The predictions, over the range of experimental data considered, were dependent upon the assumed value of the transition Reynolds number as well as the turbulent Prandtl or Schmidt number. However, at the relatively high Reynolds number outside the data range, the transition assumption did not influence the predictions. The turbulent Schmidt number was generally lower than the turbulent Prandtl number.

4. In order to explain the difference between the turbulent Prandtl and Schmidt numbers, present experimental data should be extended to fluids of larger laminar Prandtl and Schmidt numbers. It would be valuable to make these measurements at Reynolds numbers large enough for transition to have very minor influence on the flow.

κ=.42, λ = .085, $\sigma_{h,\ell}$=.72, $\sigma_{j,\ell}$=2.4	$\Omega r_o/V_{1,\infty}$	κ	λ	$\sigma_{h,t}$	$\sigma_{j,t}$	Re_{tran}
Disc in still air (β=0.0):						
Average heat transfer:						
Cobb and Saunders (1956)				0.85	--	1.8×10^5
McComas and Hartnett (1970)				0.85	--	2.5×10^5
Dennis, Newstead and Ede (1970)				0.85	--	1.5×10^5
Average mass transfer:						
Tien and Campbell (1963)				--	0.45	2.3×10^5
Kreith, Taylor and Chong (1959)				--	0.85	2.0×10^5
Cone of 60 degree vertex angle in still air (β=5.0):						
Average heat transfer:						
Kreith (1966)				0.85	--	1.0×10^5
Average mass transfer:						
Tien and Campbell (1963)				--	0.85	1.1×10^5
Cone of 30 degree vertex angle in axially-directed air stream (β=0.0):						
Local heat transfer:						
Ruggeri and Lewis (1957)	0.35	.40	.085	0.9	--	8.0×10^4
Local mass transfer:						
Salzberg and Kezios (1965)	2.29	.40	.10	--	0.6	1.0×10^4

Table 8.1 Empirical parameters in the turbulent transport hypothesis used for calculating heat and mass transfer from discs and cones spinning in free surroundings.

CHAPTER 9

CONCLUSIONS AND RECOMMENDATIONS

In this final chapter, the principal conclusions are summarised, with emphasis on the generality of application of the different models of turbulence. Recommendations are then made on the most promising path for future work.

9.1 Conclusions

(a) The mixing-length model

(i) The first model of turbulence considered was based on the use of the mixing-length concept, suitably extended to swirling boundary layers, to determine an isotropic effective viscosity. The average circumferential drag could be well predicted for four flow configurations: free disc and cone, cylinder in axial stream, and closely spaced parallel discs with outflow. However, it was found that the magnitude of the empirical constants in the mixing-length formulation depends on the particular flow configuration as well as the flow condition.

(ii) When the mixing length is augmented to account for the effect of swirl body-forces by making it a linear function of the swirl Richardson number, a marked improvement in the universality of the constants is shown. Reasonably good predictions of the average circumferential drag were obtained for the cases mentioned above with a single set of constants.

(iii) The concept of an isotropic effective viscosity is, however, not generally applicable to swirling boundary layers. If the mixing-length variation is determined from matching predictions with experimental data for the circumferential drag, then the agreement between predictions and data for the longitudinal drag

is poor, and vice versa. An isotropic viscosity model is quite unable to predict the complete flow field and the model suffers a serious drawback in this respect.

(b) The energy.length-scale model

(i) The mixing-length concept implies the local structure of the flow is determined by local conditions alone, and neglects any upstream influences on the flow. A more realistic model was developed in which the turbulence features of the flow are characterised by the kinetic energy of turbulence and a length scale, both quantities being determined from differential equations. A body-force term was introduced in the length-scale equation to account for the effects of swirl on the turbulence structure. Furthermore, the ratio of the effective viscosities in the mainstream and swirl directions was presumed constant.

(ii) Prediction of the entire flow field near a cylinder spinning in an axial stream were in good agreement with experimental data, but there were large variations in the adjustable parameters of the turbulence model for the two flow conditions considered. This lack of generality reflects the main deficiency of the model; namely, that the ratio of effective viscosities is not a constant across the boundary layer.

(c) The anisotropic mixing-length model

(i) The anisotropic nature of the effective viscosity was considered more closely, especially in the near-wall region, in the third model of turbulence. The two effective viscosities were calculated from a mixing-length based formulation, modified by Van Driest's expressions which were made functions of the local shear-stress components corresponding to the effective viscosities. Away from the wall the viscosities were assumed equal. This model

was based mainly on intuition and trials; but it is justified by the good agreement between the predictions and the data and by the fairly satisfactory level of generality of the empirical parameters.

(ii) For all the cases investigated, free disc and cone,and cylinder in axial stream, the predictions based on this model suggest that the viscosity ratio differed substantially from unity in the sublayer. The velocity vector in this region twists relative to the shear-stress vector; that is they do not act in the same direction as implied by isotropic viscosity assumptions.

(iii) Although the anisotropic mixing-length model lacks a sound physical basis, it nonetheless shows that it is the anisotropic nature of the viscosity in the near-wall region which plays an important part in the development of the whole flow field. The anisotropic nature of the viscosity also appears to have a larger influence on the flow than the effects of swirl body-forces.

(d) The algebraic Reynolds stress model

(i) The fourth, and last, model of turbulence developed provided algebraic relations for all six Reynolds stress components for fully turbulent flow. The stresses were expressed in terms of the time-average velocity components, the dissipation rate of turbulence energy, and the stresses themselves. They also yield an analytical expression for the ratio of the effective viscosities.

(ii) The algebraic Reynolds stress model was employed to predict free swirling jets, and good agreement with the mean-flow data as well as data for the Reynolds stress components was obtained. The calculated variation of the viscosity ratio was in close accord with the empirical formulae used by other workers.

(ii) For wall flows, the assumption of high Reynolds number is not satisfied in the near-wall region; the algebraic Reynolds stress model was matched with the anisotropic mixing-length based model in this region. The complete flow field near free spinning discs and cylinders rotating in axial streams was well predicted. This is an encouraging pointer to the generality of this approach.

(e) Heat and mass transfer

Finally, the heat and mass transfer from spinning discs and cones was investigated. The effective heat and mass exchange coefficients were made linear functions of the effective viscosity, the latter being calculated from the isotropic mixing-length model. The agreement between predictions and data was generally satisfactory over the range of experimental conditions considered. However, for those cases where the data barely extends into the fully turbulent region, the predictions were dependent upon the assumed transition Reynolds number.

9.2 Recommendations

The simplest model of turbulence considered, the isotropic mixing-length model with the Richardson term addition, is probably the most useful one under present circumstances to design engineers, when all that is required is a single overall quantity such as the circumferential drag or the longitudinal drag, but not both. A judicious choice of empirical constants will result in good agreement between predictions and measurements. It is important, however, to appreciate the limits of the model, and to realise that frequent and arbitrary adjustments of the constants lower its universality and attractiveness. As such, it is of limited use when operating conditions are extended much beyond the range for which it has been developed.

The non-isotropic features of turbulent swirling flows require characterisation by many variables. Increased universality can only be obtained by increasing the number of differential equations employed in a model of turbulence, at the expense of increased complexity of the analytical and computational problems.

Short of solving the complete Reynolds stress differential equations, the algebraic Reynolds stress model offers itself as a practicable and economical intermediate stage, and also provides a useful degree of universality. In particular, the extension of the algebraic stress model to the near-wall region is of special importance if the goal of reasonably wide application and unified treatment is to be attained.

For the more practical and realistic problem of three-dimensional recirculating flow, the effective viscosities corresponding to the three Reynolds shear-stress components can differ by an order of magnitude or more. To develop a model of turbulence which possesses a satisfactory level of universality for this problem will require the abandonment of the effective viscosity concept. The algebraic Reynolds stress approach, because of its small demand of computer time compared to that required for solving the differential equations for the Reynolds stresses, offers the most promise for future research.

NOMENCLATURE

Symbols	Definitions
$\mathbf{a}$	acceleration vector.
A	area.
C_B, C_D, C_R, C_S, C_W, C_q	constants in the energy-length-scale equation.
C_1, C_2, $C_{2,n}$, $C_{2,t}$	constants in the algebraic Reynolds stress model of turbulence.
$\overline{C}_f$	$=8\pi\sin\alpha\int_0^\delta \rho r^2 V_1 V_3\, dy / \Omega^2 r^5$, $\int_0^\delta V_1 V_3\, dy / \Omega R^2 V_{1,\infty}$, average drag coefficient for free disc and cone, and for cylinder respectively.
C_p	$=\rho r_o^2 (p_\infty - \bar{p}) / \mu_\ell^2$, pressure coefficient for parallel discs.
C_W	$=2\pi\int_0^\delta \rho r V_1\, dy / r_o \mu_\ell$, mass flow coefficient for parallel discs.
d	orifice diameter.
D	dissipation.
$\mathscr{D}$	diffusion coefficient in Fick's law.
Df	diffusion.
g	gravitational acceleration.
$\mathbf{G}$	mass velocity vector.
G	component of $\mathbf{G}$.
h	specific enthalpy.
$\tilde{h}$	stagnation enthalpy.
H	$=\int_0^\delta \frac{V_3}{\Omega r} dy \Big/ \int_0^\delta \frac{V_3}{\Omega r}\left(1-\frac{V_3}{\Omega r}\right) dy$, shape factor for disc.
$\mathbf{i}$	unit vector.
$\mathbf{J}$	diffusional flux.
k	$=\frac{1}{2}(\overline{V_1^2}+\overline{V_2^2}+\overline{V_3^2})$, turbulence energy.
k_a, k_d	thermal conductivity.

ℓ	length scale of turbulence; metric length.
ℓ_m	mixing-length.
$\ell_{m,c}$	mixing-length modified by Richardson function.
L	length of cone measured in the x_1-direction.
$\dot{m}$	mass flow rate.
m_j	mass fraction.
Nu	$= \dot{q}''_w x \sigma_{h,\ell} / c_p (T_w - T_\infty) \mu_\ell$, local Nusselt number.
$\overline{Nu}$	$= \left[2 \int_0^{x_o} r \dot{q}''_w \, dx / x_o r_o \right] x_o \sigma_{h,\ell} / c_p (T_w - T_\infty) \mu_\ell$, average Nusselt number.
p	pressure.
P	production.
Pr	Prandtl number.
Ps	pressure-strain.
$\dot{q}''$	heat flux.
Q	$= 2 \int_0^\delta \rho V_1 \, dy / \Omega r^2$, radial volumetric flow rate for disc.
Q_{rad}	radiation heat transfer per unit volume.
r	distance from axis of symmetry.
R	radius of cylinder.
Rc	radius of base of cone.
Re	$= \rho \Omega r x / \mu_\ell$, Reynolds number for free disc and cone; $= \rho V_{1,\infty} R / \mu_\ell$, Reynolds number for cylinder.
Ri	Richardson number.
Rj	rate of generation of chemical species.
S	$= \int_0^\infty \rho V_1 V_3 r^2 \, dr \Big/ \frac{d}{2} \int_0^\infty \rho V_1^2 r \, dr$, swirl number for free jet.
Sc	Schmidt number.
Sh	$= \dot{m}''_w x \sigma_{j,\ell} / \mu_\ell (m_{j,w} - m_{j,\infty})$, local Sherwood number.

$\overline{Sh}$ $= \left[2\int_0^{x_0} \dot{m}''_w r\,dx / x_0 r_0\right] x_0 \sigma_{j,l} \Big/ \frac{\mu}{l}(m_{j,w} - m_{j,\infty})$, average Sherwood number.

$\overline{T}$ temperature.

T, τ shear-stress.

v, v' fluctuating velocity.

V time-average velocity.

$\mathbf{V}$ instantaneous velocity vector.

$\overline{v}$ average velocity across boundary layer or slot exit; time-average value of instantaneous velocity.

x coordinate direction;
$\equiv x_1$, coordinate measured along the surface.

y $\equiv x_2$, coordinate measured normal to the surface.

α angle made by direction-1 with symmetry axis.

β parameter in the Monin-Oboukhov formula.

Γ exchange coefficient.

δ boundary layer thickness where $V/V_m = 0.01$, or 0.99.

$\delta_{1,2}$ $= \int_0^{\delta} \frac{V_1}{V_\infty}\left(1 - \frac{V_1}{V_\infty}\right) dy$, axial momentum thickness for cylinder.

$\delta_{2,3}$ $= \int_0^{\delta} V_1 V_3\, dy \Big/ \Omega R V_\infty$, circumferential momentum thickness for cylinder.

δ_{ij} Kronecker's delta.

ε dissipation.

η dimensionless radial coordinate for free jet.

ϑ angle of revolution about symmetry axis.

χ, λ mixing-length constants.

μ	viscosity
ν	μ_ℓ/ρ
ξ	coordinate in orthogonal system.
ρ	density.
σ_h, σ_j	Prandtl number and Schmidt number.
σ_1, σ_2	diffusion constants in energy-length model.
$\sigma_{2,3}$	effective viscosity ratio.
τ	shear stress.
ϕ	dependent variable.
Φ	source term.
Ψ	stream function.
ω	dimensionless stream function.
Ω	rotational speed.

Subscripts	Definitions
1,2,3	coordinate directions in orthogonal system.
δ	where the velocity is 1% or 99% of some reference value.
eff	effective value.
i,j,k	indices relating to the i, j and k directions respectively.
I, E	inner and outer edges of boundary layer.
h	enthalpy.
i,j , i,k etc.	denote the ij plane, the ik plane, etc.
j	chemical species.
k	energy of turbulence.
$k\ell$	energy-length scale product.
ℓ	laminar.
m	maximum value.

o	outer or maximum value.
ø	dependent variable.
R	resultant value.
s	slot value; surface value.
t	turbulent.
w	wall value.
∞	free stream.
.01, .99, $\frac{1}{2}$, $\frac{1}{5}$	relate to point where V/V_m is equal to .01, .99, $\frac{1}{2}$ and $\frac{1}{5}$ respectively.

Superscripts	Definitions
'	fluctuating value.
"	per unit area.
—	time-average or space-average value.

REFERENCES

1. ARIS, R. (1962) 'Vectors, tensors, and the basic equations of fluid mechanics'.
Prentice Hall Int., London.

2. BACKSHALL, R.G. and LANDIS, F. (1969) 'The boundary layer velocity distribution in turbulent swirling pipe flow'.
J. Basic Engineering, Trans. ASME, Vol. 91, pp. 728-733.

3. BAYLEY, F.J. and OWEN, J.M. (1969) 'Flow between a rotating and a stationary disc'.
Aeronautical Quarterly, Vol. 20, pp. 333-352.

4. BAYLEY, F.J. and OWEN, J.M. (1970) 'The fluid dynamics of a shrouded disk system with a radial outflow of coolant'.
J. Eng. Power, Trans. ASME, Vol. 92, p. 335.

5. BRADSHAW, P. (1969) 'The analogy between streamline curvature and buoyancy in turbulent shear flow'.
Journal of Fluid Mechanics, Vol. 36, pt. 1, pp. 177-191.

6. BRYER, D.W. and PANKHURST, R.C. (1971) 'Pressure-probe methods for determining wind speed and flow direction'.
H.M.S.O., National Physical Laboratory, London.

7. CHAM, T-S. and HEAD, M.R. (1969) 'Turbulent boundary-layer flow on a rotating disk'.
J. Fluid Mechanics, Vol. 37, pt. 1, pp. 129-147.

8. CHAM, T-S. and HEAD, M.R. (1970) 'The turbulent boundary layer on a rotating cylinder in an axial stream'.
J. Fluid Mechanics, Vol. 42, pt. 1, pp. 1-15.

9. CHAM, T-S. and HEAD, M.R. (1971) 'The turbulent boundary layer on a rotating nose-body'.
Aeronautical Quarterly, Vol. 22, Pt. 4, pp. 389-402.

10. CHIGIER, N.A. (1972) 'Gasdynamics of swirling flow in combustion systems'.
Astronautica Acta, Vol. 17, pp. 387-395.

11. CHIGIER, N.A. and BEER, J.M. (1964) 'Velocity and static pressure distributions in swirling air jets issuing from annular and divergent nozzles'.
J. Basic Engineering, Trans ASME, Vol. 86, Pt. 4, pp. 788-796.

12. CHIGIER, N.A. and CHERVINSKY, A. (1966) 'Experimental and theoretical study of swirling jets issuing from a round orifice'.
Israel J. Technology, Vol. 4, No. 1, pp. 44-54.

13. CHIGIER, N.A. and CHERVINSKY, A. (1967) 'Experimental investigation of swirling vortex motion in jets'.
J. Applied Mechanics, Trans ASME, Vol. 89, pp. 443-451.

14. CHERVINSKY, A. and LORENZ, D. (1967) 'Decay of turbulent axisymmetrical free flows with rotation'.
J. Applied Mechanics, Trans. ASME, Vol. 89, pp. 806-812.

15. CHOU, P.Y. (1945) 'On velocity correlations and the solution of the equations of turbulent fluctuation'.
Quart. Appl. Math., Vol. 3, p. 31.

16. COBB, E.C. and SAUNDERS, O.A. (1956) 'Heat transfer from a rotating disk'.
Proceedings Royal Society, Vol. A236, pp. 343-351.

17. COCHRAN, W.G. (1934) 'The flow due to a rotating disk'.
Proc. Camb. Phil. Soc., Vol. 30, pp. 365-375.

18. COOPER, P. (1971) 'Turbulent boundary layer on a rotating disk calculated with an effective viscosity'.
AIAA Journal, Vol. 9, No. 2, pp. 255-261.

19. CRAYA, A. and DARRIGOL, M. (1967) 'Turbulent swirling jet'.
The Physics of Fluids Supplement, pp. S197-199.

20. DALY, B.J. and HARLOW, F.H. (1970) 'Transport equations in turbulence'.
Physics of Fluids, Vol. 13, p. 2634.

21. DAVIES, D.B. (1959) 'On the calculation of eddy viscosity and heat transfer in a turbulent boundary layer near a rapidly rotating disk'.
Quart. J. of Mech. and Appl. Math., Vol. 12, Pt. 2, pp. 211-221.

22. DENNIS, R.W., NEWSTEAD, C. and EDE, A.J. (1970) 'The heat transfer from a rotating disc in an air cross flow'.
4th Int. Heat Transfer Conference, Paris-Versailles, Vol. III, FC 7.1

23. DONALDSON, C. DU P. (1972) 'Calculations of turbulent shear flows for atmospheric and vortex motions'.
AIAA Journal, Vol. 10, pp. 4-12.

24. DORFMAN, L.A. (1963) 'Hydrodynamic resistance and the heat loss of rotating solids'.
Oliver and Boyd, London.

25. DORFMAN, L.A. (1965) 'Calculation of the boundary layer on an arbitrary axisymmetric surface rotating in a still medium'. J. Appl. Mech. and Tech. Phys., No. 3, pp. 62-65.

26. DORFMAN, L.A. and MIRONOVA, V.A. (1970) 'Solutions of equations for the thermal boundary layer on a rotating axisymmetric surface'. Int. J. Heat Mass Transfer, Vol. 13, pp. 81-92.

27. DORFMAN, L.A. and SERAZETDINOV, A.Z. (1965) 'Laminar flow and heat transfer near rotating axisymmetric surface'. Int. J. Heat Mass Transfer, Vol. 8, pp. 317-327.

28. EAST, L.F. (1972) 'A prediction of the law of the wall in compressible three dimensional turbulent boundary layers'. Royal Aircraft Establishment TR72178.

29. ERIAN, F.F. and TONG, Y.H. (1971) 'Turbulent flow due to a rotating disk'. The Physics of Fluids, Vol. 14, No. 12, p. 2588.

30. ESCUDIER, M.P. (1965) 'The distribution of the mixing length in turbulent flows near walls'. Imperial College, Mech. Eng. Dept. Rep., TWF/TN/1.

31. FORSTALL, W. and SHAPIRO, A.H. (1950) 'Momentum and mass transfer in coaxial jets'. J. Appl. Mech.,Trans. ASME, Vol. 17, p. 399.

32. FURUYA, Y., NAKAMURA, I. and KAWACHI, H. (1966) 'The experiment on the skewed boundary layer on a rotating body'. Bull. JSME, Vol. 9, No. 36, pp. 702-710.

33. GOLDSTEIN, S. (1935) 'On the resistance to the rotation of a disc immersed in a fluid'.
Proceedings Camb. Phil. Soc., Vol. 31, pp. 232-241.

34. GOSMAN, A.D., PUN, W.M., RUNCHAL, A.K., SPALDING, D.B. and WOLFSHTEIN, M. (1969) 'Heat and mass transfer in recirculating flows'.
Academic Press, London.

35. GREGORY, N., STUART, J.T. and WALKER, W.S. (1955) 'On the stability of three-dimensional boundary layers with application to the flow due to a rotating disk'.
Phil. Trans. Royal Soc., Vol. A248, pp. 155-199.

36. HANJALIC, K. and LAUNDER, B.E. (1972) 'A Reynolds-stress model of turbulence and its application to thin shear flows'.
J. Fluid Mechanics, Vol. 52, Pt. 4, pp. 609-638.

37. HANNAH, D.M. (1947) 'Forced flow against a rotating disk'.
ARC report R&M No. 2772, London.

38. HARTNETT, J.P. and DELAND, E.C. (1961) 'The influence of Prandlt number on the heat transfer from rotating non isothermal disks and cones'.
J. Heat Transfer, Trans. ASME, Vol. 83, pp. 95-96.

39. HARTNETT, J.P., TSAI, S. and JANTSCHER, H.N. (1965) 'Heat transfer to a nonisothermal rotating disk with a turbulent boundary layer'.
J. Heat Transfer, Trans. ASME, Vol. 87, pp. 362-368.

40. HAYDAY, A.A. (1965) 'On heat transfer from isothermal and nonisothermal spinning bodies of revolution'.
J. Heat Transfer, Trans. ASME, Vol. 87, pp. 445-451.

41. HINZE, J.O. (1959) 'Turbulence'.
McGraw-Hill, London.

42. HOMANN, F. (1936) 'Der Einfluss grösser Zähigkeit bei der Strömung um den Zylinder und um die Kugel'.
Z. angew. Math. Mech., Vol. 16, p. 153.

43. HUGHES, D.W. and HORLOCK, J.H. (1971) 'Effect of rotation on the development of the turbulent boundary layer'.
Symposium on internal flows, U. of Salford, England, Paper 18, pp. B.78-B.88.

44. JOHNSTON, J.P. (1970) 'Measurements in a three-dimensional turbulent boundary layer induced by a swept, forward-facing step'.
J. Fluid Mechanics, Vol. 42, pp. 823-844.

45. KARMAN, T. VON (1921) 'Über laminare und turbulent Reibung'.
Z. angew. Math. Mech., Vol. 1, pp. 233-252.
Translated as NACA TM 1092, 1946.

46. KESTIN, J. and RICHARDSON, P.D. (1963) 'Heat transfer across turbulent, incompressible boundary layers'.
Int. J. Heat Mass Transfer, Vol. 6, pp. 147-189.

47. KOH, J.C.Y. and PRICE, J.F. (1967) 'Nonsimilar boundary layer heat transfer of a rotating cone in forced flow'.
J. Heat Transfer, Trans. ASME, Vol. 89, pp. 139-145.

48. KOLMOGOROV, A.N. (1942) 'Equations of turbulent motion in an incompressible fluid'.
Izv. Academy of Sciences, USSR, Physics, Vol. 6, No. 1, 2, pp. 56-58.

49. KOOSINLIN, M.L. and LOCKWOOD, F.C. (1971) 'The prediction of boundary layers on rotating axially-symmetrical bodies'.
Imperial College, Mech. Eng. Dept., HTS/71/6.

50. KREITH, F. (1966) 'Frictional drag and convective heat transfer on rotating cones in mixed and turbulent flow'.
Proceedings of the 1966 Heat Transfer and Fluid Mechanics Institute, Stanford University Press.

51. KREITH, F. (1968) 'Advances in heat transfer'.
Vol. 5,Academic Press, New York.

52. KREITH, F., ELLIS, D. and GIESING, J. (1962) 'Boundary layer and transition characteristics of a rotating cone'.
ASME paper No. 62-WA-105.

53. KREITH, F., ELLIS, D. and GIESING, J. (1962) 'An experimental investigation of the flow engendered by a rotating cone'.
Appl. Sci. Res., Vol. A11, p. 430.

54. KREITH, F., TAYLOR, J.H. and CHONG, J.P. (1959) 'Heat and mass transfer from a rotating disk'.
Journal of Heat Transfer, Trans. ASME, Vol. 81, pp. 95-105.

55. LAUNDER, B.E. and SPALDING, D.B. (1972) 'Mathematical Models of turbulence'.
Academic Press, London and New York.

56. LEE, M. (1966) 'Effect of boundary layer control on heat transfer from a rotating disk'.
D.I.C. Thesis, Imperial College, London.

57. LEWIS, J.P. and RUGGERI, R.S. (1956) 'Investigation of heat transfer from a stationary and rotating ellipsoidal forebody of fineness ratio 3'.
NACA TN 3837.

58. LILLEY, D.G. (1973) 'Prediction of inert turbulent swirl flows'.
AIAA Journal, Vol. 11, No. 7, pp. 955-960.

59. LILLEY, D.G. and CHIGIER, N.A. (1971) 'Nonisotropic exchange coefficients in turbulent swirling flames from mean value distributions'.
Combustion and Flame, Vol. 16, pp. 177-189.

60. LILLEY, D.G. and CHIGIER, N.A. (1971) 'Nonisotropic turbulent stress distribution in swirling flows from mean value distributions'.
Int. J. Heat Mass Transfer, Vol. 14, p. 573-585.

61. LIU, K.T. and STEWART, W.E. (1972) 'Asymptotic solutions for forced convection from a rotating disk'.
Int. J. Heat Mass Transfer, Vol. 15, pp. 187-189.

62. MABUCHI, I., KOTAKE, Y. and TANAKA, T. (1971) 'Studies on the convective heat transfer from a rotating disk'.
Bull. JSME, Vol. 15, No. 84, pp. 766-773.

63. MABUCHI, I, TANAKA, T. and SAKAKIBARA, Y. (1967) 'Studies on the convective heat transfer from a rotating disk'.
Bull. JSME, Vol. 10, No. 37, pp. 104-112.

64. MCCOMAS, S.T. and HARTNETT, J.P. (1970) 'Temperature profiles and heat transfer associated with a single disk rotating in still air'.
4th Int. Heat Transfer Conference, Paris-Versailles, Vol. III, FC7.7.

65. MILLSAPS, K. and POHLHAUSEN, K. (1952) 'Heat transfer by laminar flow from a rotating plate'.
J. Aeronautical Sciences, Vol. 19, pp. 120-126.

66. NAOT, D., SHAVIT, A. and WOLFSHTEIN, M. (1970) 'Interactions between components of the turbulent velocity correlation tensor due to pressure fluctuations'.
Israel J. Technology, Vol. 8, pp. 259-269.

67. NG, K.H. (1972) 'Predictions of turbulent boundary-layer developments using a two-equation model of turbulence'.
Ph.D. Thesis, U. of London.

68. NG, K.H., PATANKAR, S.V. and SPALDING, D.B. (1968) 'Proceedings of the 'Conference on computation of turbulent-boundary layers-1'.
Ed. Kline, S.J ., Morkovin, M.V., Sovran, G. and Cockrell, D.J.,
Standford University.

69. NG, K.H. and SPALDING, D.B. (1972) 'Turbulence model for boundary layers near walls'.
Physics of Fluids, Vol. 15, pp. 20-30.

70. OSTRACH, S. and THORNTON, P.R. (1958) 'Compressible laminar flow and heat transfer about a rotating isothermal disk'.
NACA TN 4320.

71. OWEN, J.M. (1969) 'Flow between a rotating andastationary disc'.
Ph.D. Thesis, U. of Sussex, England.

72. OWEN, J.M. (1971) 'The effect of forced flow on heat transfer from a disc rotating near a stator'.
Int. J. Heat Mass Transfer, Vol. 14, p. 1135-1147.

73. OWEN, J.M., HAYNES, C.M. and BAYLEY, F.J. (1972) 'Heat transfer from an air-cooled rotating disk'.
Mech. Eng. Lab., School Appl. Sci., U. of Sussex, Rep. 72/Me/43 and /44.

74. PARR, VON O. (1963) 'Untersuchungen der dreidimensionalen Grenzschicht an rotierenden Drehkörpern bei axialer Anströmung'.
Ing. Arch., Vol. 32, pp. 393-413.

75. PATANKAR, S.V. and SPALDING, D.B. (1970) 'Heat and mass transfer in boundary layers'.
Intertext Books, London.

76. PRANDTL, L. (1925) 'Bericht über Untersuchungen zur ausgebildeten Turbulenz'.
Z. angew. Math. Mech., Vol. 5, p. 136.

77. PRANDTL, L. and WEIGHARDT, K. (1945) 'Über ein neues Formelsystem fur die ausgebildete Turbulenz'.
Nach. Akad. Wiss., Goettingen, Math. Phys., Vol. 19, p. 6.

78. PRATTE, B.D. and KEFFER, J.R. (1972) 'The swirling turbulent jet'.
J. Basic Engineering, Trans. ASME, Paper No. 72-FE-18.

79. PRATTE, B.D. and KEFFER, J.R. (1972a) 'Private communication'.

80. RICHARDSON, P.D. (1958) 'Some studies of the flow and heat transfer associated with a rotating disk'.
Ph.D. Thesis, U. of London.

81. ROBERTS, L.W. (1972) 'Turbulent swirling flows with recirculation'.
Ph.D. Thesis, U. of London.

82. RODI, W. (1970) 'Basic equations for turbulent flow in Cartesian and cylindrical coordinates'.
Imp. Col., Dept. of Mech. Eng., Rep. HTS/70/4.

83. RODI, W. (1973) 'The prediction of free turbulent boundary layers by use of a two-equation model of turbulence'.
Ph.D. Thesis, U. of London.

84. RODI, W. and SPALDING, D.B. (1970) 'A two-parameter model of turbulence, and its application to free jets'.
Wärmeund Stoffübertragung, Vol. 3, pp. 85-95.

85. ROSE, W.G. (1962) 'A swirling round turbulent jet'.
J. Applied Mechanics, Trans. ASME, Vol. 29, Pt. 4, pp. 615-625.

86. ROTTA, J.C. (1951) 'Statistiche Theorie nichthomogener Turbulenz'.
Zeit. Phys., Vol. 129, pp. 547-572.

87. ROTTA, J.C. (1962) 'Turbulent boundary layers in incompressible flows'.
Progress in Aeronautical Sciences, Macmillan, Vol. 2, pp. 1-221.

87a. RUGGERI, R.S. and LEWIS, J.P. (1957) 'Investigation of heat transfer from a stationary and a rotating conical forebody'.
NACA TN 4093.

88. SALZBERG, F. and KEZIOS, S.P. (1965) 'Mass transfer from a rotating cone in axisymmetric flow'.
J. Heat Transfer, Trans. ASME, Vol. 87, pp. 469-476.

89. SCHLICHTING, H. (1953) 'Die laminare Strömung um einen axial angeströmten rotierenden Drenkörper'.
Ingenieur-Archiv, Vol. 21, No. 4, pp. 227-244.
Translated as: 'Laminar flow about a rotating body of revolution in an axial airstream'.
NACA TM 1415, 1956.

90. SCHLICHTING, H. (1968) 'Boundary layer theory'.
McGraw-Hill, London.

91. SCHLICHTING, H. and TRUCKENBRODT, E. (1952) 'The flow around a rotating disk in a uniform stream'.
J. Aero. Sci., Readers Forum, Vol. 18, p. 639.

92. SCHNURR, N.M. (1964) 'Heat transfer from a rotating disk with a stepwise discontinuous surface temperature'.
J. Heat Transfer, Trans. ASME, Vol. 86, pp. 467-468.

93. SIDDHARTHA, V. (1971) 'Boundary layers with swirl'.
Ph.D. Thesis, U. of London.

94. SPALDING, D.B. (1967) 'Theories of the turbulent boundary layer'.
Appl. Mech. Review, Vol. 20, p. 735.

95. SPARROW, E.M. and GREGG, J.L. (1959) 'Heat transfer from a rotating disk to fluids of any Prandtl number'.
J. Heat Transfer, Trans. ASME, Vol. 81, pp. 249-250.

96. SPARROW, E.M. and GREGG, J.L. (1960) 'Mass transfer, flow and heat transfer about a rotating disk'.
J. Heat Transfer, Trans. ASME, Vol. 82, pp. 294-302.

97. SPARROW, E.M. and HARTNETT, J.P. (1961) 'Condensation on a rotating cone'.
J. Heat Transfer, Trans. ASME, Vol. 83, pp. 101-102.

98. SUBBA RAO, B.K. (1967) 'Heat transfer from a disc with uniform wall heat flux rotating in air'.
J. Institution of Engineers (India), Vol. XLVII, No. 7, Pt. ME4, pp. 289-304.

99. SYRED, N., BEER, J.M. and CHIGIER, N.A. (1971) 'Turbulence measurements in swirling recirculating flows'.
Proceedings of Salford Symposium on Internal Flow, Institution of Mechanical Engineers.

100. THEODORSEN, T. and REGIER, A. (1944) 'Experiments on drag of revolving disks, cylinders, and streamline rods at high speed'.
NACA. Rep. 793.

101. TIEN, C.L. (1960) 'Heat transfer by laminar flow from a rotating cone'.
J. Heat Transfer, Trans. ASME, Vol. 82, pp. 252-253.

102. TIEN, C.L. (1965) 'Heat transfer by the induced flow about a rotating cone of non-uniform surface temperature'.
Int. J. Heat Mass Transfer, Vol. 8, pp. 411-418.

103. TIEN, C.L. and CAMPBELL, D.T. (1963) 'Heat and mass transfer from rotating cones'.
J. Fluid Mechanics, Vol. 17, pp. 105-112.

104. TIEN, C.L. and TSUJI, J. (1964) 'Heat transfer by laminar forced flow against a non-isothermal rotating disk'.
Int. J. Heat Mass Transfer, Vol. 7, pp. 247-252.

105. TIEN, C.L. and TSUJI, J. (1965) 'A theoretical analysis of laminar forced flow and heat transfer about a rotating cone'.
J. Heat Transfer, Trans. ASME, Vol. 87, pp. 184-190.

106. TRUCKENBRODT, E. (1952) 'Method of quadrature for calculation of the laminar and turbulent boundary-layer in case of plane and rotationally symmetrical flow'.
Ing. Arch., Vol. 20, pp. 211-228.
Translated as NACA TM 1379.

107. VAN DRIEST, E.R. (1956) 'On turbulent flow near a wall'.
J. Aeronautical Sciences, Vol. 23, pp. 1007-1011.

108. WAGNER, C. (1948) 'Heat transfer from a rotating disk to ambient air'.
J. Applied Physics, Vol. 19, pp. 837-839.

109. WISLICENUS, G.F. and YEH, H.A. (1952) 'A program of research in the field of turbulent flow in ducts, in a space of revolution, and in turbo-machinery'.
John Hopkins University, Mech. Eng. Dept., Internal Flow Research Report I-8.

110. WU, C.S. (1959) 'The three dimensional incompressible laminar boundary on a spinning cone'.
Appl. Sci. Res., Vol. 8, pp. 140-146.

111. YU, J.P., SPARROW, E.M., ECKERT, E.R.G., HENNECKE, D.K. and SHAMSUNDAR, N. (1972) 'Experiments on a shrouded, parallel disk system with rotation and coolant through flow'.
Heat Transfer Laboratory, Mech. Eng. Dept., U. of Minnesota, Rep. HTL TR No. 105.

APPENDIX 1

Previous Theoretical Work

1.1 INTRODUCTION

A comprehensive survey of the various prediction procedures in existence up to about 1958 has been provided by Dorfman (1963). Another extensive review of subsequent advances in the field has been made by Kreith (1968). From these two reviews, which appear in book form, it is evident that the field of rotating flows is extremely vast, even when only boundary-layer flows are considered. The present review, therefore, does not cover all the previous work on swirling boundary-layer flows, but focuses on the principal theoretical

approaches for unshrouded flow situations. However, it adequately summarises the present status of the subject for other geometries as well since the theoretical methods developed for shrouded geometries are mostly extensions of methods which work well for the unshrouded cases.

In Section 1.2 the previous theoretical work on laminar flow hydrodynamics and heat transfer is covered. Consideration of the laminar flow solutions represents an essential step in the study of any class of flows. These solutions serve two main purposes: firstly, they provide exact or near exact solutions with which the accuracy of proposed prediction procedures can be tested; and secondly, they provide an insight into the physical nature of the flow under consideration. The flow configurations reviewed are: discs, cones and axisymmetrical bodies of arbitary geometry rotating in unconfined surroundings.

The turbulent flow work is surveyed in Section 1.3-1. All of the early theoretical procedures have been comprehensively summarised by Dorfman (1963) and Kreith (1968). The present review extends the coverage to 1972, and shows the gradual shift in prediction procedures from integral-profile to finite-difference methods. The turbulence models associated with the latter procedures are described. The flows covered range from free discs, parallel discs, free cones and cylinders, to free swirling jets.

Lastly, Section 1.3-2 is concerned with the analytical work on the heat transfer from discs and cones rotating in stagnant surroundings.

1.2 LAMINAR FLOW

1.2-1 Discs

(a) Hydrodynamics

The first theoretical analysis of the flow near a rotating body was performed by von Karman (1921). He considered the induced flow near a disc, and showed that the general forms of the momentum equations reduce to a set of ordinary differential equations. Using Pohlhausen's integral-profile method von Karman solved these for the drag on the disc and showed that the boundary layer was of uniform thickness. Cochran (1934) obtained very accurate solutions of the same equations for the velocity field and the drag by means of a numerical integration procedure. For the case where the surrounding fluid moves with uniform speed towards the disc parallel to its axis, Schlichting and Truckenbrodt (1952) used an integral-profile method similar to von Karman's to obtain an approximate solution for the drag. Hannah (1947) showed that similarity solutions also exist for this case; she used a numerical integration method like that of Cochran, and presented exact solutions for the velocity and pressure distributions, and for the drag.

(b) Heat Transfer

Wagner (1948) and Millsaps and Pohlhausen (1952) made use of Cochran's (1934) results and solved the energy equation to determine the heat transfer from an isothermal disc rotating in stagnant surroundings. This work was extended by Ostrach and Thornton (1958) to include the influence of variable fluid properties, and to fluids of any Prandtl number by Sparrow and Gregg (1959). Asymptotic solutions for large and small Prandtl numbers have been

obtained by Liu and Stewart (1971).

The influence of injection or suction, or phase change at the disc surface, on the heat transfer and velocity field have been examined by Sparrow and Gregg (1960). The heat transfer from a disc with a stepwise discontinuous surface temperature has been studied by Schnurr (1964); he used Pohlhausen's integral method to obtain an energy balance in the thermal boundary layer.

For the more general problem of a disc rotating in a uniform axial stream, Tien and Tsuji (1964) have extended the flow analysis of Hannah (1947) to the heat-transfer problem. Their analysis was based on power-law wall-temperature distribution, with the isothermal wall boundary condition as a special case. They also presented results for a wide range of Prandtl numbers. Mabuchi (1967) included viscous dissipation effects in the energy equation and obtained similar results to Tien and Tsuji.

1.2-2 Cones

Wu (1959) demonstrated that, by appropriate transformations, the hydrodynamic solution for the flow on a disc rotating in stagnant surroundings can be used to determine the flow on a rotating cone (the disc is, of course, a special case: a cone of 180 degree vertex angle). Tien (1960) subsequently showed that, under boundary-layer approximations, heat transfer obtained for an isothermal disc, with viscous dissipation included, can be applied to the rotating cone. Hartnett and Deland (1961) obtained solutions in this way for the case of cones having a power-law variation of surface temperature, and for fluids of different Prandtl number. Sparrow and Hartnett (1961) reported solutions for the case of condensation on the surface of a cone.

The more general problem of a cone spinning in a uniform axial stream is not amenable to a similarity type of treatment, Schlichting (1953, 1968). Tien and Tsuji (1965) obtained asymptotic solutions of the velocity and temperature distributions for a slow rotating cone using a perturbation scheme, and for a fast rotating cone by means of a series-expansion procedure. The general problem was successfully analysed by Koh and Price (1967) by means of a finite-difference technique. They solved the boundary-layer form of the momentum and energy equations to determine the flow and heat transfer on an isothermal cone. They presented results for various Prandtl numbers, for several ratios of the rotational to free stream velocity, for a disc and for a cone of 53.5 degree vertex angle.

1.2-3 Other Geometries

Hayday (1965) showed that similarity solutions of the boundary-layer equations exist for a body of revolution rotating in quiescent fluid, the radius of which varies according to a power-law with respect to distance measured along its surface; when there is heat transfer, the surface temperature must also obey a power-law. He further showed that the technique of superposition can be employed to extend similarity solutions for the temperature field to the case where the surface temperature varies in an arbitrary way.

The work of Dorfman and his coworkers (1965, 1970) probably represents the ultimate in usefulness of the similarity approach. They described an approximate procedure in which the boundary-layer similarity solutions are employed to obtain solutions for a rotating body of revolution of arbitrary shape. The body is divided into finite segments by planes at right angles to its axis and the flow over each surface element is determined approximately

by assuming that the similarity solution corresponding to a power-law variation of radius applies.

1.3 TURBULENT FLOW

1.3-1 Hydrodynamics

(a) Discs

Von Karman (1921) solved the integral forms of the momentum equations to obtain the frictional resistance and boundary-layer thickness on a disc rotating in stagnant surroundings. He assumed velocity profiles of the 1/7th power-law form and a wall shear stress relation from Blasius' friction formula for smooth pipes. Goldstein (1935) and later Dorfman (1963) obtained the overall drag on the disc using logarithmic velocity profiles in place of the 1/7th power-law. Of these three, Dorfman's method gives the best agreement with the experimental data.

Cham and Head (1969) also calculated the velocity field using an integral-profile method and an auxiliary equation for entrainment. The circumferential velocity profiles were represented by a two-parameter family, and the radial profiles by a quadratic expression. The entrainment was governed by the circumferential velocity. They obtained excellent agreement with their experimental measurements of entrainment and velocity distributions.

Recently, several workers have made use of finite-difference procedures to predict swirling flows. Bayley and Owen (1969, 1970) and Owen (1969), in connection with the gas-turbine disc-cooling problem, have integrated the turbulent boundary-layers which form on the stator and rotor of a parallel discs system with radial outflow. These authors used the original finite-difference method of Patankar and Spalding (1970) for the numerical solution of the

equations governing their problem. The radial and circumferential shear stress components in the momentum equations were respectively expressed as:

$$\tau_{1,2} \equiv \mu_{1,2} \frac{\partial V_1}{\partial y} \quad , \quad \text{and} \quad \tau_{2,3} \equiv \mu_{2,3} \frac{\partial V_3}{\partial y} \quad .$$

The effective viscosities $\mu_{1,2}$ and $\mu_{2,3}$ were calculated from the following extension of Prandtl's (1925) mixing-length hypothesis:

$$\mu_{1,2} = \mu_\ell + \rho \ell_m^2 \left| \frac{\partial V_1}{\partial y} \right| \quad , \quad \text{and} \quad \mu_{2,3} = \mu_\ell + \rho \ell_m^2 \left| \frac{\partial V_3}{\partial y} \right| \quad .$$

In the regions close to the rotor and stator, the van Driest (1956) damping function was employed with $\kappa = 0.4$:

$$\mu_{1,2} = \mu_\ell + \rho \kappa^2 y^2 \left[1 - \exp\left(-y \sqrt{\rho \tau_{1,2}} / 26 \mu_\ell \right) \right]^2 \left| \frac{\partial V_1}{\partial y} \right| \quad ,$$

$$\mu_{2,3} = \mu_\ell + \rho \kappa^2 y^2 \left[1 - \exp\left(-y \sqrt{\rho \tau_{2,3}} / 26 \mu_\ell \right) \right]^2 \left| \frac{\partial V_3}{\partial y} \right| \quad .$$

In the region remote from the solid boundaries the mixing-length ℓ_m was assumed equal to half the spacing between the rotor and the stator. The authors obtained qualitative agreement of circumferential drag and radial pressure distributions between their predictions and their experimental measurements over the whole range of data. However, quantitative discrepancies of certain flow conditions led Bayley and Owen to remark that the simple mixing-length hypothesis used in their analysis is not universally adequate.

Cooper (1971) solved the continuity and momentum equations for the case of a free rotating disc by a two-dimensional finite-difference method, modelling the Reynolds stress terms by a two-layer scalar effective viscosity. In the layer close to the wall the effective viscosity was computed from the resultant of the radial and circumferential velocity gradients, and from Prandtl's

(1925) mixing-length modified by van Driest's (1956) damping function:

$$\mu_{1,2} = \mu_{2,3} = \mu_\ell + \rho \kappa^2 y^2 \left[1 - \exp\left(-y\sqrt{\tau/\rho}/26\mu_\ell\right)\right]^2 \left[\left(\frac{\partial V_1}{\partial y}\right)^2 + \left(\frac{\partial V_3}{\partial y}\right)^2\right]^{\frac{1}{2}},$$

where $\kappa = 0.4$, and τ is the local effective shear stress calculated as the product of the effective viscosity and the resultant of the velocity gradients. For the outer part of the layer Cooper assumed that the viscosity was proportional to the circumferential velocity displacement thickness and an intermittency factor. He initiated his predictions at the centre of the disc and assumed a step transition from laminar to turbulent flow at a rotational Reynolds number of 3.04×10^5. His predictions compared well with the circumferential drag and velocity field data.

(b) Cones

The integral profile analysis of von Karman (1921) for a disc was generalised by Kreith (1966) to calculate the drag on cones of arbitrary vertex angles. He obtained satisfactory agreement with his drag measurements for a cone of 60 degree vertex angle.

(c) Cylinders

For the case of a cylinder in a uniform stream flowing parallel to its axis of rotation, Parr (1963) used a momentum integral approach to predict the axial and circumferential momentum thicknesses. Cham and Head (1970) extended their method for the disc flow to the cylinder flow. The velocity profiles were assumed from a two parameter family, and the auxiliary equation for entrainment was made a function of the velocity defect in the outer part of the layer and of the ratio of rotational to free stream velocity. They obtained very good agreement with the drag and

velocity field measurements of Parr. Furuya, Nakamura and Kawachi (1966) represented the velocity components by fourth order polynomials; they achieved fair agreement with their data for the velocity field.

(d) Nose-Body

Cham and Head (1971) have recently applied their entrainment method (based on the use of momentum integral equations in the streamwise and cross-stream directions) to the study of the boundary layer on a nose-body rotating in an axial stream of uniform velocity. The problem was formulated in orthogonal coordinates which were then transformed to a system of streamline coordinates appropriate to their solution procedure. They present solutions of the velocity field, and axial and circumferential drag coefficients, for a single set of conditions based on the free-stream Reynolds number and a rotational velocity parameter. Experimental measurements are not available for their geometry.

(e) Free Swirling Jet

The most comprehensive study of axisymmetrical swirling jets in stagnant surroundings is undoubtedly that of Chigier and his coworkers. Chigier and Chervinsky (1966, 1967) used an integral-profile method and assumed that, at some distance from the jet orifice a fully developed flow field is established in which the velocity profiles have similar shapes. The axial and swirl components of velocity were specified as third order polynomials. Their analysis was extended by Chervinsky and Lorenz (1967) to general axisymmetrical free swirling flows: a jet issuing into a stagnant medium, a jet issuing into a co-axial stream, and a wake behind a rotating body. The solutions are, again, only valid in the region of

the flow where the assumption of similarity holds. The predictions of axial and swirl velocity decay compared well with the data for jets in stagnant surroundings.

Lilley (1973) adopted a different approach; he employed the finite-difference procedure of Patankar and Spalding (1970) to solve the equations governing the jet swirling in a stagnant medium. He assumed that the effective viscosities are related via a viscosity ratio, $\sigma_{2,3} = \mu_{1,2}/\mu_{2,3}$, and evaluated $\mu_{1,2}$ from an extension of Prandtl's mixing-length hypothesis:

$$\mu_{1,2} = \rho \ell_m^2 \left[\left(\frac{\partial V_1}{\partial x_2} \right)^2 + \left(r \frac{\partial V_3/r}{\partial x_2} \right)^2 \right]^{\frac{1}{2}} ,$$

$$\ell_m = .08 \left(1 + .6 S \right) r_{.05} ,$$

$$\sigma_{2,3} = 1 + 5S^{\frac{1}{3}} .$$

$r_{.05}$ is the value of r where the axial velocity decays to 5% of its value at the axis. Both the mixing-length ℓ_m and the viscosity ratio $\sigma_{2,3}$ were made functions of the local swirl number S, a measure of the axial flux of swirl and axial momenta. Lilley's predictions of jet growth, entrainment and decay were in good agreement with the data of Chigier and Chervinsky (1966, 1967).

In addition to the mixing-length formulation, Lilley also employed a different model of turbulence to repeat his predictions. The effective viscosity $\mu_{1,2}$ was calculated in terms of the kinetic energy of turbulence k and a length scale ℓ appropriate to the energy containing eddies: $\mu_{1,2} = \rho k^{\frac{1}{2}} \ell$ and $\mu_{2,3} = \mu_{1,2}/\sigma_{2,3}$ where $\sigma_{2,3} = 1 + 2S^{\frac{1}{3}}$. The two turbulence quantities k and ℓ were determined from their own differential equations. These equations were developed by Rodi and Spalding (1970) and Ng and Spalding (1972) for non-swirling boundary layers, and extended during

the course of the present research to swirling boundary layers; this latter work was reported in an internal report at Imperial College: Koosinlin and Lockwood (1971). Since these equations are described in the main text of the present thesis, it is sufficient here to note that Lilley's predictions were in good agreement with the data.

1.3-2 Heat Transfer

(a) Discs

Dorfman (1963) presented predictions of the Nusselt number for a disc rotating in stagnant surroundings and having an arbitrary distribution of surface temperature. He employed von Karman's (1921) results for the frictional drag, assumed a quadratic variation of surface temperature, and applied Reynolds analogy. He then solved the energy equation assuming an one parameter family of temperature profiles; the constants in this equation were determined from the Reynolds analogy results. Dorfman found that the Nusselt number varies with Reynolds number to the 0.8 power, and with Prandtl number to the 0.6 power.

A procedure for the case of an isothermal disc in air was proposed by Davies (1959). He assumed 1/7th power velocity profiles, and solved the integral radial momentum equation alone, making use of von Karman's results to obtain the radial component of shear stress. The diffusivity of the radial momentum was then equated to the diffusivity of heat, and the temperature equation solved to determine the heat transfer; the Nusselt number was found to vary as the Reynolds number to the power 0.8.

Hartnett, Tsai and Jantscher (1965) pointed out that the analytical procedure of Davies is also applicable when the

surface temperature of the disc is a power-law function of the radius. They extended Davies' solution to non-isothermal discs, but equated the circumferential instead of the radial diffusivity of momentum to the diffusivity of heat. Their own predictions, along with those of Dorfman and Davies, were compared with the experimental heat and mass transfer data for isothermal discs rotating in still air; the predictions of Dorfman were the most reliable.

(b) Cones

Tien (1965) showed that the analytical heat-transfer prediction for non-isothermal discs can be applied to obtain solutions for non-isothermal rotating cones, and also for discs and cones having a step distribution of surface temperature. Kreith (1966) determined that the Nusselt number for an isothermal cone varies with Reynolds number to the 0.8 power, and with Prandtl number to the 0.75 power. This result was derived from the earlier work of Kreith, Taylor and Chong (1959) who assumed a 'law of the wall' type profile, and solved the mass-transfer equation.

APPENDIX 2

Previous Experimental Work

2.1 INTRODUCTION

The availibility of reliable experimental data is paramount to the successful development of prediction procedures; in particular, they are essential to the framing of a proper model for the turbulence structure of the flow under consideration. These data play a major role in the determination of the constants or functions appearing in the turbulence models, and in assessing the general validity of such models. It is therefore necessary to identify the most reliable experimental data. However, for many swirling flow configurations the data are limited or unreliable; but they are none-the-less the only ones available for comparison with predictions. The following review therefore covers the most reliable experimental measurements for the

few cases when several sets of data are available; it also indicates the limited amount, the unreliability, and the plain lack of data for several flow situations.

The experimental measurements of mean flow quantities for rotating discs, cones and cylinders, and for free swirling jets in stagnant surroundings, under conditions of turbulent flow, are reviewed in Section 2.2. The laminar flow data have been comprehensively covered by Dorfman (1963) and Kreith (1968).

Section 2.3 covers the measurements of turbulence quantities for rotating discs and swirling jets in stagnant surroundings. These are the only two flows for which turbulence measurements have been reported.

Section 2.4 deals with the heat and mass transfer from discs and cones rotating in stagnant air. Also reviewed are isothermal discs and cones rotating in co-axial air streams. Both laminar and turbulent flows are considered.

2.2 HYDRODYNAMIC EXPERIMENTS

2.2-1 Discs

One of the earliest reported experiments is that of Theodorsen and Regier (1944) who measured the drag on a disc rotating in still air. At high Reynolds numbers, when turbulent flow prevailed over most of the disc surface, their results and the more recent drag measurements of Owen (1969) confirm Dorfman's (1963) turbulent flow predictions.

Measurements of the velocity field near a disc in the laminar, transitional and turbulent flow regions were made by Gregory, Stuart and Walker (1955); they found that the transition Reynolds number lies between 2.7×10^5 and 3×10^5. Their circumferential

velocity profiles were in good agreement with Cochran's (1934) predictions for laminar flow, but the agreement for the radial velocity profiles was not good. For turbulent flow, both the 1/7th power profile assumed by von Karman (1921) and the logarithmic profile assumed by Goldstein (1935) represented well the circumferential velocity measurements. The radial velocity profile was in good agreement with von Karman's power-law assumption close to the surface, but Goldstein's logarithmic profile was superior away from the surface.

Recently, Cham and Head (1969) have reported comprehensive measurements of the velocity field and entrainment into the boundary layer on a free rotating disc. These authors obtained excellent agreement with their calculations using the circumferential and radial momentum equations with an auxiliary equation for entrainment.

2.2-2 Cones

Kreith, Ellis and Giesing (1962) investigated the transition characteristics of cones rotating in a motionless medium, and found a rapid increase in the transition Reynolds number with increasing cone vertex angle. They further measured the velocity field on a cone of 53.5 degree vertex angle for laminar flow; the results confirmed their predictions based on boundary-layer theory. Kreith (1966) has also performed a few measurements of the drag on a 60 degree cone rotating in stagnant air in turbulent flow conditions; the experimental data substantiate well his theoretical predictions.

2.2-3 Cylinders

Parr (1963), and Furuya, Nakamura and Kawachi (1966) have measured the velocity distribution on a cylinder having a streamline fore-portion rotating in an axial air stream of uniform velocity. The measurements were carried out on the cylindrical part of the body, and

have been well predicted by Cham and Heads' (1970) integral-profile method.

2.2-4 Free Jets

The first reliable experimental velocity measurements of an axisymmetrical swirling jet were reported by Rose (1962) for a weak degree of swirl relative to the axial velocity; the jet issued from a rotating pipe. The same technique was used by Pratte and Keffer (1972) to generate a jet of moderate swirl. Chigier and Beer (1964), and Chigier and Chervinsky (1966, 1967) obtained jets for a wide range of degrees of swirl by injecting air through tangential slots into an axial flow in a pipe. The results of all these experiments showed a rapid decay of the swirl component of velocity to less than 5% of the orifice value at 10 diameters downstream; they also showed that the mean velocity profiles and pressure profiles were effectively similar from an axial distance of 4 orifice diameters for low and moderate swirl. Chigier and Chervinsky (1966, 1967) found good agreement between the experimental mean velocity data and their predictions based on an integral-profile method.

2.3 TURBULENCE MEASUREMENTS

2.3-1 Discs

The only experimental measurements of turbulence quantities for the flow over axisymmetrical rotating bodies are those recently reported by Erian and Tong (1971) for a disc rotating in stagnant air. They measured the Reynolds stresses $\overline{v_1^2}$ and $\overline{v_3^2}$ associated with the radial and circumferential directions, but not the cross-stream normal stress $\overline{v_2^2}$, nor the radial-normal $\overline{v_1 v_2}$ and circumferential-normal $\overline{v_3 v_2}$ shear stresses because of experimental difficulties. This is rather unfortunate since these latter three stresses are the most significant ones in the

boundary layer on the disc.

Erian and Tong's work has however exposed several experimental problems; for example, as a result of manufacturing tolerances, the movement of the surface in the cross-stream direction is usually of larger magnitude than the scale of fluctuating motions. Accurate positioning of the measuring probe from the surface is not easily achieved, leading to inaccurate measurements owing to the steep gradients of flow properties. Direct measurement of the two significant shear stresses on a disc would require positioning a hot wire in a plane normal to the disc surface, thus sensing average values over most of the boundary-layer thickness, rather than local values.

2.3-2 Free Jets

The turbulence characteristics of axisymmetrical jets swirling in stagnant surroundings have been investigated experimentally by Rose (1962), Craya and Darrigol (1967), and Pratte and Keffer (1972). The measurements of Rose were restricted to the turbulence energy for a jet having a low degree of swirl, whereas the measurements of Craya and Darrigol covered all three normal stresses as well as two shear stresses for degrees of swirl varying from weak to very strong. However, very few of their data have been published.

The only other measurements of all the stress components have been made by Pratte and Keffer for a jet having a moderate degree of swirl. They found that the normal turbulence intensities tended towards a self-similar state downstream of the orifice, long after the mean flow had achieved a self-similar state. The data for the shear stresses however, showed a considerable degree of scatter and precluded anything more than a simple order of magnitude estimate. Pratte and Keffer also reported appreciable experimental difficulties

in measuring the Reynolds shear stresses; these measurements involved subtraction of hot wire signals, with increasing errors as these differences became small.

2.4 HEAT AND MASS TRANSFER EXPERIMENTS

2.4-1 Laminar Flow

Measurements of the average heat transfer from an isothermal disc rotating in still air under conditions of laminar flow have been performed by Cobb and Saunders (1956), Richardson (1958), Lee (1966), McComas and Hartnett (1970), and Dennis, Newstead and Ede (1970). All the results show that the average Nusselt number is proportional to the Reynolds number to the power 0.5, but they differ in the proportionality constant. These results are summarised in Table 2.1 below in which the measured values of the constant are recorded for a fluid of Prandtl number 0.72; the proportionality constant determined in the various theoretical studies are also given.

Experimental Work		Theoretical Work	
Cob and Saunders (1956)	0.36	Millsaps and Pohlhausen (1952)	0.35
Richardson (1958)	0.40	Sparrow and Gregg (1959)	0.33
Lee (1966)	0.35	Hartnett and Deland (1961)	0.33
McComas and Hartnett (1970)	0.34	Dorfman and Serazetdinov (1965)	0.33
Dennis, Newstead and Ede (1970)	0.40		

Table 2.1 Proportionality constant determind from $\overline{Nu}/Re^{0.5}$

The experimentally measured constants are generally higher than the predicted ones. These discrepancies arise from the inevitable errors due to extraneous heat losses associated with heat-transfer experiments.

In order to avoid the heat-loss problem, and also the experimental difficulty of obtaining an isothermal surface condition, several workers have preferred to perform mass-transfer experiments. Most have studied the mass transfer from naphtalene coated surfaces for which the Schmidt number is 2.4. The earliest work of this kind seems to be that of Krieth, Taylor and Chong (1959) who made measurements for the mass transfer from a disc rotating in stagnant air. Similar experiments were carried out by Tien and Campbell (1963) for cones with vertex angles ranging from 60 to 180 degrees. The results of both groups of workers are consistent, and are closely approximated by the expression $\overline{Sh}=0.625\ Re^{0.5}$ predicted by Millsaps and Pohlhausen (1952), Sparrow and Gregg (1959), and others in their theoretical analyses. The Reynolds number is defined as $Re=\Omega r x/\nu$ and the expression for the Sherwood number is valid for discs and cones; x is the distance measured from the centre or apex along the surface.

Salzberg and Kezios (1965) investigated the mass transfer from a 30 degree cone under laminar flow conditions for the case where the surrounding air flows axially past the cone. Their data confirmed the predictions of Schlichting (1953). A step-change in the surface temperature of cones of vertex angles 60 to 180 degrees was simulated by Tien (1965) by allowing mass transfer to occur from part of the surface only; the results are well represented by Tien's predictions. Mabuchi, Kotake and Tanaka (1971) measured the local and the average mass transfer from a disc, with a stepwise discontinuous

naphtalene covered surface, rotating in an uniform axial laminar air stream. The measurements supported their analytical predictions very well.

2.4-2 Turbulent Flow

The average heat transfer from an isothermal disc rotating in still air under conditions of turbulent flow has been investigated by Cobb and Saunders (1956), McComas and Hartnett (1970), and Dennis, Newstead and Ede (1970); mass-transfer measurements were reported by Kreith, Taylor and Chong (1959). Similar mass-transfer experiments have been made by Tien and Campbell (1963) for cones of 60 to 180 degrees vertex angles.

For an isothermal surface all of the theoretical analyses reviewed in Appendix 1, Section 1.3, were based on the assumption that turbulent flow prevailed over the whole cone or disc surface. The analyses resulted in an expression for the average Nusselt (or Sherwood) number of the form $\overline{Nu} = C\sigma^{A}Re^{0.8}$; C and A are constants and σ is the Prandtl (or Schmidt) number. The Reynolds number is, as in the laminar flow case, defined as $Re = \Omega r x / \nu$. The theoretical results together with the experimental ones are summarised in Table 2.2 below.

Theory		Constant C	A	$\sigma = .72$ $C\sigma^A$	$\sigma \doteq 2.4$ $C\sigma^A$
Davies	(1959)	.0166	1.0	.012	.040
Dorfman	(1965)	.0184	.6	.015	.031
Hartnett, Tsai and Jantscher	(1965)	.025	1.0	.018	.060
Dorfman, modified by Hartnett et al	(1965)	.0198	1.0	.014	.047
Kreith	(1968)	.020	.75	.015	.038
McComas and Hartnett	(1970)	.0154	.33	.014	.021
Experiment					
Cobb and Saunders	(1956)	Heat transfer		.015	
Kreith, Taylor and Chong	(1959)	Mass transfer			.040
Tien and Campbell	(1963)	Mass transfer			.042
McComas and Hartnett	(1970)	Heat transfer		.014	
Dennis, Newstead and Ede	(1970)	Heat transfer		.015	

Table 2.2 Constants in the average Nusselt number expression for isothermal discs and cones in turbulent flow: $\overline{Nu} = C\sigma^A Re^{0.8}$.

The predictions of Dorfman, Kreith, and Hartnett and his co-workers, display good agreement with the three sets of heat-transfer data; and those of Davies, and Kreith,are well supported by the mass-transfer data. It should however be remarked that none of these experiments reached a sufficiently high Reynolds number for fully turbulent flow. Consequently, the extrapolation of the data to the

limiting condition of turbulent flow over the whole surface is subject to some uncertainty.

The case of uniform surface heat flux for a disc rotating in air has been studied by Subba Rao (1967) who measured the average heat transfer. From his measurements of heat flux and surface temperature distribution, Subba Rao deduced the local heat transfer rate by applying a local heat balance over annular segments, for several radii. The results are closely represented by the following empirical formulae:

$$Nu_r = .0416Re_r^{0.8} \qquad \text{and} \qquad \overline{Nu} = .0148Re_R^{0.8} .$$

The subscripts r and R refer to the local and maximum radii respectively; Nu_r and $\overline{Nu}$ are the local and average Nusselt numbers. Since the average Nusselt number is in close agreement with that for isothermal discs, Subba Rao concluded that the difference between the two boundary conditions does not influence the average heat transfer. A similar result can be inferred from the work of Lewis and Ruggeri (1956, 1957); they investigated the heat transfer for these two boundary conditions for an ellipsoidal-nose body and a conical-nose body which were rotated in a co-axial air stream of uniform velocity.

In order to simulate a step-change in the surface temperature of cones, Tien (1965) allowed mass-transfer to take place from only part of the surface. His measurements are well represented by his own predictions. The experimental investigation of Salzberg and Kezios (1965) of the mass transfer on a 30 degree cone rotating in a co-axial air stream confirms the analytical predictions of Truckenbrodt (1952).

Recirculating Flow

Owen and his co-workers (1972) have recently reported measurements

of average heat transfer for a shrouded parallel discs system with a radial outflow of coolant. Their data cover a wide range of rotational Reynolds number, coolant flow rate, discs spacing, and shroud-disc spacing. Yu and his co-workers (1972) measured the local as well as the average heat transfer for a different shrouded parallel discs system, see Fig. 2.1. They investigated much larger inter-disc spacing to radius ratio than Owen.

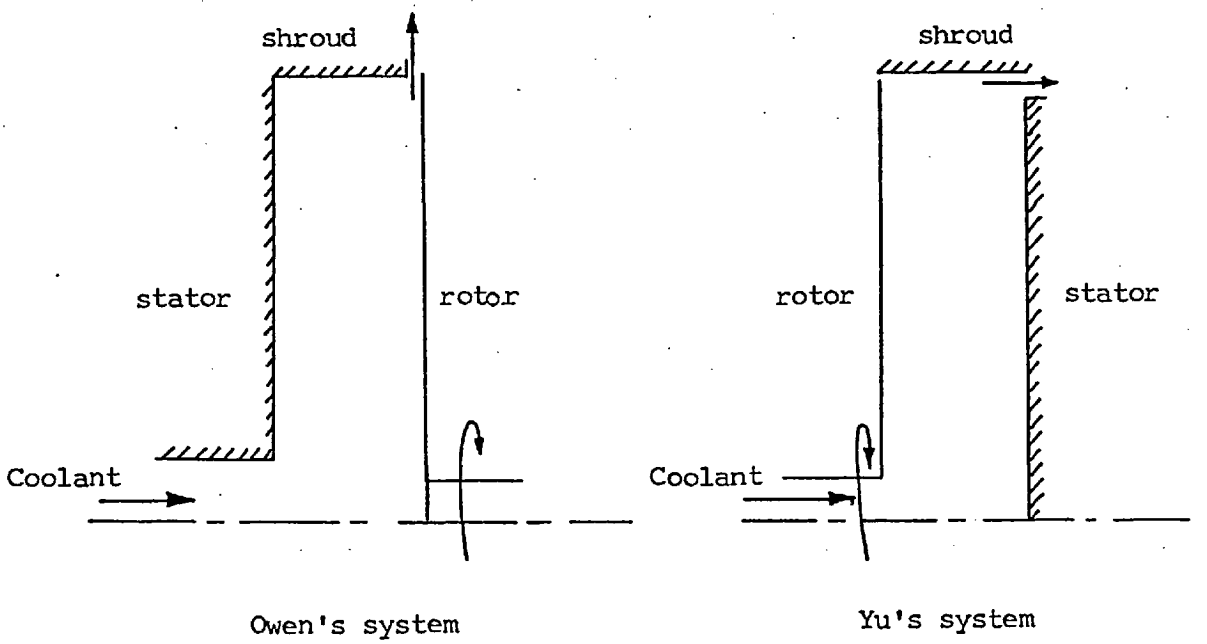

Fig. 2.1 Shrouded parallel discs systems

Although they do not fall into the present class of swirling boundary-layer flows, since they are of the recirculating flow class, these two experimental investigations are briefly reviewed because they are comprehensive and have been accurately performed. They will play an important part in the extension of turbulent transport hypothesis from boundary-layer to recirculating flows.

APPENDIX 3

Wall-Functions

3.1 INTRODUCTION

Close to a wall, the fluxes of mass, momentum and energy are only significant in the direction normal to the wall. The transport of these quantities by convection is negligible since the streamwise and cross-stream velocities close to the wall are small. Consequently, this is a region of one-dimensional or Couette flow. A finite-difference grid covering this region has to be closely spaced, on account of the steep gradients of the dependent variables, and is therefore uneconomical in terms of computer time.

However, Patankar and Spalding (1970) showed that, since the partial differential equations reduce to ordinary equations in the Couette region, they could be solved with appropriate assumptions for the exchange coefficients to yield algebraic formulae which relate the values or fluxes of the variables at the wall to conditions at the grid node adjacent to the wall. These algebraic relations are known as 'wall-functions'.

3.2 LAMINAR FLOW

When the convection terms in the momentum, heat and mass transfer equations (Chapter 2, equations 2.34, 2.36, 2.37 and 2.38) are neglected, the equations reduce to:

$$\frac{\partial}{\partial y}\left[\mu_\ell r \frac{\partial V_1}{\partial y}\right] = r\left[\frac{\partial p}{\partial x} - \rho\frac{V_3^2}{r}\sin\alpha\right], \tag{3.1}$$

$$\frac{\partial}{\partial y}\left[\mu_\ell r^3 \frac{\partial}{\partial y}\left(\frac{V_3}{r}\right)\right] = 0, \tag{3.2}$$

$$\frac{\partial}{\partial y}\left[\frac{\mu_\ell}{\sigma_{h,\ell}} r \frac{\partial h}{\partial y}\right] = -\frac{\partial}{\partial y}\left[rV_1\tau_{1,2} + rV_3\tau_{2,3}\right], \tag{3.3}$$

$$\frac{\partial}{\partial y}\left[\frac{\mu_\ell}{\sigma_{j,\ell}} r \frac{\partial m_j}{\partial y}\right] = 0. \tag{3.4}$$

The symbol y represents the cross-stream x_2-coordinate, and x is the streamwise x_1-coordinate. In the thin Couette-flow region, the terms on the right hand side of the above equations, and also the distance r from the axis of symmetry, are assumed constant between the wall and the grid-node adjacent to the wall at the average of their values at the wall and at the near-wall node. With these assumptions, the solutions to equations 3.1 to 3.4 are:

$$\frac{\tau_{1,w}}{\rho V_1^2} = \frac{\mu_\ell}{\rho V_1 y} - \frac{y}{2\rho V_1^2}\left(\overline{\frac{\partial p}{\partial x}} - \rho\overline{\frac{V_3^2}{r}}\sin\alpha\right), \tag{3.5}$$

$$\frac{\tau_{3,w}}{\rho V_1\left(V_3 - V_{3,w}\right)} = \frac{\mu_\ell}{\rho V_1 y} \tag{3.6}$$

$$\frac{\dot{q}''_w}{\rho V_1\left(\tilde{h} - \tilde{h}_w\right)} = \frac{1}{\sigma_{h,\ell}}\frac{\mu_\ell}{\rho V_1 y} + \frac{\mu_\ell}{\rho V_1 y}\frac{1}{\left(\tilde{h} - \tilde{h}_w\right)}\left[\frac{1}{2}\left(1 - \frac{1}{\sigma_{h,\ell}}\right)\left(V_1^2 + V_3^2 - V_{3,w}^2 - \frac{2yV_{3,w}\tau_{3,w}}{\mu_\ell}\right) - \frac{y}{r}\cos\alpha\left(V_3^2 - V_{3,w}^2\right)\right], \tag{3.7}$$

$$\frac{\dot{m}''_w}{\rho V_1\left(m_j - m_{j,w}\right)} = \frac{1}{\sigma_{j,\ell}}\frac{\mu_\ell}{\rho V_1 y}. \tag{3.8}$$

The subscript w refers to wall values, the overscore to the average of the wall and near-wall node values, while all the remaining variables are evaluated at the near-wall grid-node. Equations 3.5 to 3.8 are the laminar flow wall-functions for the two momentum, the stagnation enthalpy and the mass-transport equations.

3.3 TURBULENT FLOW

For turbulent flow the grid-node adjacent to the wall can, without significant loss of accuracy, be located beyond the edge of the laminar sublayer, provided information about the effective exchange coefficients $\Gamma_{\phi,eff}$ is available. For many non-swirling two-dimensional wall flows, these coefficients are established to high degrees of accuracy; see for example Patankar and Spalding (1970), and Ng and Spalding (1972). Unfortunately, this is not the case for turbulent swirling boundary layers. The present thesis deals with four proposals to model turbulent swirling flows, and hence to determine the exchange coefficients. The near-wall procedures adopted for the different models are explained in the following subsections.

3.3-1 Mixing-Length Based Models

For the Prandtl mixing-length based models developed in Chapters 4 and 6, turbulent wall-functions are not employed simply because these models are applicable to fully turbulent flow, as well as the near-wall region and the laminar sublayer. Instead, the finite-difference grid is extended right into the laminar sublayer and consequently, the laminar wall-functions are used to determine the shear stresses, and when there is heat or mass transfer, the heat or mass fluxes at the wall.

3.3-2 Energy-Length-Scale Model

(a) Velocity

The two-equation energy-length-scale model under consideration in Chapter 5 is only applicable to fully turbulent flow. For this case, the resultant velocity V_R relative to the wall is presumed to obey the conventional log-law; see for example Backshall and Landis (1969), and also p. 76:

$$V_R \Big/ \left(\tau_{R,w}/\rho\right)^{\frac{1}{2}} = \frac{1}{0.4} \ln\left[9 \frac{y}{\mu_\ell}\left(\frac{\tau_{R,w}}{\rho}\right)^{\frac{1}{2}}\right] \qquad (3.9)$$

The axial and circumferential shear-stress components are then obtained by straightforward resolution, assuming that the resultant shear-stress at the wall, $\tau_{R,w}$, acts in the same direction as the resultant velocity evaluated at the near-wall node. It should be noted that this assumption is only made for the Couette region, and not for the remainder of the flow, in order to determine the components of the shear-stress at the wall; namely,

$$\tau_{1,w} = \tau_{R,w} V_1 \Big/ V_R \ , \qquad (3.10)$$

$$\tau_{3,w} = \tau_{R,w} \left(V_3 - V_{3,w}\right) \Big/ V_R \ . \qquad (3.11)$$

The assumption implies that the effective viscosity is isotropic in the region between the wall and the near-wall grid node.

(b) Turbulence Energy and Length Scale

Very little is known of the behaviour of the energy of turbulence, k, in the near-wall region of swirling wall flows. However, the information available for non-swirling wall flows, see Hinze (1959), indicates that the diffusion as well as the convection of k are negligible in that region. It is assumed that the same situation applies for swirling boundary layers. Consequently, when

the convection and diffusion terms are removed from the transport equation for k, equation 7.20 of Chapter 7, and the dissipation is expressed in terms of k and the length scale through equation 7.17, there results:

$$-\overline{v_1 v_2}\,\frac{\partial V_1}{\partial x_2} - \overline{v_2 v_3}\,r\,\frac{\partial (V_3/r)}{\partial x_2} = C_D k^{\frac{3}{2}} \ell^{-1} . \qquad (3.12)$$

The turbulent viscosity, assumed in the proceeding subsection to be isotropic in the region between the wall and the first near-wall node, is given in Chapter 5 as:

$$\mu_t = \rho k^{\frac{1}{2}} \ell . \qquad (3.13)$$

Furthermore, equation 3.12 implies that the production and dissipation of k are in balance, and leads, see Chapter 4, to the following expression:

$$\mu_t = \rho \ell_m^2 \left[\left(\frac{\partial V_1}{\partial x_2} \right)^2 + \left(r\,\frac{\partial (V_3/r)}{\partial x_2} \right)^2 \right]^{\frac{1}{2}} , \qquad (3.14)$$

where ℓ_m is the mixing length.

Algebraic solution of equations 3.12 to 3.14, with $-\rho\overline{v_1 v_2} \equiv \mu_t \frac{\partial V_1}{\partial x_2}$ and $-\rho\overline{v_2 v_3} \equiv \mu_t r \frac{\partial (V_3/r)}{\partial x_2}$, results in the following explicit relations for k and ℓ:

$$k = \left(\tau_{1,w}^2 + \tau_{3,w}^2 \right)^{\frac{1}{2}} / \rho C_D^{\frac{1}{2}} \qquad (3.15)$$

and

$$\ell = C_D^{\frac{1}{4}} \ell_m \qquad (3.16)$$

$\tau_{1,w}$ and $\tau_{3,w}$ correspond to the values of $-\rho\overline{v_1 v_2}$ and $-\rho\overline{v_2 v_3}$ at the wall, and are the components of the resultant wall shear-stress $\tau_{R,w}$.

Also, in the turbulent region outside the sublayer, the mixing-length ℓ_m is simply proportional to the distance from the wall (see Schlichting (1968)). Hence, equations 3.15 and 3.16 can be rewritten as:

$$k = \tau_{R,W} / \rho C_D^{\frac{1}{2}} \quad , \tag{3.17}$$

$$\ell = \kappa C_D^{\frac{1}{4}} y \quad . \tag{3.18}$$

These expressions for k and ℓ are evaluated for the near-wall node, and serve as the inner boundary conditions to the solution of the differential equations for k and the combined variable $k\ell$. Consequently, the grid node adjacent to the wall must always be located outside the sublayer in the turbulent part of the flow for the above analysis to remain valid. This treatment was employed by Ng and Spalding (1972) for predicting several non-swirling wall boundary layers, and is also adopted in the present work.

3.3-3 Algebraic Stress Model

The algebraic stress model presented in Chapter 7 is applicable to fully turbulent flow, but is matched near the wall to the anisotropic mixing-length model developed in Chapter 6. This procedure allows the use of the laminar wall-functions to obtain the wall shear stress components $\tau_{1,w}$ and $\tau_{3,w}$, and furthermore, it does not necessitate any assumption about the behaviour of the shear stress and velocity vectors in the near-wall region.

An analysis similar to that in Section 3.3-2 (b) above now shows that the near-wall value of k, to be used as the inner boundary condition to the solution of its transport equation, is given by:

$$k = \left(\tau_{1,w}^2 + \sigma_{2,3}\,\tau_{3,w}^2\right)^{\frac{1}{2}} \Big/ \rho C_\mu^{\frac{1}{2}} \,. \qquad (3.19)$$

The parameter $\sigma_{2,3}$ is the effective viscosity ratio obtained from the anisotropic mixing-length model for the near-wall region. For the length scale, equation 3.18 remains valid.

APPENDIX 4

STREAM-WISE PRESSURE GRADIENT FOR SHROUDED FLOWS

The pressure gradient is estimated from a one-dimensional analysis of the flow. The mass flow rate, with the density and velocity averaged across the stream, is given by:

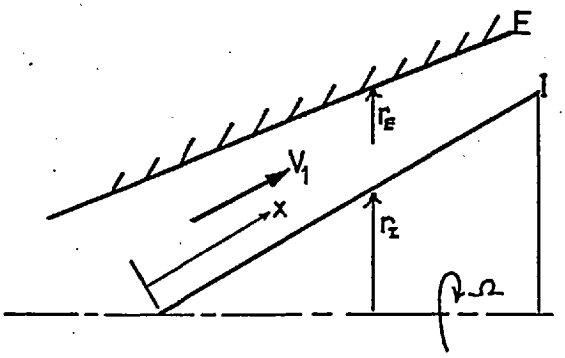

$$\dot{m} = \bar{\rho}\bar{V}_1 A \qquad (4.1)$$

That is, $$d\dot{m} = \bar{\rho}\bar{V}_1 dA + \bar{\rho} A d\bar{V}_1 + \bar{V}_1 A d\bar{\rho} \quad , \qquad (4.2)$$

where the symbol A represents the calculated area of the flow.

A force balance in the stream-wise direction yields:

$$\frac{dp}{dx} A \delta x + (r_I \tau_I + r_E \tau_E)\delta x - \rho \frac{\overline{V_3^2}}{r} \sin\alpha \, A \delta x - \frac{d}{dx}(\dot{m}\bar{V}_1)\delta x = 0 . \qquad (4.3)$$

For a steady flow of constant density, $d\dot{m}$ and $d\bar{\rho}$ are zero; hence, equations 4.2 and 4.3 result in the following final form of the pressure gradient equation:

$$\frac{dp}{dx} = -\frac{(r_I \tau_I + r_E \tau_E)}{A} + \rho \frac{\overline{V_3^2}}{r} \sin\alpha + \frac{\dot{m}}{A^2}\bar{V}_1 \frac{\delta A}{\delta x} \qquad (4.4)$$

The term δA is a measure of the difference between the calculated area of the flow and the geometrical area between the shroud and the rotating body, and is calculated from:

$$A = (A_{geometrical,D} - A_U) f \; ; \qquad (4.5)$$

δx is simply equal to $x_D - x_U$. The subscripts U and D symbolise the upstream and downstream stations. This formulation always causes the

pressure gradient to alter such that the discrepancy between the calculated flow area and the geometrical area is reduced. The need to iterate in order to obtain exact agreement between the two areas is eliminated. The fraction f controls the magnitude of the area correction; (a value of 0.05 was used for the shrouded disc geometry described in Section 4.3-4 of Chapter 4).

APPENDIX 5

Turbulent Mean Velocity Measurements on a Rotating Cone

5.1 INTRODUCTION

Measurements of the mean velocity within the boundary layer on a rotating cone, of half angle 40 degrees, are reported. The measurements are intended to augment the rather limited available data, as revealed in Appendix 2, for boundary layers near axisymmetric rotating bodies. The experiment was designed to ensure the provision of a significant number of data for fully turbulent Reynolds number since these are particularly scarce.

The chosen geometry was that of a rotating cone with provision for a wall jet issuing from a concentric annular slot near the apex. A wide range of conditions were obtained by varying the rotational speed, and the slot height and slot Reynolds number. The dimensions and speed of the cone were large enough to ensure a substantial length of fully turbulent flow.

5.2 APPARATUS

5.2-1 Air Supply and Cone

The overall arrangement of the apparatus is shown in Fig. 5.1. Air from a radial fan passes into a large settling chamber,

containing two wire-mesh filters. The air leaves the chamber to flow through a length of pipe which terminates in a circular diffuser placed concentrically over the cone apex. At the diffuser exit, velocity fluctuations were less than 5% for velocities lower than 3 m/s, decreasing to less than 1% for velocities greater than 10 m/s.

The lip of the diffuser was machined to a thickness of 0.1 mm to minimise its downstream influence. The axial position of the diffuser was adjustable allowing the slot height, between the diffuser lip and the cone surface, to be varied. The alignment of the diffuser was such that the maximum circumferential variation in slot velocity was 3% at the maximum experimental velocity of 20 m/s decreasing to less than 1% for velocities of less than 3 m/s.

The cone was machined from 4 layers of 76 mm aluminium plates, secured together by internal screws. The maximum variation recorded when the cone was slowly rotated and its surface 'clocked' was $\pm$ .025 mm. The cone was driven by a synchronous motor through a timing belt and pulley arrangement offering a wide selection of precise rotational speeds.

The cone half-angle of 40° was sufficiently large to ensure the development of a boundary-layer on its surface when rotating in stagnant surroundings. The substantial length of its conical surface of 0.356 m permitted a significant range of fully turbulent Reynolds numbers to be attained. Fig. 5.2 shows the Reynolds numbers provided by the apparatus as a function of surface position and rotational speeds up to the maximum safe speed for the cone of 1500 rpm. The extent of the laminar, transitional and turbulent regimes as established by Kreith and his co-workers (1962) are indicated on the figure.

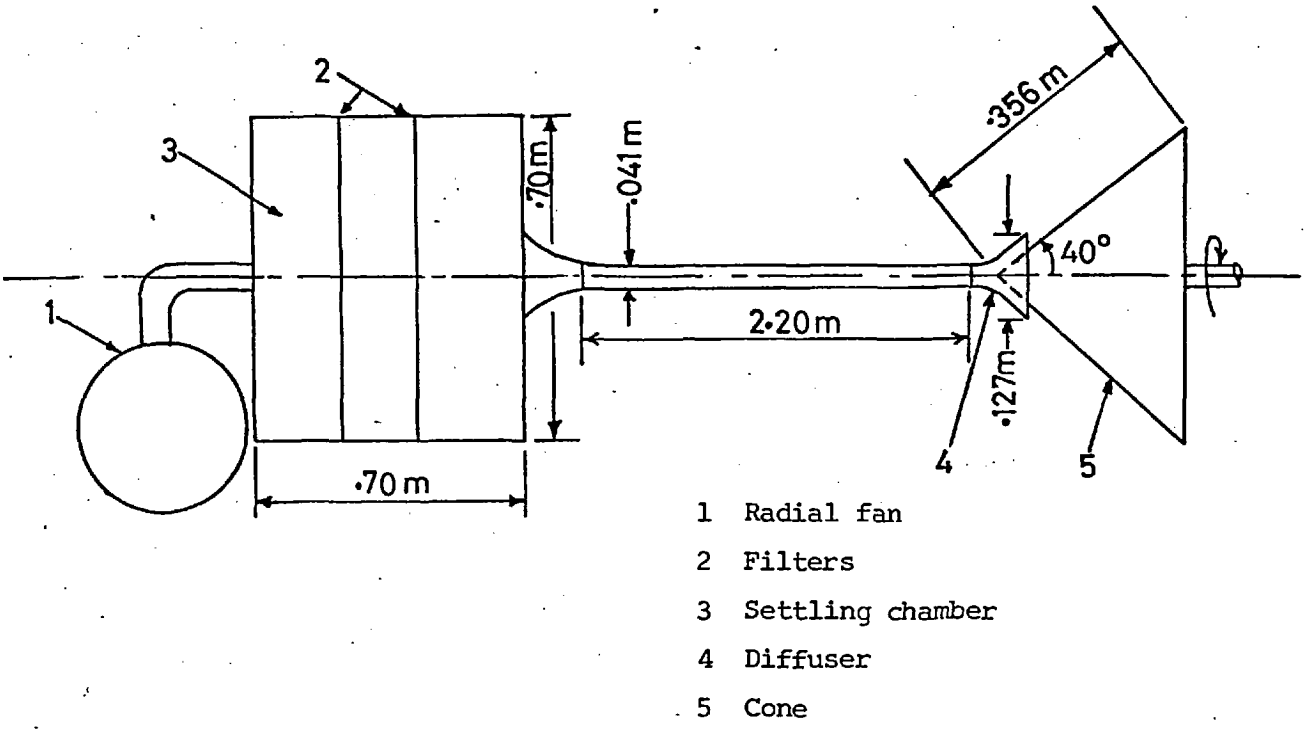

Fig. 5.1 General arrangement of apparatus

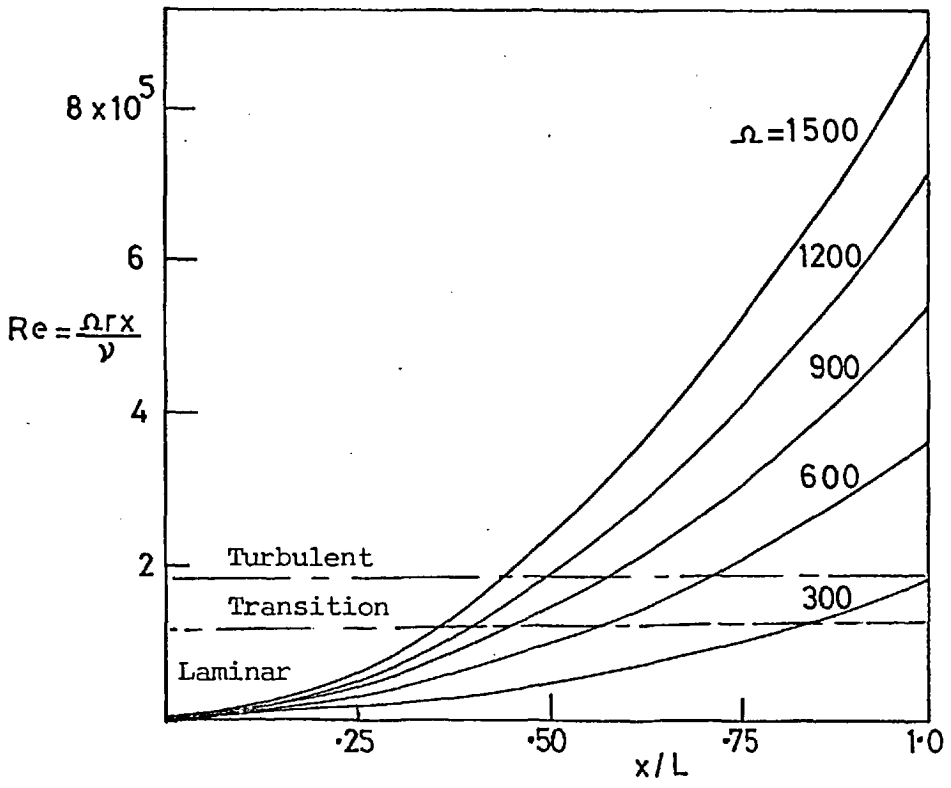

Fig. 5.2 Flow regimes and Reynolds numbers attainable with the apparatus

5.2-2 Instrumentation

The magnitude and direction of the resultant velocity were measured using the three-hole Pitot probe shown in Fig. 5.3. The design and construction of the probe were based on the recommendations of Bryer and Pankhurst (1971). A traversing mechanism allowed the probe to be moved parallel to the conical surface, normal to the cone surface in steps of 0.02 mm, and to be rotated about an axis normal to the cone surface.

The three pressures sensed by the probe were measured using an electronic micromanometer to an accuracy of .5%. The response of the probe to misalignment with the resultant velocity was determined by a wind-tunnel calibration. The direction of the resultant velocity could be measured to an accuracy of $\pm$ 0.2° for velocities larger than 5 m/s, decreasing to $\pm$ 0.5° for velocities lower than 2 m/s.

5.3 RESULTS

Measurements were made for the eight sets of condition given in Table 5.1 below. The full reduced numerical data are presented in Section 5.5.

Run	Ω (rpm)	Y_{slot} (mm)	x_{slot} (mm)	$\overline{V_1}_{,slot}$ (ms^{-1})	$Re_{slot} X10^3$	$Re_L X10^5$
1	892.9	slot absent (i.e. free rotating cone in stagnant surroundings)				5.00
2	1111.1					6.22
3	1428.6					8.00
4	0	2.59	95.5	17.1	2.93	
5	1111.1	2.59	95.5	17.0	2.90	6.22
6	0	3.81	94.0	13.5	3.38	
7	562.5	3.81	94.0	13.4	3.36	3.15
8	1111.1	3.81	94.0	13.6	3.42	6.22

Table 5.1 Experimental conditions

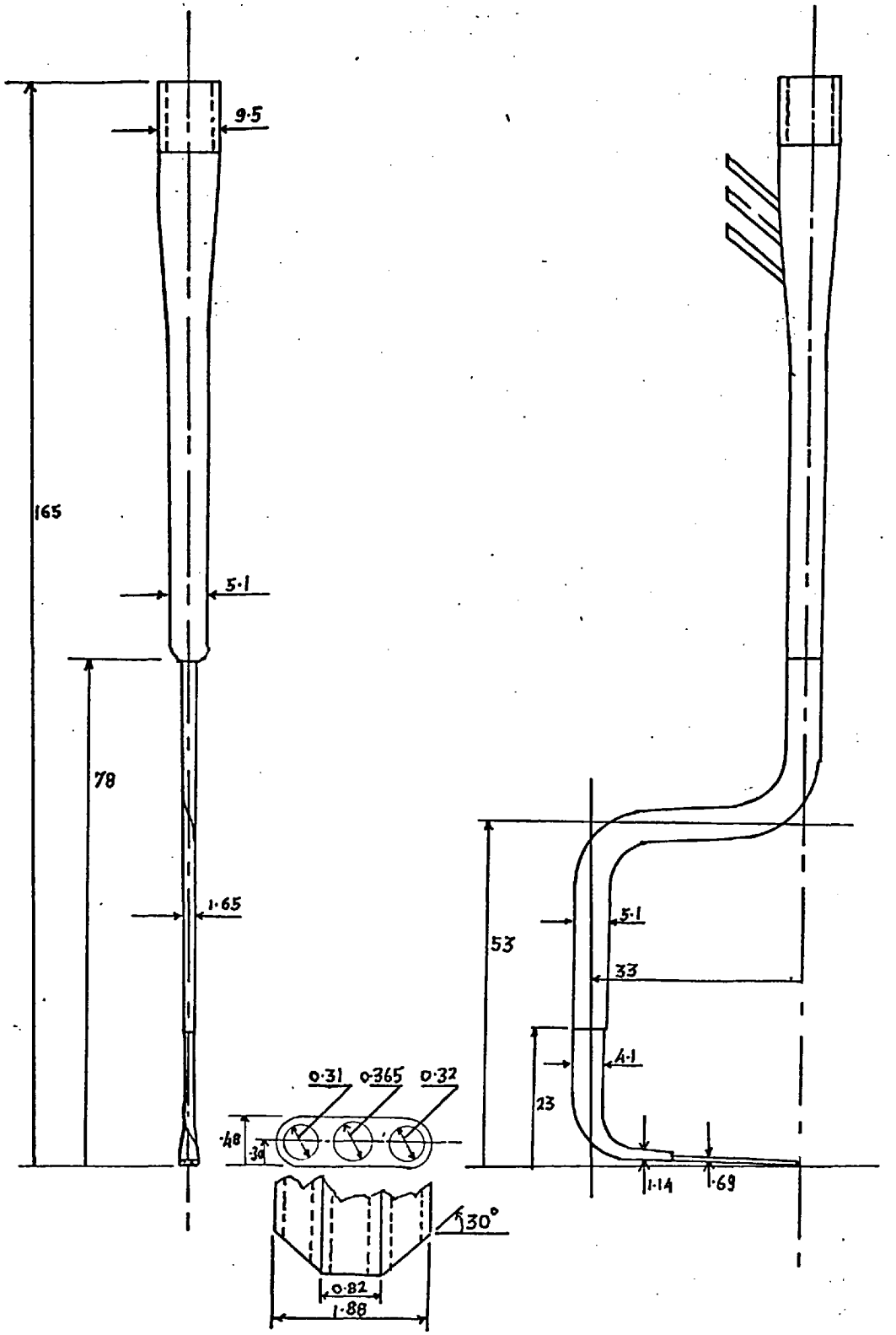

Fig. 5.3 Dimensions (mm) of 3-hole Pitot probe

A selection of these results is presented in graphical form in Fig. 5.4 to 5.6. Panels (a) and (b) of Fig. 5.4 show the longitudinal and circumferential velocity profiles for Run 2 in which the cone was rotating in stagnant air at 1111 rpm, while panel (c) displays the variation of the angle between the resultant velocity and a plane through the axis. Fig. 5.5 shows plots of similar information for Run 5 where the cone was rotating in the presence of a finite slot flow. Fig. 5.6 displays some features of the developing boundary layer: the growth of longitudinal (direction - 1) and circumferential (direction - 3) profiles for Runs 6, 7 and 8.

5.4 NOMENCLATURE

L	length of cone surface = 0.356 m
r	radius; $r = x \sin 40^\circ$
Re_{slot}, Re_L	Reynolds numbers: $\overline{V_{1,slot}} y_{slot}/\nu$ and $\Omega L^2 \sin 40^\circ/\nu$
V_1, $\overline{V_{1,slot}}$	longitudinal velocity, average slot value; $V_1 = V_R \cos\beta$
V_3, $V_{3,S}$	circumferential velocity, value at surface; $V_3 = V_R \sin\beta$
V_R	resultant velocity
x, x_{slot}	distance from apex along cone surface, value at diffuser exit
y, y_{slot}	normal distance from cone surface, slot height
$y_{\frac{1}{2}}$, $y_{1/5}$	values of y at which velocity has fallen to $\frac{1}{2}$ and 1/5 of its maximum value
β	angle between resultant velocity and an axial plane
Ω	rotational speed in rpm

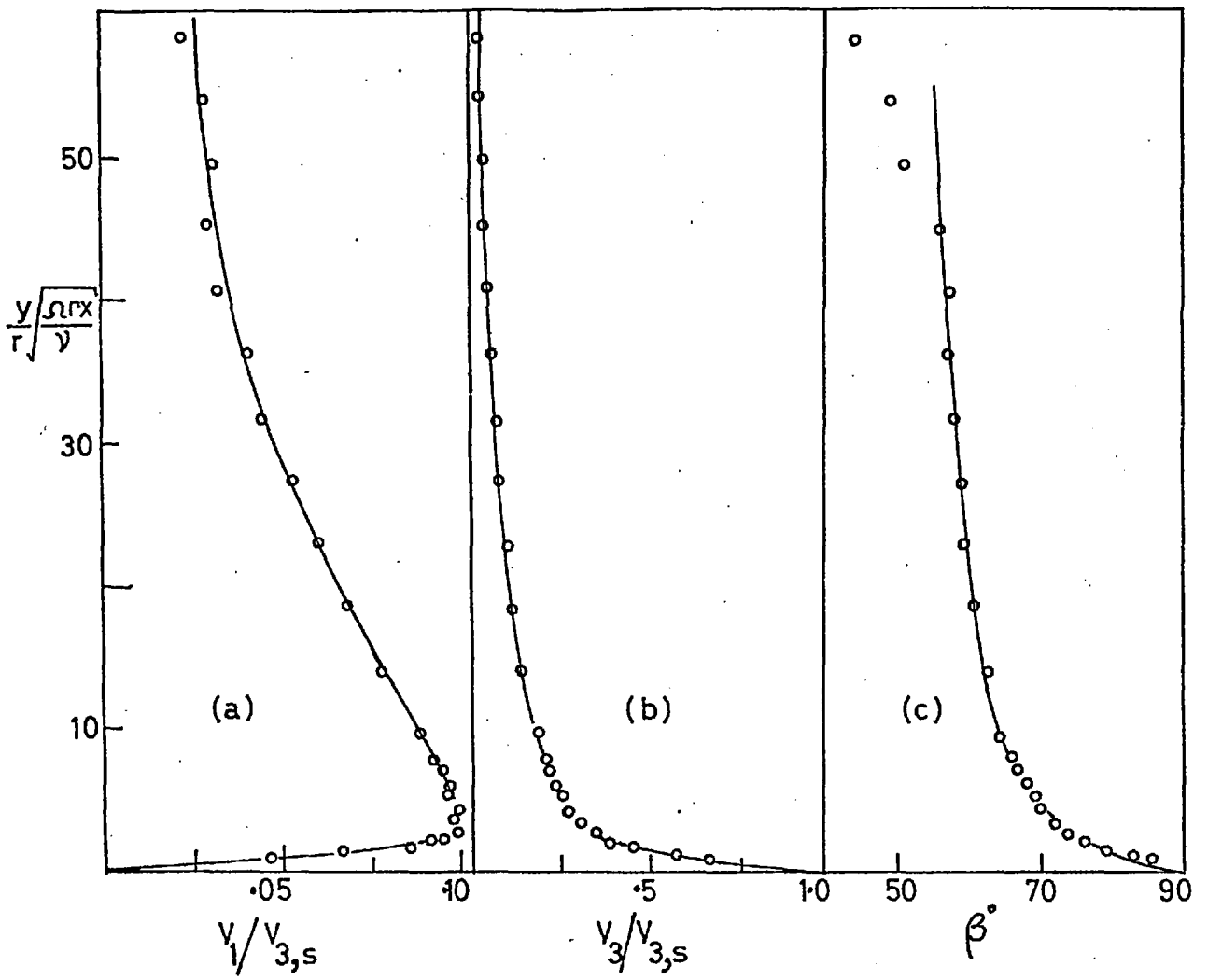

Fig. 5.4 Cone rotating in stagnant air: Run 2, x/L = .857

(a) profile of longitudinal velocity V_1

(b) profile of circumferential velocity V_3

(c) angle between resultant velocity and an axial plane

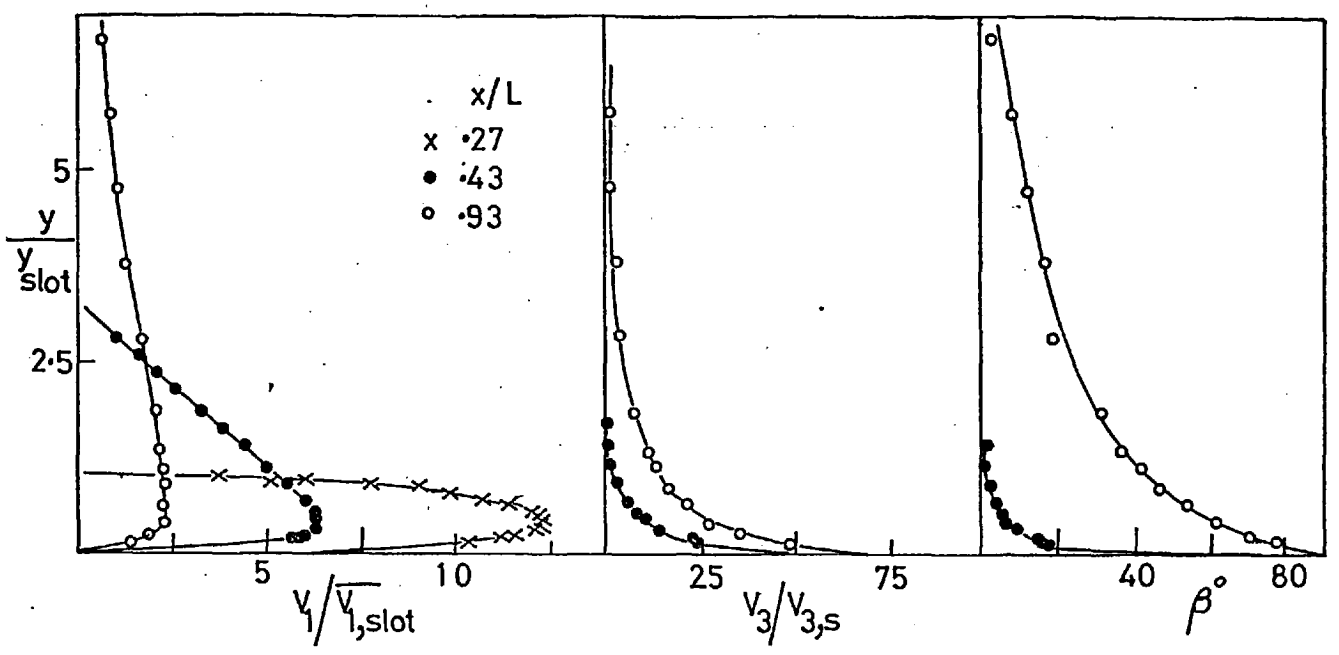

Fig. 5.5 Distributions of V_1, V_3, and β for Run 5

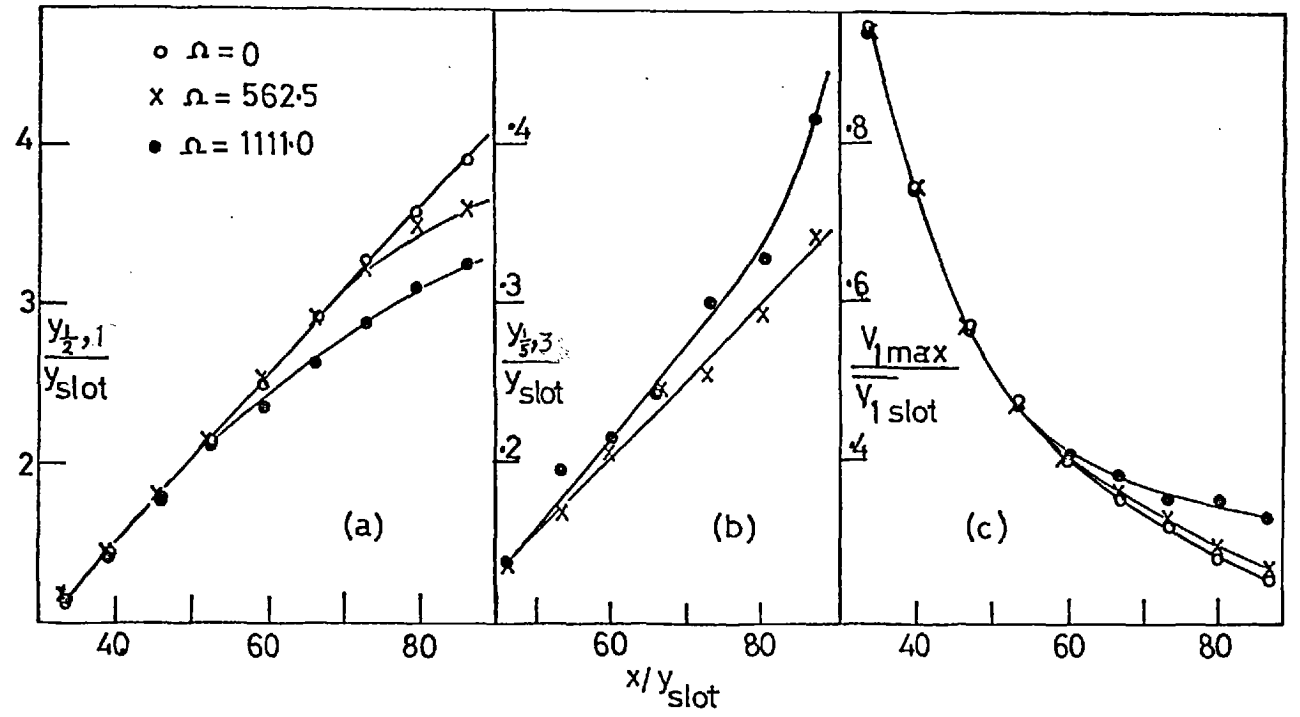

Fig. 5.6 Boundary layer development for Runs 6, 7, 8

(a) Growth of longitudinal boundary layer

(b) Growth of circumferential boundary layer

(c) Decay of longitudinal maximum velocity

5.5 REDUCED NUMERICAL DATA

Distances are measured in 10^{-3} metres (millimetres), velocities in metres per second.

x/L = .64			x/L = .715			x/L = .785			x/L = .855			x/L = .93		
y	V_R	β	y	V_R	β	y	V_R	β	y	V_R	β	y	V_R	β
.356	10.82	83.0	.343	11.04	83.2	.317	11.92	84.3	.432	10.13	83.4			
.406	10.17	82.0	.394	10.18	81.8	.356	10.98	83.6	.457	9.76	82.5	.368	12.28	82.8
.457	9.59	81.0	.444	9.42	80.8	.406	9.93	82.3	.483	9.36	81.7	.394	11.78	82.6
.533	8.58	79.0	.571	7.34	78.6	.457	9.07	81.1	.508	9.04	81.0	.419	11.05	81.6
.660	7.19	76.0	.698	6.69	76.1	.508	8.39	80.1	.559	8.54	80.1	.444	10.71	81.2
.787	6.07	74.0	.825	5.97	75.1	.635	7.24	78.5	.686	7.43	78.0	.495	9.82	80.2
1.04	4.54	72.5	1.08	4.96	72.4	.762	6.41	77.1	.813	6.92	76.5	.521	9.50	79.7
1.30	3.95	69.3	1.33	4.35	72.3	.889	6.04	76.4	.940	6.49	75.7	.546	9.16	79.3
1.55	2.85	70.9	1.59	3.93	72.5	1.02	5.63	75.7	1.07	6.12	75.0	.673	8.13	77.6
2.18	2.00	72.2	2.22	2.91	75.5	1.27	5.12	73.9	1.32	5.85	73.5	.927	6.98	75.7
3.45	0.58	75.5	2.86	2.54	76.9	1.65	4.57	73.2	1.57	5.18	72.5	1.18	6.41	74.3
4.72	0.57	65.0	3.49	2.08	77.5	2.29	3.89	71.9	1.83	4.84	71.9	1.44	5.90	72.8
			4.13	1.73	77.5	2.92	3.31	71.4	2.21	4.42	70.0	1.69	5.48	72.1
			5.40	1.41	72.0	3.56	2.96	71.5	2.59	4.05	69.2	1.94	5.15	71.6
			6.67	1.00	70.0	4.19	2.64	71.0	3.10	3.73	68.5	2.20	4.82	71.2
			7.94	0.82	66.5	4.83	2.30	70.6	3.73	3.36	67.0	2.45	4.71	70.2
			9.21	0.41	64.0	5.46	2.04	70.6	4.37	2.96	66.5	3.09	4.09	68.9
						6.10	1.82	70.3	5.00	2.70	66.0	3.73	3.64	67.3
						6.73	1.63	70.0	5.64	2.37	65.7	4.36	3.38	66.7
						7.37	1.35	69.0	6.27	2.19	65.5	4.99	3.10	66.0
						8.64	0.91	67.0	6.91	1.95	65.0	5.63	2.88	66.0
						9.91	0.71	65.0	7.54	1.73	64.1	6.26	2.54	65.3
						11.2	0.58	63.0	8.18	1.58	63.9	6.90	2.41	65.0
						12.4	0.41	61.0	8.81	1.41	63.5	7.53	2.19	64.0
									9.45	1.15	62.5	8.80	1.82	63.5
									10.7	1.00	61.5	10.1	1.52	62.0
									12.0	0.81	60.5	11.3	1.22	62.0
									13.3	0.41	59.5	12.6	1.00	61.0
												13.9	0.91	60.0
												15.2	0.71	57.0

RUN 1: Ω = 892.9 rpm., $Re_L = 5.0 * 10^5$

x/L = .57			x/L = .715			x/L = .785			x/L = .855			x/L = .93		
y	V_R	β	y	V_R	β	y	V_R	β	y	V_R	β	y	V_R	β
.317	10.72	86.8	.317	14.05	86.5	.343	13.73	84.5	.317	15.64	86.0	.394	14.42	83.5
.343	10.14	85.7	.368	11.95	84.0	.394	11.97	82.1	.368	13.63	83.5	.444	12.48	80.5
.394	9.24	83.7	.495	9.24	79.0	.521	9.67	78.1	.495	10.96	79.5	.571	10.69	77.5
.470	7.74	82.5	.662	7.93	76.0	.648	8.57	75.5	.622	9.47	76.5	.698	9.67	75.5
.597	6.59	77.0	.876	6.66	73.0	.902	7.29	73.0	.749	8.69	74.7	.825	9.03	74.2
.851	5.57	73.0	1.13	5.89	71.0	1.16	6.57	71.0	1.00	7.67	72.5	.952	8.53	73.5
1.10	4.61	71.5	1.77	4.84	68.0	1.41	6.01	70.0	1.26	7.00	70.7	1.08	8.11	72.5
1.61	3.80	69.0	2.40	4.15	66.0	1.92	5.29	67.2	1.51	6.54	70.0	1.33	7.58	70.6
2.12	3.18	67.3	3.67	3.18	62.5	2.55	4.61	65.0	1.77	6.11	68.5	1.59	7.03	70.0
3.39	2.51	63.5	4.94	2.61	60.5	3.19	4.07	63.0	2.02	5.76	67.5	1.84	6.62	68.5
4.66	1.68	59.5	6.21	1.95	58.5	4.46	3.21	61.5	2.27	5.45	66.5	2.10	6.16	68.0
5.93	1.15	57.5	7.48	1.58	56.5	5.73	2.58	59.5	2.78	4.87	65.0	2.35	5.96	67.0
7.20	0.81	49.0	8.75	1.29	54.5	7.00	2.15	58.0	4.05	3.93	62.9	2.98	5.31	65.0
8.47	0.58	44.5	10.0	1.00	50.5	8.27	1.82	57.0	5.32	3.28	61.0	3.62	4.80	63.6
x/L = .64			11.3	0.58	49.5	9.54	1.41	55.3	6.59	2.76	60.0	4.25	4.35	62.5
.330	11.94	85.5				10.8	1.15	54.5	7.86	2.41	59.5	4.89	4.05	61.5
.457	9.08	80.5				12.1	0.81	50.8	9.13	2.00	58.5	5.52	3.73	61.0
.584	7.51	77.0				13.3	0.41	49.5	10.4	1.73	57.5	6.16	3.41	61.0
.711	6.63	74.5							11.7	1.41	57.0	6.79	3.15	60.8
.838	6.10	73.5							12.9	1.22	56.5	7.43	3.02	60.1
1.09	5.39	71.0							14.2	1.15	51.0	8.70	2.61	59.5
1.60	4.44	68.5							15.5	1.00	49.5	9.97	2.34	59.0
2.87	3.28	65.5							16.8	0.71	44.5	11.2	2.08	58.5
4.14	2.51	62.0										12.5	2.00	58.5
5.41	1.82	59.5										13.8	1.78	58.5
6.68	1.52	55.5										15.0	1.68	58.5
7.95	1.15	53.5										16.3	1.52	58.5
9.22	0.81	51.5										17.6	1.41	55.5

RUN 2: Ω = 1111 rpm, $Re_L = 6.22*10^5$

x/L = .57			x/L = .715			x/L = .785			x/L = .855			x/L = .93		
y	V_R	β	y	V_R	β	y	V_R	β	y	V_R	β	y	V_R	β
.381	11.90	82.6	.432	11.95	81.0	.381	14.67	82.9	.381	16.21	83.0	.406	15.30	81.2
.432	11.22	80.1	.457	11.38	80.1	.432	13.15	80.8	.432	14.19	80.6	.432	14.99	80.5
.483	9.88	78.2	.508	10.75	79.0	.483	12.27	79.5	.483	13.24	79.1	.483	13.84	79.0
.610	8.36	75.6	.559	10.08	78.0	.533	11.66	78.7	.533	12.68	78.0	.533	13.23	78.0
.737	7.30	73.7	.686	9.18	76.4	.660	10.30	76.5	.635	11.66	76.4	.610	12.39	77.0
.991	6.03	73.0	.940	7.95	74.2	.914	8.97	74.1	.762	10.77	74.8	.737	11.45	75.5
1.24	5.17	73.0	1.19	7.13	73.0	1.17	8.03	72.7	1.02	9.48	73.1	.864	10.82	74.3
1.75	4.05	75.5	1.45	6.62	71.7	1.42	7.46	71.4	1.27	8.71	71.2	1.12	9.85	72.5
2.39	2.99	77.3	1.83	5.97	70.0	1.80	6.78	70.0	1.52	8.03	70.1	1.37	9.08	71.0
3.02	2.19	76.0	2.46	5.09	68.4	2.44	5.72	67.8	1.90	7.39	68.5	1.63	8.47	70.0
3.66	1.63	77.0	3.10	4.42	67.0	3.07	5.20	66.0	2.54	6.41	66.8	2.13	7.50	68.0
4.29	1.41	76.0	3.73	3.89	66.0	3.71	4.50	65.0	3.17	5.61	65.5	2.64	6.85	66.5
5.56	0.81	58.0	4.37	3.53	65.0	4.98	3.60	64.0	4.44	4.59	63.0	3.28	6.08	64.5
x/L = .64			5.64	2.58	63.5	6.25	2.91	63.0	5.71	3.84	62.0	3.91	5.51	63.2
.343	13.81	86.2	6.91	2.00	63.0	7.52	2.37	62.0	6.98	3.18	61.2	4.55	5.01	63.0
.394	12.32	83.8	8.18	1.41	62.0	8.79	1.78	61.0	8.25	2.54	60.5	5.18	4.70	61.6
.444	11.00	81.8	9.45	0.81	58.0	10.1	1.47	59.0	9.52	2.15	60.0	6.45	3.86	60.3
.495	10.08	80.3	10.7	0.71	54.0	11.3	0.81	58.0	10.8	1.52	59.5	7.72	3.38	60.5
.622	8.76	77.7	12.0	0.41	53.0	12.6	0.58	58.0	12.1	1.41	57.0	8.99	2.70	59.5
.749	7.97	76.0							13.3	0.71	55.0	10.3	2.23	59.0
1.00	7.02	74.4							14.6	0.41	55.0	11.5	1.78	58.5
1.26	6.31	73.0										12.8	1.52	58.0
1.64	5.51	71.5										14.1	1.08	58.0
2.02	4.96	70.8										15.3	0.81	58.0
2.40	4.59	69.5												
3.67	3.28	66.5												
4.94	2.41	65.0												
6.21	1.68	63.0												
7.48	1.08	61.0												
8.75	0.71	54.0												
10.0	0.41	50.0												

RUN 3: Ω = 1429 rpm, $Re_L = 8.0*10^5$

x/y_{slot}=36.9		x/y_{slot}=49.0		x/y_{slot}=58.8		x/y_{slot}=68.6		x/y_{slot}=78.4	
y	V_R	y	V_R	y	V_R	y	V_R	y	V_R
.305	17.52	.305	12.62	.305	8.75	.305	6.18	.356	4.91
.432	18.80	.356	13.14	.432	9.64	.356	6.38	.483	5.66
.559	19.58	.432	13.81	.813	10.74	.483	7.22	.737	6.39
.813	20.57	.559	14.40	1.07	10.80	.737	7.85	.991	6.67
.940	20.81	.686	14.57	1.32	10.68	.991	8.11	1.24	6.88
1.07	20.93	.940	14.57	1.70	10.41	1.24	8.19	1.50	6.89
1.19	20.81	1.57	13.51	2.34	9.63	1.88	8.11	2.01	6.88
1.32	20.69	2.21	11.81	2.97	8.57	2.51	7.60	3.28	6.30
1.57	20.00	2.84	9.85	3.61	7.87	3.15	7.27	4.55	5.63
1.83	18.93	3.48	7.83	4.24	6.67	3.78	6.74	5.82	4.94
2.08	17.57	4.11	5.90	4.88	5.66	5.05	5.49	7.09	4.09
2.21	16.24	4.75	4.07	5.51	4.70	6.32	4.27	8.36	3.46
2.34	13.93	5.38	2.51	6.15	3.78	7.59	3.18	9.63	2.34
2.44	11.08			6.78	2.85	8.86	2.12	10.9	1.63
2.49	9.02			7.42	2.00	10.1	1.22	12.2	0.81
2.59	6.69			8.05	1.29				

x/y_{slot}=88.2		x/y_{slot}=98.0		x/y_{slot}=107.8		x/y_{slot}=117.8		x/y_{slot}=127.5	
y	V_R	y	V_R	y	V_R	y	V_R	y	V_R
.305	3.71	.305	3.13	.305	2.30	.356	2.30	.356	2.12
.356	4.01	.381	3.38	.559	3.36	.737	3.15	.991	3.07
.483	4.52	.508	3.91	1.19	3.93	1.37	3.59	1.63	3.48
.737	5.25	.762	4.42	1.83	4.17	2.01	3.84	2.26	3.55
.991	5.51	1.02	4.68	2.46	4.25	2.64	3.89	2.90	3.62
1.50	5.80	1.65	4.92	3.10	4.19	3.91	3.82	3.53	3.53
2.13	5.72	2.29	5.10	4.37	4.11	5.18	3.78	4.80	3.46
2.77	5.66	3.56	4.75	5.64	3.84	7.72	3.21	7.34	3.21
4.04	5.25	4.83	4.50	6.91	3.53	10.3	2.76	9.88	2.70
5.31	4.70	6.10	4.15	8.18	3.28	12.8	2.19	12.4	2.30
6.58	4.19	7.37	3.73	9.45	2.94	15.3	1.73	15.0	2.08
7.85	3.69	8.64	3.31	10.7	2.51	17.9	1.35	17.5	1.73
9.12	3.18	9.91	2.82	12.0	2.27	20.4	0.81	20.0	1.22
10.4	2.58	11.2	2.51	13.3	2.00				
11.7	1.95	12.4	2.04	14.5	1.73				
12.9	1.35	13.7	1.77	15.8	1.29				

RUN 4: Ω = 0 rpm, y_{slot} = 2.59 , $\overline{V}_{1,slot}$ =17.1 ,

x_{slot} = 95.5

x/y_{slot}=36.9			x/y_{slot}=49.0			x/y_{slot}=58.8			x/y_{slot}=68.6			x/y_{slot}=78.4		
y	V_R	β	y	V_R	β	y	V_R	β	y	V_R	β	y	V_R	β
.305	17.66	3.0	.330	12.62	7.2	.356	9.98	17.0	.356	8.42	45.8	.356	9.19	60.5
.432	18.97	3.0	.406	13.51	7.1	.432	10.53	15.0	.406	8.15	38.8	.406	8.31	50.5
.559	19.79	3.0	.533	14.29	6.6	.813	10.76	9.2	.483	7.97	27.5	.483	7.73	41.2
.813	20.69	2.1	.660	14.52	6.0	1.07	10.80	7.2	.737	8.34	17.1	.737	7.27	26.3
.940	20.93	1.8	.914	14.57	4.0	1.32	10.71	5.9	.991	8.49	13.5	.991	7.21	19.8
1.07	21.09	1.5	1.55	13.45	2.0	1.70	10.41	4.2	1.24	8.49	11.0	1.24	7.15	16.6
1.19	21.01	1.3	2.18	11.66	1.1	2.34	9.54	2.5	1.88	8.44	5.8	1.50	7.11	14.0
1.32	20.77	1.2	2.82	9.72	0.7	2.97	8.57	1.2	2.51	7.86	4.7	2.01	7.00	10.5
1.57	19.53	1.1	3.45	7.73	0.3	3.61	7.71	0.7	3.15	7.27	3.3	3.28	6.30	5.3
1.83	18.35	1.0	4.09	5.83	0.0	4.24	6.69	0.5	3.78	6.77	2.2	4.55	5.51	3.3
2.08	16.84	0.9	4.72	4.07	0.0	4.88	5.58	0.3	5.05	5.46	1.5	5.82	4.63	2.5
2.21	15.51	0.7	5.36	2.51	0.0	5.51	4.57	0.2	6.32	4.25	0.0	7.09	3.86	1.7
2.34	13.14	0.5				6.15	3.60	0.0	7.59	2.99	0.0	8.36	2.88	1.5
2.44	10.46	0.3				6.78	2.76	0.0	8.86	2.30	0.0	9.63	2.12	1.0
2.49	8.74	0.1				7.42	1.78	0.0				10.9	1.29	0.0
2.59	6.44	0.0												

x/y_{slot}=88.2			x/y_{slot}=98.0			x/y_{slot}=107.8			x/y_{slot}=117.6			x/y_{slot}=127.5		
y	V_R	β	y	V_R	β	y	V_R	β	y	V_R	β	y	V_R	β
.330	10.97	74.5	.330	11.89	78.6	.330	12.12	79.5	.381	11.86	76.5	.381	12.44	79.0
.381	9.73	66.5	.406	10.27	72.0	.457	9.64	68.0	.508	9.78	69.0	.635	9.51	69.7
.508	7.89	51.0	.533	8.30	57.3	.584	8.23	59.8	.762	8.15	59.7	1.02	7.92	61.0
.762	6.90	46.5	.787	6.96	45.8	1.22	6.41	44.4	1.40	6.64	49.5	1.65	6.63	53.7
1.02	6.56	39.5	1.04	6.47	39.0	1.85	5.72	35.4	2.03	5.85	42.5	2.29	5.87	47.3
1.52	6.30	21.0	1.68	5.83	28.7	2.46	5.15	27.9	2.67	5.28	35.5	2.92	5.26	42.0
2.13	6.07	16.0	2.31	5.25	21.7	3.10	4.78	22.5	3.91	4.44	26.5	3.53	4.77	37.0
2.77	5.77	11.8	3.56	5.07	13.6	4.37	4.31	15.0	5.18	3.93	19.1	4.80	4.11	31.0
4.04	5.15	7.4	4.83	4.50	9.2	5.64	3.83	10.3	7.72	3.21	10.5	7.34	3.15	19.0
5.31	4.55	4.2	6.10	4.07	7.0	6.91	3.50	9.0	10.3	2.58	8.5	9.88	2.34	16.5
6.58	4.01	3.0	7.37	3.60	5.0	8.18	3.02	6.8	12.8	2.04	7.0	12.4	1.95	12.0
7.85	3.33	2.0	8.64	3.23	4.5	9.45	2.73	6.5	15.3	1.58	6.0	15.0	1.47	8.0
9.12	2.76	1.5	9.91	2.79	4.0	10.7	2.34	6.0	17.9	1.22	5.0	17.5	1.08	2.5
10.4	1.95	1.0	11.2	2.27	3.0	12.0	1.82	5.5						
11.7	1.82	0.5	12.4	1.82	2.0	13.3	1.58	4.5						
						14.5	1.35	2.0						

RUN 5: Ω = 1111 rpm, y_{slot}=2.59, $\overline{V_1}_{,slot}$=17.00

x_{slot}=95.5

x/y_{slot}=24.7		x/y_{slot}=33.3		x/y_{slot}=40.0		x/y_{slot}=46.7		x/y_{slot}=5	
y	V_R	y	V_R	y	V_R	y	V_R	y	V_R
0.305	12.35	0.305	10.70			0.305	5.85		
0.356	12.88	0.432	11.95	0.432	9.03	0.381	6.16	0.356	4.89
0.406	13.48	0.559	12.59	0.559	9.68	0.457	6.63	0.483	5.54
0.457	13.87	0.686	12.88	0.686	10.06	0.584	7.25	0.610	5.92
0.508	14.23	0.813	13.01	0.813	10.26	0.838	7.71	0.737	6.08
0.559	14.52	1.07	13.17	1.07	10.40	1.09	7.92	0.864	6.30
0.686	15.13	1.32	13.14	1.32	10.40	1.73	7.98	1.12	6.53
0.813	15.56	1.57	12.88	1.57	10.32	2.36	7.69	1.37	6.61
1.07	16.22	1.83	12.49	1.83	10.16	3.63	6.69	1.63	6.61
1.32	16.50	2.08	11.98	2.08	9.91	4.90	5.73	1.88	6.59
1.57	16.47	2.34	11.48	2.34	9.70	6.17	4.64	2.13	6.57
1.83	16.19	2.84	10.26	2.84	9.04	7.44	3.55	2.51	6.45
2.34	15.19	3.48	8.74	3.48	8.17	8.71	2.54	3.15	6.16
2.84	13.69	4.11	7.23	4.11	7.37	9.98	1.68	3.78	5.86
3.05	13.01	4.75	5.75	4.75	6.47			4.42	5.51
3.30	11.95	5.38	4.39	5.38	5.49			5.69	4.84
3.56	9.55	6.65	1.59	6.65	3.80			6.96	4.09
3.78	4.73			7.92	2.31			8.23	3.31
3.81	2.88							9.50	2.73
								10.8	2.04
								12.0	1.29

x/y_{slot}=60.0		x/y_{slot}=66.7		x/y_{slot}=73.3		x/y_{slot}=80.0		x/y_{slot}=86.7	
y	V_R	y	V_R	y	V_R	y	V_R	y	V_R
		0.305	3.02	0.305	2.54	0.305	2.04	0.305	1.87
0.356	3.97	0.356	3.16	0.356	2.61	0.356	2.19	0.356	2.04
0.483	4.57	0.406	3.59	0.406	2.79	0.483	2.61	0.406	2.12
0.610	4.87	0.533	3.91	0.533	3.21	0.610	2.96	0.533	2.41
0.864	5.28	0.660	4.07	0.660	3.55	0.737	3.15	0.787	2.82
1.12	5.46	0.914	4.42	0.914	3.86	0.991	3.43	1.42	3.23
1.37	5.55	1.17	4.61	1.17	4.17	1.24	3.62	2.06	3.36
1.63	5.61	1.55	4.80	1.68	4.37	1.50	3.69	2.69	3.43
2.01	5.64	2.18	4.85	2.31	4.46	1.88	3.82	3.33	3.48
2.64	5.58	2.82	4.78	2.95	4.41	2.51	3.89	3.96	3.46
3.91	5.22	3.45	4.64	5.49	3.99	3.78	3.84	4.60	3.38
5.18	4.71	5.99	4.05	8.03	3.36	5.05	3.71	5.23	3.31
6.45	4.19	8.53	3.31	10.6	2.73	7.59	3.36	7.14	3.02
7.72	3.71	11.1	2.51	13.1	2.15	10.1	2.67	9.68	2.73
8.99	3.18	13.6	1.82	15.6	1.58	12.7	2.19	12.2	2.27
10.3	2.64	16.2	1.15	18.2	1.00	15.2	1.68	14.8	1.73
11.5	2.30					17.8	1.35	17.3	1.47
12.8	1.53					20.3	0.71	19.8	1.29
14.1	1.15								

RUN 6: Ω = 0 rpm., y_{slot}=3.81 , $\overline{V}_{1,slot}$=13.47 , x_{slot}=94 .

x/y_{slot}=24.7			x/y_{slot}=33.3			x/y_{slot}=40.0			x/y_{slot}=46.7			x/y_{slot}=53.3		
y	V_R	β	y	V_R	β	y	V_R	β	y	V_R	β	y	V_R	β
.330	13.51	2.5	.432	12.08	3.9	.432	9.17	6.8	.381	6.23	16.0	.368	5.53	35.0
.432	14.34	2.0	.559	12.62	3.1	.559	9.79	6.0	.457	6.67	13.0	.483	5.69	21.0
.559	15.08	2.0	.686	13.04	2.7	.686	10.12	5.3	.584	7.25	10.0	.610	6.01	14.0
.686	15.56	1.6	.813	13.23	2.4	.813	10.26	4.7	.838	7.71	7.8	.737	6.22	12.5
.813	15.93	1.5	1.07	13.39	1.7	1.07	10.40	3.8	1.09	7.94	6.5	.864	6.34	11.0
1.07	16.45	1.2	1.32	13.39	1.5	1.32	10.40	3.0	1.73	7.99	4.6	1.12	6.56	8.5
1.32	16.75	1.0	1.57	12.95	1.2	1.57	10.26	2.5	2.36	7.73	3.1	1.37	6.66	7.0
1.57	16.70	0.6	1.83	12.49	0.8	1.83	10.06	2.0	3.63	6.82	0.4	1.63	6.69	6.0
1.83	16.24	0.5	2.08	12.02	0.5	2.08	9.87	1.5	4.90	5.83	0.0	1.88	6.67	5.5
2.08	15.67	0.4	2.34	11.52	0.3	2.34	9.57	1.0	6.17	4.70	0.0	2.13	6.61	4.5
2.34	14.97	0.3	2.84	10.22	0.1	2.84	8.94	0.5	7.44	3.55	0.0	2.51	6.48	3.0
2.84	13.51	0.2	3.48	8.71	0.0	3.48	8.17	0.2	8.71	2.58	0.0	3.15	6.28	2.0
3.35	11.52	0.0	4.11	7.13	0.0	4.11	7.25	0.0	9.98	1.73	0.0	3.78	5.93	1.0
3.81	2.88	0.0	4.75	5.69	0.0	4.75	6.34	0.0				4.42	5.61	0.0
			5.38	4.39	0.0	5.38	5.42	0.0				5.69	4.85	0.0
			6.65	1.73	0.0	6.65	3.69	0.0				6.96	4.07	0.0
						7.92	2.12	0.0				8.23	3.35	0.0
												10.8	1.95	0.0

x/y_{slot}=60.0			x/y_{slot}=66.7			x/y_{slot}=73.3			x/y_{slot}=80.0			x/y_{slot}=86.7		
y	V_R	β	y	V_R	β	y	V_R	β	y	V_R	β	y	V_R	β
			.343	7.00	70.0	.343	7.62	74.0	.356	8.35	78.0	.356	8.47	77.0
.381	5.63	49.0	.394	6.42	64.0	.381	6.86	66.5	.406	7.41	72.0	.406	7.62	72.0
.508	5.29	33.5	.432	5.87	53.5	.432	6.14	59.5	.533	5.99	59.5	.444	6.89	68.0
.635	5.29	24.0	.559	5.18	40.0	.559	5.45	47.5	.660	5.28	50.0	.571	5.82	59.0
.889	5.49	16.5	.686	5.06	32.0	.686	4.96	37.5	.787	4.94	42.5	.825	4.94	46.5
1.13	5.60	13.5	.927	4.99	23.2	.940	4.78	27.5	1.03	4.55	33.0	1.45	4.25	32.5
1.38	5.75	11.5	1.18	5.05	18.4	1.18	4.73	21.5	1.27	4.39	28.0	2.07	4.03	26.0
1.64	5.80	10.0	1.55	5.05	14.0	1.69	4.64	16.5	1.52	4.29	24.5	2.71	3.86	20.5
2.02	5.77	8.5	2.18	4.99	11.0	2.31	4.59	12.5	1.90	4.23	21.0	3.33	3.80	17.5
2.65	5.66	6.0	2.82	4.97	8.3	2.95	4.46	10.0	2.54	4.15	15.0	3.96	3.64	15.0
3.92	5.36	3.5	3.45	4.78	6.5	5.49	4.03	4.0	3.78	3.91	11.0	4.60	3.60	12.5
5.19	4.78	2.5	5.99	4.15	3.0	8.03	3.36	1.0	5.05	3.61	8.0	5.23	3.50	10.5
6.46	4.33	1.0	8.53	3.36	2.0	10.6	2.73	0.0	7.59	3.26	3.0	7.14	3.10	6.0
7.73	3.73	0.0	11.1	2.54	1.0	13.1	2.12	0.0	10.1	2.67	2.0	9.68	2.76	5.0
9.00	3.18	0.0	13.6	1.87	0.0	15.6	1.58	0.0	12.7	2.19	1.0	12.2	2.23	4.0
10.3	2.61	0.0	16.2	1.15	0.0	18.2	1.00	0.0	15.2	1.68	0.0	14.8	1.73	3.0
11.5	2.15	0.0							17.8	1.29	0.0	17.3	1.41	2.0
12.8	1.58	0.0							20.3	0.71	0.0	19.8	1.29	1.0

RUN 7: Ω = 562.5 rpm., y_{slot}=3.81 , $\overline{V}_{1,slot}$=13.40 , x_{slot}=94

x/y_{slot}=24.7			x/y_{slot}=33.3			x/y_{slot}=40.0			x/y_{slot}=46.7			x/y_{slot}=53.3		
y	V_R	β	y	V_R	β	y	V_R	β	y	V_R	β	y	V_R	β
.330	14.11	2.5	.432	12.08	10.5	.356	9.47	24.5	.356	8.87	57.0	.356	9.95	65.0
.457	14.91	1.5	.559	12.69	10.0	.406	9.65	19.0	.406	8.15	42.5	.406	8.90	56.0
.711	15.98	1.0	.686	13.07	9.0	.660	10.22	12.0	.533	7.62	28.0	.457	8.10	47.5
.965	16.65	0.5	.813	13.26	8.0	.914	10.40	9.0	.635	7.75	21.5	.559	7.26	34.5
1.22	16.89	0.4	1.07	13.45	6.5	1.17	10.38	7.0	.889	7.99	15.5	.813	6.89	22.5
1.47	16.79	0.3	1.32	13.39	6.0	1.42	10.38	5.5	1.14	8.04	13.0	1.07	6.84	16.5
1.73	16.39	0.2	1.57	12.95	5.0	1.68	10.23	4.8	1.40	8.10	10.3	1.32	6.82	13.5
1.98	15.83	0.1	1.96	12.29	4.3	1.93	9.99	3.7	1.65	8.02	8.6	1.57	6.77	11.0
2.24	15.24	0.0	2.59	10.93	3.5	2.18	9.73	2.6	1.90	7.94	7.5	1.96	6.72	8.5
2.49	14.69	0.0	3.23	9.29	2.0	2.69	9.20	2.0	2.29	7.81	6.0	2.59	6.45	5.5
2.74	13.87	0.0	8.86	7.83	1.5	3.33	8.40	1.0	3.56	6.88	3.0	3.23	6.24	2.5
3.00	13.14	0.0	4.50	6.18	1.0	3.96	7.51	0.5	4.83	5.90	1.5	4.50	5.44	1.0
3.25	12.08	0.0	5.13	4.99	0.0	5.23	5.61	0.0	6.10	4.73	1.0	5.77	4.70	0.0
3.51	9.98	0.0	5.77	3.64	0.0	6.50	4.03	0.0	7.37	3.60	0.7	7.04	3.97	0.0
3.81	3.15	0.0	6.40	2.30	0.0	7.77	2.58	0.0	9.91	2.08	0.0	8.31	3.43	0.0
						8.41	1.29					9.58	2.67	0.0
												12.1	1.68	0.0

x/y_{slot}=60.0			x/y_{slot}=66.7			x/y_{slot}=73.3			x/y_{slot}=80.0			x/y_{slot}=86.7		
y	V_R	β	y	V_R	β	y	V_R	β	y	V_R	β	y	V_R	β
.356	10.82	72.5	.356	12.19	72.0	.317	14.29	80.5	.343	14.49	75.5	.381	14.63	74.5
.381	9.59	64.0	.457	9.14	58.5	.343	13.07	78.0	.457	10.91	65.0	.432	12.78	71.0
.432	8.52	56.5	.711	7.17	42.0	.394	11.54	72.0	.584	9.30	59.5	.483	11.52	68.0
.508	8.07	51.5	.965	6.52	34.0	.521	9.31	62.5	.838	7.87	51.2	.559	10.62	65.5
.559	7.42	45.5	1.47	5.93	25.0	.635	8.24	56.5	1.09	7.15	47.0	.686	9.55	61.5
.686	6.83	37.5	1.85	5.69	19.5	.762	7.61	51.5	1.35	6.61	42.5	.940	8.39	56.5
.914	6.56	29.0	2.24	5.45	15.5	1.02	6.90	44.5	1.60	6.16	39.5	1.19	7.60	52.5
1.30	6.16	21.5	2.87	5.22	10.0	1.65	5.99	34.5	1.98	5.76	35.0	1.45	7.14	50.0
1.93	5.82	14.5	3.51	5.01	7.0	2.29	5.43	26.5	2.62	5.14	29.0	2.08	6.11	43.5
2.57	5.54	9.5	4.78	4.55	2.5	2.92	5.02	22.0	3.25	4.78	25.0	2.72	5.51	38.0
3.84	5.15	4.5	6.05	4.03	1.5	3.56	4.82	17.5	3.89	4.44	21.5	3.35	4.85	32.0
6.38	4.07	1.0	7.32	3.60	0.5	5.46	4.15	8.5	5.16	4.07	15.0	4.60	4.27	24.5
8.92	3.02	0.0	8.59	3.21	0.5	7.98	3.38	3.0	6.43	3.78	10.5	7.11	3.50	14.5
11.5	1.95	0.0	9.86	2.85	0.5	10.5	2.64	1.0	7.70	3.28	8.0	9.65	2.61	9.0
14.0	1.35	0.0	11.1	2.44	0.5	13.1	2.19	0.0	8.97	3.02	5.0	12.2	2.12	5.0
			12.4	2.12	0.0	15.6	1.58	0.0	10.2	2.76	4.0	14.7	1.73	3.0
			13.7	1.78	0.0				11.5	2.44	3.0	17.3	1.41	2.0
			14.9	1.58	0.0				14.0	2.08	1.0			
									16.6	1.29	0.0			

RUN 8: Ω = 1111 rpm., y_{slot}=3.81 , $\overline{V}_{1,slot}$=13.60 ,

x_{slot}=94.0

APPENDIX 6

Derivation of the Transport Equations for the Double Velocity Correlations

6.1 INTRODUCTION

It is shown in Section 7.2-1 of Chapter 7 that the convection and production terms of the double velocity correlation can be deduced from the Navier-Stokes equations by algebraic manipulation of only the convection terms of the latter equations. The exact expressions representing the diffusion, pressure-strain and dissipation processes are not at present solved. Consequently, in the following derivation of the transport equations for the double velocity correlations the complete expressions for these three processes are not deduced.

The Navier-Stokes equations for steady incompressible flow are in vector notation, Aris (1962):

$$\underbrace{(\mathbf{V}\cdot\nabla)\mathbf{V}}_{\text{convection}} = \underbrace{-\nabla p/\rho}_{\text{pressure}} + \underbrace{\nu\nabla^2\mathbf{V}}_{\text{viscous diffusion}} \qquad (6.1)$$

The term $(\mathbf{V}.\nabla)\mathbf{V}$ can be expressed in short as an acceleration term symbolised by $\mathbf{a}$. In the curvilinear orthogonal system of coordinates illustrated in Fig. 2.1 of Chapter 2, the components of the convection terms in, for example, the i-direction are:

$$\left[(V\cdot\nabla)V\right]_i = a_i = \sum_{k=1,3} \frac{V_k}{\ell_k}\left[\frac{\partial V_i}{\partial x_k} + V_i\frac{\partial \ell_i}{\ell_i \partial x_k} - V_k\frac{\partial \ell_k}{\ell_i \partial x_i}\right] \qquad (6.2)$$

The acceleration term **a** and all the velocity components V represent instantaneous values.

6.2 EQUATIONS IN CURVILINEAR ORTHOGONAL COORDINATES

If for example $\overline{v_i v_j}$ is the double velocity correlation being considered, then the relevant Navier-Stokes equations are those for the i and j directions:

$$a_i = \left[-\frac{1}{\rho}\nabla p + \nu\nabla^2 V\right]_i \qquad (6.3)$$

$$a_j = \left[-\frac{1}{\rho}\nabla p + \nu\nabla^2 V\right]_j \qquad (6.4)$$

The sequence of algebra necessary to obtain the desired transport equation for the double velocity correlation from equations 6.3 and 6.4 is now described:

(a) Equations 6.3 and 6.4 are multiplied by V_j and V_i respectively, and the products summed; after some simplifications:

$$\frac{V_k}{\ell_k}\left[\frac{\partial V_i V_j}{\partial x_k} + V_i V_j\left\{\frac{\partial \ell_i}{\ell_i \partial x_k} + \frac{\partial \ell_j}{\ell_j \partial x_k}\right\} - V_k\left\{\frac{V_j}{\ell_i}\frac{\partial \ell_k}{\partial x_i} + \frac{V_i}{\ell_j}\frac{\partial \ell_k}{\partial x_j}\right\}\right] = V_j\left[-\frac{\nabla p}{\rho} + \nu\nabla^2 V\right]_i + V_i\left[-\frac{\nabla p}{\rho} + \nu\nabla^2 V\right]_j \qquad (6.5)$$

The instantaneous values of V are separated into their mean component $\overline{V}$ and their fluctuating component v':

$$\left[\frac{\overline{V_k}+v_k'}{\ell_k}\right]\left[\frac{\partial}{\partial x_k}\left\{\overline{V_i V_j} + v_i'\overline{V_j} + v_j'\overline{V_i} + \overline{v_i' v_j'}\right\} + \left\{\overline{V_i V_j} + v_i'\overline{V_j} + v_j'\overline{V_i} + \overline{v_i' v_j'}\right\}\left\{\frac{\partial \ell_i}{\ell_i \partial x_k} + \frac{\partial \ell_j}{\ell_j \partial x_k}\right\}\right.$$
$$\left. - \left\{\overline{V_k}+v_k'\right\}\left\{\frac{\overline{V_j}+v_j'}{\ell_i}\frac{\partial \ell_k}{\partial x_i} + \frac{\overline{V_i}+v_i'}{\ell_j}\frac{\partial \ell_k}{\partial x_j}\right\}\right] = \left(\overline{V_j}+v_j'\right)\left(-\frac{\nabla p}{\rho} + \nu\nabla^2 V\right)_i + \left(\overline{V_i}+v_i'\right)\left(-\frac{\nabla p}{\rho} + \nu\nabla^2 V\right)_j \qquad (6.6)$$

(b) Equations 6.3 and 6.4 are multiplied by the mean values of V_j and V_i respectively, and the products summed:

$$\overline{V_j}\frac{V_k}{\ell_k}\left[\frac{\partial V_i}{\partial x_k} + \frac{V_i}{\ell_i}\frac{\partial \ell_i}{\partial x_k} - \frac{V_k}{\ell_i}\frac{\partial \ell_k}{\partial x_i}\right] + \overline{V_i}\frac{V_k}{\ell_k}\left[\frac{\partial V_j}{\partial x_k} + \frac{V_j}{\ell_j}\frac{\partial \ell_j}{\partial x_k} - \frac{V_k}{\ell_j}\frac{\partial \ell_k}{\partial x_j}\right] = \overline{V_j}\left(-\frac{\nabla p}{\rho} + \nu\nabla^2 V\right)_i + \overline{V_i}\left(-\frac{\nabla p}{\rho} + \nu\nabla^2 V\right)_j \qquad (6.7)$$

The instantaneous values of V are once again separated into mean and fluctuating components:

$$\overline{V_j}\left(\frac{\overline{V_k}+v_k'}{\ell_k}\right)\left[\frac{\partial}{\partial x_k}\left(\overline{V_i}+v_i'\right)+\frac{\overline{V_i}+v_i'}{\ell_i}\frac{\partial \ell_i}{\partial x_k}-\frac{\overline{V_k}+v_k'}{\ell_i}\frac{\partial \ell_k}{\partial x_i}\right]+\overline{V_i}\left(\frac{\overline{V_k}+v_k'}{\ell_k}\right)\times$$
$$\left[\frac{\partial}{\partial x_k}\left(\overline{V_j}+v_j'\right)+\frac{\overline{V_j}+v_j'}{\ell_j}\frac{\partial \ell_j}{\partial x_k}-\frac{\overline{V_k}+v_k'}{\ell_j}\frac{\partial \ell_k}{\partial x_j}\right]=\overline{V_j}\left(-\frac{\nabla p}{\rho}+\nu\nabla^2 V\right)_i+\overline{V_i}\left(-\frac{\nabla p}{\rho}+\nu\nabla^2 V\right)_j \qquad (6.8)$$

(c) Equations 6.6 and 6.8 are time-averaged; from the definition of the fluctuating velocity component it follows that $\overline{v'} = 0$, so that only double and triple velocity correlations now remain. The overscores and primes for the velocity components on the left side of the following equations are omitted for convenience. The time-average of equation 6.6 gives:

$$\frac{V_k}{\ell_k}\left[\frac{\partial}{\partial x_k}\left(V_iV_j+\overline{v_iv_j}\right)+\left(V_iV_j+\overline{v_iv_j}\right)\left(\frac{\partial \ell_i}{\ell_i\partial x_k}+\frac{\partial \ell_j}{\ell_j\partial x_k}\right)-\left(\frac{V_jV_k+\overline{v_jv_k}}{\ell_i}\frac{\partial \ell_k}{\partial x_i}+\frac{V_iV_k+\overline{v_iv_k}}{\ell_j}\frac{\partial \ell_k}{\partial x_j}\right)\right]$$
$$+\frac{v_k}{\ell_k}\left[\frac{\partial}{\partial x_k}\left(\overline{v_iV_j}+\overline{v_jV_i}+\overline{v_iv_j}\right)+\left(\overline{v_iV_j}+\overline{v_jV_i}+\overline{v_iv_j}\right)\left(\frac{\partial \ell_i}{\ell_i\partial x_k}+\frac{\partial \ell_j}{\ell_j\partial x_k}\right)-\left(\frac{\overline{v_kV_j}+\overline{v_jV_k}+\overline{v_jv_k}}{\ell_i}\frac{\partial \ell_k}{\partial x_i}+\right.\right.$$
$$\left.\left.\frac{\overline{v_kV_i}+\overline{v_iV_k}+\overline{v_iv_k}}{\ell_j}\frac{\partial \ell_k}{\partial x_j}\right)\right]=\overline{\left(\overline{V_j}+v_j'\right)\left(-\frac{\nabla p}{\rho}+\nu\nabla^2 V\right)_i}+\overline{\left(\overline{V_i}+v_i'\right)\left(-\frac{\nabla p}{\rho}+\nu\nabla^2 V\right)_j} \qquad (6.9)$$

The time-average of 6.8 gives:

$$\frac{V_k}{\ell_k}\left[\frac{\partial V_iV_j}{\partial x_k}+V_iV_j\left(\frac{\partial \ell_i}{\ell_i\partial x_k}+\frac{\partial \ell_j}{\ell_j\partial x_k}\right)-\left(\frac{V_jV_k}{\ell_i}\frac{\partial \ell_k}{\partial x_i}+\frac{V_iV_k}{\ell_j}\frac{\partial \ell_k}{\partial x_j}\right)\right]+\frac{v_k}{\ell_k}\left[V_j\frac{\partial v_i}{\partial x_k}+V_i\frac{\partial v_j}{\partial x_k}+\right.$$
$$\left.\frac{v_iV_j}{\ell_i}\frac{\partial \ell_i}{\partial x_k}+\frac{v_jV_i}{\ell_j}\frac{\partial \ell_j}{\partial x_k}-\frac{v_kV_j}{\ell_i}\frac{\partial \ell_k}{\partial x_i}-\frac{v_kV_i}{\ell_j}\frac{\partial \ell_k}{\partial x_j}\right]$$
$$=\overline{V_j\left(-\frac{\nabla p}{\rho}+\nu\nabla^2 V\right)_i}+\overline{V_i\left(-\frac{\nabla p}{\rho}+\nu\nabla^2 V\right)_j} \qquad (6.10)$$

(d) Finally, equation 6.10 is subtracted from equation 6.9 giving:

$$\left(\frac{V_k+v_k}{\ell_k}\right)\left[\frac{\partial v_iv_j}{\partial x_k}+v_iv_j\left(\frac{\partial \ell_i}{\ell_i\partial x_k}+\frac{\partial \ell_j}{\ell_j\partial x_k}\right)-\left(v_jv_k\frac{\partial \ell_k}{\ell_i\partial x_i}+v_iv_k\frac{\partial \ell_k}{\ell_j\partial x_j}\right)\right]$$
$$+\frac{v_k}{\ell_k}\left[v_i\frac{\partial V_j}{\partial x_k}+v_j\frac{\partial V_i}{\partial x_k}+v_iV_j\frac{\partial \ell_j}{\ell_j\partial x_k}+v_jV_i\frac{\partial \ell_i}{\ell_i\partial x_k}-v_jV_k\frac{\partial \ell_k}{\ell_i\partial x_i}-v_iV_k\frac{\partial \ell_k}{\ell_j\partial x_j}\right]$$
$$=\overline{v_j'\left(-\frac{\nabla p}{\rho}+\nu\nabla^2 V\right)_i}+\overline{v_i'\left(-\frac{\nabla p}{\rho}+\nu\nabla^2 V\right)_j} \qquad (6.11)$$

The left hand side of equation 6.11 comprises the convection and production terms for the double velocity correlations, as well as some turbulent diffusion terms represented by the triple velocity correlations. These diffusion terms, together with the right hand side terms representing viscous diffusion, pressure diffusion, pressure-strain and dissipation are not considered in the remainder of the present analysis. Section 7.3 of Chapter 7 describes how they are modelled.

The transport equation can therefore be represented as:

Convection = Production + Diffusion + Pressure-strain + Dissipation.

6.3 AXISYMMETRIC CASES WITH CONSTANT ANGLE α

In the present work the stress equations are only employed for cases when the geometrical angle α is a constant, see Figure 6.1.

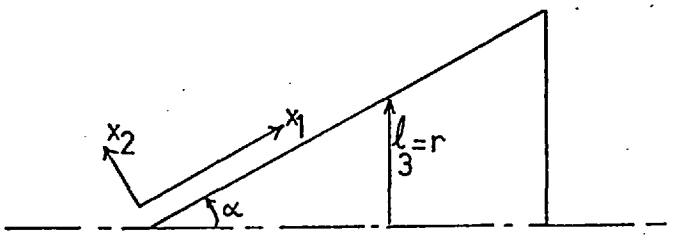

Fig. 6.1

The metric coefficients ℓ_1 and ℓ_2 are then equal to unity, and for axisymmetrical flow ℓ_3 is equivalent to the radius r. Furthermore, derivatives with respect to the circumferential direction x_3, are zero. Equation 6.11 is considerably simplified and can be expanded for each of the six double velocity correlations as:

$$V_k \frac{\partial v_1^2}{\partial x_k} - 4 v_1 v_3 \frac{V_3}{r} \frac{\partial r}{\partial x_1} + 2 v_1 v_k \frac{\partial V_1}{\partial x_k} = \left(D_f + P_s + D \right)_{1,1} \qquad (6.12)$$

$$V_k \frac{\partial v_2^2}{\partial x_k} - 4 v_2 v_3 \frac{V_3}{r} \frac{\partial r}{\partial x_2} + 2 v_2 v_k \frac{\partial V_2}{\partial x_k} = \left(D_f + P_s + D \right)_{2,2} \qquad (6.13)$$

$$V_k\left(\frac{\partial v_3^2}{\partial x_k}+\frac{2}{r}v_3^2\frac{\partial r}{\partial x_k}\right)+2v_3v_k\left(\frac{\partial V_3}{\partial x_k}+\frac{V_3}{r}\frac{\partial r}{\partial x_k}\right)=\left(Df+P_s+D\right)_{3,3} \qquad (6.14)$$

$$V_k\frac{\partial v_1v_2}{\partial x_k}-2\frac{V_3}{r}\left(v_2v_3\frac{\partial r}{\partial x_1}+v_1v_3\frac{\partial r}{\partial x_2}\right)+v_1v_k\frac{\partial V_2}{\partial x_k}+v_2v_k\frac{\partial V_1}{\partial x_k}=\left(Df+P_s+D\right)_{1,2} \qquad (6.15)$$

$$V_k\left(\frac{\partial v_1v_3}{\partial x_k}+\frac{v_1v_3}{r}\frac{\partial r}{\partial x_k}\right)-2v_3^2\frac{V_3}{r}\frac{\partial r}{\partial x_1}+v_1v_k\frac{\partial V_3}{\partial x_k}+v_3v_k\frac{\partial V_1}{\partial x_k}+v_1v_k\frac{V_3}{r}\frac{\partial r}{\partial x_k}=\left(Df+P_s+D\right)_{1,3} \qquad (6.16)$$

$$V_k\left(\frac{\partial v_2v_3}{\partial x_k}+\frac{v_2v_3}{r}\frac{\partial r}{\partial x_k}\right)-2v_3^2\frac{V_3}{r}\frac{\partial r}{\partial x_2}+v_2v_k\frac{\partial V_3}{\partial x_k}+v_3v_k\frac{\partial V_2}{\partial x_k}+v_2v_k\frac{V_3}{r}\frac{\partial r}{\partial x_k}=\left(Df+P_s+D\right)_{2,3} \qquad (6.17)$$

6.4 BOUNDARY LAYER EQUATIONS

For boundary layer flows, if direction -1 and -2 are assumed to be the predominant and cross-stream direction of flow respectively, the following approximations are valid:

$$V_1 \simeq V_3 \simeq \partial V/\partial x_1 \simeq O(1)\,,$$

$$V_2 \simeq O(e)\,,\ \partial V/\partial x_2 \simeq O(1/e)\,,\quad e \ll 1\,.$$

When these approximations together with the continuity equation $\frac{\partial}{\partial x_1}(rV_1)+\frac{\partial}{\partial x_2}(rV_2)=0$ are applied to equations 6.12 to 6.17, the following boundary layer equations are obtained:

$$V_k\frac{\partial v_1^2}{\partial x_k}-4v_1v_3\frac{V_3}{r}\frac{\partial r}{\partial x_1}+2v_1v_2\frac{\partial V_1}{\partial x_2}+2v_1^2\frac{\partial V_1}{\partial x_1}=\left(Df+P_s+D\right)_{1,1} \qquad (6.18)$$

$$V_k\frac{\partial v_2^2}{\partial x_k}-4v_2v_3\frac{V_3}{r}\frac{\partial r}{\partial x_2}=\left(Df+P_s+D\right)_{2,2} \qquad (6.19)$$

$$V_k\frac{\partial v_3^2}{\partial x_k}+4v_1v_3\frac{V_3}{r}\frac{\partial r}{\partial x_1}+4v_2v_3\frac{V_3}{r}\frac{\partial r}{\partial x_2}+2v_2v_3r\frac{\partial(V_3/r)}{\partial x_2}+2v_3^2\frac{V_1}{r}\frac{\partial r}{\partial x_1}=\left(Df+P_s+D\right)_{3,3} \qquad (6.20)$$

$$V_k \frac{\partial v_1 v_2}{\partial x_k} + v_2^2 \frac{\partial V_1}{\partial x_2} - 2\frac{V_3}{r}\left(v_2 v_3 \frac{\partial r}{\partial x_1} + v_1 v_3 \frac{\partial r}{\partial x_2}\right) + v_1 v_2 \frac{\partial V_1}{\partial x_1} = \left(Df + Ps + D\right)_{1,2} \quad (6.21)$$

$$V_k \frac{\partial v_1 v_3}{\partial x_k} + v_1 v_2 r \frac{\partial (V_3/r)}{\partial x_2} + v_2 v_3 \frac{\partial V_1}{\partial x_2} + 2 v_1 v_2 \frac{V_3}{r}\frac{\partial r}{\partial x_2} + 2\frac{V_3}{r}\left(v_1^2 - v_3^2\right)\frac{\partial r}{\partial x_1}$$
$$+ v_1 v_3 \left(\frac{\partial V_1}{\partial x_1} + \frac{V_1}{r}\frac{\partial r}{\partial x_1}\right) = \left(Df + Ps + D\right)_{1,3} \quad (6.22)$$

$$V_k \frac{\partial v_2 v_3}{\partial x_k} + v_2^2 r \frac{\partial (V_3/r)}{\partial x_2} + 2\left(v_2^2 - v_3^2\right)\frac{V_3}{r}\frac{\partial r}{\partial x_2} + 2 v_1 v_2 \frac{V_3}{r}\frac{\partial r}{\partial x_1}$$
$$+ v_2 v_3 \frac{V_1}{r}\frac{\partial r}{\partial x_1} = \left(Df + Ps + D\right)_{2,3} \quad (6.23)$$

APPENDIX 7

Local Heat Transfer Measurements from a Disc of Non-Uniform Temperature Rotating in Stagnant Air

7.1 INTRODUCTION

The local heat transfer by convection from the surface of a disc rotating in stagnant air was investigated, for a range of rotational speeds and arbitrary radial distributions of heat flux. The local heat transfer coefficients were found directly by measurements of the heat input to and the temperature of the disc's surface.

The experimental apparatus is described in Section 7.2, and the experimental procedure and results are presented in Sections 7.3 and 7.4. The local Nusselt numbers, determined from the experimental measurements, are compared with predicted values in Section 4.2 of Chapter 8.

7.2 APPARATUS

The experimental apparatus is sketched in Fig. 7.1; it consisted of a vertically mounted disc driven by an electric motor through a variable pulley arrangement. The construction and function of the main components are described in the following subsections.

7.2-1 Disc and Heaters

The local heat transfer coefficients were determined using the thin, electrically heated sheet technique. The thin-sheet, concentric, annular strips of stainless steel, .254 mm thick and 50.8 mm wide, were glued to the front face of the disc at intervals of 2.5 mm. There were a total of 8 of these annular strips, hereafter referred to as the heaters, located at the radii as shown in Fig. 7.2. The heaters were, for convenience, identified by the numbers 1 to 8 from the centre outwards, and their electrical resistances, measured using a potentionmeter, were .038, .056, .074, .093, .111, .130, .148 and .166, $\pm$ .0005 ohm.

The heaters could be independently heated and a wide range of non-uniform surface temperature or heat -flux

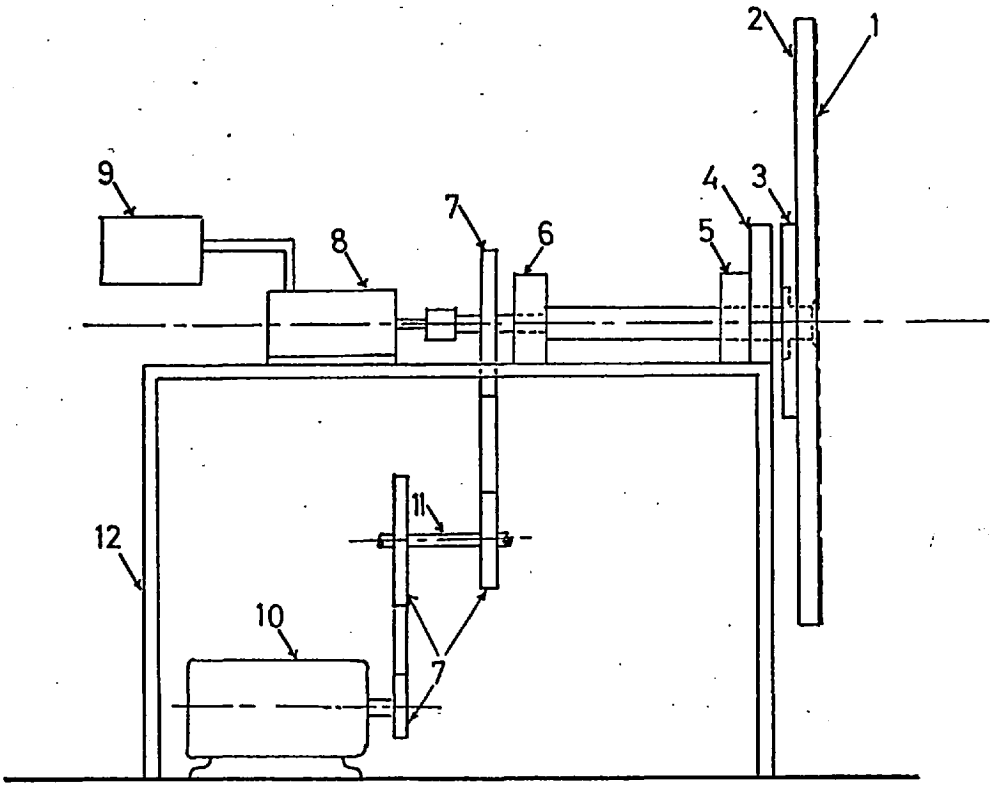

1. Concentric annular heaters.
2. Disc.
3. Slip-ring assembly for heaters current.
4. Holder for current carrying brushes.
5. Roller bearing.
6. Thrust ball bearing .
7. Pulleys .
8. Slip-rings for thermocouples.
9. Digital voltmeter for reading thermocouples output.
10. Synchronous motor.
11. Movable pulley assembly.
12. Mild steel frame, .025 m square section, supported on dampers and bolted to the floor.

Fig. 7.1 Lay-out of apparatus

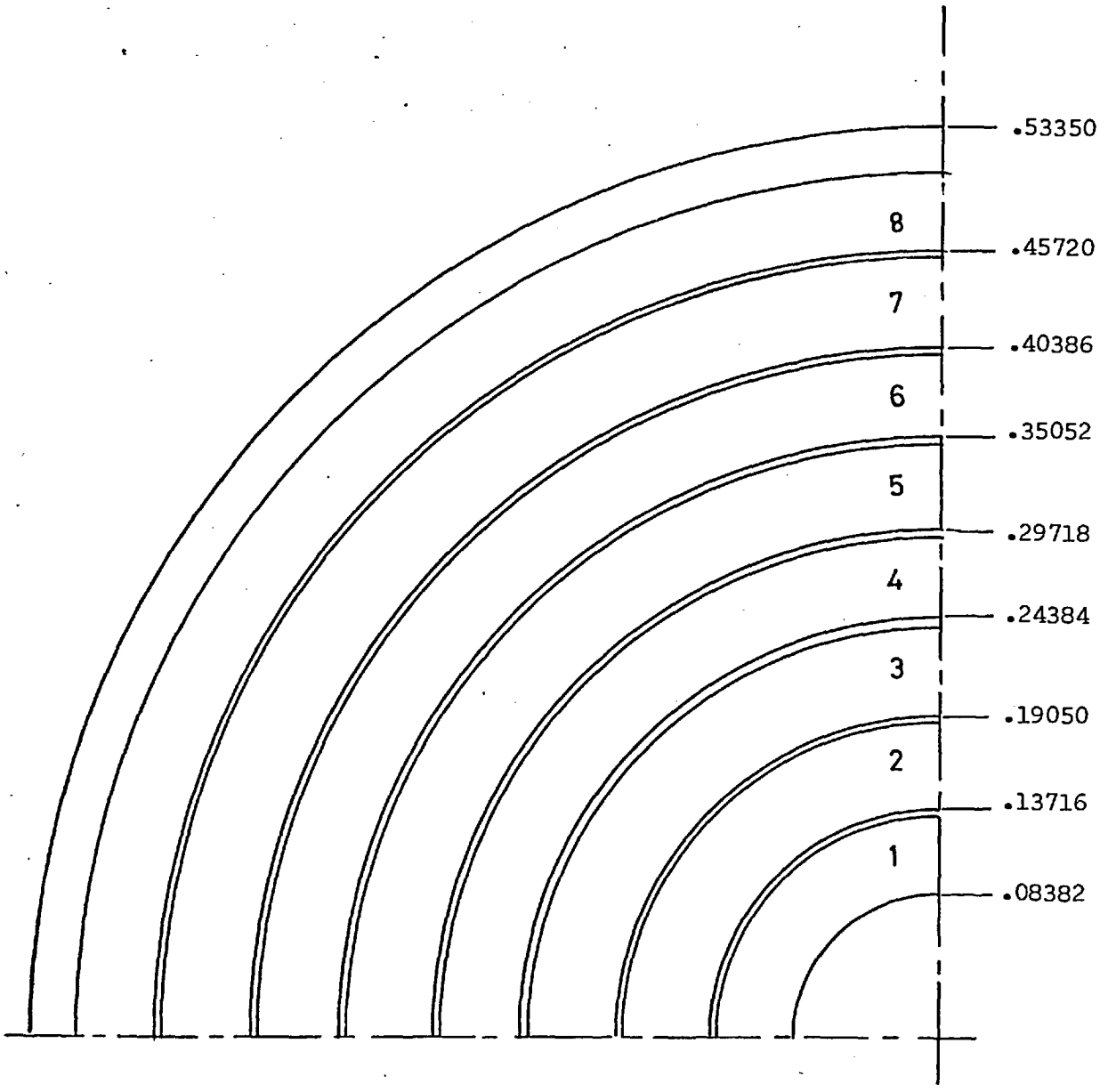

Fig. 7.2 Location of heaters 1 to 8 (dimensions in metres)

distribution could be achieved. The maximum power output was 35 watts for heater-1, rising to 150 watts for heater-8; these corresponded to a maximum heat flux of 1000 watts/m^2.

In order to minimise the error in the heat-transfer measurements due to heat loss, the disc on which the heaters were mounted was made of glass fibre. This material possessed a satisfactory combination of two properties required by the experimental design: it had a low thermal conductivity, thereby limiting the heat-loss by conduction; and it had adequate strength to withstand the stresses induced by rotation. The fibre-glass disc* was 0.0254 m thick and 1.067 m in diameter.

7.2-2 Motor and Speed Transmission

A synchronous motor of 4.47 kW(6hp) running at 1500 rpm was used to drive the apparatus. The motor-speed could be stepped-down through a two stage timing-belt and pulley set-up to provide disc speeds in the range of 140 to 1500 rpm; these speeds correspond to rotational Reynolds numbers based on disc radius of $2.5X10^5$ to $2.6X10^6$. At the highest Reynolds number 90% of the disc surface would be covered by fully turbulent flow.

The drive system guaranteed that there was no slip in speed transmission between motor and disc, and thereby ensured a constant and known speed for any preset experimental condition. The driven shaft, onto which the disc was mounted, was 50.8 mm in diameter

---

* The disc was cut from a .0254·m thick sheet of "Scotchply reinforced plastic, Crossply Type 1002", manufactured by the Minnesota Mining and Manufacturing Co. of Minnesota 55101, USA. The properties of the material were: Tensile strength: $5X10^8 N/m^2$, Tensile Modulus: $2.55X10^{10}$ N/m^2, Thermal conductivity: .339J/msdegK, Thermal coefficient of linear expansion: $1.278X10^{-5}$ m/m/degK, Specific gravity: 1.84

machined from mild steel.

7.2-3 Electrical Power Input

The heaters were electrically heated from a low voltage (5 to 15 V) transformer capable of supplying a total current of 250 A. The electrical circuit to one of the heaters is sketched in Fig. 7.3.

From the transformer, the current was conducted through 5mm square copper leads to a 30A fuse, a variable resistance*, and a 0-50A ammeter with an accuracy of ± 0.5A for currents less than 10A and ±0.2A for currents between 10 and 50A. The current was transmitted to the rotating heaters through spring loaded, water-cooled, copper/carbon (95%/5%) brushes making contact with concentric brass slip-rings. From the slip-rings the leads were fixed radially to the back of the fibre-glass disc, and then connected to bus-bars through the disc to the heaters.

The slip-ring assembly, see Fig. 7.3, consisted of an .18 mm thick Tufnol disc with machined concentric grooves into which 6.5 mm wide brass slip-rings were fixed, mounted on a 7.5 mm mild steel backing plate.

The path of the coolant through a copper/carbon brush is shown in Fig. 7.4. The coolant, tap water, was circulated from a central reservoir through individual flexible tubes to each brush, then to a common sink.

---

* Variable resistances were 'Zenith' Carbon Plate Type Rheostats capable of dissipating 200 watts to the surroundings.

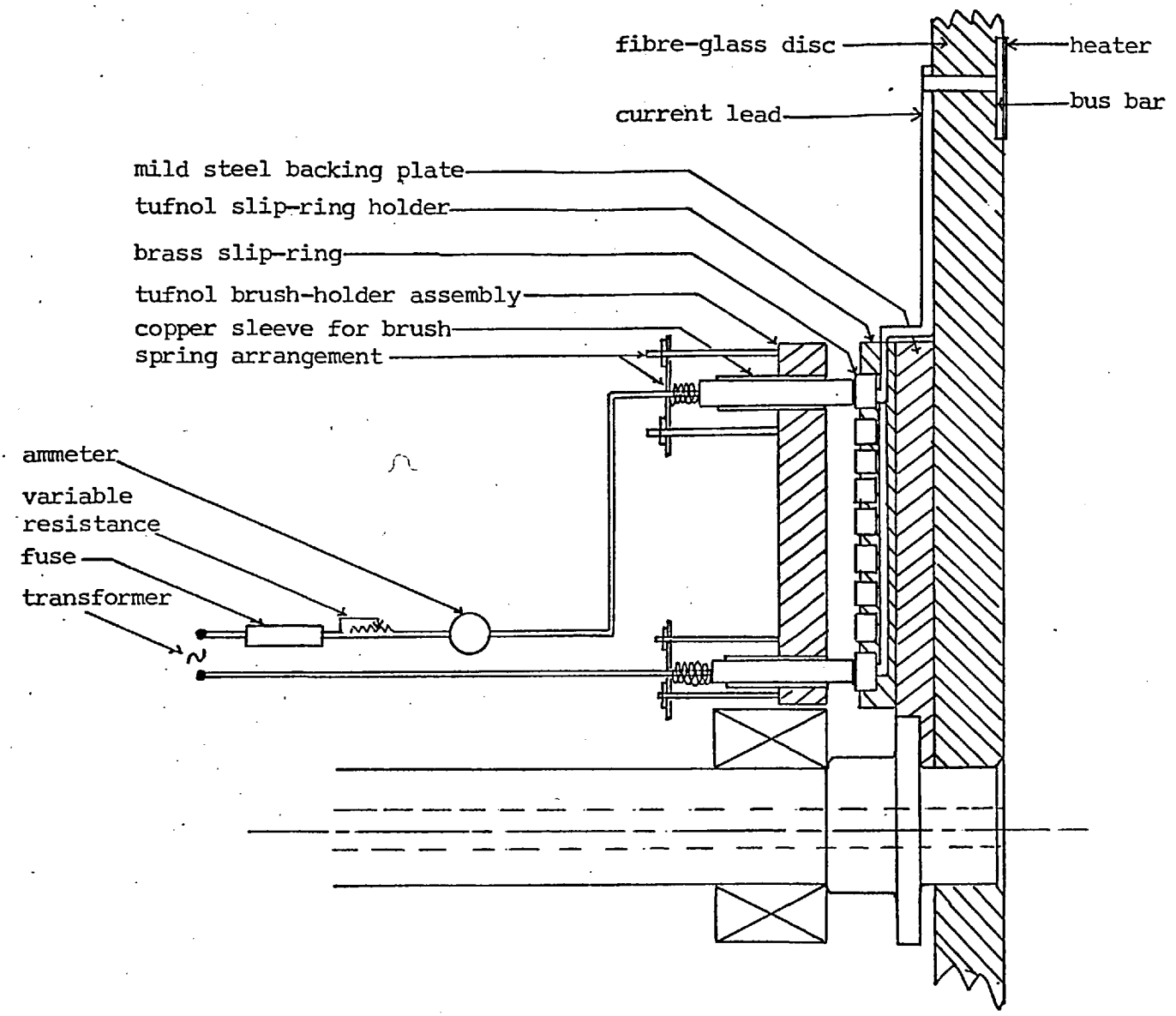

Fig. 7.3 Current path and slip-ring assembly

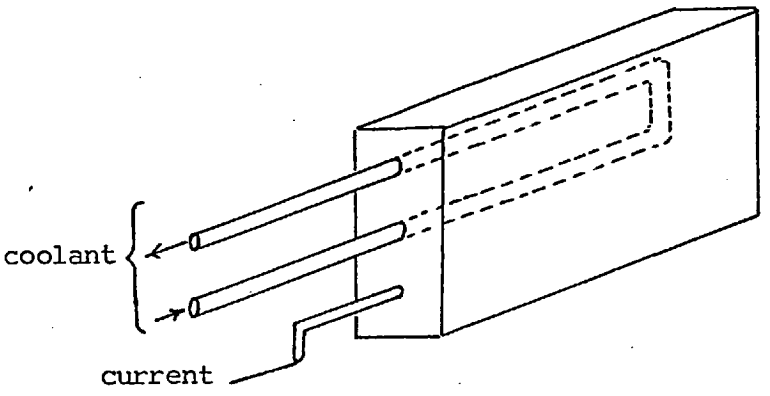

Fig. 7.4 Coolant path in copper/carbon brush

7.2-4 Temperature Measurement

The temperature of the heaters could be continuously measured by means of 40 copper-constantan thermocouples of 0·5 mm diameter. The thermocouples were fitted in grooves flush with the surface of the fibre-glass disc, led along a circumference for about 50 wire-diameters to minimise lead conduction, channelled in the radial direction towards the centre of the disc, and thence into the hollow shaft. The thermocouple leads were, on emerging from the shaft, connected to silver-coated slip-rings*, and the outputs transmitted to a digital voltmeter (DVM). The location of one of the thermocouples and its leads are sketched in Fig. 7.5; the figure is not drawn to scale.

1. disc
2. heater
3. thermocouple hot-junction
4. leads
5. digital volt-meter
6. slip-ring assembly
7. thermocouple cold-junction
8. coupling between shaft and slip-rings
9. drive pulley
10. bearing
11. hollow shaft

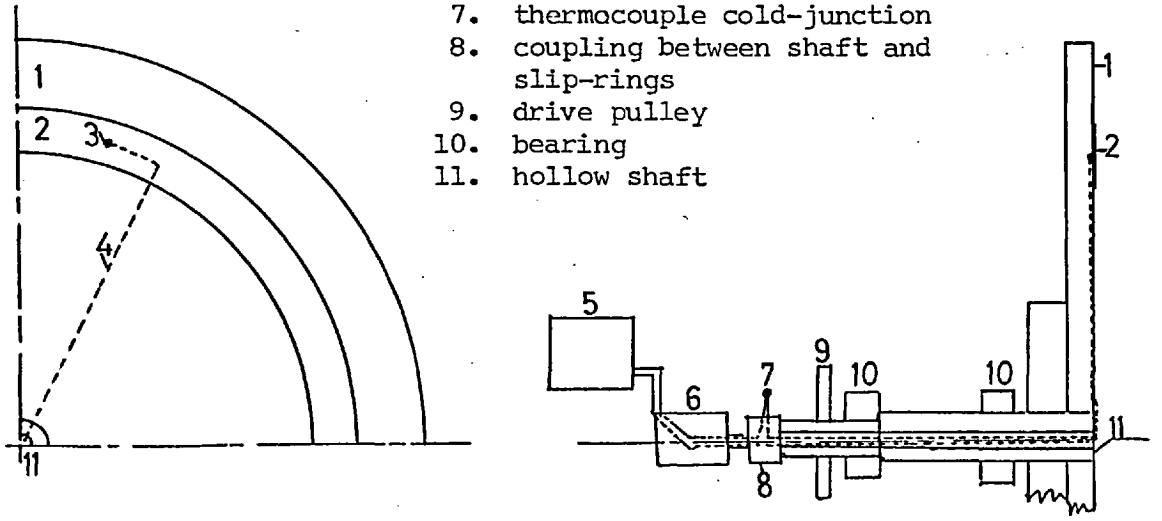

Fig. 7.5 Thermocouple lay-out

* Thermocouple slip-rings were twelve-channels Type PL12 from IDM Electronics Ltd.

The 'cold' junctions of the thermocouples were, as shown in Fig. 7.5, located close to the thermocouple slip-rings. These junctions rotated with the disc, and consequently ambient temperature was used as the reference temperature.

The signal (voltage) obtained from the thermocouples was calibrated, .0389 mV corresponding to a temperature difference of 1 degree K, and ranged between 0 and .6 mV. The electrical noise at 1000 rpm from the slip-rings was negligible; it was specified by the manufacturers as 5μV/mA. The digital voltmeter recording the signals from the thermocouples could be read to an accuracy of ±5μV. The maximum error in temperature measurement was therefore 12% decreasing to less than 2% for temperature differences between the heaters and ambient of 1 and 10 degrees K respectively.

7.2-5 Extraneous Heat Sources

When the apparatus was run without any power input to the heaters, frictional heating generated in the bearings, and between the brushes and slip-rings, caused an increase in temperature above ambient of 10 deg K for heater-1 decreasing to 1 degree for heater-8. This heat source was estimated to be in the region of 100 watts, which is far above the maximum heat input to heaters 1 to 4.

Furthermore, when the current was switched on to the heaters, the contact resistance between the brushes and slip-rings was measured to be between .05 and .15 ohm. With the maximum currents employed in the experiment, the heat generated at these sliding contact points was of the order of 90 watts.

The total, these extraneous heat sources were about 5 times the maximum electrical power input to heater-1, and of the same order as the power input to heater-8.

To overcome the problem of these large unwanted heat sources, it was decided to disregard the innermost two heaters since they were the worst affected and to keep the temperatures of heaters 3 and 4 constant by adjusting their current supply. Under these conditions, the radial conduction in the annular segment of the disc covered by heaters 3 and 4 was minimised, thereby insulating the remaining four outermost heaters from the effects of the heat sources. In other words, the heat from extraneous sources conducted to that part of the disc where $r > .30$ m was minimized.

7.3 EXPERIMENTAL PROCEDURE

Pulley ratios were selected to provide the desired speed, the motor was switched on, followed by the power input to the heaters. The apparatus achieved a steady state after about 3 hours, when the thermocouples outputs from the heaters had settled to a constant value.

The readings of the ammeters were recorded, and the outputs from the thermocouples were read in turn from a digital voltmeter.

7.4 EXPERIMENTAL RESULTS

Four experimental conditions were investigated for only two rotational speeds, 458.5 and 781 rpm; the reasons why only these few conditions were considered are explained later in Section 7.5. The temperatures and current inputs are recorded in the tables below, for each of the four experimental runs. The data are shown graphically in Fig. 7.6 and 7.7 and illustrate the non-uniform temperature or heat-flux distribution achieved by the apparatus.

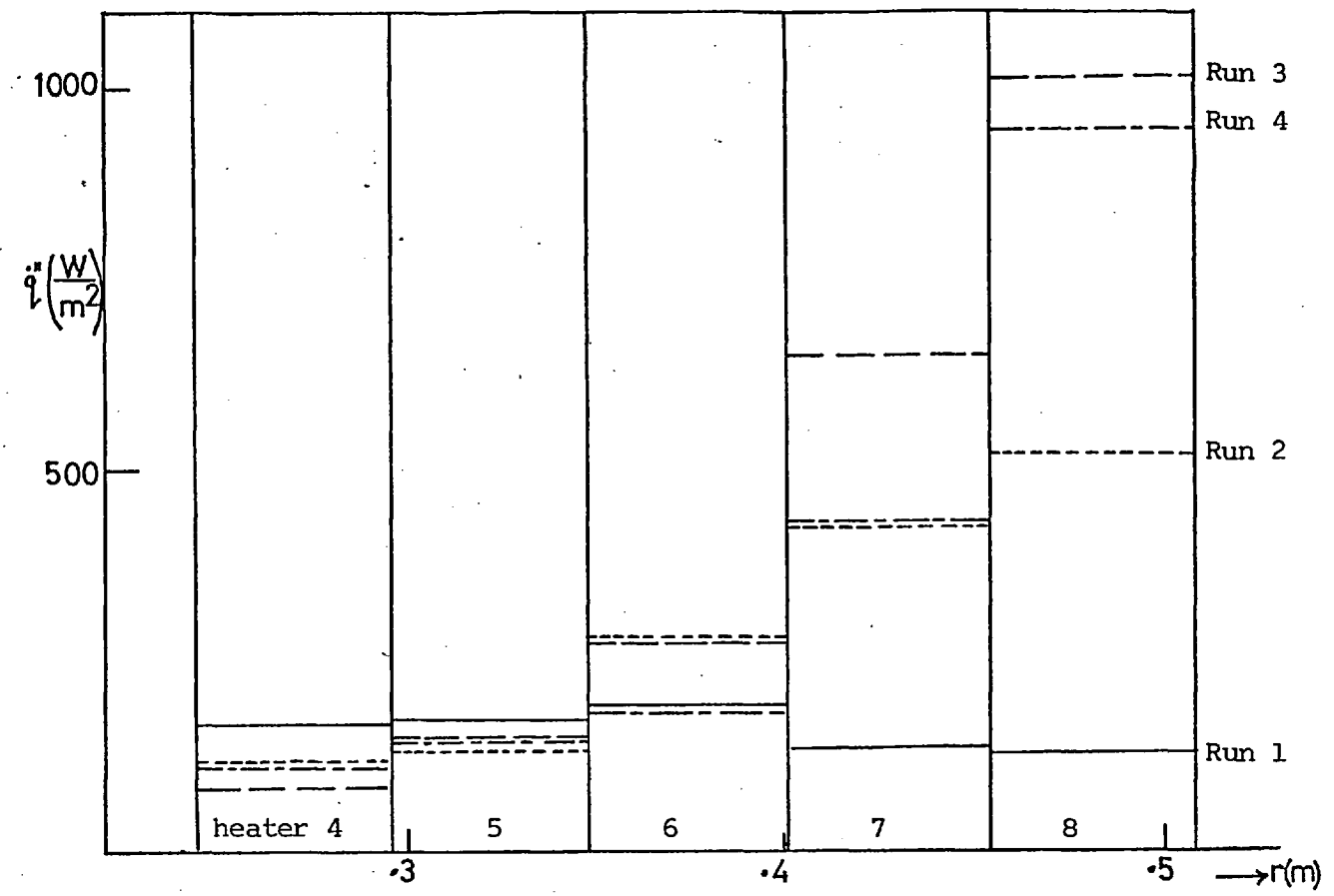

Fig. 7.6 Electrical heat flux distributions for Runs 1 to 4

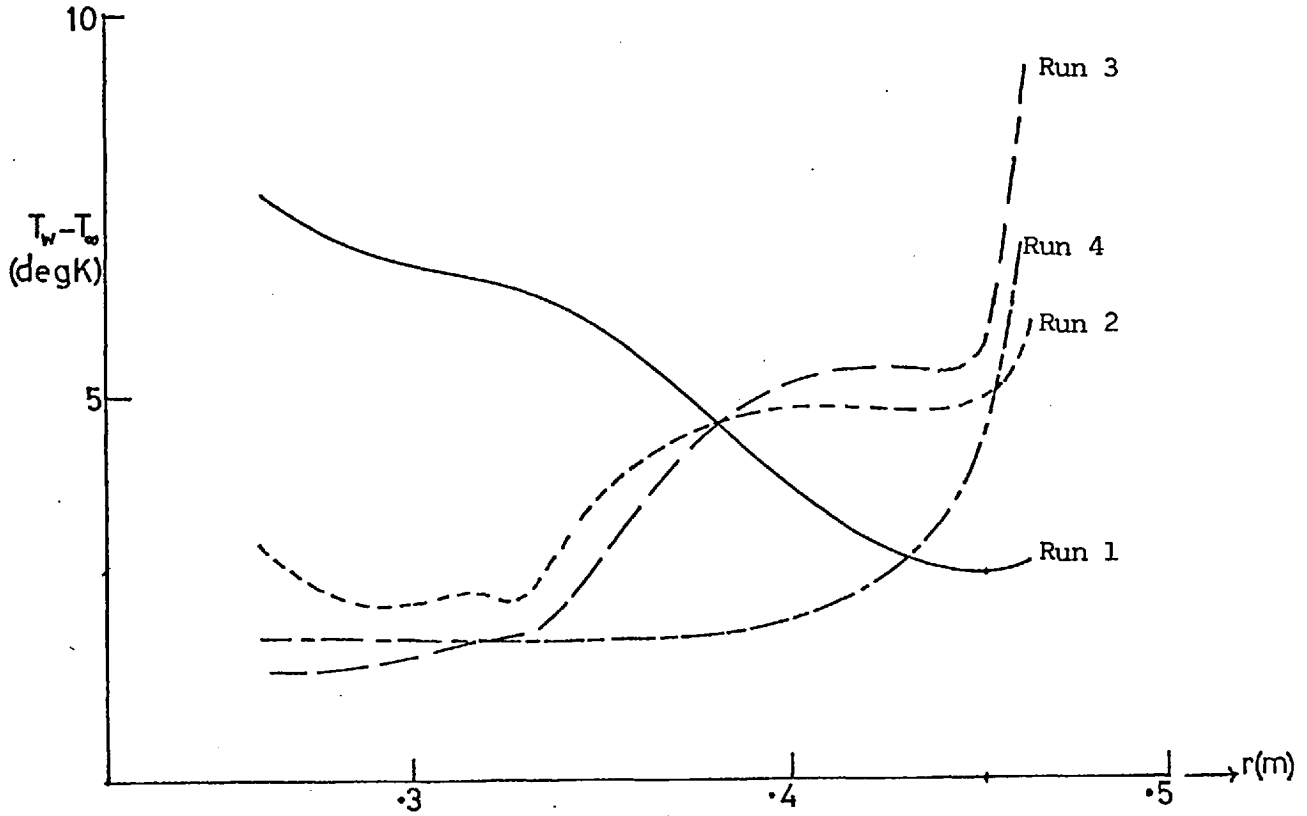

Fig. 7.7 Temperature distribution of heaters for Runs 1 to 4

The heat transfer by conduction through the disc was accounted for by a simple heat conduction calculation, neglecting any conduction in the radial direction in the disc material as well as the metal heater.

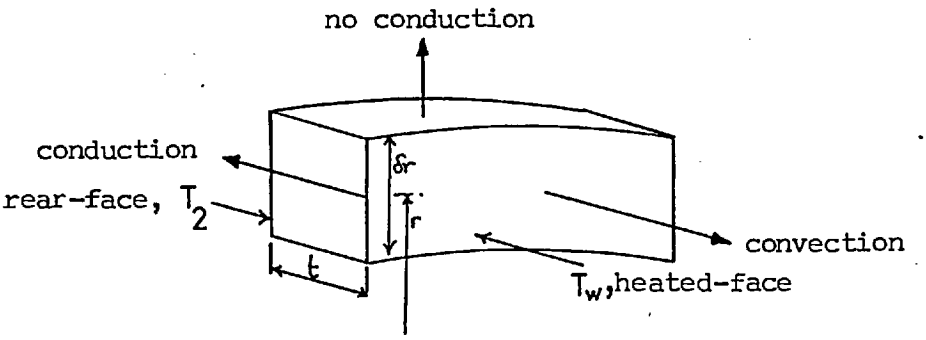

The temperature T_2 of the rear face of the disc, at the radial position corresponding to a value T_w measured for the heated face, was obtained from the recorded radial temperature distribution for the rear face. The heat conducted through the disc was then calculated as : $k_d \frac{T_w - T_2}{t}$, and consequently, the convective heat flux was computed as:

$$\dot{q}''_{convective} = I^2R/\text{Area of heater} - k_d(T_w - T_2)/t \quad . \qquad (7.1)$$

The local Nusselt number was subsequently determined from the known convective heat flux and surface temperature:

$$Nu = \frac{\dot{q}''}{k_a(T_w - T_\infty)} \quad . \qquad (7.2)$$

7.5 ASSESSMENT OF EXPERIMENTAL PROGRAMME AND SUGGESTIONS FOR IMPROVEMENT

The extraneous heat sources mentioned in Section 7.2-5 were the cause of the major set back to the experimental programme; the magnitudes of these sources were reduced by extensive cooling of the brushes and slip-rings transmitting the electrical power, but they were still rather large. Despite the attempt to isolate that part of the disc where the measurements were made from the influence of the heat sources, the temperature of the rear face of the disc was not constant and furthermore, different from the front face (heater) temperature. This was, of course, to be expected since heat conduction in the disc proceeded in the axial as well as the radial direction. This means that the effects of frictional and extraneous electrical heat sources on the disc for a radius larger than 0.30 m were not entirely eliminated.

The heat conduction in the disc can, in principle, be accurately calculated provided the radial surface temperature distribution for the heated and rear faces are measured. In the present experiment, a few temperatures were recorded for reasons explained in the following paragraph; consequently, an accurate two-dimensional heat conduction analysis was not performed.

Forty thermocouples were originally glued in channels flush with the fibre-glass disc's surface, under the heaters. However, when the measurements were made only 16 were functioning, and by the time Run 4 was made only 12 remained in working order. The design of the apparatus did not allow for replacement of failed thermocouples. Failure resulted from two main causes: (i) the 40 cold junctions were spinning in air and were therefore exposed to damage; and, (ii) since the thermocouple slip-ring assembly had only twelve channels, a selector switch, rotating with the disc, was incorporated between

the thermocouples and the slip-rings. The numerous lead-connections involved were very prone to failure.

In view of the uncertainty in the heat-flux and temperature measurements, they were not considered accurate enough to be of use and of lasting value. Under these circumstances, and also because of the long time and expenses required, but unavailable, to modify and improve the apparatus, it was decided to curtail the experimental programme to four runs only.

Further, these runs were restricted to speeds below 800 rpm because of large vibrations during the start-up period at speeds above 800 rpm. A resistance-type starter was used in conjunction with the synchronous motor to bring the apparatus from rest to the desired speed in a time interval of 10 seconds. This interval should be extended to over 60 seconds in order to have a gradual and slow build-up of speed, and therefore suppress the start-up vibrations.

In retrospect, the experimental programme was not successful in its main objective: the accurate measurements of surface heat flux and temperature to determine the local heat transfer rate.

The existing apparatus will only achieve the above objective after extensive modification and reconstruction to: (i) arrange for a large number of thermocouples to monitor the complete temperature distribution of the disc, connected directly to an equivalent number of slip-rings, with easy access for replacements in case of failure; (ii) locate the brushes and slip-rings assembly for electrical power transmission, at present fixed to the back of the disc, away from the disc, and arrange for extensive cooling; (iii) cool the bearings.

These modifications will undoubtedly present several complex design problems and it may be, that a new approach to the problem can be more fruitful. Remote sensors could be placed facing the disc's

heated face to record both the local temperature and the heat flux; these sensors could be automatically traversed in the radial direction recording a continuous distribution of heat flux and temperature. The existing apparatus would then not require any modifications whatsoever. The extraneous heat sources would contribute to the surface heat flux, and the current to the heaters would be adjusted to increase or decrease the heat flux for one or more of the 8 heaters, and thereby simulate any arbitrary heat flux.

Local heat transfer measurements for a rotating disc

			Heat flux (W/m^2)			$(T_w - T_\infty)$degK			
Heater	Radius (m)	Current (A)	Input	Conducted	Convected	Heated face	Rear face	Reynolds no. x 10^5	Local Nusselt no. x 10^2
	<.245					10.20	11.05		
4	.263	12.2	161.1	42.5	118.6	7.63	4.45	2.17	1.58
	.275			39.3	121.8	7.24	4.30	2.37	1.79
5	.315	12.5	168.4	37.9	130.5	6.58	3.74	3.11	2.41
	.329			38.4	130.0	6.44	3.56	3.40	2.56
6	.371	13.2	188.8	25.3	163.5	5.05	3.16	4.32	4.64
7	.423	11.0	130.7	13.4	117.3	3.10	2.10	5.62	6.18
	.448			12.3	118.4	2.80	1.88	6.30	7.32
8	.463	10.85	126.8	14.9	111.9	2.90	1.78	6.73	6.90

Run 1 : T_∞ = 20.75°C , rpm = 458.5

			Heat flux(W/m^2)			(T_w-T_∞)degK			
Heater	Radius (m)	Current (A)	Input	Conducted	Convected	Heated face	Rear face	Reynolds no. x 10^5	Local Nusselt no. x 10^2
	<.245					5.50	14.20		
4	.263	10.3	114.8	-3.3	118.1	3.00	3.25	2.17	4.00
	.275			-8.3	123.1	2.48	3.10	2.37	5.27
5	.315	11.1	132.8	-2.7	135.5	2.46	2.66	3.11	6.70
	.329			-2.9	135.7	2.32	2.54	3.40	7.43
6	.371	16.0	277.3	26.0	251.3	4.47	2.52	4.32	8.05
7	.423	19.85	425.6	29.5	396.1	4.81	2.60	5.62	13.45
	.448			28.6	397.0	4.74	2.60	6.30	14.49
8	.463	22.0	521.5	41.5	480.0	5.71	2.60	6.73	15.03

Run 2 : T_∞ = 21.80^oC , rpm = 458.5

			Heat flux (W/m^2)			(T_w-T_∞)degK			
Heater	Radius (m)	Current (A)	Input	Conducted	Convected	Heated face	Rear face	Reynolds no. x 10^5	Local Nusselt no. x 10^3
	<.245					1.75	15.80		
4	.263	8.7	81.9	-9.3	91.2	1.50	2.20	3.70	.618
	.275			-7.6	89.5	1.47	2.04	4.05	.645
5	.315	11.9	152.6	1.0	151.6	1.84	1.76	5.31	1.002
	.329			2.1	150.5	1.83	1.67	5.79	1.045
6	.371	16.0	277.3	36.7	240.6	4.21	1.46	7.36	.819
7	.423	24.5	648.3	53.1	595.2	5.34	1.36	9.57	1.820
	.448			50.6	597.7	5.29	1.50	10.73	1.954
8	.463	30.6	1008.9	102.9	906.0	9.21	1.50	11.46	1.759

Run 3: T_∞ = 21.00°C , rpm = 781

			Heat flux (W/m^2)			$(T_w - T_\infty)$degK			
Heater	Radius (m)	Current (A)	Input	Conducted	Convected	Heated face	Rear face	Reynolds no. $\times 10^5$	Local Nusselt no. $\times 10^3$
	<.245					1.80	10.50		
4	.263	10.1	110.4	12.0	98.4	1.75	0.85	3.70	.571
5	.315	11.9	152.6	24.0	128.6	1.80	0.0	5.31	.869
6	.371	13.0	183.1	21.6	161.5	1.80	0.18	7.36	1.285
7	.448	20.0	432.0	30.7	401.3	3.70	1.40	10.73	1.876
8	.463	29.6	944.1	71.1	873.0	6.78	1.45	11.46	2.302

Run 4: $T_\infty = 21.00^\circ C$, rpm = 781